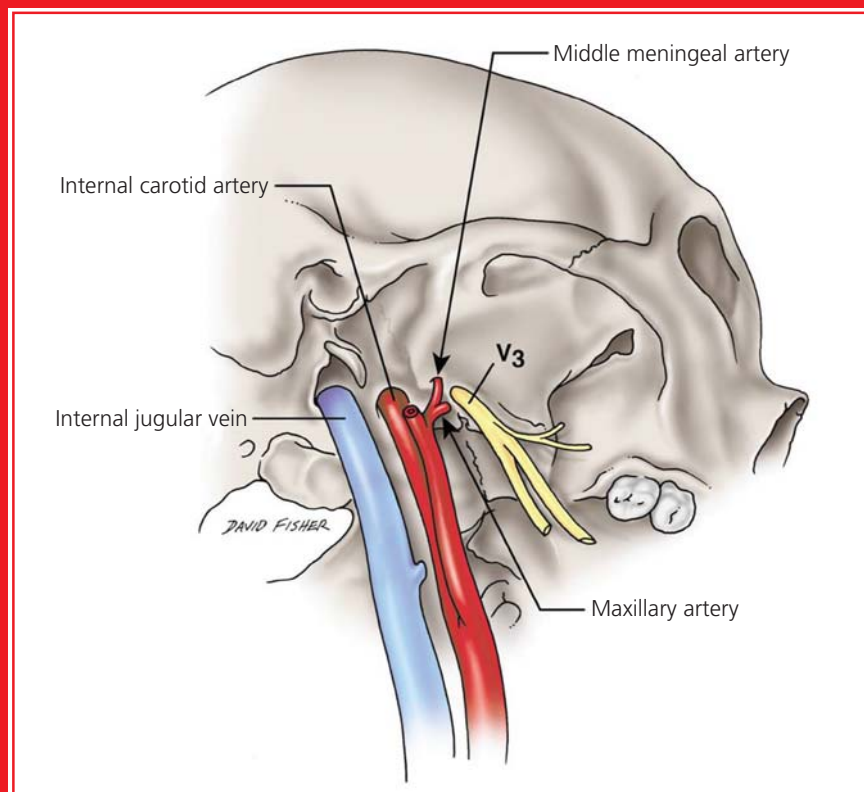


anatomy

An International Journal of Experimental and Clinical Anatomy

Volume 10 / Issue 3 / December 2016

Published three times a year



Official Publication of the Turkish Society of Anatomy and Clinical Anatomy

Aim and Scope

Anatomy, an international journal of experimental and clinical anatomy, is a peer-reviewed journal published three times a year with an objective to publish manuscripts with high scientific quality from all areas of anatomy. The journal offers a forum for anatomical investigations involving gross, histologic, developmental, neurological, radiological and clinical anatomy, and anatomy teaching methods and techniques. The journal is open to original papers covering a link between gross anatomy and areas related with clinical anatomy such as experimental and functional anatomy, neuroanatomy, comparative anatomy, modern imaging techniques, molecular biology, cell biology, embryology, morphological studies of veterinary discipline, and teaching anatomy.

Publication Ethics

Anatomy is committed to upholding the highest standards of publication ethics and observes the principles of Journal's Publication Ethics and Malpractice Statement which is based on the recommendations and guidelines for journal editors developed by the Committee on Publication Ethics (COPE), Council of Science Editors (CSE), World Association of Medical Editors (WAME) and International Committee of Medical Journal Editors (ICMJE). For detailed information please visit the online version of the journal which is available at www.anatomy.org.tr

Authorship

All persons designated as authors should have participated sufficiently in the work to take public responsibility for the content of the manuscript. Authorship credit should be based on substantial contributions to (1) conception and design or analysis and interpretation of data, (2) drafting of the manuscript or revising it for important intellectual content and, (3) final approval of the version to be published. The Editor may require the authors to justify assignment of authorship. In the case of collective authorship, the key persons responsible for the article should be identified and others contributing to the work should be recognized with proper acknowledgment.

Copyright

Copyright © 2016, by the Turkish Society of Anatomy and Clinical Anatomy, TSACA. All rights reserved. No part of this publication may be reproduced, stored or transmitted in any form without permission in writing from the copyright holder beforehand, exceptionally for research purpose, criticism or review. The publisher and the Turkish Society of Anatomy and Clinical Anatomy assume no liability for any material published in the journal. All statements are the responsibility of the authors. Although all advertising material is expected to conform ethical standards, inclusion in this publication does not constitute a guarantee or endorsement of the quality or value of such product or of the claims made of it by its manufacturer. Permission requests should be addressed to the publisher.

Publication Information

Anatomy (p-ISSN 1307-8798; e-ISSN 1308-8459) is published by Deomed Publishing, Istanbul, for the Turkish Society of Anatomy and Clinical Anatomy, TSACA. Due the Press Law of Turkish Republic dated as June 26, 2004 and numbered as 5187, this publication is classified as a periodical in English language.

Ownership

On behalf of the Turkish Society of Anatomy and Clinical Anatomy, Ahmet Kağan Karabulut, MD, PhD; Konya

Responsible Managing Editor

Nihal Apaydın, MD, PhD; Ankara

Administrative Office

Güven Mah. Güvenlik Cad. Onlar Ap. 129/2 Aşağı Ayrancı, Ankara
Phone: +90 312 447 55 52-53

Publisher

Deomed Publishing
Gür Sok. No:7/B Kadıköy, Istanbul, Turkey
Phone: +90 216 414 83 43 (Pbx) / Fax: +90 216 414 83 42
www.deomed.com / e-mail: medya@deomed.com

Submission of Manuscripts

Contributions should be submitted for publication under the following categories to:

Gülgün Şengül, MD
Editor-in-Chief, *Anatomy*

Department of Anatomy,
Faculty of Medicine, Ege University,
35100, Bornova, Izmir, Turkey
Phone: 0090 232 390 39 84
Fax: 0090 232 342 21 42
e-mail: gulgun.sengul@gmail.com; gulgun.sengul@ege.edu.tr

Categories of Articles

- **Original Articles** describe substantial original research that falls within the scope of the Journal.
- **Teaching Anatomy** section contains regular or all formats of papers which are relevant to comparing teaching models or to introducing novel techniques, including especially the own experiences of the authors.
- **Reviews** section highlights current development in relevant areas of anatomy. The reviews are generally invited; other prospective authors should consult with the Editor-in-Chief.
- **Case Reports** include new, noteworthy or unusual cases which could be of help for basic notions and clinical practice.
- **Technical Note** articles cover technical innovations and developments with a specific technique or procedure or a modification of an existing technique. They should be sectioned like an original research article but not exceed 2000 words.
- **Viewpoint** articles give opinions on controversial topics or future projections, some of these are invited.
- **Historical View** category presents overview articles about historical sections from all areas of anatomy.
- **Terminology Zone** category is a platform for the articles which discuss some terminological controversies or opinions.

The categories above are peer-reviewed. They should include abstract and keywords. There are also categories including Letters to the Editor, Book Reviews, Abstracts, Obituary, News and Announcements which do not require a peer review process.

For detailed instructions concerning the submission of manuscripts, please refer to the Instructions to Authors.

Subscription

Please send your order to Deomed Publishing, Gür Sok. No: 7/B Kadıköy, Istanbul, Turkey. e-mail: aliko@deomed.com

- **Annual rates:** Institutional 100 EUR, Individual 50 EUR (include postage and local VAT). Supplements are not included in the subscription rates.
- Membership of the Turkish Society of Anatomy and Clinical Anatomy, TSACA includes a reduced subscription rate to this journal.
- **Change of address:** Please send to the publisher at least six weeks in advance, including both old and new addresses.
 - **Cancellations:** Subscription cancellations will not be accepted after the first issue has been mailed.

The online version of this journal is available at www.anatomy.org.tr

Advertising and Reprint Requests

Please direct to publisher. e-mail: medya@deomed.com

Printing and Binding

Birmat Press, Istanbul, Turkey, Phone: +90 212 629 05 59-60
Printed in Turkey on acid-free paper (January 2017).

Honorary Editor

Doğan Akşit, Ankara, Turkey

Founding Editors

Salih Murat Akkın, Gaziantep, Turkey

Hakan Hamdi Çelik, Ankara, Turkey

Former Editor-in-Chief &

Advising Editor

Salih Murat Akkın, Gaziantep, Turkey

Editor-in-Chief

Gülgün Şengül, Izmir, Turkey

Editors

Nihal Apaydın, Ankara, Turkey

Kyung Ah Park, Seoul, Korea

George Paxinos, Sydney, Australia

Luis Puelles, Murcia, Spain

Mustafa F. Sargon, Ankara, Turkey

Ümit S. Şehirli, Istanbul, Turkey

Shane Tubbs, Birmingham, AL, USA

Emel Ulupınar, Eskişehir, Turkey

Associate Editors

Vaclav Baca, Prague, Czech Republic

Çağatay Barut, Istanbul, Turkey

Jon Cornwall, Dunedin, New Zealand

Ayhan Cömert, Ankara, Turkey

Georg Feigl, Graz, Austria

Zeliha Kurtoğlu, Mersin, Turkey

Scott Lozanoff, Honolulu, HI, USA

Levent Sarıkçıoğlu, Antalya, Turkey

Cristian Stefan, Boston, MA, USA

Executive Board of Turkish Society of Anatomy and Clinical Anatomy

Erdoğan Şendemir (President)

Emel Ulupınar (Vice President)

Ümit S. Şehirli (Vice President)

Esat Adıgüzel (Secretary General)

Nihal Apaydın (Treasurer)

Gülgün Şengül (Member)

Ferruh Yücel (Member)

Scientific Advisory Board

Peter H. Abrahams
Cambridge, UK

Halil İbrahim Açar
Ankara, Turkey

Esat Adıgüzel
Denizli, Turkey

Marian Adamkov
Martin, Slovakia

Mustafa Aktekin
Istanbul, Turkey

Serap Arbak,
Istanbul, Turkey

Mahindra Kumar Anand
Gujarat, India

Doychin Angelov
Cologne, Germany

Alp Bayramoğlu
Istanbul, Turkey

Brion Benninger
Lebanon, OR, USA

Susana Biasutto
Cordoba, Argentina

Dragica Bobinac
Rijeka, Croatia

David Bolender
Milwaukee, WI, USA

Eric Brenner
Innsbruck, Austria

Richard Halti Cabral
Sao Paulo, Brazil

Safiye Çavdar
Istanbul, Turkey

Katharina D'Herde
Ghent, Belgium

Özlem Yılmaz
Izmir, Turkey

Fabrice Duparc
Rouen, France

Behice Durgun
Adana, Turkey

İzzet Duyar
Istanbul, Turkey

Mirela Eric
Novi Sad, Serbia

Cumhur Ertekin
Izmir, Turkey

Mete Ertürk
Izmir, Turkey

Reha Erzurumlu
Baltimore, MD, USA

Ali Firat Esmer
Ankara, Turkey

António José Gonçalves Ferreira
Lisboa, Portugal

Quentin Fogg
Melbourne, Australia

Christian Fontaine
Lille, France

Rod Green
Bendigo, Australia

Bruno Grignon
Nancy Cedex, France

Nadir Gülekon
Ankara, Turkey

Mürvet Hayran
Izmir, Turkey

David Heylings
Norwich, UK

Lazar Jelev
Sofia, Bulgaria

David Kachlík
Prague, Czech Republic

Samet Kapakin
Erzurum, Turkey

Ahmet Kağan Karabulut
Konya, Turkey

Necdet Kocabıyık
Ankara, Turkey

Cem Kopuz
Samsun, Turkey

Mustafa Ayberk Kurt
Bursa, Turkey

Piraye Kervancıoğlu
Gaziantep, Turkey

Hee-Jin Kim
Seoul, Korea

Marios Loukas
Grenada, West Indies

Veronica Macchi
Padua, Italy

Mehmet Ali Malas
Izmir, Turkey

Petru Matusz
Timisoara, Romania

Bernard Moxham
Cardiff, Wales, UK

Konstantinos Natsis
Thessaloniki, Greece

Helen Nicholson
Dunedin, New Zealand

Davut Özbağ
Malatya, Turkey

P. Hande Özdinler
Chicago, IL, USA

Adnan Öztürk
Istanbul, Turkey

Mehmet Hakan Öztürk
Mersin, Turkey

Friedrich Paulsen
Erlangen, Germany

Wojciech Pawlina
Rochester, MN, USA

Tuncay Veysel Peker
Ankara, Turkey

Vid Persaud
Winnipeg, MB, Canada

David Porta
Louisville, KY, USA

Jose Ramon Sanudo
Madrid, Spain

Tatsuo Sato
Tokyo, Japan

Mohammadali M. Shoja
Birmingham, AL, USA

Ahmet Sinav
Gaziantep, Turkey

Takis Skandalakis
Athens, Greece

Vildan Sümbüloğlu
Gaziantep, Turkey (*Biostatistics*)

Muzaffer Şeker
Konya, Turkey

Erdoğan Şendemir
Bursa, Turkey

İbrahim Tekdemir
Ankara, Turkey

Hironubu Tokuno
Tokyo, Japan

Trifon Totlis
Thessaloniki, Greece

Mehmet İbrahim Tuğlu
Manisa, Turkey

Selçuk Tunali
Ankara, Turkey

Uğur Türe
Istanbul, Turkey

Mehmet Üzel
Istanbul, Turkey

Ivan Varga
Bratislava, Slovakia

Tuncay Varol
Manisa, Turkey

Charles Watson
Sydney, Australia

Andreas H. Weiglein
Graz, Austria

Bülent Yalçın
Ankara, Turkey

M. Gazi Yaşargil
Istanbul, Turkey

Hiroshi Yorifuji
Gunma, Japan

Anatomy, an international journal of experimental and clinical anatomy, is the official publication of the Turkish Society of Anatomy and Clinical Anatomy, TSACA. It is a peer-reviewed journal that publishes scientific articles in English. For a manuscript to be published in the journal, it should not be published previously in another journal or as full text in congress books and should be found relevant by the editorial board. Also, manuscripts submitted to *Anatomy* must not be under consideration by any other journal. Relevant manuscripts undergo conventional peer review procedure (at least three reviewers). For the publication of accepted manuscripts, author(s) should reveal to the Editor-in-Chief any conflict of interest and transfer the copyright to the Turkish Society of Anatomy and Clinical Anatomy, TSACA.

In the Materials and Methods section of the manuscripts where experimental studies on humans are presented, a statement that informed consent was obtained from each volunteer or patient after explanation of the procedures should be included. This section also should contain a statement that the investigation conforms with the principles outlined in the appropriate version of 1964 Declaration of Helsinki. For studies involving animals, all work must have been conducted according to applicable national and international guidelines. Prior approval must have been obtained for all protocols from the relevant author's institutional or other appropriate ethics committee, and the institution name and permit numbers must be provided at submission.

Anatomical terms used should comply with Terminologia Anatomica by FCAT (1998).

No publication cost is charged for the manuscripts but reprints and color printings are at authors' cost.

Preparation of manuscripts

During the preparation of the manuscripts, uniform requirements of the International Committee of Medical Journal Editors, a part of which is stated below, are valid (see ICMJE. Uniform requirements for manuscripts submitted to biomedical journals. Updated content is available at www.icmje.org). The manuscript should be typed double-spaced on one side of a 21x 29.7 cm (A4) blank sheet of paper. At the top, bottom and right and left sides of the pages a space of 2.5 cm should be left and all the pages should be numbered except for the title page.

Manuscripts should not exceed 15 pages (except for the title page). They must be accompanied by a cover letter signed by corresponding author and the Conflicts of Interest Disclosure Statement and Copyright Transfer Form signed by all authors. The contents of the manuscript (original articles and articles for Teaching Anatomy category) should include: 1- Title Page, 2- Abstract and Keywords, 3- Introduction, 4- Materials and Methods, 5- Results, 6- Discussion (Conclusion and/or Acknowledgement if necessary), 7- References

Title page

In all manuscripts the title of the manuscript should be written at the top and the full names and surnames and titles of the authors beneath. These should be followed with the affiliation of the author. Manuscripts with long titles are better accompanied underneath by a short version (maximum 80 characters) to be published as running head. In the title page the correspondence address and telephone, fax and e-mail should be written. At the bottom of this page, if present, funding sources supporting the work should be written with full names of all funding organizations and grant numbers. It should also be indicated in a separate line if the study has already been presented in a congress or likewise scientific meeting. Other information such as name and affiliation are not to be indicated in pages other than the title page.

Abstract

Abstract should be written after the title in 100–250 words. In original articles and articles prepared in IMRAD format for Teaching Anatomy category the abstract should be structured under sections Objectives, Methods, Results and Conclusion. Following the abstract at least 3 keywords should be added in alphabetical order separated by semicolons.

References

Authors should provide direct references to original research sources. References should be numbered consecutively in square brackets, according to the order in which they are first mentioned in the manuscript. They should follow the standards detailed in the NLM's Citing Medicine, 2nd edition (Citing medicine: the NLM style

guide for authors, editors, and publishers [Internet]. 2nd edition. Updated content is available at www.ncbi.nlm.nih.gov/books/NBK7256). The names of all contributing authors should be listed, and should be in the order they appear in the original reference. The author is responsible for the accuracy and completeness of references. When necessary, a copy of a referred article can be requested from the author. Journal names should be abbreviated as in *Index Medicus*. Examples of main reference types are shown below:

- **Journal articles:** Author's name(s), article title, journal title (abbreviated), year of publication, volume number, inclusive pages

- *Standard journal article:* Sargon MF, Celik HH, Aksit MD, Karaagaoglu E. Quantitative analysis of myelinated axons of corpus callosum in the human brain. *Int J Neurosci* 2007;117:749–55.

- *Journal article with indication article published electronically before print:* Sengul G, Fu Y, Yu Y, Paxinos G. Spinal cord projections to the cerebellum in the mouse. *Brain Struct Funct Epub* 2014 Jul 10. DOI 10.1007/s00429-014-0840-7.

- **Books:** Author's name(s), book title, place of publication, publisher, year of publication, total pages (entire book) or inclusive pages (contribution to a book or chapter in a book)

- *Entire book:*

- *Standard entire book:* Sengul G, Watson C, Tanaka I, Paxinos G. Atlas of the spinal cord of the rat, mouse, marmoset, rhesus and human. San Diego (CA): Academic Press Elsevier; 2013. 360 p.

- *Book with organization as author:* Federative Committee of Anatomical Terminology (FCAT). Terminologia anatomica. Stuttgart: Thieme; 1998. 292 p.

- *Citation to a book on the Internet:* Bergman RA, Afifi AK, Miyauchi R. Illustrated encyclopedia of human anatomic variation. Opus I: muscular system [Internet]. [Revised on March 24, 2015] Available from: <http://www.anatomyatlases.org/AnatomicVariants/AnatomyHP.shtml>

- *Contribution to a book:*

- *Standard reference to a contributed chapter:* Potten CS, Wilson JW. Development of epithelial stem cell concepts. In: Lanza R, Gearhart J, Blau H, Melton D, Moore M, Pedersen R, Thomson J, West M, editors. Handbook of stem cell. Vol. 2, Adult and fetal. Amsterdam: Elsevier; 2004. p. 1–11.

- *Contributed section with editors:* Johnson D, Ellis H, Collins P, editors. Pectoral girdle and upper limb. In: Standring S, editor. Gray's anatomy: the anatomical basis of clinical practice. 29th ed. Edinburgh (Scotland): Elsevier Churchill Livingstone; 2005. p. 799–942.

- *Chapter in a book:*

- *Standard chapter in a book:* Doyle JR, Botte MJ. Surgical anatomy of the hand and upper extremity. Philadelphia (PA): Lippincott Williams and Wilkins; 2003. Chapter 10, Hand, Part 1, Palmar hand; p. 532–641.

Illustrations and tables

Illustrations and tables should be numbered in different categories in the manuscript and Roman numbers should not be used in numbering. Legends of the illustrations and tables should be added to the end of the manuscript as a separate page. Attention should be paid to the dimensions of the photographs to be proportional with 10x15 cm. Some abbreviations out of standards can be used in related illustrations and tables. In this case, abbreviation used should be explained in the legend. Figures and tables published previously can only be used when necessary for a comparison and only by giving reference after obtaining permission from the author(s) or the publisher (copyright holder).

Control list

- Length of the manuscript (max. 15 pages)
- Manuscript format (double space; one space before punctuation marks except for apostrophes)
- Title page (author names and affiliations; running head; correspondence)
- Abstract (100–250 words)
- Keywords (at least three)
- References (relevant to *Index Medicus*)
- Illustrations and tables (numbering; legends)
- Conflicts of Interest Disclosure Statement and Copyright Transfer Form
- Cover letter

Ultrastructure of the placenta in gestational diabetes mellitus

Abdelghany Hassan, Tarek M. Essa

Department of Anatomy and Embryology, School of Medicine, Alexandria University, Alexandria, Egypt

Abstract

Objectives: The placenta plays critical roles during pregnancy and is essential for fetal growth and development. Its functions are determined by the ultrastructure of the placental barrier that is an important feature to maintain the exchange surface area between the fetus and the mother. Gestational diabetes mellitus (GDM) comprises unfit conditions for embryonic and fetoplacental development, and may result in placental abnormalities. The aim of this study was to detect the ultrastructural changes of the placenta in women with GDM.

Methods: The placentas of 10 women with GDM without pregestational diabetics, hypertension and chronic diseases and 10 controls were studied. Six control women were delivered vaginally and the remaining cases by caesarian section at a gestational age of 36 to 39 weeks. Placental samples were measured for their thickness and prepared for light and transmission electron microscopy study.

Results: Light microscopic study of the control placentas showed numerous densely packed microvilli with syncytial knots and thin-walled blood vessels and wide intervillous spaces. The placentas of GDM cases showed reduced number of microvilli with syncytial knots, thick-walled vessels, edematous spaces, areas of fibrosis and perivillous fibrinoid degeneration. Electron microscopic study of the placentas of the control women showed terminal villi with a thick layer of syncytiotrophoblasts (Sy) with a lot of regular cylindrical microvilli and a thin layer of cytotrophoblasts (Cy). There were some endoplasmic reticulum cisternae besides few mitochondria. The underlying villus core was harboring fetal capillaries lined with flat endothelial cells and thin basement membrane. There was no fibrosis or edema. In the placenta of GDM women, there was hypertrophy of Cy with atrophy of Sy with multiple vacuoles and areas for glycogen storage. The subtrophoblastic membrane was thick and the microvilli were scarce. The villous core showed congested capillaries, stromal macrophages, edematous spaces, glycogen storage areas and fibrosis.

Conclusion: All the changes in placentas of gestational diabetes were attributed to associated hypoxia and oxidative stress due to decreased uteroplacental flow that was aggravated by the thick placental barrier and the presence of edema, fibrosis and glycogen storage areas that increased the distance of transfer between the fetus and mother.

Keywords: cytotrophoblast; fetal; gestational diabetes; microvilli; placenta; syncytiotrophoblast

Anatomy 2016;10(3):159–169 ©2016 Turkish Society of Anatomy and Clinical Anatomy (TSACA)

Introduction

The placenta, situated between the mother and fetus, is essential for fetal growth and development.^[1] Placenta performs essential functions during pregnancy, including the exchange of nutrients, water, respiratory gases and waste products, and synthesis of various hormones which regulate the transport of maternal nutrients to the fetus and facilitate maternal metabolic adaptation to different pregnancy stages. These functions are determined by the ultrastructure of the placental exchange barrier.^[2]

The placental barrier that separates the fetal and maternal blood is composed of different structures including a continuous maternal-facing layer of syncytiotrophoblasts (Sy) with multiple apical microvilli, a thin layer of cytotrophoblasts (Cy) which gets thinner as pregnancy proceeds but persists until term, the endothelial lining and underlying basal membrane (BM) of the fetal capillaries, and the villous connective tissue between them. This barrier is mostly important to maintain the exchange surface area between the fetus and the mother.^[2,3] A proper coordination of trophoblast proliferation, differentiation and invasion is required for placental development.^[3,4]

The physiological changes that occur during pregnancy can only be sustained if there is an appropriate nutrient supply to ensure placental and fetal development. To make sure that the supply of nutrients is essential to fetal survival, the placenta continuously undergoes changes in weight, structure, shape and function during gestation. Some forms of intrauterine fetal growth abnormalities have been correlated with abnormalities of placental blood flow and transfer of nutrients from the mother to the fetus.^[1]

Gestational diabetes mellitus (GDM) is defined as the glucose intolerance with onset or first recognition during pregnancy. GDM is associated with short- and long-term morbidity in both offspring and mother. The short-term adverse outcomes include macrosomia, neonatal hypoglycemia, neonatal jaundice, preeclampsia, preterm delivery and cesarean delivery, while the long-term complications include obesity, abnormal glucose tolerance, and diabetes in adolescence or early adulthood.^[5,6]

The diabetic environment can be regarded as a network of substances (hormones, nutrients, cytokines) with altered concentrations.^[7] In diabetes, the placenta undergoes a variety of structural and functional changes. The nature and extent of these changes depend on a range of variables including the quality of glycemic control achieved during the critical periods in placental development and the modality of treatment.^[7,8]

Despite currently available treatment, maternal diabetes comprises unfit conditions for embryonic and fetoplacental development and placental structure. However, reports on the pathology of placenta are usually incompatible with diabetes mellitus. The inconsistency may be explained partially by the fact that the category of diabetic pregnant women is not homogeneous. Moreover, the analysis of placental lesions in maternal diabetes has been complicated by superimposed hypertensive and other associated complications.^[1]

Few studies have investigated the ultrastructural changes in human term placentas in GDM.^[2] Therefore, this study was undertaken to detect the ultrastructural changes of the placenta in women with GDM.

Materials and Methods

The placentas of 20 women, 10 control and 10 with GDM, were studied with free consents approved by the Committee of Ethics in Alexandria University, School of Medicine. Women with a history of pregestational diabetes, hypertension or other chronic diseases were excluded. The age of the women ranged from 28 to 30 years for the controls and 27 to 31 years for the GDM group. Fasting blood glucose level was measured after an overnight fast of at least 10 h at 24–28 weeks of gestation. The diagnosis of GDM was made based on the criteria of

the American Diabetes Association (2011).^[5] Control women were within the accepted normal range of blood glucose levels from 90 to 115 mg/dL throughout gestation, while the GDM women showed levels ranging from 120 to 180 mg/dL. GDM women were asked to control their diet besides insulin therapy, so that their fasting blood glucose levels were kept in the 100 to 135 mg/dL range until delivery. Two GDM women had higher fasting blood glucose ranging from 140 to 165 mg/dL due to poor diet control and interrupted therapy. The maternal weight at gestation ranged from 62 to 65.5 kg for the control, and from 65 to 68.5 kg for GDM group. All GDM women were delivered by caesarian section and the gestational weeks at delivery ranged from 36 to 38 weeks for the GDM. Six control women were delivered vaginally, while four were delivered by caesarian section at a gestational age ranging from 36 to 39 weeks. All deliveries were done at the Department of Gynecology and Obstetrics, Alexandria University, School of Medicine. The fetal birth weight ranged from 2.8 to 3.15 kg in the control group, while it ranged from 3.21 to 3.4 kg in the GDM group. The embryonic membranes and the umbilical cords were trimmed from the placentas. The placenta weight ranged from 450 to 480 g in the control group, and 470 to 500 g in the GDM group. The whole thickness of the placenta was measured at the center of the placenta, beside the site of attachment of the umbilical cord. Paraffin-embedded blocks from formaldehyde-fixed tissues were prepared and cut on a microtome at a thickness of 0.5 μ m from each block and stained with hematoxyline and eosin (HE) to be examined under Optika B-150 (Optika SRL, Ponteranica, Italy) light microscope. Blocks for electron microscopy were fixed in the fixative 3% glutaraldehyde and 2% paraformaldehyde in 0.1 mol/l cacodylate buffer (pH 7.3) for 24 h at 4°C. After fixation in 1.0% OsO₄ in 0.1 mol/l cacodylate buffer (pH 7.3) for 2 h at room temperature, the tissue specimens were subjected to dehydration in graded ethanol series. After immersion in propylene oxide (three times for 10 min each), the samples were immersed overnight in a mixture (1:1) of propylene oxide and Epon 812 resin (Sigma Aldrich, St. Louis, MO, USA) to be finally embedded in Epon-812 resin Semithin sections (0.5 μ m thick) were cut using an ultramicrotome (Leica Ultracut; Leica, Berlin, Germany) that were picked on copper grids and counterstained with 2% uranyl acetate and lead citrate.^[9] The specimens were then examined by transmission electron microscopy JEM-100CXi, (Jeol, Tokyo, Japan) at the electron microscope unit of Alexandria University School of Medicine.

The results were analyzed statistically using SPSS 17 (SPSS Inc, Chicago, IL, USA). Mean \pm standard deviation (SD) of the two groups were compared using paired-samples t-test and the level of significance was accepted as $p < 0.05$.

Results

There was no statistically significant difference for the increase in gestational age in the control women compared to the GDM. Also, the higher maternal age in GDM women compared to the control was not statistically significant ($p>0.5$). On the other hand, the neonatal weight, neonatal weight and plasental weight were significantly increased in the GDM compared to controls (**Table 1**).

Light microscopy of the control placenta showed a large number of densely packed microvilli. The intervillous spaces were narrow and explicit and filled with blood cells. The microvilli showed syncytial knots which are aggregations of the nuclei of the Sy occupying vari-

Table 1
Parameters of the studies control and GDM cases.

Variables	Control	GDM	t-test	p value
Gestational age	36.9±0.91	36.4±0.6	1.88	0.076
Neonatal weight	2.93±0.127	3.15±1.91	5.955	0.001*
Maternal age	28.85±0.88	29.20±1.36	0.941	0.358
Maternal weight	63.97±1.14	65.64±0.53	5.807	0.001*
Placental weight	460.25±8.96	485.25±11.47	6.216	0.001*

*Significant at $p<0.05$

able areas at the poles of the microvilli. The villous core showed small and thin-walled blood vessels showing a number of blood cells (**Figure 1**). In placenta of GDM,

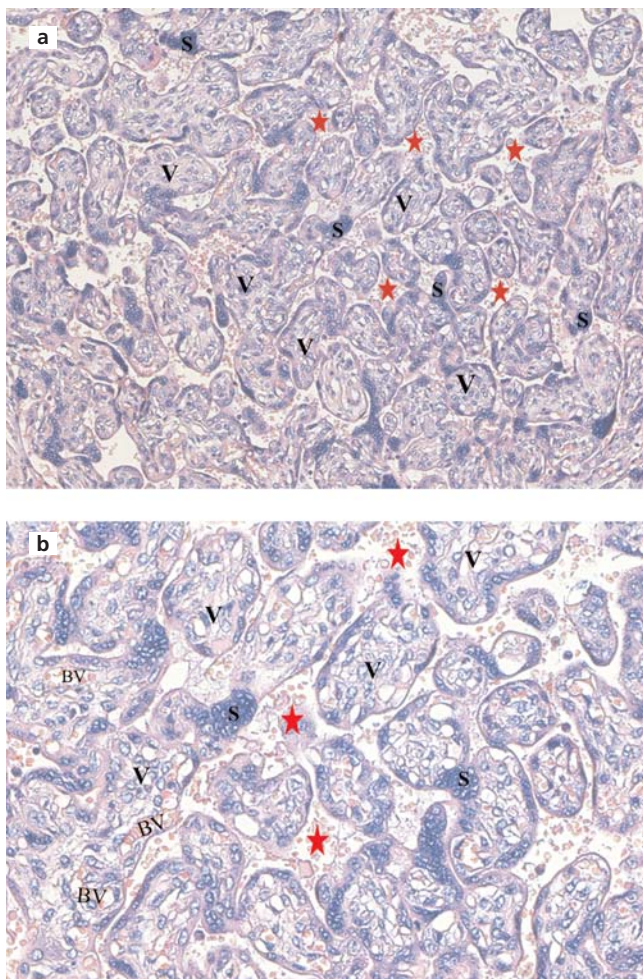


Figure 1. (a, b) Photomicrographs of the control placenta showing numerous microvilli (V) with narrow intervillous spaces (red star) filled with blood cells. The microvilli show syncytial knots (S) at their poles. The villous core shows thin-walled blood vessels (BV) containing blood cells. Haematoxyline and eosin stain, $\times 200$ (a); $\times 400$ (b). [Color figure can be viewed in the online issue, which is available at www.anatomy.org.tr]

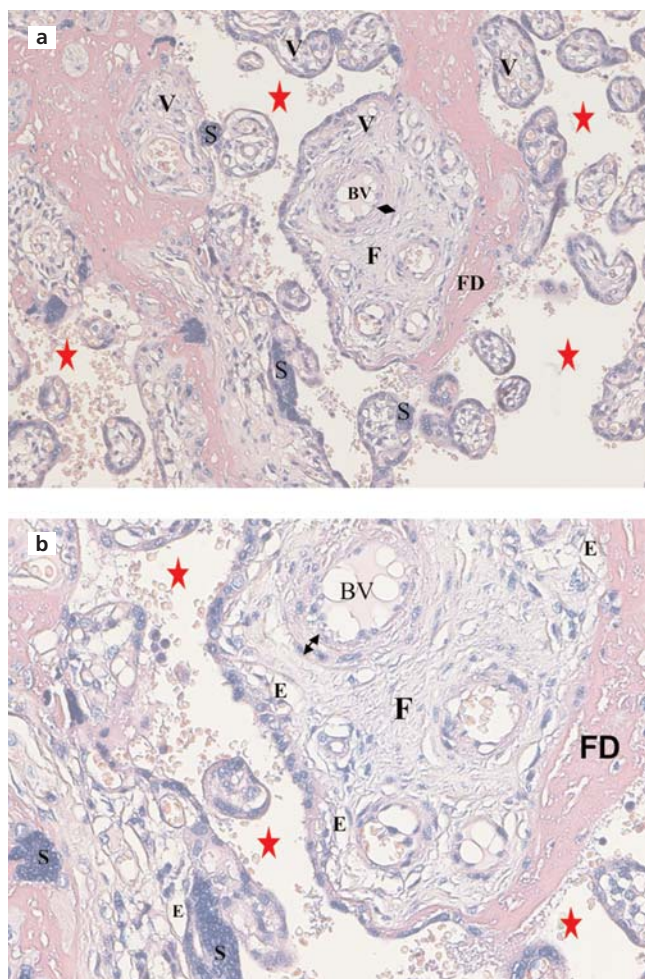


Figure 2. (a, b) A photomicrograph of GDM placenta showing reduced number of microvilli (V) showing syncytial knots (S) with wide intervillous spaces (red star) filled with blood cells. The villous core shows areas of fibrosis (F), spaces of edema (E) and blood vessels (BV) containing blood cells and their walls (black arrow) were thick. There were areas of perivillous fibrinoid degeneration (FD). $\times 200$ (a); $\times 400$ (b). [Color figure can be viewed in the online issue, which is available at www.anatomy.org.tr]

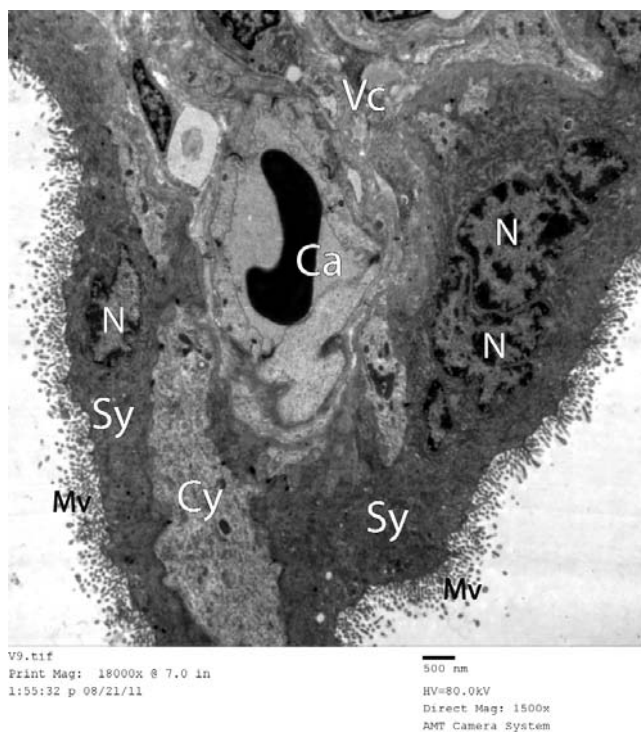


Figure 3. An electron micrograph of a terminal chorionic villus of a placenta from a control woman showing that the covering trophoblastic layer is formed basically of Sy that exhibits a relatively dense cytoplasm surrounding multiple nuclei (N), with a lot of long cylindrical microvilli (Mv) on the surface. The underlying villus core (Vc) is harboring a capillary (Ca). Cytotrophoblast (Cy). Magnification $\times 1500$, Scale bar = 500 nm.

the number of microvilli was less than the controls with syncytial knots. The intervillous spaces were wide. A number of the microvilli showed areas of fibrosis and scattered spaces of edema in the villous core. The blood vessels in some of the micovilli were dilated and showed thickening of their walls. There were areas of perivillous fibrinoid degeneration shown in bright pink appearance (Figure 2).

Electron microscopic study of the full-term placenta of control women showed that the terminal chorionic villi had a covering of a thick layer of Sy which had a lot of cylindrical and regular microvilli (Figures 3 and 4). The cytoplasm of Sy was relatively dense surrounding multiple nuclei with rough endoplasmic reticulum (rER) and mitochondria (Figures 3–6). Deeper to SY there was a thin layer of Cy where the cytoplasm of its cells was paler and harbored some rER cisternae beside few mitochondria (Figures 4 and 6). In some areas of the villi, there was only Sy, but no Cy (Figures 3 and 5). The underlying villous core was harboring fetal capillaries that were lined with flat endothelial cells held together by dense junctions (Figures 5 and 7). The BM was too thin

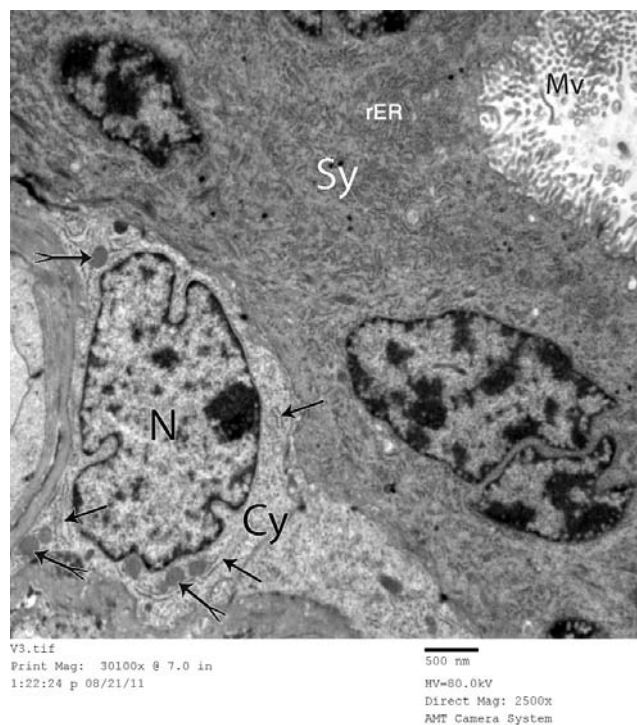


Figure 4. A higher Electron micrograph of a terminal chorionic villous of a control placenta. The Sy has its cytoplasm rich in rER profiles and bears slender and regular microvilli (Mv). The Cy forms a thinner deep layer; the cytoplasm of this cell seemed paler and harbored some rER cisternae (arrows) beside few mitochondria (forked arrows). Magnification $\times 2500$, Scale bar = 500 nm.

to be resolved. The capillaries were externally limited by fenestrated concentric arrays of reticular fibers (Figures 5 and 7).

In the placenta of GDM women, there was hypertrophy of Cy with atrophy of the Sy (Figure 8). The cytoplasm of both types of trophoblasts was occupied by a lot of membrane-bounded irregular vesicular structures that contained a low electron-dense material (Figures 8–10). Areas rich in glycogen granules and few mitochondria appeared in the Cy cells (Figure 9). In the Sy, there were inclusion bodies inside the nucleus that assumed a concentric lamellar appearance with a halo around (Figure 10). The microvilli on the surface were scarce and some had terminal club ends (Figure 10). The subtrophoblastic BM was thick and separated from the fetal capillary by a subtrophoblastic space (Figure 9). The fetal capillaries underneath the trophoblast were congested with much dark and few pale red blood cells (RBCs) (Figure 8). The endothelial cells lining the capillaries showed aggregates of glycogen granules near the nucleus together with the presence of dilated cisternae of endoplasmic reticulum (Figure 11). There were edematous clear

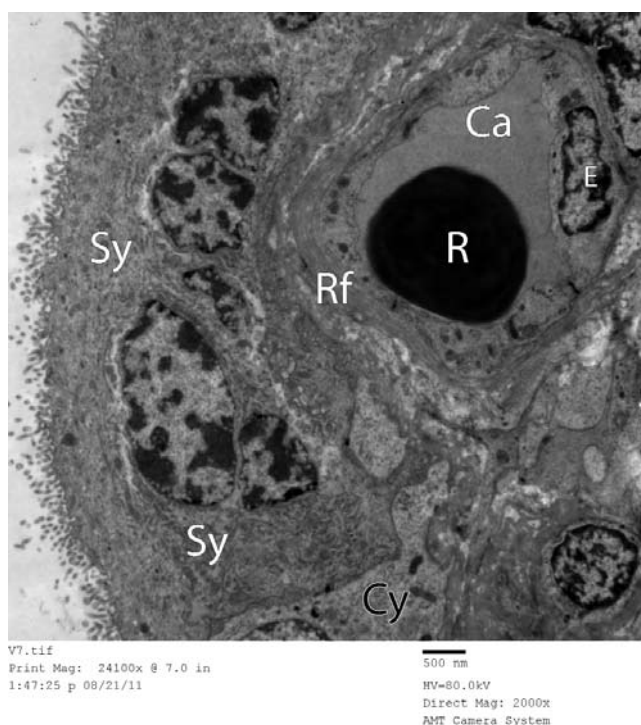


Figure 5. Electron micrograph of a terminal chorionic villous of a control placenta showing predominance of Sy and almost complete exclusion of the Cy in the placental barrier. The fetal capillary (Ca) is lined by flat endothelium (E) that is surrounded by multiple layers of reticular fibers (Rf). Fetal RBC (R). Magnification $\times 2000$, Scale bar = 500 nm.

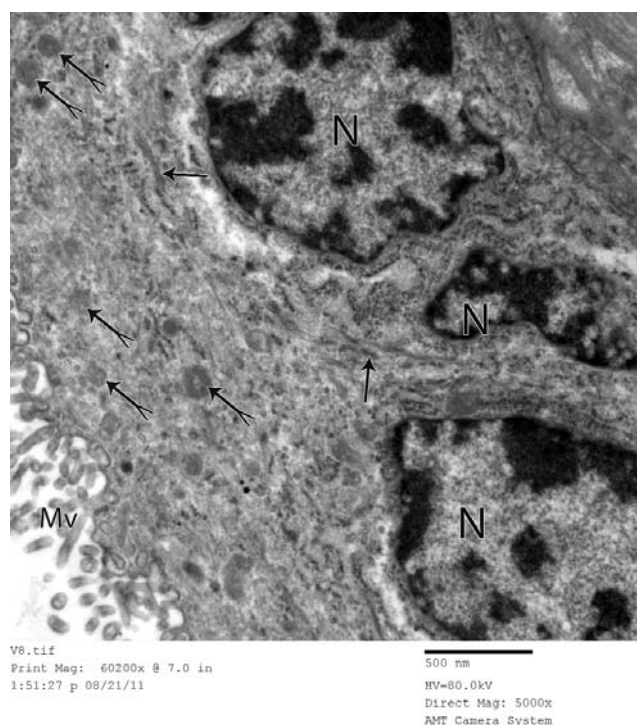


Figure 6. A magnified part from Figure 3 to reveal the ultra-structure of the Sy; rER (arrows), mitochondria (forked arrows), microvilli (Mv) and multiple nuclei (N). Magnification $\times 5000$, Scale bar = 500 nm.

spaces and well-defined storage areas in the matrix of the villous core (Figures 12 and 13). These storage areas were well-circumscribed by microcapsules of coarse matrix fibers and enclosed scattered dense short fibrillar and granular content on a homogenous background of moderate electron density (Figure 13). There was fibrosis inside a chorionic villous core where fibroblasts and collagenous bundles were exceptionally prevalent (Figure 14). Stromal macrophages were observed with lysosomes containing a material with a density comparable to that of hemoglobin of the extra-vascular fetal RBCs (Figure 12).

Discussion

The placenta is a complex organ that fulfills vital roles during fetal growth. Because of its unique position, the placenta is exposed to changes in both maternal and fetal environments. The diabetic environment can be regarded as a network of nutrients and hormones. Diabetes affects both maternal and fetal environments with multiple effects on different body organs including the placenta that shows alterations from non-diabetic placenta.^[7]

Study of the placenta of the control group showed that the placental terminal villi were formed of a thick layer of Sy with multiple nuclei and a thin layer of Cy with a thin BM. The trophoblast showed some rER and mitochondria. Terminal villi contained regular and cylindrical microvilli. The villous core contained capillaries lined with flat endothelial cells with a thin BM with no evidence of fibrosis or edematous spaces. Meng et al.^[2] observed the same findings for the trophoblastic covering and the core of the placental villi.

Placental growth is essentially a result of the coordination of trophoblast proliferation and differentiation. The microvilli projecting from the Sy and their terminal branches play an important role in the fetal-maternal exchange. The thickness of the trophoblastic layers determine the microvillous density and the degree of trophoblastic maturation.^[2]

In the control group, a thin layer of Cy is shown due to proper syncytial fusion. Sy cannot grow by itself, but syncytial growth and surface expansion throughout pregnancy together with endometrial invasion depend on continuous incorporation of Cy by syncytial fusion. This

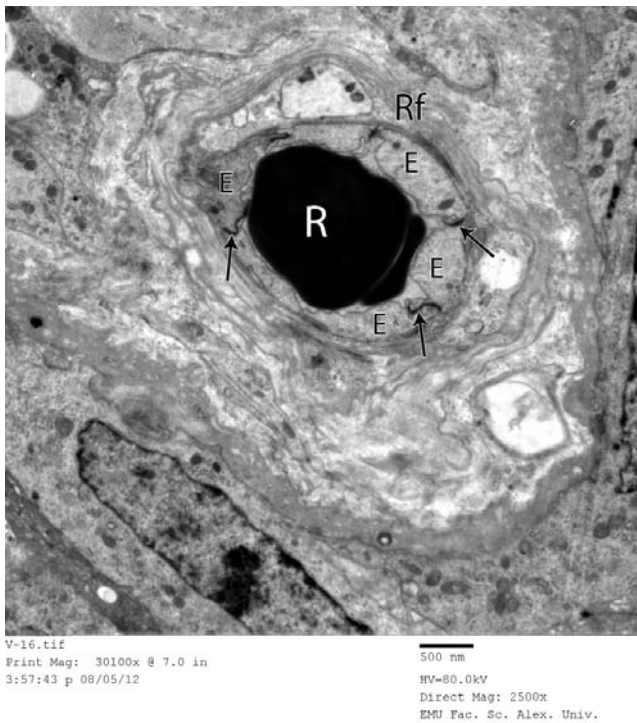


Figure 7. Detailed ultrastructure of a fetal capillary from a control placenta. This micro-vessel is lined by flat endothelial cells (E) that are held together by dense junctions (arrows). The BM is too thin to be resolved; however, the capillary is externally limited by fenestrated concentric arrays of reticular fibers (Rf). Fetal RBCs (R). Magnification $\times 2500$, Scale bar = 500 nm.

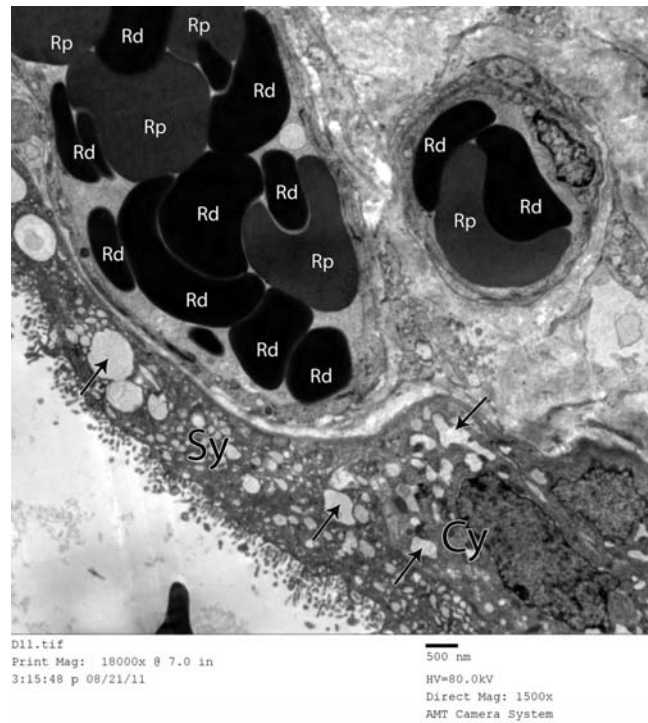


Figure 8. Electron micrograph of a terminal chorionic villous of a placenta from a woman with GDM. Notice hypertrophy of Cy on the expense of the atrophic Sy; the cytoplasm of both is occupied by dilated membrane-bound vesicular structures (arrows). The capillaries underneath the trophoblast are congested with much dark (Rd) and few pale (Rp) fetal RBCs inside. Magnification $\times 1500$, Scale bar = 500 nm.

fusion is also important for the syncytial hormonal function.^[4] Thin Cy and hence the placental barrier increase the utero-placental blood flow into the intervillous spaces, thus ensuring adequate maternal nutrient supply to the fetus.^[2,4] Moreover, thin Cy cells ensure proper invasion to the endometrium and its spiral arteries as the Cy at the tips of the villi grows out to penetrate into the decidualised uterus.^[4] Placental invasion and establishment of enough maternal blood supply are key processes in placental development, their dysregulation is associated with pregnancy diseases.^[2,3]

The placental barrier represents the site of interface between the maternal and fetal circulations. In the control group, it was formed of Sy, a thin layer of Cy and a thin layer of vascular endothelial cells with a thin BM together with a villous core made up of stroma without edema or fibrosis. Gude et al.^[10] and Meng et al.^[2] stated that this structure is suitable to ensure proper oxygenation and nutrition of the embryo as proper oxygenation of the placenta and the embryo is essential for a successful pregnancy.^[2,10]

The rER is the intracellular organelle where synthesis of proteins occurs prior to its eventual extrusion into the extracellular matrix to share in the production of placental hormones. Mitochondria are double-membrane organelles with multiple essential functions, such as cellular survival, energy metabolism, and intracellular adenosine triphosphate (ATP) production by oxidative phosphorylation necessary for the active organ. Oxidative phosphorylation is a highly efficient process in which cells use enzymes to oxidize nutrients, thereby releasing energy which is used to form ATP. Under normal conditions, increased activity and oxidative phosphorylation of placental mitochondria throughout gestation result in overproduction of reactive oxygen species (ROS) such as superoxide and hydrogen peroxide as natural by-products of the normal metabolism of oxygen. Physiological ROS levels play a crucial role in placental development through cellular signaling, but increased ROS can inactivate certain enzymes thus expose the placenta to oxidative stress even in normal pregnancies. This is dealt with by the placental antioxidant defense capacities which induce conversion of ROS to water and molecular oxygen.^[11,12]

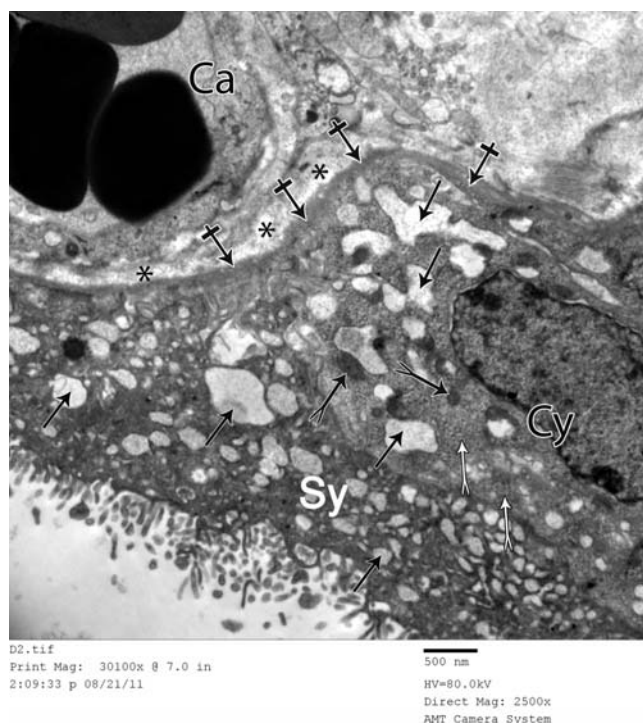


Figure 9. Higher magnification of Figure 6; the cytoplasm of both types of trophoblast is occupied by a lot of membrane-bounded irregular vesicular structures (black arrows) that contain a low electron-dense material. Areas rich in glycogen granules (white forked arrows) and few mitochondria (black forked arrows) appear in the Cy cell (Cy). The sub-trophoblastic BM (crossed arrows) is obviously thick and is separated from the fetal capillary (Ca) by a sub-trophoblastic space (*). Magnification $\times 2500$, Scale bar = 500 nm.

The present study on placentas from women with GDM showed that the Sy was thin with thick Cy and scarce microvilli. Similar observations were found by Meng et al.,^[2] Gheorman et al.,^[8] Slukvin et al.^[13] and Gul et al.^[1] who found reduced number of or even absent placental microvilli with immature villous Sy and persistent Cy with GDM.

It has been suggested that diabetes induces abnormal uncontrolled cell proliferation in the placenta similar to that seen in other organs, with increased proliferative activity in villous Cy.^[4,14] This adds to the uteroplacental ischemia and hypoxia as the cells of the thick Cy layer at the tips of the villi do not invade properly to the endometrial vessels. This strongly suggests an influence of the maternal diabetic environment on trophoblastic invasion. Invasion is a complex process involving a range of invasion inhibiting and invasion promoting factors. The diabetic environment appears to shift the balance towards invasion inhibition as a response to accompanying diabetic oxidative stress.^[1,15] This shallow invasion

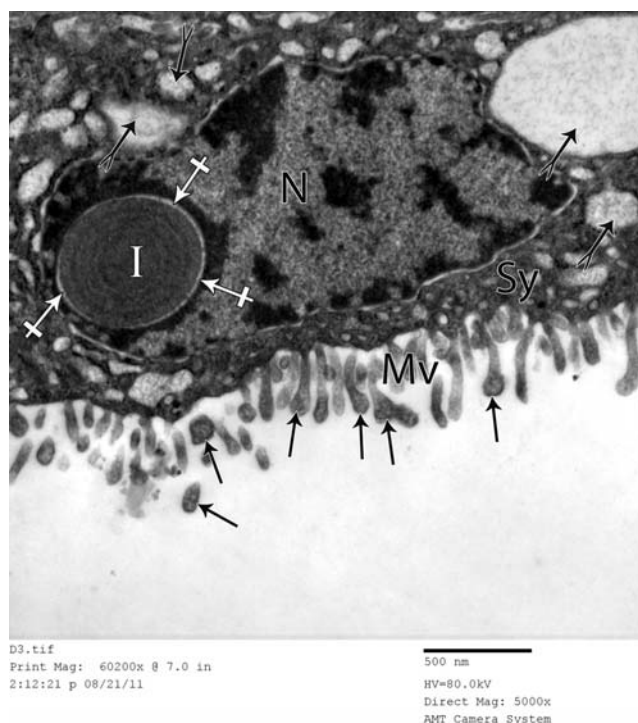


Figure 10. Electron micrograph of Sy in the placenta in a diabetic woman. It demonstrates the appearance of an inclusion body (I) inside the nucleus (N); it assumes a concentric lamellar appearance with a halo around (crossed arrows). Microvilli (Mv) on the surface are scarce and some have terminal club ends (black arrows). There are cytoplasmic vesicular structures (forked arrows). Magnification $\times 5000$, Scale bar = 500 nm.

reduces the uteroplacental blood flow resulting in hypoxia, increased placental infarction areas and Sy cell degeneration with shedding and reduction of the number of the villi.^[2,13] It was suggested that villous Cy proliferation without syncytial fusion, as observed in severe hypoxia, might be accompanied by syncytial degeneration.^[3]

Oxidative stress and mitochondrial dysfunction are now emerging as a front-runner in the mechanism of diabetic pathogenesis. Recently, a two fold increase in trophoblastic mitochondrial ROS production through incomplete reduction of oxygen under hyperglycemic conditions when compared to normoglycemic levels with the reduction of antioxidant capacity was reported. ROS causes a biological molecular damage leading to inactivation of specific enzymatic reactions together with loss of function and cell death with the resulting oxidative stress. Thus, the trophoblasts are affected by the hyperglycemic environment with reduction of its proliferation.^[16-18]

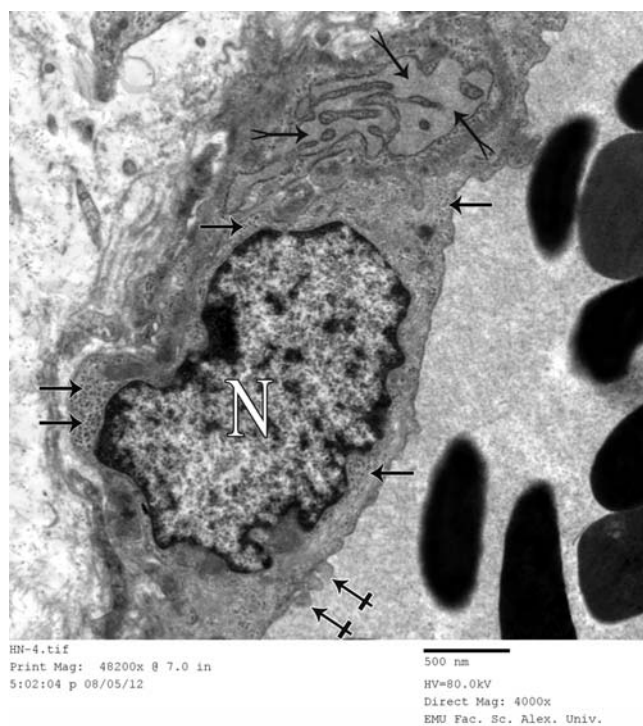


Figure 11. Electron micrograph with very high power magnification of a fetal capillary in a diabetic woman. Aggregates of glycogen granules (arrows) are stored particularly near the nucleus (N) of an endothelial cell. Also, dilated cisternae of endoplasmic reticulum (forked arrows) are shown where a homogeneous material of moderate electron density is stored. Notice blebblings of capillary endothelial cytoplasm into the capillary lumen (crossed arrows). Magnification $\times 4000$, Scale bar = 500 nm.

The present study showed thick trophoblastic BM in diabetic placentas. Similar results were obtained by Gheorman et al.,^[8] Magee et al.^[19] and Meng et al.^[2] who found thick BM of the villous trophoblast in women with GDM. The same was found by Gul et al.^[1] in the placenta of diabetic rats. BM thickening might be attributed to mucopolysaccharide storage and impaired villous trophoblastic activity such as increased production or decreased turnover of BM molecules, as it is known that the constituents of the BM components are produced by the secretion of trophoblasts.^[8] BM thickening is also attributed to fat droplet accumulation due to an effect of diabetes on fatty acid oxidation.^[1,13] These changes may result in uteroplacental vascular insufficiency further aggravating the hypoxic state.^[1]

Also, the current study showed the presence of vacuoles in both layers of the trophoblasts. It was hypothesized that a slight vacuolation may be present in the normal human placenta as a natural and physiological form of cell degradation which promotes survival.^[20,21] Meng et al.^[2] found much more trophoblastic vacuoles in placen-

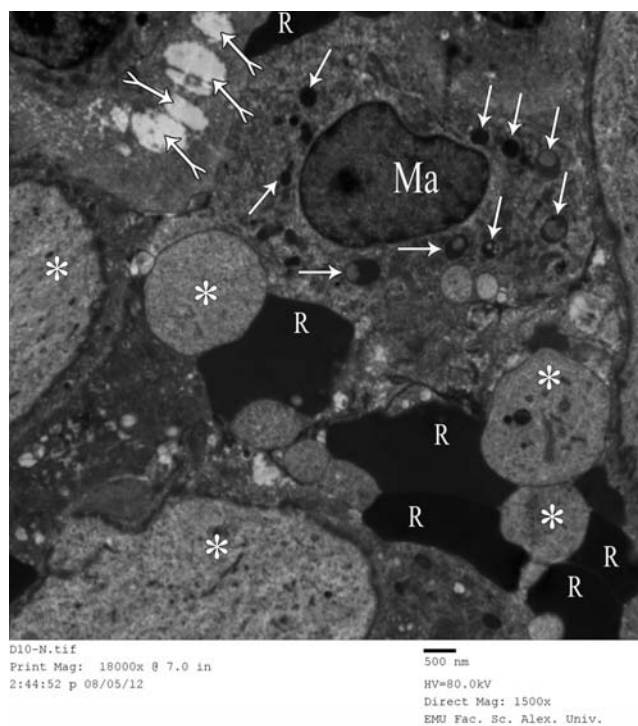


Figure 12. Electron micrograph of the core of a terminal chorionic villus of a diabetic woman. Notice, edematous clear spaces (forked arrows) and well-defined storage areas (*) inside the villous core matrix. A stromal macrophage (Ma) is seen that contains lysosomes (arrows) with a dense material comparable to that of hemoglobin of the extra-vasated fetal RBCs (R). Magnification $\times 1500$, Scale bar = 500 nm.

tas of GDM compared to controls.^[2] Hyperglycemia and hypoxia which have a role in the etiology of GDM may enhance the lysosome/vacuole functions of the trophoblasts, which result in widespread cytoplasmic vacuolation and altered transplacental metabolic exchange that may lead to cell death. So, in the context of disease, vacuolation is observed as a response to stress and oxygen restriction.^[2,21,22]

Regarding the villous core, the present study showed that edematous spaces were obviously seen in women with GDM. Gauster et al.^[23] and Slukvin et al.^[13] mentioned that the placental villi showed spaces consistent with villous edema in GDM women. The same was found by Gul et al.^[1] on diabetic rat placentas. Gheorman et al.^[8] attributed the villous edema to the mucopolysaccharide deposits that consisted mainly of hyaluronic acid molecules that can retain water. This edema fluid is interposed as a barrier to the exchange between the mother and fetus.^[1]

Also, the present study showed dilatation of the endoplasmic reticulum in the cytoplasm of the vascular

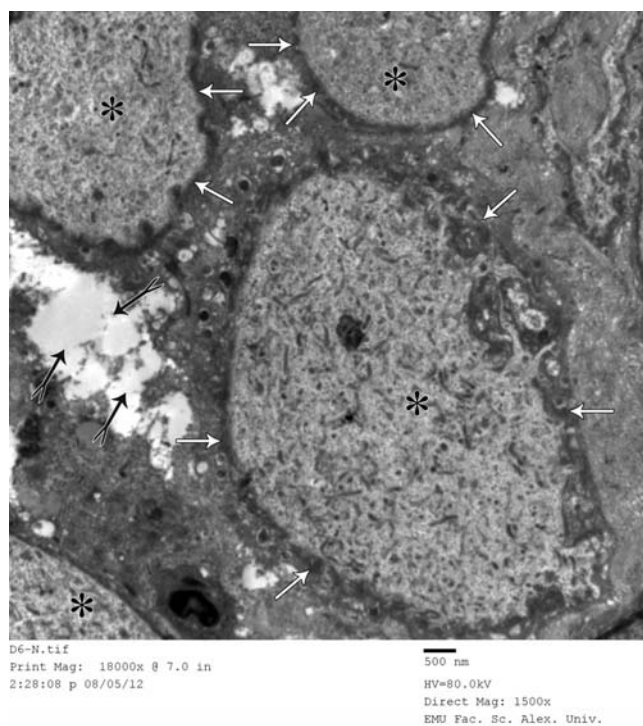


Figure 13. Electron micrograph of the core of terminal chorionic villous of a diabetic woman showing the detailed structure of the storage areas (*) of these areas are well-circumscribed by micro-capsules (arrows) of coarse matrix fibers and enclose scattered dense short fibrillar and granular content on a homogenous background of moderate electron density. Notice, edematous clear spaces (forked arrows). Magnification $\times 1500$, Scale bar = 500 nm

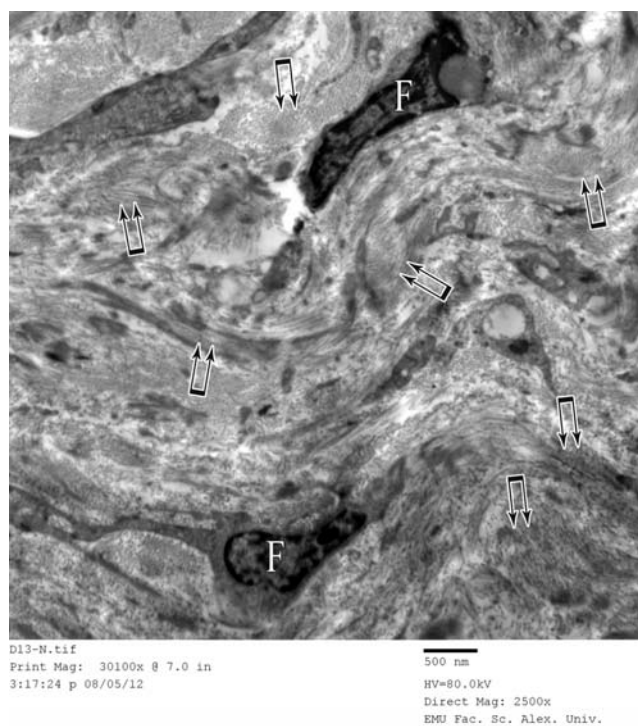


Figure 14. Electron micrograph revealing fibrosis inside a chorionic villus core of a diabetic woman; fibroblasts (F) and collagenous bundles (double arrows) are exceptionally prevalent. Magnification $\times 2500$, Scale bar = 500 nm.

endothelial cells. Same findings were observed by Meng et al.^[2] and Gul et al.^[1] on diabetic rats. rER is one of the most vulnerable organelles susceptible to hyperglycemia and hypoxia.^[12] Massively dilated rER, however, is an ultrastructural indication of improper processing associated with a disorder that prevents proper folding and extrusion of protein products, and this was attributed to oxidative stress induced cell injury in diabetes.^[1,24] The abnormal ultrastructure of rER could have impacts on metabolic functions and synthesis in the placenta.^[2]

Also, the present study showed areas of glycogen storage inside the trophoblast and villous core. Gheorman et al.^[8] showed the presence of glycogen storage areas in placentas of diabetic mothers. Gul et al.,^[1] Yoruk et al.^[25] and Padmanabhan and Shafiullah^[26] found increased glycogen content in the placental villi in diabetic rats. This glycogen deposition around the villous capillaries was related to the extent of maternal hyperglycemia that caused increased insulin levels in the fetal circulation. Fetal hyperinsulinemia stimulates what is called the buffer action of the placenta by stimulating

endothelial glucose uptake and glycogen synthesis.^[7] Placenta is glucose dependent and the only fetal tissue that can store excess glucose. Moreover, glucose itself activates glycogen synthase and deactivates glycogen phosphorylase that destroys glycogen.^[1,25] Also, the high affinity glucose transporter 3 (GLUT3) is expressed in the placental endothelium, where it co-localizes with glycogenin, the protein precursor for glycogen synthesis.^[1] These areas filled with glycogen may disrupt blood flow and placental exchange by increasing the transfer distance from the maternal blood.^[1]

Fibroblasts and fibrin deposition were found in the villous core in GDM women in the current study. Gheorman et al.,^[8] Gauster et al.^[23] and Mayhew and Sampson^[15] found greater deposition of fibrin in the placenta of diabetic women. The same was described by Meng et al.^[2] and Shams et al.^[27] The interruption of blood supply to the placenta causes placental infarcts and fibrosis. Small placental infarcts with minimal fibrosis are considered to be normal at term. However, large placental infarcts and marked fibrosis are associated with

vascular abnormalities as in GDM. Fibrin deposits may reflect changes in the nature of the villi and this might affect transport of oxygen and nutrients to the fetus.^[15,27]

The current study revealed the presence of perivillous fibrinoid degeneration in GDM placentas. This was also shown in earlier studies by Jarmuzek et al.^[28] and Gabbay-Benziv and Baschat.^[29] This fibrinoid degeneration as a special form of necrosis was attributed to the deposition of molecules derived from the hypoxic degenerative processes or blood clotting, or complexes of antigens and antibodies of hypersensitivity reactions together with fibrin that leaked outside the vessels giving the characteristic pink appearance. The fibrinoid may replace the degenerative Sy at the maternofetal exchange surfaces, thus acting as a kind of substitute barrier. Moreover, it is used to adapt the intervillous space to optimized flow conditions to counteract intervillous stasis or turbulence of maternal blood.^[28,30] Moreover, the present study showed stromal macrophages outside the villous capillaries. Guo et al.^[31] showed that these stromal macrophages represented the stromal vascular fraction that was stated in many regeneration processes and diabetes-related complications. Stromal vascular fraction was suggested to achieve healing and regeneration by angiogenesis and extracellular matrix secretion.^[31]

Conclusion

This study showed that hyperglycemia and hypoxia are two key factors in the pathophysiologic process of GDM complications, and that it is hyperglycemia that induces hypoxia and oxidative stress in the placenta. Also, the thickened placental barrier, edematous spaces, fibrin deposition and trophoblastic vacuoles in GDM potentially reduce transplacental transport and exchange with aggravation of ischemia and hypoxia.

References

- Gül M, Bayat N, Çetin A, Kepekçi RA, Şimşek Y, Kayhan B, Turhan U, Otlu A. Histopathological, ultrastructural and apoptotic changes in diabetic rat placenta. *Balkan Med J* 2015;32:296–302.
- Meng Q, Shao L, Luo L, Mu Y, Xu W, Gao C, Gao L, Liu J, Cui Y. Ultrastructure of placenta of gravidas with gestational diabetes mellitus. *Obstet Gynecol Int* 2015;2015:283124.
- Aires MB, Dos Santos AC. Effects of maternal diabetes on trophoblast cells. *World J Diabetes* 2015;6:338–44.
- Castellucci M, Kaufmann P. Basic structure of the villous trees. In: Benirschke K, Kaufmann P, Baergen RN, editors. *Pathology of the human placenta*. 5th ed. New York (NY): Springer; 2006. p. 50–120.
- American Diabetes Association. Standards of medical care in diabetes-2011. *Diabetes Care* 2011;34:S11–61.
- Zhang F, Dong L, Zhang CP, Li B, Wen J, Gao W, Sun S, Lv F, Tian H, Tuomilehto J, Qi L, Zhang CL, Yu Z, Yang X, Hu G. Increasing prevalence of gestational diabetes mellitus in Chinese women from 1999 to 2008. *Diabet Med* 2011;28:652–7.
- Desoye G, Hauguel-de Mouzon S. The human placenta in gestational diabetes mellitus. The insulin and cytokine network. *Diabetes Care* 2007;30 Suppl 2:S120–6.
- Gheorman L, Pleşea IE, Gheorman V. Histopathological considerations of placenta in pregnancy with diabetes. *Rom J Morphol Embryol* 2012;53:329–36.
- Hayat MA. Principles and techniques of electron microscopy: biological applications. 3rd ed. New York (NY): CRC Press; 1989. p. 24–74.
- Gude NM, Roberts CT, Kalionis B, King RG. Growth and function of the normal human placenta. *Thromb Res* 2004;114:397–407.
- Lemasters JJ, Theruvath TP, Zhong Z, Nieminen AL. Mitochondrial calcium and the permeability transition in cell death. *Biochim Biophys Acta* 2009;1787:1395–401.
- Pagliarini DJ, Calvo SE, Chang B, Sheth SA, Vafai SB, Ong SE, Walford GA, Sugiana C, Boneh A, Chen WK, Hill DE, Vidal M, Evans JG, Thorburn DR, Carr SA, Mootha VK. A mitochondrial protein compendium elucidates complex I disease biology. *Cell* 2008;134:112–23.
- Slukvin II, Salamat MS, Chandra S. Morphologic studies of the placenta and autopsy findings in neonatal-onset glutaric acidemia type II. *Pediatr Dev Pathol* 2002;5:315–21.
- Zorn TM, Zuniga M, Madrid E, Tostes R, Fortes Z, Giachini F, San Martín S. Maternal diabetes affects cell proliferation in developing rat placenta. *Histol Histopathol* 2011;26:1049–56.
- Mayhew TM, Sampson C. Maternal diabetes mellitus is associated with altered deposition of fibrin-type fibrinoid at the villous surface in term placentae. *Placenta* 2003;24:524–31.
- Joshi M, Kotha SR, Malireddy S, Selvaraju V, Satoskar AR, Palesty A, McFadden DW, Parinandi NL, Maulik N. Conundrum of pathogenesis of diabetic cardiomyopathy: role of vascular endothelial dysfunction, reactive oxygen species, and mitochondria. *Mol Cell Biochem* 2014;386:233–49.
- Frohlich JD, Huppertz B, Abuja PM, König J, Desoye G. Oxygen modulates the response of first-trimester trophoblasts to hyperglycemia. *Am J Pathol* 2012;180:153–64.
- Jauniaux E, Burton GJ. The role of oxidative stress in placental-related diseases of pregnancy. *J Gynecol Obstet Biol Reprod (Paris)* 2016;45:775–85.
- Magee TR, Ross MG, Wedekind L, Desai M, Kjos S, Belkacemi L. Gestational diabetes mellitus alters apoptotic and inflammatory gene expression of trophoblasts from human term placenta. *J Diabetes Complications* 2014;28:448–59.
- Kobayashi S. Choose delicately, reuse adequately: the newly recycled process of autophagy. *Biol Pharm Bull* 2015;38:1098–103.
- Curtis S, Jones CJ, Garrod A, Hulme CH, Heazell AE. Identification of autophagic vacuoles and regulators of autophagy in villous trophoblast from normal term pregnancies and in fetal growth restriction. *J Matern Fetal Neonatal Med* 2013;26:339–46.
- Holmes VA, Young IS, Patterson CC, Pearson DW, Walker JD, Maresh MJ, McCance DR. Optimal glycemic control, pre-eclampsia, and gestational hypertension in women with type 1 diabetes in the diabetes and pre-eclampsia intervention trial. *Diabetes Care* 2011;34:1683–8.
- Gauster M, Desoye G, Tötsch M, Hiden U. The placenta and gestational diabetes mellitus. *Curr Diab Rep* 2012;12:16–23.

24. Shapiro F, Mulhern H, Weis MA, Eyre D. Rough endoplasmic reticulum abnormalities in a patient with spondyloepimetaphyseal dysplasia with scoliosis, joint laxity and finger deformities. *Ultrastruct Pathol* 2006;30:393–400.
25. Yoruk M, Kanter M, Meral I, Agaoglu Z. Localization of glycogen in the placenta and fetal and maternal livers of cadmium-exposed diabetic pregnant rats. *Biol Trace Elem Res* 2003;96:217–26.
26. Padmanabhan R, Shafiullah M. Intrauterine growth retardation in experimental diabetes: possible role of the placenta. *Arch Physiol Biochem* 2001;109:260–71.
27. Shams F, Rafique M, Samoo NA, Irfan R. Fibrinoid necrosis and hyalinization observed in normal, diabetic and hypertensive placentae. *J Coll Physicians Surg Pak* 2012;22:769–72.
28. Jarmuzek P, Wielgos M, Bomba-Opon D. Placental pathologic changes in gestational diabetes mellitus. *Neuro Endocrinol Lett* 2015;36:101–5.
29. Gabbay-Benziv R, Baschat AA. Gestational diabetes as one of the “great obstetrical syndromes” – the maternal, placental, and fetal dialog. *Best Pract Res Clin Obstet Gynaecol* 2015;29:150–5.
30. Augustine G, Pulikkathodi M, Renjith S, Jithesh TK. A study of placental histological changes in gestational diabetes mellitus on account of fetal hypoxia. *Int J Med Sci Public Health* 2016;5:2457–60.
31. Guo J, Nguyen A, Banyard DA, Fadavi D, Toronto JD, Wirth GA, Paydar KZ, Evans GR, Widgerow AD. Stromal vascular fraction: a regenerative reality? Part 2: mechanism of regenerative action. *J Plast Reconstr Aesthet Surg* 2016;69:180–8.

Online available at:
www.anatomy.org.tr
 doi:10.2399/ana.16.019
 QR code:



deomed®

Correspondence to: Abdelghany Hassan, MD
 Department of Anatomy and Embryology, Faculty of Medicine,
 Alexandria University, Alexandria, Egypt
 Phone: +201 115 509 509
 e-mail: abdelghanyha@yahoo.com

Conflict of interest statement: No conflicts declared.

This is an open access article distributed under the terms of the Creative Commons Attribution-NonCommercial-NoDerivs 3.0 Unported (CC BY-NC-ND3.0) Licence (<http://creativecommons.org/licenses/by-nc-nd/3.0/>) which permits unrestricted noncommercial use, distribution, and reproduction in any medium, provided the original work is properly cited. *Please cite this article as:* Hassan A, Essa TM. Ultrastructure of the placenta in gestational diabetes mellitus. *Anatomy* 2016;10(3):159–169.

Moringa protects against nicotine-induced morphological and oxidative damage in the frontal cortex of Wistar rats

Ismail Temitayo Gbadamosi, Gabriel Olaiya Omotoso, Olayemi Joseph Olajide, Shakirat Opeyemi Dada-Habeeb, Tolulope Timothy Arogundade, Ezra Lambe, Kosisochukwu Kingsley Obasi

Department of Anatomy, Faculty of Basic Medical Sciences, College of Health Sciences, University of Ilorin, Ilorin, Kwara State, Nigeria

Abstract

The use of nicotine-containing substances has been implicated in oxidative-induced neuronal damage in several neurological dysfunctions. This study assessed the antioxidant potentials of Moringa tea on the frontal cortex of Wistar rats. Twenty female Wistar rats were divided into 4 groups of 5 animals each. Group A (control) received normal saline, Group B received 5.71 mg/kg of Moringa tea, Group C was treated with 13.76 mg/kg nicotine, while Group D received 5.71 mg/kg of Moringa tea and 13.76 mg/kg nicotine, for 21 days. Homogenate of excised frontal cortex of rats obtained on day 22 was used to assess the level of malondialdehyde, catalase, superoxide dismutase and glutathione peroxidase. Histological sections were stained with hematoxylin and eosin. Results showed increased activities of malondialdehyde and catalase in group C and a slight increase in group D compared with the control, while the activity of superoxide dismutase and glutathione peroxidase was reduced. The histological sections showed a normal architecture of the frontal cortex of rats treated with Moringa tea, but disrupted morphology in the group treated with Moringa tea and nicotine and further distortion in those that received nicotine only, when compared with the control group. These results suggest that Moringa tea may reduce the oxidative stress associated with nicotine consumption and limit the extent of structural damage in the frontal cortex of Wistar rats.

Keywords: frontal cortex; Moringa tea; nicotine; oxidative damage

Anatomy 2016;10(3):170–176 ©2016 Turkish Society of Anatomy and Clinical Anatomy (TSACA)

Introduction

Nicotine is one of the principal components of tobacco; other constituents include many toxins and carcinogens such as tar, polycyclic aromatic hydrocarbon, heavy metals, carbon monoxide, arsenic and hydrogen cyanide that are linked to various diseases in the body.^[1,2] The commonest source of nicotine is through cigarette smoking - the practice of burning tobacco and inhaling the smoke.^[3] Nicotine replacement therapy (NRT) is used to decrease withdrawal symptoms triggered by smoking cessation in individuals who want to quit smoking and thus avoid the harmful effects of smoking and chewing tobacco.^[4] Underlying the supposed connection between nicotine and cognitive enhancement is the role of nicotinic acetylcholine receptors (nAChRs) in attention, learning, mem-

ory, and cortical plasticity.^[5] nAChRs normally bind endogenous neurotransmitter acetylcholine, but are also particularly responsive to nicotine. They are abundant in brain regions associated with learning and memory, including the frontal cortex,^[6] and in primate and rodent models, depletion of acetylcholine in the prefrontal cortex results in impaired attentional performance.^[5] Nicotine replacement products are most beneficial for heavy smokers who smoke more than 15 cigarettes per day. There are not adequate studies to show that NRT helps those who smoke fewer than 10 cigarettes per day.^[7]

Moringa oleifera commonly known as drumstick or horseradish tree,^[8] is indigenous to the Northwestern part of India, but also widely distributed in the tropics, West Africa and Central America as well as the

Caribbean.^[9] Various parts of the tree have been used traditionally for the treatment of diabetes, rheumatism, hepatotoxicity, renal diseases and a variety of other diseases.^[9-11] Given its therapeutic advantages, Moringa leaves have been processed into tea bags for easy consumption. The aim of the present study was to determine the effect of Moringa tea on oxidative stress markers and histoarchitecture of the frontal cortex following nicotine administration.

Materials and Methods

A total of 20 adult female Wistar rats with an average weight of 185 ± 3.32 g were used for the study. Following the approval of the Ethics Committee of the University of Ilorin, the animals were housed in a wire gauzed cage in the animal house of the Faculty of Basic Medical Sciences at the University of Ilorin. The animals were allowed to acclimatize for two weeks prior to the commencement of the study.

The animals were divided into four groups (A–D) of five animals each. Group A was orally treated with 1ml of distilled water, Group B was treated with 5.71 mg/kg body weight of Moringa tea, Group C was treated with 13.76 mg/kg nicotine in 0.1 ml of vehicle once daily as the maximum tolerated dose in an earlier study,^[12] while Group D was treated with 5.71 mg/kg body weight of oral Moringa tea and 13.76 mg/kg nicotine i.p. once daily. All groups were treated for 21 consecutive days. *Moringa oleifera* leaves were obtained and identified at the Department of Plant Biology of the University of Ilorin, Kwara State, Nigeria. Following weeks of sundrying, an aqueous extraction of the dry *Moringa oleifera* leaves was made and concentrated. Rats were weighed at 7-day intervals, beginning from day one of administration.

24 h after the final administration of *Moringa oleifera*, animals for histology were euthanized using 20 mg/kg of ketamine i.p. and perfused transcardially with normal saline, followed by 4% paraformaldehyde (PFA). The brains were excised and post-fixed for 24 h in 4% PFA and processed manually for haematoxylin and eosin stain. Rats processed for enzymatic studies were sacrificed by cervical dislocation to eliminate the meddling of ketamine-induced change in biochemical status. The brains were excised following proper decapitation and dissection, and placed in 30% sucrose solution. The frontal cortices of the right and left lobes of each animal were obtained and then homogenized manually with 30% sucrose solution. Each homogenate was centrifuged at 3000 rpm for 10 min and the supernatant was extracted for further enzymatic analysis. Enzymatic studies were carried out using the enzyme linked immunosorbent assay.

The results obtained from enzymatic analysis were subjected to statistical analysis using the GraphPad Prism software, Version 6 (GraphPad Software Inc., San Diego, CA, USA). Malondialdehyde (MDA), glutathione peroxidase (GSH), catalase (CAT) and superoxide dismutase (SOD) results were plotted in one way ANOVA with Tukey's multiple comparisons test. Data obtained were presented as mean \pm standard error of mean, with determination of level of significance at p value less than 0.05. The outcomes were represented in bar charts with error bars to show the mean and standard error of mean, respectively.

Results

Body weight changes

The body weights of the animals were obtained on days 1, 7, 14 and 21. The animals in the nicotine group were observed to reduce the amount of daily food intake. Statistical analysis of the body weight of the animals revealed that the body weight of animals in the control group increased linearly over the period of treatment. There was an initial decrease in the body weight of animals treated with Moringa tea, but the weight gradually increased. Weight changes in the nicotine-treated group continuously decreased. Animals co-treated with nicotine and Moringa tea had reduced weight initially, followed by steady body weight over the period of administration (Figure 1).

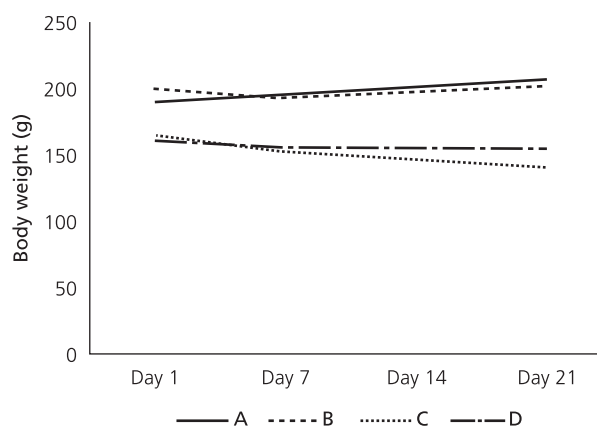


Figure 1. Linear graph showing changes in body weight over the period of administration. Line A: control (Group A); Line B: Moringa tea (Group B); Line C: nicotine (group C), and Line D: nicotine and Moringa tea (Group D). Group A showed a continuous linear increase in weight, while group B showed an initial subtle decrease and then a continuous increase in body weight. Group C had a continuous linear decrease in weight, but Group D showed mild decrease until day 7, and thereafter weight was fairly stable.

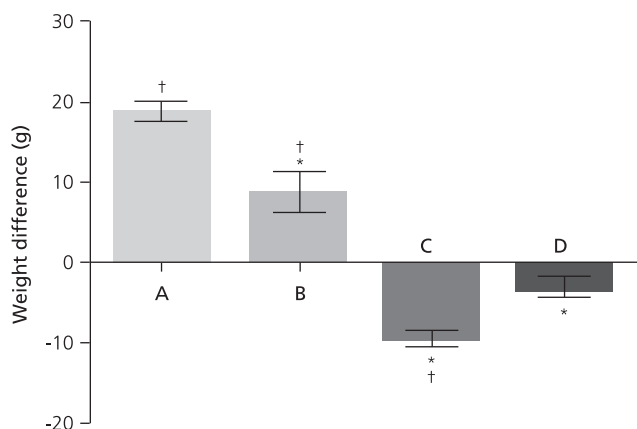


Figure 2. Changes in body weight. A: control; B: Moringa tea; C: nicotine and D: nicotine and Moringa tea. * $p < 0.05$ compared with the control; † $p < 0.05$ compared with Group D. Group B showed a significantly lesser weight gain, while Groups C and D showed significant weight loss when compared to A. C shows a significantly higher weight loss when compared to D.

Biochemical analysis

The biochemical data obtained in this study for each group which include MDA, GSH, CAT and SOD are shown in Figures 3-6. The results showed increased MDA and CAT activities in group C and a slight increase in group D compared to group A, while reverse was the case for SOD and GSH.

The histological sections of the frontal cortices of saline-treated and Moringa-treated animals showed a proper and normal cortical neuronal cells layout from the outermost molecular layer to the innermost multi-form layer. The nicotine-treated frontal cortices showed

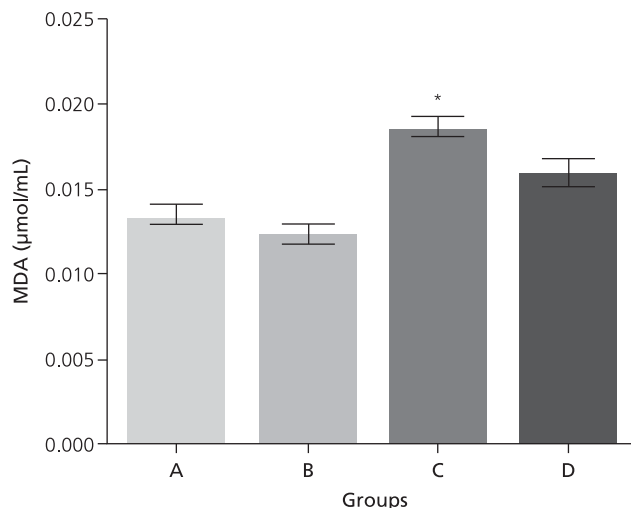


Figure 3. Graph showing the changes in the levels of MDA. **Figure 4.** Graph showing the changes in the levels of GSH. A: control; B: Moringa tea; C: nicotine and D: nicotine and Moringa tea. * $p < 0.05$ in comparison with the control group. Group B showed significant increase and Group C significant decrease, while there was no significant change in the MDA level in Group D.

a distorted cellular layout. The extent of distortion in the animals treated with combined Moringa and nicotine was limited when compared to the nicotine-treated animals. This may be attributed to the presence of Moringa tea, as well as the increase in lipid peroxidation marked by the raised levels of MDA in the nicotine-treated group. Nicotine increases the levels of free radicals in, precisely O_2^- which scavenges electrons from the lipids of the cell membrane of the neuronal cells.^[24-26] The increase in MDA levels was also indicated in (Figure 7)

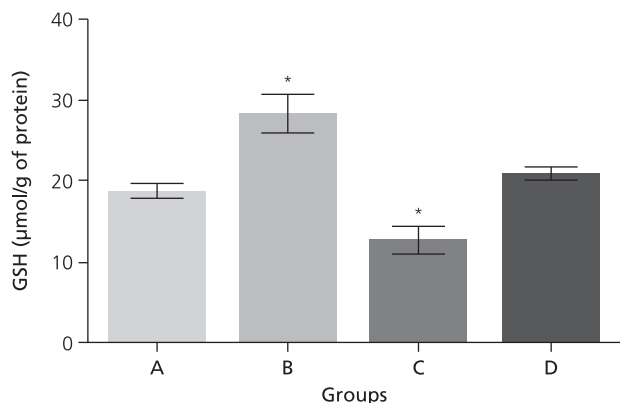


Figure 4. Graph showing the changes in the levels of GSH. A: control; B: Moringa tea; C: nicotine and D: nicotine and Moringa tea. * $p < 0.05$ in comparison with the control group. Group B showed significant increase and Group C significant decrease, while there was no significant change in the GSH level in Group D.

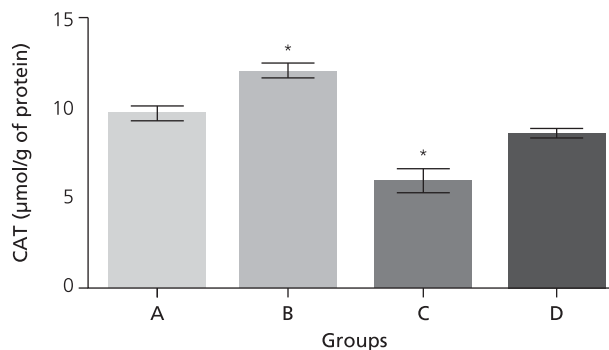


Figure 5. Graph showing the changes in the levels of CAT. A: control; B: Moringa tea; C: nicotine and D: nicotine and Moringa tea. * $p < 0.05$ in comparison with the control group. Group B showed significant increase and Group C significant decrease, while there was no significant change in the CAT level in Group D.

that showed intact cell membrane in A and B, but poor demarcation in C due to the degraded lipid bilayer of the neuronal and non-neuronal cell membranes. The conspicuous delineation in the frontal cortex of animals Group D can be attributed to the neuroprotective effects of Moringa to on the neuronal cells against the neurodegenerative tendencies of nicotine.

In the internal granular layer of dorsolateral frontal cortex of Wistar rats treated with normal saline and Moringa tea, nuclei of the neuronal and non-neuronal were eosinophilic and deeply-stained with small pyramidal cells characterized by apical and basal dendrites sparsely distributed among the dominating stellate (granule) cells (Figure 8a, b). In rats treated with nicotine, neurons were apoptotic with poorly stained nuclei (Figure 8c). Histology of Moringa tea treatment in nicotine rats showed an improvement with healthy granule cells and few in apoptotic stages (Figure 8d).

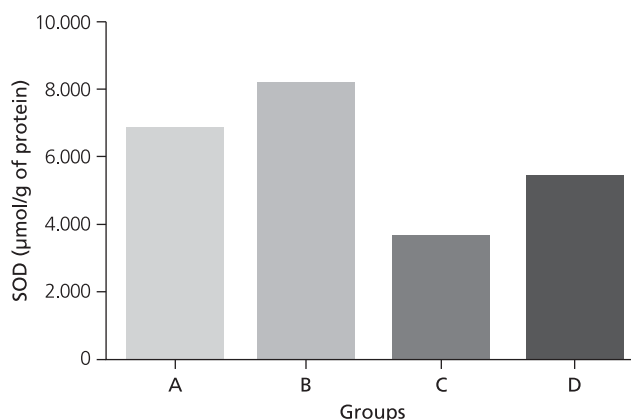


Figure 6. Graph showing the changes in the levels of SOD. A: control; B: Moringa tea; C: nicotine, and D: nicotine and Moringa. *p<0.05 in comparison with the control group. Group B showed significant increase and Group C significant decrease, while there was no significant change in the SOD level in Group D.

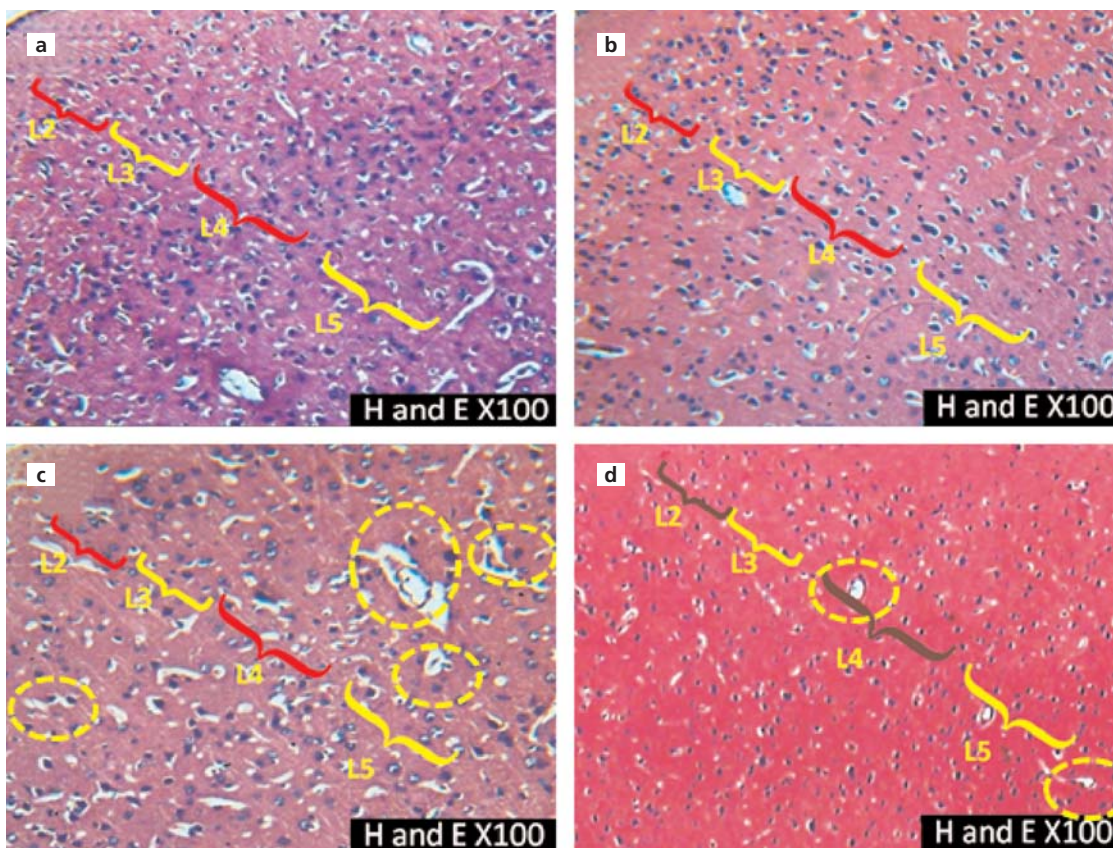


Figure 7. Photomicrographs showing the dorsolateral frontal cortex of Wistar rats treated with normal saline (a), Moringa tea (b), nicotine (c), and Moringa tea with nicotine (d). a (control) and b show normal cortical cell distribution, from the molecular layer (layer I) to the multiform layer (layer 6) with adequate and typical cellular density in the internal molecular and internal pyramidal layer (L3 and L4). c shows distorted cell distribution and poor cellular delineation more than found in d. Density and size of neurons were reduced in c and d in comparison to a and b. Perineural spaces and fragmented neuropils (yellow dotted circles) were noticeable in d. Neuronal cells were laconically expressed in d. Heamatoxylin and eosin stain x100. [Color figure can be viewed in the online issue, which is available at www.anatomy.org.tr]

Discussion

Nicotine is known to decrease insulin sensitivity^[13] and cause significant reduction in body weight of animals. There is a significant reduction in adipose tissue, particularly white fat masses, as fat deposits might be used as an energy supply under these conditions of negative energy balance.^[14] The pattern of change in body weight of animals in the control group showed a continuous linear increase over the period of administration. Animals in the Moringa-treated group showed an initial slight decrease in body weight after which there was a linear progression in the body weight. The nicotine-treated group experienced a continuous decrease in body weight over the period of administration. This pattern of continuous weight loss experienced by animals in the nicotine-treated group was reversed by the actions of

Moringa in the group treated synergistically with nicotine and Moringa.

Food intake in all the treated animals was reduced compared with the control animals, although Perkins et al.^[15] reported no difference in total caloric intake or micronutrient or taste selection in smokers and non-smoker. Also, the work of Winders and Grunberg^[16] reported that nicotine administration produced no comparable cumulative effect on growth rate even though he reported changes in food consumed and body weight. The findings in the present study corroborate some earlier works that substantial weight loss was detected in animals exposed to cigarette smoke, which was a factor of reduction in food intake.^[17-20]

Nicotine affects a variety of cellular processes ranging from secretion of hormones to modulation of enzy-

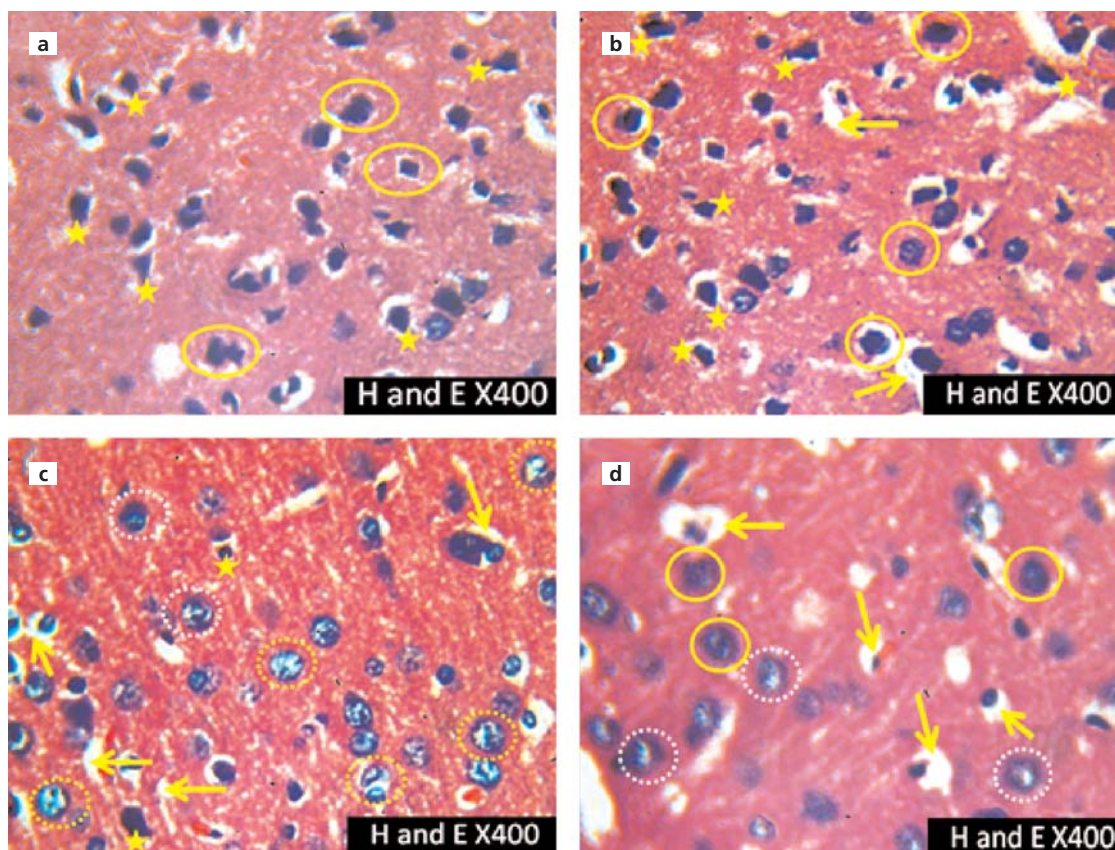


Figure 8. Photomicrographs of the internal granular layer of dorsolateral frontal cortex of Wistar rats treated with normal saline (a), Moringa tea (b), nicotine (c), and Moringa tea with nicotine (d). a and b show small pyramidal cells characterized by apical and basal dendrites (yellow stars) sparsely distributed among the dominating stellate (granule) cells (yellow circles) characterized by their several dendritic processes. Nuclei of the neuronal and non-neuronal cells found in a and b are adequately eosinophilic and deeply stained. Many of the granule cells in c are in their early apoptotic (white dotted circles) or late apoptotic (yellow dotted circles) stages characterized by their poorly stained nuclei. d is marked by healthy granule cell (yellow circles) and few granule cells in their early apoptotic stages (white dotted circles). c and d express perineural spaces (yellow arrows) which are predominant in c (Haematoxylin and eosin stain $\times 100$). [Color figure can be viewed in the online issue, which is available at www.anatomy.org.tr]

matic activities.^[8] MDA is a marker of lipid peroxidation, and in the present study, its levels increased significantly in the nicotine group as well as in the group treated concurrently with Moringa tea and nicotine, with animals given nicotine only having a higher level. Nicotine increases MDA levels in the vascular wall of rat offspring^[21] and maternal foetal brain tissues.^[8] The expression of NADPH oxidase increases following nicotine treatment, which is linked to an increase in O²⁻ production and oxidative damage of the vasculature as indicated by the increase in MDA levels.^[21]

A significant increase and decrease in the levels of catalase was observed in Moringa-treated and the nicotine-treated groups. However, the level of decrease was not significant in rats administered with both Moringa tea and nicotine. This observation was due to the counterbalancing actions of Moringa tea against that of the nicotine that was administered to animals in this group.

The level of GSH increased significantly in the group treated with Moringa tea unlike the nicotine-treated group which had a significant decrease. There was an increase in the level of GSH in the group that received the combined treatment of Moringa tea and nicotine, but the level of increase was not significant. The partial increase in the levels of GSH in the group given Moringa tea and nicotine compared to the decrease in nicotine-treated group could be attributed to the effect Moringa tea that was concomitantly administered to the former group.

A significant increase in the levels of SOD was observed in Moringa-treated animals compared with the nicotine-treated rats. The reduced level of SOD in animals that received the combination of Moringa tea and nicotine, though not significant, could be ascribed to the compensating actions of Moringa against nicotine. This observation is in agreement with previous report by Xia et al. (2011) that nicotine treatment significantly decreased the level of the antioxidant enzyme activities such as SOD.^[21]

In the current study, assessment of the level of MDA showed that treatment with Moringa tea counterbalanced the neurotoxic effect of nicotine. This can be related from **Figures 3–6** that showed a decrease in the level of MDA and increase in the levels of SOD, GSH and CAT in the group that was treated in tandem with Moringa tea and nicotine. The extremely defensive effects of *Moringa oleifera* against nicotine-induced neurotoxicity has been sustained by the findings of Gupta et al. who demonstrated its therapeutic efficacies.^[13] The present study is also in line with studies by Luqman et al.^[22] who reported that Moringa decreased lipid oxidation and increased antioxidant activity in mice. Faiza^[8] also suggested that the pro-

TECTIVE effects of *Moringa oleifera* extract on glutathione and MDA concentration may be attributed to the presence of phytoconstituents that scavenge free radicals, activate the antioxidant enzymes and inhibit oxidases. *Moringa oleifera* may decrease oxidative stress by other mechanisms such as the decreased oxidative stress generation capacity through the mitochondrial or inflammatory mechanisms.^[23]

Conclusion

The use of Moringa tea may reduce the morphological alterations and oxidative damage associated with nicotine-induced neurotoxicity in the frontal cortex. This could offer clinical benefits in neurological dysfunctions associated with consumption of nicotine-containing substances.

References

1. Secretan B, Straif k, Baan R, Grosse Y, Ghissassi F, Buovard, V, Benbrahim-Tallaa L, Guha N, Freeman C, Galichet L, Coglian V. A review of human carcinogens – Part E: tobacco, areca nut, alcohol, coal smoke and salted fish. *Lancet Oncol* 2009;10:1033–4.
2. Zainul Z. Dark nights behind the white clouds – risks of tobacco smoking on human health besides the oral health and malignancy. *EXCLI J* 2011;10:69–85.
3. Gately I. Tobacco: a cultural history of how an exotic plant seduced civilization. New York (NY): Grove; 2001. p. 3–7.
4. Stead LF, Perera R, Bullen C, Mant D, Hartmann-Boyce J, Cahill K, Lancaster T. Nicotine replacement therapy for smoking cessation. *Cochrane Database Syst Rev* 2012;11:CD000146.
5. Wallace TL, Bertrand D. Importance of the nicotinic acetylcholine receptor system in the prefrontal cortex. *Biochem Pharmacol* 2013;85:1713–20.
6. Poorthuis RB, Goriounova NA, Couey JJ, Mansvelder HD. Nicotinic actions on neuronal networks for cognition: general principles and long-term consequences. *Biochem Pharmacol* 2009;78:668–76.
7. Rigotti NA. Clinical practice. Treatment of tobacco use and dependence. *N Engl J Med* 2002;346:506–12.
8. Faiza A. Effect of Moringa oleifera extract on nicotine induced neurotoxicity in female rat and their embryos. *Global Veterinaria* 2013; 11:131–8.
9. Jaiswal D, Kumar PR, Kumar A, Mehta S, Watal G. Effect of Moringa oleifera Lam. leaves aqueous extract therapy on hyperglycemic rats. *J Ethnopharmacol* 2009;123:392–6.
10. Babu R, Chaudhuri M. Home water treatment by direct filtration with natural coagulant. *J Water Health* 2005;3:27–30.
11. Verma AR, Vijayakumar M, Mathela CS, Rao CV. In vitro and in vivo antioxidant properties of different fractions of Moringa oleifera leaves. *Food Chem Toxicol* 2009;47:2196–201.
12. Gabriel OO, Mercy OA, Abayomi AA, Josephine OI, Olalekan AO, Bernard UE. Neurohistochemical studies of adolescent rats' prefrontal cortex exposed to prenatal nicotine. *Ibnosina Journal of Medicine and Biomedical Sciences* 2014;6:1.

13. Gupta R, Kannan GM, Sharma M, S Flora SJ. Therapeutic effects of *Moringa oleifera* on arsenic-induced toxicity in rats. *Environ Toxicol Pharmacol* 2005;20:456–64.
14. Chen H, Vlahos R, Bozinovski S, Jones J, Anderson GP, Morris MJ. Effect of short-term cigarette smoke exposure on body weight, appetite and brain Neuropeptide Y in mice. *Neuropsychopharmacology* 2005; 30:713–9.
15. Perkins KA, Sexton JE, DiMarco A, Fonte C. Acute effects of tobacco smoking on hunger and eating in male and female smokers. *Appetite* 1994;22:149–58.
16. Winders SE, Grunberg NE. Effects of nicotine on body weight, food consumption and body composition in male rats. *Life Sci* 1990;46: 1523–30.
17. Albanes D, Jones DY, Micozzi MS, Mattson ME. Association between smoking and body weight in the US population: analysis of NHANES II. *Am J Public Health* 1987;77:439–44.
18. Bellinger L, Cepeda-Benito A, Wellman PJ. Meal patterns in male rats during and after intermittent nicotine administration. *Pharmacol Biochem Behav* 2003;74:495–504.
19. Bishop C, Parker GC, Coscina, DV. Systemic nicotine alters whole-body fat utilization in female rats. *Physiol Behav* 2004;80:563–7.
20. Omotoso GO, Babalola FA. Histological changes in the cerebelli of adult wistar rats exposed to cigarette smoke. *Niger J Physiol Sci* 2014;29:43–6.
21. Xiao D, Huang X, Yang S, Zhang L. Antenatal nicotine induces heightened oxidative stress and vascular dysfunction in rat offspring. *Br J Pharmacol* 2011;164:1400–9.
22. Luqman S, Srivastava S, Kumar R, Maurya AK, Chanda D. Experimental assessment of *Moringa oleifera* leaf and fruit for its anti-stress, antioxidant and scavenging potential using in vitro and in vivo assays. *Evid Based Complement Alternat Med* 2012;2012:519084.
23. Kirisattayakul W, Wattanathorn J, Tong-Un T, Muchimapura S, Wannanon P, Jittiwat J. Cerebroprotective effect of *Moringa oleifera* against focal ischemic stroke induced by middle cerebral artery occlusion. *Oxid Med Cell Longev* 2013;2013:951415.
24. Marnett LJ. Lipid peroxidation - DNA damage by malondialdehyde. *Mutat Res* 1999;424:83–95.
25. Zou XL, Chem JM. Serum SOD activity and lipid peroxidation. A handbook of hematology from Wuhan University. 6th ed. Wuhan: Wuhan University Press; 2005. p. 43–71.
26. Michel F, Bonnefont-Rousselot D, Mas E, Draï J, Thérond P. Biomarkers of lipid peroxidation: analytical aspects. *Ann Biol Clin (Paris)* 2008; 66:605–20.

Online available at:
www.anatomy.org.tr
 doi:10.2399/ana.16.020
 QR code:



deomed®

Correspondence to: Ismail Temitayo Gbadamosi

Department of Anatomy, Faculty of Basic Medical Sciences, College of Health Sciences, University of Ilorin, Ilorin, Kwara State, Nigeria

Phone: +234 806 903 1960

e-mail: ismail.tayo@yahoo.com

Conflict of interest statement: No conflicts declared.

This is an open access article distributed under the terms of the Creative Commons Attribution-NonCommercial-NoDerivs 3.0 Unported (CC BY-NC-ND3.0) Licence (<http://creativecommons.org/licenses/by-nc-nd/3.0/>) which permits unrestricted noncommercial use, distribution, and reproduction in any medium, provided the original work is properly cited. *Please cite this article as:* Gbadamosi IT, Omotoso GO, Olajide OJ, Dada-Habeeb SO, Arogundade TT, Lambe E, Obasi KK. *Moringa* protects against nicotine-induced morphological and oxidative damage in the frontal cortex of Wistar rats. *Anatomy* 2016;10(3):170–176.

Reporting detailed information and acknowledging donor-cadavers: good practice recommendation for anatomists

İlke Ali Gürses, Esranur Korkmaz, Adnan Öztürk

Department of Anatomy, Istanbul Faculty of Medicine, Istanbul University, Istanbul, Turkey

Abstract

Objectives: In order to facilitate a healthy and trusting relationship between anatomists and their society, appreciating the anatomical gift of the individuals that donated their bodies to science in every way possible remains central. Apart from memorial services and monuments, scientific articles themselves can be a good platform to show this appreciation. In this article, we aimed to create awareness among anatomists and researchers by evaluating the information given regarding donor-cadavers in their articles and see if they acknowledged them.

Methods: We evaluated all articles that used human cadaveric specimens by Turkish anatomists published between January 2011 and April 2016 and assessed if researchers provided data on the age, gender, preservation technique(s), source, and ethical / legal permissions regarding the cadavers used.

Results: Majority of the articles provided data about gender (74.5%) and age (68.9%). Preservation technique (56.6%) and source of specimens (50.5%) were reported less frequently. While 28.3% of the articles provided data on some form of ethical approval, only 11.8% of the articles provided data on the consent of the individuals. Ten (4.7%) articles acknowledged the cadavers and/or their families.

Conclusion: We believe it is the duty of anatomists to promote body donation within their society by building a trustworthy relationship. Scientific articles that depend on donor-cadavers should also be used to promote this relationship. Therefore, awareness among anatomists should be raised to discuss ethical grounds for scientific research on cadavers.

Keywords: anatomy; cadaver; guideline, medical ethics; research

Anatomy 2016;10(3):177–181 ©2016 Turkish Society of Anatomy and Clinical Anatomy (TSACA)

Introduction

Cadavers are essential for medical education and research.^[1,2] Despite their importance, dissection courses sometimes traumatize the students and result in materialization of the cadavers to form a level of detachment.^[3,4] Additionally, majority of scientific journals use the term “material(s)” to define the cadavers and forget that they were once individuals.^[5] It is important for the anatomists and related researchers to form a healthy and trustworthy relationship with the society which is the source of their specimens for future research and continuous medical education. There are a few options available for maintaining this relationship; reflection practices and commemoration services,^[6,7] recorded donor interviews,^[8] de-anonymization of donor-cadavers,^[9] and donor monuments^[10] are good opportunities for future doctors to emphasize with the

donor-cadavers and their relatives. These practices create a reciprocal appreciation between the anatomists and the community they live in. Another supportive way expressing appreciation is the actual work that depends on the gifts of donor-cadavers *i.e.* the scientific articles. Providing detailed information regarding the donor-cadavers including demographics, preservation methods, source of specimens, formal approvals, and donors’ consent in articles is not only important for the repeatability of the work, but also essential to emphasize that human cadavers are treated with respect and dignity just like a living person rather than freely accessible materials with limited rights bestowed by whomever claims them.

A few recent studies have evaluated the amount of information provided in articles published in orthopaedics and anatomy journals in order to create an awareness

among scientific community.^[5,11] These studies showed that there was not a standard way of reporting information and some information (source, formal approval, and consent) were mostly neglected by researchers.

In this study, we aimed to investigate the amount of information provided in the articles authored or co-authored by Turkish anatomists that used human cadaveric specimens. We also aimed to see how common do anatomists acknowledge the gift of their donor-cadavers and/or their families. Lastly, we aimed to create an awareness regarding the value of donor-cadavers among Turkish researchers who use human cadaveric materials in their studies.

Materials and Methods

We performed an electronic search on Google Scholar^[12] to find all articles that were authored or co-authored by Turkish anatomists from medical and dental schools. The time filter was set between January 2011 and April 2016. We evaluated articles published in international journals indexed and not indexed in Science Citation Index and Science Citation Index-Expanded. Articles published in national journals indexed in TÜBİTAK ULAKBİM database were also included. We included articles that used tissues, organs, and bodies of deceased individuals, infants, and fetuses with different gestational stages. Review articles, educational studies that did not use cadaveric specimens, surgical and radiologic studies performed on patients, studies performed on surgical excision specimens, and pre-existing osteological collections were excluded from the study. For avoiding iteration, we cross-checked authors and titles of every article and excluded repeating studies. Articles that were published online, but not printed as of April 2016 were also excluded.

First, the demographic (age and gender) and technical (preservation) data provided in the articles regarding the donor-cadavers were evaluated. We accepted the source of specimens as any institution that provided the specimens. The terms that implied consent of the donor-cadavers including “written consent”, “donor”, “donation”, “donated”, “bequest”, “bequeath”, and “bequeathal” were evaluated, and if any information was provided about the ethical or formal approval for the study, this was noted. Finally, we determined if the authors acknowledged the donor-cadavers and/or their families as proposed previously.^[13]

Results

Table 1 summarizes our results and comparison with previous studies. We evaluated 375 authors from 85 institutions. Two hundred and twelve articles met our inclusion criteria. The majority of articles (158, 74.5%) provided information regarding gender. Ninety-nine (46.7%) articles provided the age of the specimens as mean and 47 (22.2%) articles as range.

We found that 120 (56.6%) articles provided information about the preservation technique. Only 5 articles mentioned more than one method. The techniques used included embalming with a specific method in 96 (45.3%), embalming with an unspecified method in 9 (4.2%), fresh in 12 (5.6%), fresh-frozen in 7 (3.3%), and plastination in 1 (0.5%) articles.

Only 107 (50.5%) articles reported the source of the specimens. Two articles reported more than one source for the specimens used. The source of the specimens was anatomy departments in 97 (45.7%), the Forensic Institution of the Ministry of Justice in 10 (4.7%), and an institution in 2 (0.9%) articles.

Table 1
Information provided in articles authored by Turkish anatomists compared with previous studies.

	Present study		Gürses et al. ^[11]		Winkelmann et al. ^[5]	
	n	%	n	%	n	%
Total number of articles investigated	212	100	586	100	345	100
Number of articles reporting information regarding						
Age	146	68.9	405	69.1	260	75
Gender	158	74.5	425	72.5	196	57
Preservation method	120	56.6	426	72.7	295	86
Source of specimens	107	50.5	319	54.4	78	23
Consent	25	11.8	154	26.3	139	40
Formal approval	60	28.3	190	32.4	58	17
Acknowledgment for donors / family	10	4.7	104	17.7	2	0.6

Some form of ethical approval was reported in 60 (28.8%) articles. In 51 (24%) articles institutional review board was obtained, 8 (3.8%) articles complied with institutional guidelines, and 1 (0.5%) article conformed state legislations. Among the 51 studies that obtained ethical approval, 30 were performed on fetal and 21 on adult cadavers. Studies that obtained Institutional Review Board for Protection of Human Subjects (IRB) approval were performed in 18 different institutions.

We found that 25 (11.8%) articles mentioned a degree of consent of the donor-cadavers. In 19 (9%) articles written consent was obtained and in 6 (2.8%) articles terms implying a donation was used. One hundred eighty seven (88.2%) articles did not provide information on the consent of the cadavers.

The authors acknowledged the donor-cadavers and their families in 10 (4.7%) articles. **Figure 1** shows the number of acknowledgements per year.

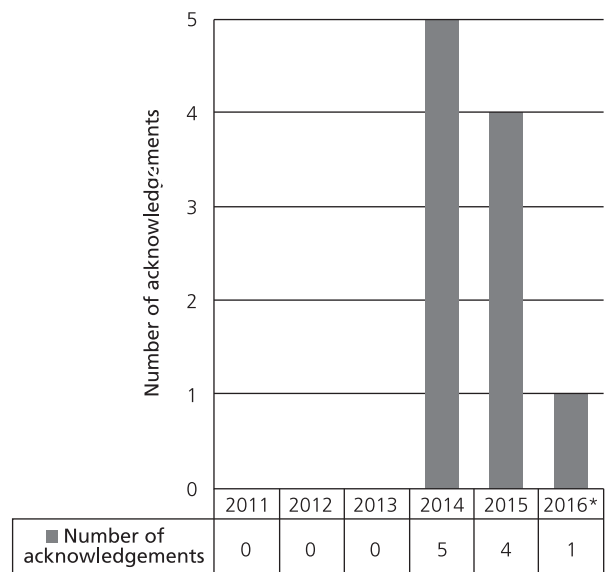
Discussion

We found that Turkish Anatomists were similar to their colleagues worldwide for reporting demographic information regarding cadaveric specimens (**Table 1**).^[5,11] Researchers from the field of orthopedics reported the age of the cadavers more often (75% vs. 68.9% for Turkish anatomists and 69.1% for international anatomists). Anatomists, on the other hand, reported information on gender with a higher frequency (74.5% for Turkish anatomists and 72.5% for international anatomists vs. 57%) (**Table 1**). The reason(s) for not reporting demographics remains unclear. It is possible, either the researchers have omitted the information that they see irrelevant to the study at hand, or the information was not available. While the former is unacceptable, the latter is debatable. The unavailability of information may be due to the use of unclaimed cadavers or a legal limitation. For example in France, the Civil Code which regulates body donation also entails complete anonymity of the donors as well.^[14] Therefore, the information remains unavailable for most researchers. Nevertheless, reporting demographics of donor-cadavers in research articles is a must for scientific methodology and should be promoted whenever possible. If not, authors should mention the reasons for not reporting this information.

Articles from musculoskeletal researchers surprisingly reported their preservation method more often compared to anatomists (86% vs. 56.6% for Turkish anatomists and 73.2% for international anatomists).^[5,11] We found that nearly half of Turkish anatomists did not mention a preservation method as if they took this step of their research for granted. Although the reasons for this inade-

quacy is a topic for further research, reporting detailed methodology including embalming or preservation methods should be promoted by national associations and journal editors. It should be kept in mind that describing the steps of methodology is essential for comparing and repeating the study data. Therefore, skipping this step may be considered as inadequate reporting of study design and methodology.

Turkish anatomists reported the source of the specimens they used in a similar way with their international colleagues.^[11] Although it is important to report the source of specimens for maintaining a healthy relationship with their society, the authors may not have neglected this information intentionally. The authors may have chosen to remove this information in order to blind the manuscript for submission processes or to accord word count limits of the journals. Not reporting the source is a serious topic. This may give public the opinion that the specimens used are freely available, which is not the case in majority of the world. As suggested previously, the authors either take available cadavers for granted or just consider this unnecessary. A new reason behind this may be the foreign source of cadavers. Not-for-profit and for-profit companies are usual sources of cadavers in North American countries.^[2,5] Within the last couple of years, some European countries have started to import foreign cadavers with high costs. Bodies imported from the USA are used at private training centers in Italy.^[15] Similarly, a



*Note that acknowledgements for 2016 are from January to April.

Figure 1. Number of donor-cadaver acknowledgements by Turkish anatomists per year.

recent editing to the related Law (No: 2238) in 2014 allowed Turkish institutions to import cadavers from the USA and China.^[16-20] This practice has a few major problems. In Turkey, body donation is still a taboo and importing cadavers may end up alienating the society from the idea of body donation itself. Secondly, the consent of the imported cadavers remains uncertain. The companies do not provide that the consent of the donors included the transport and use of their bodies in foreign countries. Additionally, any profit based practice has a risk of labeling human bodies or body parts as disposable property.^[21] Nevertheless, it is important to report the source of cadaveric specimens to avoid giving a false impression that human cadaveric material is easy to acquire and use.

Nearly one third of Turkish anatomists provided some form of ethical approval for their studies. This rate is similar to the rate of international anatomical community.^[11] Applying and reporting ethical approval for studies performed on human cadaveric specimens is an ongoing debate. For example in Turkey, procurement of human bodies is governed with a legislation (No: 2238) and its related regulation.^[16,22] Although a legislation is present that regulates procurement of human bodies for education and research, our results show that practices regarding ethical approval for cadaveric studies remain uncertain in Turkey. We found that 51 studies have already obtained IRB approval for cadaveric studies. We also found that fetal cadaveric studies were more likely to apply for a formal ethical approval (n=30 vs. n=21). It is apparent that practices among institutional review boards within different institutions differ in Turkey. For example, both boards of two medical faculties at Istanbul University request IRB approval for studies performed on human cadavers and skeletons since January 2016. Same situation is present for The Scientific and Technological Research Council of Turkey (TÜBİTAK) and Bezmialem University.^[23,24] This dispute roots from the ethical status of cadavers which previously showed that it was not the same as living human beings under current legal and ethical framework.^[5,25] Despite this lack of framework, every cadaver (donated or not) deserves respect until the final disposition of the body.^[26,27] From this point of view, Winkelmann et al.^[5] argued that an IRB application would set the cadavers' status as of a living individual, thus making it possible for the society to perceive this as showing respect to the cadavers and reinforcing the notion of body donation.

Articles authored by Turkish anatomists were less likely to report the consent of cadavers compared to articles published in international anatomy and orthopaedic journals.^[5,11] It is not clear whether the authors choose not to provide this information or refrained from something else. Gürses et al.^[11] argued that researchers who used

unclaimed bodies may have hesitated in order to avoid unwanted ethical disputes during peer-review process of articles. Although most Western scientists consider using unclaimed bodies for medical research as dubious,^[28] this practice is still the major body procurement method for many countries where donation is infrequent or absent.^[15] In Turkey, despite the inception of a nation-wide donation campaign^[29] and a few news reports^[18,30] pointing out the dire situation, donations remain exceptional. One should hope this situation is transitional and body donation becomes the only way of body procurement gradually.

We found that 4.7% of the articles acknowledged their cadavers and their families starting from 2014. Although this rate is lower when compared to international anatomical community, it is still heart-warming to see researchers appreciating the contributions of donor-cadavers to their work. The cadavers used in research studies may not fulfill the requirements for authorship,^[31] but their contribution to the study should not go unnoticed as well. Acknowledging is a sincere way to honor any individual who contributed to a given study. Therefore, acknowledging donor-cadavers and their families in anatomical research articles is a healthy way of showing appreciation and also empowers the relationship of trust between the anatomists and the society that they depend on future research. Gürses et al.^[11] proposed that this method of appreciation should be promoted and remain voluntary as well.

There were a few limitations in our study. Firstly, we did not investigate if single-center studies reported the source or not. We also accepted first author's institution as the place of research. By doing so, we neglected multi-center studies and authors with more than one affiliation.

Conclusion

As proposed earlier,^[5] a standard order for reporting information regarding human cadaveric specimens needs to be established. This standard reporting should include the age, gender, preservation/research method(s), and the source of specimens without exception. It is important to report the information regarding consent, but using unclaimed bodies should not be set as an obstacle without considering the country of research and its cultural background for body donation. Since Turkish legislations do not provide a framework for ethical approval for cadaveric studies and institutional practices differ, it is up to the researchers to apply for institutional review board approval. Finally, without doubt, every anatomist and researcher who appreciates the contribution of their society by acknowledging cadavers (donor or not) and their families should be promoted.

References

- Dyer GSM, Thorndike EL. Quidne mortui vivos docent? The evolving purpose of human dissection in medical education. *Acad Med* 2000;75:969–70.
- Winkelmann A. Anatomical dissection as a teaching method in medical school: a review of the evidence. *Med Educ* 2007;41:15–22.
- Hildebrandt S. What is happening in our anatomical dissection rooms? *Clin Anat* 2014;27:833–4.
- Lemmp HK. Perceptions of dissection by students in one medical school: beyond learning about anatomy. A qualitative study. *Med Educ* 2005;39:318–25.
- Winkelmann A, Heinze AK, Hendrix S. Acknowledging tissue donation: human cadaveric specimens in musculoskeletal research. *Clin Anat* 2016;29:65–9.
- Jones TW, Lachman N, Pawlina W. Honoring our donors: a survey of memorial ceremonies in United States anatomy programs. *Anat Sci Educ* 2013;7:219–23.
- Subasinghe SK, Jones DG. Human body donation programs in Sri Lanka: Buddhist perspectives. *Anat Sci Educ* 2015;8:484–9.
- Bohl M, Holman A, Mueller DA, Gruppen LD, Hildebrandt S. The willed body donor interview project: medical student and donor expectations. *Anat Sci Educ* 2012;6:90–100.
- Talarico EF. A change in paradigm: giving back identity to donors in the anatomy laboratory. *Clin Anat* 2013;26:161–72.
- Bolt S. Bodies does matter: Gift giving and the unveiling of body donor monuments in the Netherlands. *Med Anthropol Q* 2012;26:613–34.
- Gürses İA, Coşkun O, Gürtekin B, Kale A. The amount of information provided in articles published in *Clinical Anatomy and Surgical and Radiologic Anatomy* regarding human cadaveric materials and trends in acknowledging donors/cadavers. *Surg Radiol Anat* 2016;8:1225–31.
- Google Scholar [database on the Internet]. Mountain View (CA): c2004 Google Inc; [cited 2016, Apr 20]. Available from: <http://www.scholar.google.com>
- Benninger B. Formally acknowledging donor-cadaver-patients in the basic and clinical science research arena. *Clin Anat* 2013;26:810–3.
- McHanwell S, Brenner E, Chirculescu ARM, Drukker J, van Mameren H, Mazzotti G, Pais D, Paulsen F, Plaisant O, Caillaud MM, Laforet E, Riederer BM, Sanudo JR, Bueno-Lopez JL, Donate-Oliver F, Sprumont P, Teofilovski-Parapid G, Moxham BJ. The legal and ethical framework governing body donation in Europe – A review of current practice and recommendations for good practice. *Eur J Anat* 2008;12:1–24.
- Riederer BM. Body donations today and tomorrow: what is best practice and why? *Clin Anat* 2016;29:11–8.
- Organ ve doku alınması, saklanması, aşılması ve nakli hakkında kanun. Kanun numarası: 2238. <http://www.mevzuat.gov.tr/MevzuatMetin/1.5.2238.pdf> Accessed 20 April 2016
- Sağlık Bakanlığı ve bağlı kuruluşların teşkilat ve görevleri hakkında kanun hükmünde kararname ile bazı kanunlarda değişiklik yapılmasına dair kanun. <http://www.resmigazete.gov.tr/eskiler/2014/01/20140118.pdf> Accessed 20 April 2016
- Çubukçu B. Kadavrasız anatomi dersi. *Al Jazeera Türk* 09 February 2016 <http://www.aljazeera.com.tr/al-jazeera-ozel/kadavrasiz-anatomidersi> Accessed 20 April 2016
- Hürriyet. Doktor adaylarına ithal kadavra. *Hürriyet Kelebek*. 23 January 2016 <http://www.hurriyet.com.tr/doktor-adaylarina-ithal-kadavra-40044207> Accessed 20 April 2016
- Sözcü. Çin'den kadavra ithal edeceğiz. *Sözcü Gazetesi*. 28 April 2015. <http://www.sozcu.com.tr/2015/gundem/cinden-kadavra-ithal-edecegiz-816673/> Accessed 20 April 2016
- Champney TH. The business of bodies: ethical perspectives on for-profit body donation companies. *Clin Anat* 2016;29:25–9
- İnsan cesedi üzerinde bilimsel araştırma yapılmasına ilişkin yönetmelik. <http://www.resmigazete.gov.tr/main.aspx?home=http://www.resmigazete.gov.tr/arsiv/17727.pdf&main=http://www.resmigazete.gov.tr/arsiv/17727.pdf> Accessed 20 April 2016
- TÜBİTAK. Etik kurul onay belgesi bilgi notu. Temmuz 2014. http://tubitak.gov.tr/sites/default/files/etik_onay_bilgi_notu_23_07_13.pdf Accessed 22 December 2016
- Bezmi Alem Vakıf Üniversitesi Sağlık Bilimleri Enstitüsü. Etik kurul yönlendirme seması. http://sbe.bezmi Alem.edu.tr/Documents/BVU_Etik_Kurul_Yonlendirme_Semasi-r.pdf Accessed 22 December 2016
- Champney TH. A proposal for a policy on the ethical care and use of cadavers and their tissues. *Anat Sci Educ* 2011;4:49–52.
- International Federation of Associations of Anatomists. (2012) Recommendations of good practice for the donation and study of human bodies and tissues for anatomical examination. *Plexus* January 2012;4-5. <http://ifaa.net/index.php/plexus/finish/3-plexus/3-plexus-2012/0> Accessed 20 April 2016
- Jones DG. Searching for good practice recommendations on body donation across diverse cultures. *Clin Anat* 2016;29:55–9.
- Jones DG, Whitaker MI. Anatomy's use of unclaimed bodies: Reasons against continued dependence on an ethically dubious practice. *Clin Anat* 2012;25:246–54.
- Turkish Society of Anatomy and Clinical Anatomy. Ulusal Anatomi Haftası Basın Bildirgesi 2012 <http://www.anatomidernegi.org.tr/kadavra-bagisi-ve-temini> Accessed 20 April 2016
- Erenoğlu C. Herkes onu konuşuyor! *HaberTürk Pazar* 02.09.2012 <http://www.haberturk.com/saglik/haber/772940-herkes-onu-konusuyor> Accessed 20 April 2016
- Defining the role of authors and contributions [homepage on the Internet]. Philadelphia: c2015 International Committee of Medical Journal Editors; [updated 2006 May 26; cited 2016 Apr 20]. Available from: <http://www.icmje.org>. Accessed 20 April 2016

Online available at:
www.anatomy.org.tr
 doi:10.2399/ana.16.032
 QR code:



deomed®

Correspondence to: Esranur Korkmaz, MD
 Department of Anatomy, Istanbul Faculty of Medicine,
 Istanbul University, Istanbul, Turkey
 Phone: +90 212 414 21 76
 e-mail: dresranurkorkmaz@gmail.com

Conflict of interest statement: No conflicts declared.

This is an open access article distributed under the terms of the Creative Commons Attribution-NonCommercial-NoDerivs 3.0 Unported (CC BY-NC-ND3.0) Licence (<http://creativecommons.org/licenses/by-nc-nd/3.0/>) which permits unrestricted noncommercial use, distribution, and reproduction in any medium, provided the original work is properly cited. *Please cite this article as:* Gürses İA, Korkmaz E, Öztürk A. Reporting detailed information and acknowledging donor-cadavers: good practice recommendation for anatomists. *Anatomy* 2016;10(3):177–181.

Reduction in *Wnt9b* and associated gene expression in the embryonic midface of *CL/Fr* mice with heritable cleft lip and palate

Brennan Takagi¹, Trudy Hong¹, Thomas E. Hynd¹, Keith S. K. Fong¹, Ben Fogelgren¹, Kazuaki Nonaka², Scott Lozanoff¹

¹Department of Anatomy, Biochemistry and Physiology, University of Hawaii John A. Burns School of Medicine, Honolulu, Hawaii, USA

²Section of Pediatric Dentistry, Faculty of Dentistry, Kyushu University, Fukuoka, Japan

Abstract

Objectives: The *CL/Fr* mouse displays cleft lip and palate (CLP) at a rate of 35%. The *clf1* mutation is associated with CLP in related "A" strain mice and affects the gene *Wnt9b*. The purpose of this study was to determine tissue specific expression of *Wnt9b* during facial prominence morphogenesis in *CL/Fr* mice and provide new details concerning gene variants associated with CLP.

Methods: Facial prominences from *CLP(-)* and *CLP(+)* *CL/Fr* and 3H1 wild-type (WT) mice at embryonic day 11.5 (E11.5) were collected for expression assays (DNA microarray analysis, qRT-PCR, immunostaining, and *in situ* hybridization). A modified Chi square test was used to analyze microarray data while a student t-test was used to statistically compare qRT-PCR values ($p < 0.05$).

Results: There was a partial and variable loss of *Wnt9b* in facial prominences of E11.5 CLP susceptible *CL/Fr* mice, with a greater loss associated with *CLP(+)*. Two genes in the *clf2* locus, *Adcy2* and *Ube2q11* also showed decreased expression. Two regulators of palatogenesis, *Runx2* and *Osr2* were significantly downregulated, while an inhibitor of cell proliferation, somatostatin (*Sst*), was elevated in *CLP(+)* relative to *CLP(-)* mice.

Conclusion: Results indicate a role for *Wnt9b* in the pathogenesis of CLP and supports previous reports concerning its involvement with CLP in "A" strain mice. Misexpression of *Sst* suggests that it may be a downstream target of *Wnt9b* causing reduced overall growth possibly hindering fusion of facial prominences and contributing to the development of CLP.

Keywords: cleft lip and palate; *CL/Fr* mice; craniofacial; *Wnt9b*

Anatomy 2016;10(3):182–192 ©2016 Turkish Society of Anatomy and Clinical Anatomy (TSACA)

Introduction

Orofacial clefts (cleft lip with or without cleft palate) are one of the most common birth defects. It occurs about 1 in 1000 live births in the United States, and over 7,000 new cases are expected annually with estimated life time treatment costs amounting to over \$697 million nationally.^[1,2] Orofacial malformations are debilitating since they can lead to difficulties in breathing, suckling, facial expression and speech in the child, and can also cause emotional hardships for the associated family. Both genetic and environmental factors contribute to these malformations and identifying the mechanisms involved

will help to provide information regarding prenatal screening methods and treatment therapies in humans.^[3]

The critical stage that is affected in CLP involves the formation of the upper lip and palate, which is normally completed when the laterally projecting maxillary prominences (MxP) and lateral nasal prominences (LNP), fuse with the medial nasal prominences (MNP). This process is regulated by complex genetic signaling pathways, and relies on precise timing of the outgrowth of the prominences, contact between epithelia of the prominences in the nasal fin region, and eventual disintegration of contiguous tissue borders to form the upper lip. This event typically occurs at 41 days of gestation in

humans and embryonic day 11.5 (E11.5) in mice. Interruption of any component of this process leads to failure of fusion and CLP.

Similarities in the genetic pathways involved in craniofacial morphogenesis in mice and humans, allow for the use of mouse models to study and understand the pathogenesis of CLP in humans. The “A” strain family of inbred mice has been useful because it exhibits spontaneous CLP.^[4,5] Of the “A” strains, CL/Fr, created by an outcross of the A/J strain with selection for CLP, has the highest risk of CLP, occurring in 35% of newborns.^[5,6] Affected newborns have altered facial geometry and abnormal morphological features that are similar to those seen in humans with CLP.

Two disease loci, *clf1* and *clf2*, are involved in the “A” strain defect.^[7–10] The *clf1* locus on distal chromosome 11 contains the genes *Wnt9b* and *Wnt3*.^[7,9] This region is syntenic to the human chromosome 17q21, which has been associated with nonsyndromic CLP in humans.^[11,12] Furthermore, SNPs within the WNT9B gene have been associated with nonsyndromic CLP in a Brazilian population.^[13] *Wnt* genes are expressed strongly during mouse craniofacial development and are involved in cell-to-cell communication, regulation of cell proliferation, and patterning in many developmental contexts.^[14] Previous gene-targeting analyses suggest that *Wnt9b* is the mutated gene involved in the *clf1* region, contributing to CLP formation in A/WySn mice.^[15] In addition, it has been hypothesized that the presence of an intracisternal A particle (IAP) transposon near the *Wnt9b* gene at the *clf1* locus and epistatic interaction of the *clf2* locus leading to hypomorphic *Wnt9b* expression, may have a role in the development of CLP in these mice as well.^[10,15,16] However, it is still unclear how reduced levels of *Wnt9b* result in a cleft lip phenotype.

In this study we measured tissue specific expression and examined spatial expression patterns of *Wnt9b* during nasal fin development and fusion in CL/Fr mice to determine whether aberrant and hypomorphic expression of *Wnt9b* is associated with an elevated risk for CLP. We also offer new details on candidate genes that may be involved in CLP formation in CL/Fr mice.

Materials and Methods

Animals

All procedures were carried out in accordance with Institutional Animal Care and Use Committee (IACUC) specifications and performed following protocols approved by the University of Hawaii Laboratory of Animal Services. Adult mice were housed under standard conditions with 12-hour light cycles and supplied with tap

water and Rodent Mouse Chow *ad libitum*. Breeding pairs were re-derived from an existing colony and reciprocally crossed. Females were examined for a vaginal plug at 8:00 AM and if absent, they were removed and re-mated the next day. The day on which a vaginal plug was observed was designated as day 0.5 of gestation (E0.5). Embryo collection was also performed on adult females from crosses between 3H1 mice. These embryos served as a control (WT) due to an extremely low incidence of CLP (< 1%) in the 3H1 strain.

Tissue collection

Pregnant CL/Fr females were isoflurane-anesthetized and sacrificed by cervical dislocation at 11.5 days of gestation. Embryos were obtained via caesarian section, placed in ice-cold phosphate-buffered saline (PBS) (pH 7.4) and verified to be Theiler stage 19 (E11.5). Facial prominences were isolated from the underlying telencephalon and the right half of the face was separated from the left along the median plane between the MNPs. Each half of the face contained one MNP, one LNP, and one MxP. The halves were placed in individual tubes containing 400 μ l of RNAlater (Ambion, Thermo Fisher Scientific, North Ride, NSW, Australia) and stored at 4°C for 24 hours. The tissues were then removed from the RNAlater for processing. WT tissues were obtained from embryos derived from 3H1 +/+ matings and collected in a similar fashion. Initial observance of phenotype was scored for non-cleft (normal) or bilateral cleft.

Quantitative real time-PCR

Total RNA from CL/Fr and 3H1 facial prominences was purified using the RNeasy Mini Kit according to the manufacturer’s protocol (Qiagen, Valencia, CA, USA). cDNA was synthesized from 400 ng of each RNA sample using the iScript cDNA Synthesis Kit (Bio-Rad Laboratories, Hercules, CA, USA). All procedures were performed according to the manufacturer’s protocols. Gene expression was determined by quantitative real-time PCR (qRT-PCR) in triple replicates (25 μ l final volume) using the iQ SYBR Green Supermix reaction procedure (Bio-Rad Laboratories) with the CFX96 Real-Time Detection System and C1000 thermocycler (Bio-Rad Laboratories). PCR conditions consisted of an initial 2-min denaturation at 94°C, followed by 40 reactions cycled through denaturation for 15 sec at 94°C, annealing for 30 sec (temperature dependent on primer pair; see **Table 1**), and extension for 60 sec at 72°C. The threshold cycle was established at the linear portion of the log scale curve and expression levels were normalized to Gapdh or Actb and calculated using the $2^{-\Delta\Delta C_t}$ method.^[17] Primer sets to amplify *Wnt9b*, *Wnt3*, *Trp63*, *Gapdh*, *Sstand Actb* were optimized for SYBR green

Table 1

PCR primers. Oligonucleotide sequences and specifications of primers used for quantitative RT-PCR. Sense oligonucleotides (F) and antisense (R) are listed.

Primer	5'-Sequence-3'	Melting temperature	Annealing temperature	Efficiency
<i>Wnt9b F</i>	GCT GGG AAG ATC TTT GAT GG	53.4 °C	59 °C	99.8%
<i>Wnt9b R</i>	TCC ATT CTT GCC TTG TAC CC	54.8 °C		
<i>Wnt3 F</i>	AGT TCC TTG TGG GCT CCT GT	61.1 °C	60 °C	94.4%
<i>Wnt3 R</i>	CCT CGG TGT CTG CTG GTT AG	60.8 °C		
<i>β-actin F</i>	CAT CCG TAA AGA CCT CTA TGC CAA C	57.3 °C	52 °C	95.7%
<i>β-actin R</i>	ATG GAG CCA CCG ATC CAC A	59.0 °C		
<i>Trp63 F</i>	CAT AGC ATG AGC TGA ACC AC	53.6 °C	51 °C	97.5%
<i>Trp63 R</i>	GCT TTC CCA AGG TAT GAA AC	51.5 °C		
<i>Gapdh F</i>	GCA TCT TGG GCT ACA CTG AG	55.6 °C	59 °C	100%
<i>Gapdh R</i>	GGT GGT CCA GGG TTT CTT AC	55.3 °C		
<i>Sst F</i>	AGA GGT CTG CCA ACT CGA AC	56.9 °C	53 °C	102.5%
<i>Sst R</i>	GGC CAG GAG TTA AGG AAG AG	54.8 °C		

real-time detection (see **Table 1** for description of primer sets). As per the Minimum Information for Publication of Quantitative Real-Time PCR Experiments (MIQE) guidelines, primers were tested for specificity and PCR efficiencies were within acceptable values (range: 94.4–100%).^[18] For the initial qRT-PCR analysis, samples sizes consisted of 18 WT, 15 CLP(-) and 8 CLP(+).

In situ hybridization

A total of 12 embryos from 3 litters, four 3H1 wild-type, four CL/Fr non-cleft, and four CL/Fr cleft embryos, were collected at E11.5, fixed in 4% PFA and stored in 100% methanol at -20°C. The embryos were subjected to *in situ* hybridization to detect *Wnt9b* expression. A 4.3 kb fragment corresponding to the *Wnt9b* mRNA was cloned into a pSPORT-P plasmid vector flanked by T7 and Sp6 transcriptional promoters.^[19] The plasmid was amplified by transforming bacteria, purified by column filtration (Sigma-Aldrich, St. Louis, MO, USA) and linearized with NotI (New England Biolabs, Ipswich, MA, USA) to generate antisense and SalI (New England Biolabs) sense ribonucleotide probes. The RNA probe was synthesized using DIG RNA labeling mix (Roche Diagnostics, Indianapolis, IN) and Sp6 and T7 RNA Polymerase (Promega, Madison, WI, USA) based on manufacturer's specifications. For *in situ* hybridization, embryos in methanol were rehydrated, hybridized with riboprobe, and incubated with anti-DIG-AP Fab (Roche) as previously described.^[20] DIG-labeled RNAs were detected with NBT/BCIP (Roche), cleared with glycerol, and examined for staining in the developing craniofacial region (MNPs, LNPs, and MxPs).

Immunohistochemistry

3H1 WT embryos, CLP(+) embryos, and CLP(-) cleft embryos were harvested at E11.5, rinsed in ice cold PBS, and flash frozen in optimum cutting temperature (OCT) compound. Sagittal and transverse sections (10 μm) were cut with selection for the contact point between facial prominences and transferred to polylysine coated microscope slides (Thermo Fisher Scientific, Waltham, MA, USA). Slides were allowed to dry for up to one hour at room temperature until fixed in ice cold methanol for 20 mins at -20°C. Slides were blocked with 5% normal donkey serum in PBS for 30 mins and incubated overnight in goat anti-*Wnt9b* primary antibody (1:100; S&D Bioscience, Manassas, VA, USA). Samples were incubated with DyLight donkey α-goat secondary antibody. To prevent rapid loss of fluorescence and photobleaching during microscopic examination, Vectashield Mounting Media for Fluorescence with DAPI (1.5 μg/ml, Vector Laboratories, Burlingame, CA, USA) was used for tissue section mounting. Identical exposure length and image processing was achieved by collecting tissue images at the constant magnifications to obviate unparallelled changes in fluorescence during processing.

DNA microarray analysis

Three biological replicates were obtained for control, CLP(-) and test CLP(+) samples. Two sets of tissue comparisons were undertaken based on these samples. First, age-matched individual CLP(-) control samples (C1,2,3) were compared to individual CLP(+) test samples (T1,2,3). A second comparison was undertaken comparing

pooled CLP(-) samples (P1) to corresponding CLP(+) samples (P2). Expression profiles were generated for these comparisons.

The anatomical right halves of the faces collected were used for the array and the anatomical left halves were reserved for corresponding qRT-PCR analysis. Total RNA was purified using the NucleoSpin RNA XS Total RNA isolation kit according to the manufacturer's protocol (Macherey-Nagel, Bethlehem, PA, USA). Gene expression profiling was achieved using the whole mouse genome 4×44K microarray kit (Agilent Technologies, Santa Clara, CA, USA). Data was analyzed using the GeneSpring Analysis Platform (Agilent Technologies) to determine the number of genes expressed in the dataset.

Attention was directed to genes in the *clf1* and *clf2* loci, other CLP candidate genes and genes that have been found to regulate craniofacial morphogenesis. In order to better define significant expression changes of these and other candidate genes, a rigorous analysis, focusing on consistency between comparisons in directionality and degree of fold change, was developed and implemented. The analysis consisted of determining fold change that was calculated iteratively among the samples paired into all 16 possible comparisons. A short subroutine was written to identify positive or negative fold change above 1.5 for all 16 comparisons. A Chi-square statistical analysis was assessed for the number of comparisons in agreement.^[21] Thus, we determined the number of comparisons that were in agreement with respect to a fold change that extended above or

below the 1.5-fold cut-off. This rigorous analysis applied a stringent level of statistical analysis to the array and enabled filtering of average gene expression comparisons as well as facilitating the identification of potential outliers.

Results

Reduced expression of *Wnt9b*, but no significant difference in levels of *Wnt3* and *Trp63* RNA in the facial prominences of CL/Fr mice

To determine whether *Wnt9b* expression is affected in CL/Fr mice, as suggested by previous genetic studies, qRT-PCR was performed using E11.5 facial prominences from CLP(-), CLP(+) and WT samples (Table 1; Figure 1). On average, *Wnt9b* expression was reduced by 30% in the CLP(-) samples relative to WT mice (Figure 1a). Additionally, CLP(+) samples showed an overall 50% decrease in expression of *Wnt9b* relative to CLP(-) embryos (Figure 1b). Since previous studies on Pbx compound mutants showed reduced expression of *Wnt3* and *Trp63* in conjunction with reduced *Wnt9b*, we also measured expression of these genes.^[22] No significant difference in the level of *Wnt3* and *Trp63* RNA was seen in the CLP(+) relative to CLP(-) embryos (Figure 1b).

To determine the spatial expression patterns of *Wnt9b* in the developing regions of the upper lip and palate, E11.5 WT, CLP(+) and CLP(-), embryos were subjected to whole mount *in situ* hybridization (Figure 2). Prominent *Wnt9b* staining can be seen in the distal ecto-

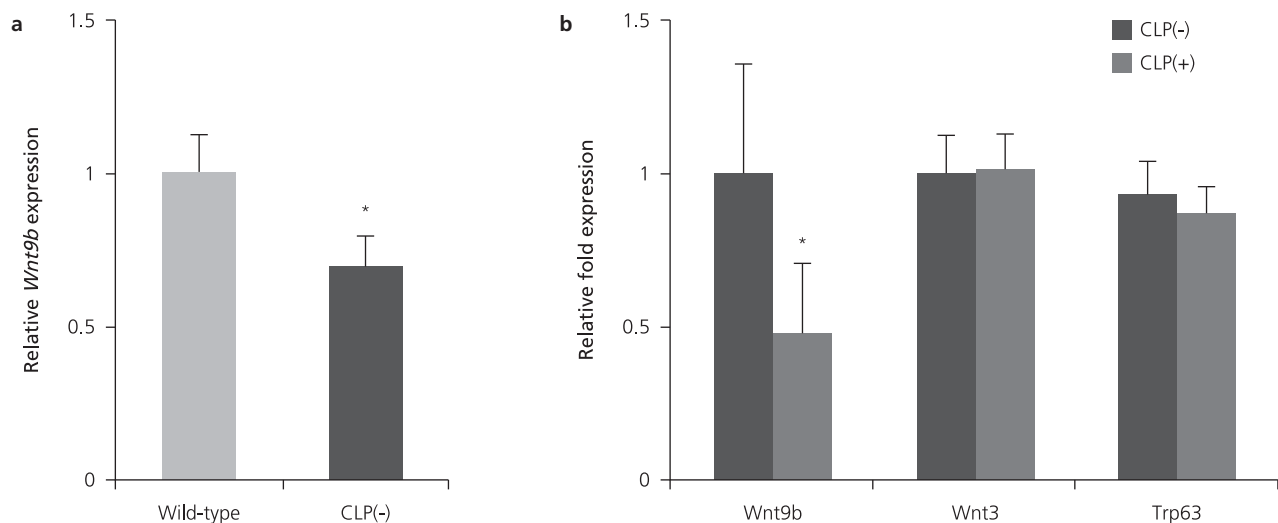


Figure 1. Reduced *Wnt9b* but not *Wnt3* or *Trp63* in CL/Fr embryos. The E11.5 facial prominences showing (a) reduced expression of *Wnt9b* in the CLP(-) relative to 3H1 wild-type mice as well as (b) CLP(+) relative to CLP(-) CL/Fr mice. However, no difference was seen for *Wnt3* and *Trp63* (B) in CL/Fr mouse comparisons based on qRT-PCR analysis. C(t) was established at the linear portion of the log scale curve and ratio of *Wnt9b* to *Actb* was calculated using the $2^{-\Delta\Delta C(t)}$ method. * $p < 0.01$.

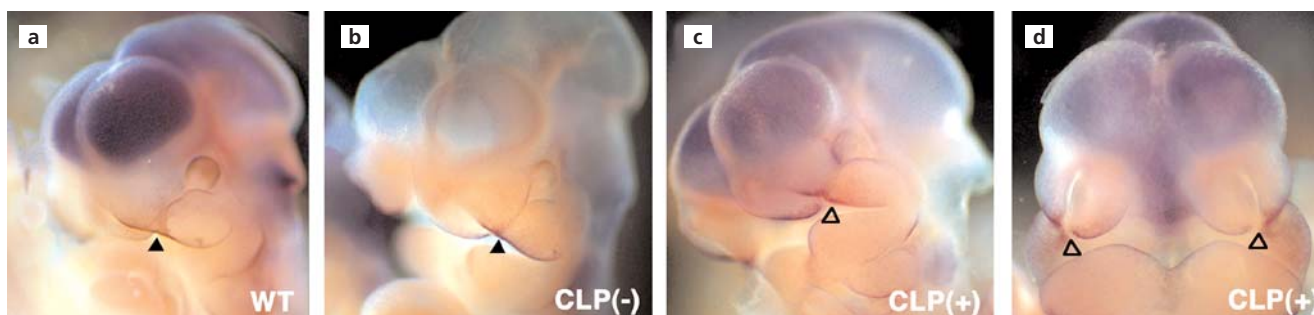


Figure 2. *In situ* hybridizations for *Wnt9b* in whole-mount E11.5 embryos. (a) 3H1 WT, (b) CLP(-) CL/Fr, (c, d) CLP(+) CL/Fr. *Wnt9b* is detected in the distal ectoderm of the MNP, LNP and MxP and in the epithelial contact sites between the fusing prominences. The CLP(+) CL/Fr embryos (c and d) show slightly reduced *Wnt9b* expression in these areas relative to the WT and CLP(-) CL/Fr (a and b). Solid triangles represent contact of the prominences in WT and CLP(-) mice. Open triangles indicate lack of contact in the CLP(+). CLP(+): presence of cleft lip and palate; CLP(-): absence of cleft lip and palate. [Color figure can be viewed in the online issue, which is available at www.anatomy.org.tr]

derm of the MNP, LNP, and MxP of the fusing prominences of WT and CLP(-) embryos. The CLP(+) embryos show reduced *Wnt9b* expression in these areas relative to the CLP(-) and WT embryos, consistent with our qRT-PCR results (Figures 1 and 2).

To visualize the localization of *Wnt9b* protein in the embryonic facial prominences during the critical time of nasal fin fusion, IHC was performed on a total of nine E11.5 WT, CLP(-) and CLP(+) mice (Figure 3). *Wnt9b* fluorescence is prominent in the area of the distal epithelial cells lining the facial prominences in WT mice (Figure

3a). *Wnt9b* fluorescence is also seen in the epithelial cells lining the mandibular component of the first branchial arch. These results are consistent with previous reports by Lan et al. (2006). Sections from CLP(-) mice display presence of *Wnt9b* protein (Figure 3c and d); however, the staining is not quite as robust compared to the WT facial prominences. The staining pattern in CLP(+) facial prominences is fundamentally different compared to both WT and CLP(-) specimens. CLP(+) prominences show greatly reduced *Wnt9b* expression (Figure 3b). The expression also appears to occur as a punctate pattern within the

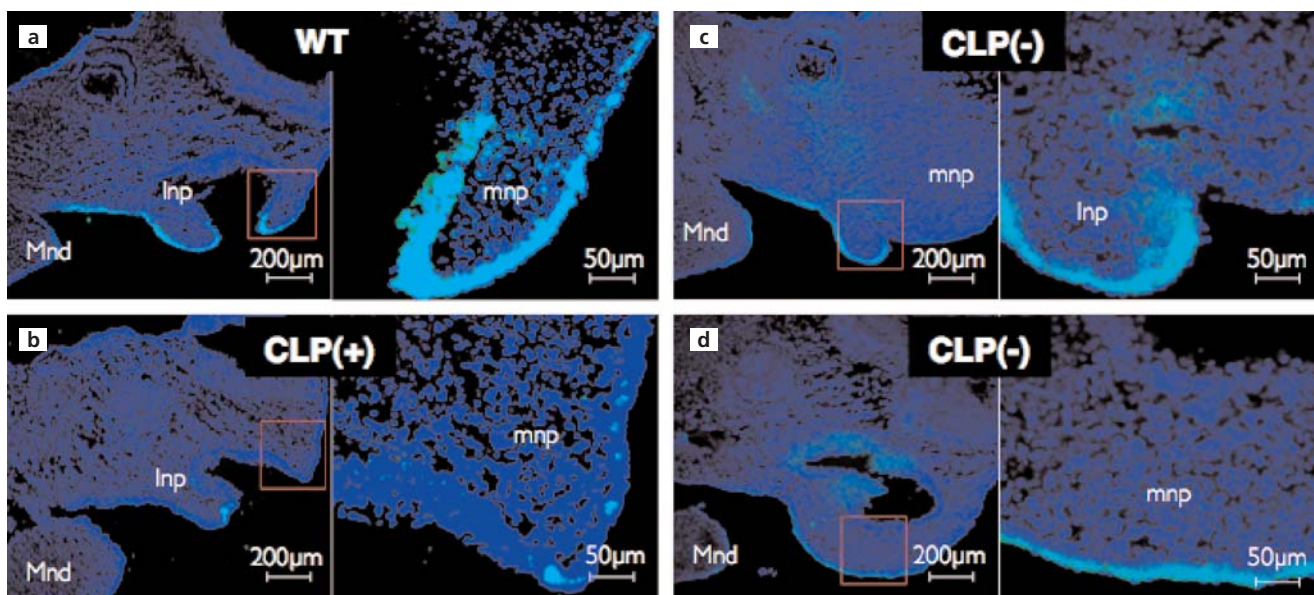


Figure 3. Immunofluorescence of *Wnt9b* in E11.5 3H1 WT, CLP(-) and CLP(+) CL/Fr embryos. Strong localization of *Wnt9b* (light blue) is seen in the facial prominence epithelial cells of E11.5 WT (a) and CLP(-) CL/Fr (c and d) embryos, relative to negative control (no primary antibody; data not shown). Reduced *Wnt9b* is seen in the epithelial cells of CLP(+) CL/Fr (b) samples compared to CLP(-) CL/Fr and WT samples. The CLP(+) is characterized by a punctate pattern of *Wnt9b* expression. Areas indicated by the red boxes were 4x magnified and are shown in the right panels. [Color figure can be viewed in the online issue, which is available at www.anatomy.org.tr]

epithelial rather than a continuous band of staining in WT and CLP(-) specimens (Figure 3b). There also appears to be a dramatic reduction of *Wnt9b*, in terms of the number of epithelial cells as well as the strength of fluorescence in the facial epithelium of the CLP(+) embryos.

Differential gene expression in the faces of CL/Fr mice

Microarray-based gene expression profiling was performed to identify genes that were differentially expressed in the facial prominences during fusion of the facial prominences in E11.5 CL/Fr mice with reduced levels of *Wnt9b* (Figure 4). Of 41,267 probes on the Agilent Mouse GE 4x44K microarray, more than 30,000 of these probes were expressed in the facial prominences in at least one sample. Of these detected probes, 117 had at least a 2-fold change in expression level with a significant probability ($p < 0.05$, Student's t-test). After the removal of probes corresponding to unknown genes and genes on sex chromosomes (gender segregation was not performed), 48 genes were identified as having increased expression in the CLP(+) samples (Table 2) compared with 46 exhibiting decreased expression (Table 3).

Consistent with aforementioned expression assays, *Wnt9b* but not *Wnt3* or *Trp63* expression was found to be significantly reduced in the gene array analysis of CLP(+) tissue (-3.11 fold; $p < 0.01$, -1.50 fold; $p < 0.02$, and -1.03 fold; $p < 0.55$ respectively). Under rigorous analysis, *Wnt9b* differed between all possible comparisons except one (Rigorous Analysis, 15/16, Table 3). Two genes within the *clf2* locus showed significant decreases based on the microarray analysis included adenylate cyclase (*Adcy2*) (-2.22 fold; $p < 0.05$) and ubiquitin-conjugating enzyme E2Q family like 1 (*Ube2q11*), (-1.83 fold; $p < 0.01$) (Table 3).

The greatest change in expression based on our microarray analysis was for somatostatin (*Sst*) (Table 2). Expression was significantly changed in CLP(+) tissue (13.35-fold; $p < 0.05$; rigorous analysis: $\chi^2 = 6.25$, $p < 0.01$, d.f.=1, N=16). A 1.72-fold up-regulation of *sst* ($p < 0.01$) was detected among individual CLP(+) tissues by qRT-PCR (Figure 5). Although this increase was not as dramatic as indicated from our array data, it supports the microarray analysis since it falls within the large range of positive fold changes for *Sst* expression in cleft samples

Discussion

The disruption of canonical WNT/ β -catenin signaling pathway has been implicated in the pathogenesis of CLP.^[23,24] In our study, we have demonstrated that the development of clefts in CL/Fr mice is associated with reduced expression of *Wnt9b*, an important member of this

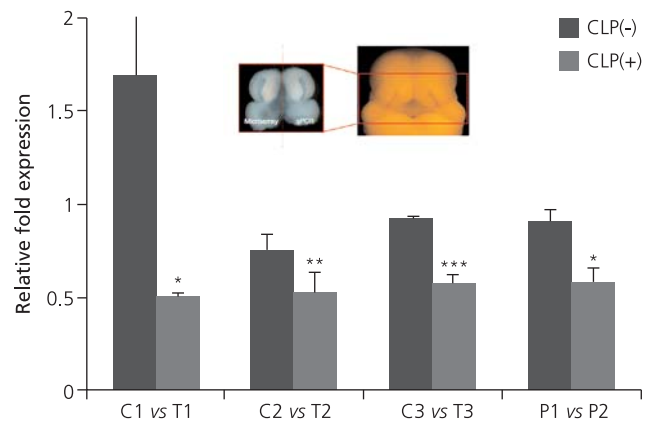


Figure 4. Relative *Wnt9b* expression in the face of CLP(-) and CLP(+) E11.5 embryos used for the microarray. Corresponding facial prominences were utilized for both qRT-PCR and microarray analyses (inset). Relative fold comparison derived from qRT-PCR analysis showing reduced *Wnt9b* expression in individual CLP(+) embryos (T1,2,3) compared with corresponding individual CLP(-) samples (C1,2,3). Pooled samples from CLP(+) animals (P1) compared to CLP(-) embryos (P2) show consistent results. Reduced expression of *Wnt9b* in the CLP(+) samples is consistent with the microarray data (see Table 3); *: $p < 0.01$, **: $p < 0.05$, ***: $p < 0.001$.

signaling pathway and CLP candidate gene. *Wnt9b* was the seventh most significantly down-regulated gene in our microarray analysis with greater than a 3-fold reduction in CLP(+) compared to CLP(-) CL/Fr embryos (Table 3). This result was confirmed by qRT-PCRs on facial prominences corresponding to those used in the array (Figures 1 and 4). This difference is greater compared to cleft versus non-cleft A/WySn mice where transcription of *Wnt9b*

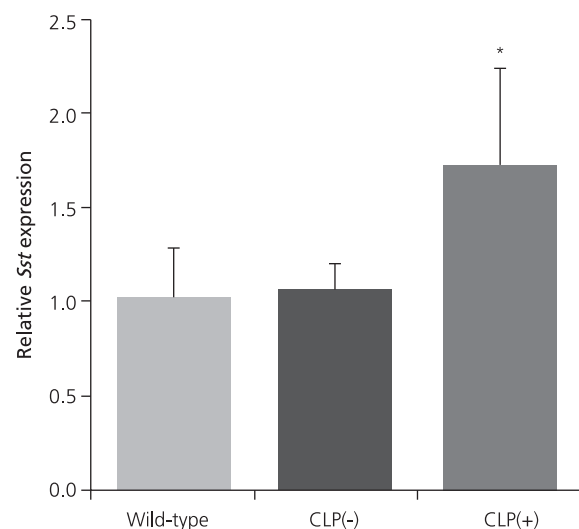


Figure 5. Expression of *Sst* in CL/Fr facial prominences. Increased expression of *Sst* in CLP(+) tissues compared to 3H1 wild-type and CLP(-) CL/Fr tissues based on qRT-PCR of E11.5 facial prominences. * $p < 0.01$.

appears to be affected by the methylated state of IAP.^[16] *Wnt9b* was also reduced in CLP(-) embryos compared to wild-type mice (Figure 1a); however, the CL/P(-)CL/Fr mice did not display clefts. This suggests that a threshold amount of *Wnt9b* is likely required for normal facial morphogenesis, and minor reductions in *Wnt9b* as seen in

CLP(-) CL/Fris not sufficient for cleft development supporting long held views of threshold growth mechanisms associated with cleft formation.^[25]

Whole mount *in situ* hybridizations on E11.5 embryos indicated that *Wnt9b* expression occurred in the facial prominences specifically in the distal ectoderm of the MNP,

Table 2
Genes exhibiting greatest increased expression in CLP(+) compared to CLP(-) samples.

Gene symbol	p-value	Fold change	Rigorous analysis	Gene name
Sst	2.33E-02	13.35	13 /16, p=0.01	somatostatin
D730050B12Rik	8.39E-03	7.42	16 /16, p=6.33E-05	RIKEN cDNA D730050B12 gene
Mstn	1.72E-02	6.05	15/16, p=4.65E-04	myostatin
Kcnj12	4.60E-02	5.45	12/16, p<0.05	potassium inwardly-rectifying channel, subfamily J, member 12
Ldhd	4.80E-02	5.35	13/16, p=0.01	lactate dehydrogenase D
Olf1423	4.52E-02	5.14	12/13, p<0.05	olfactory receptor 1423
BC049349	4.17E-02	5.13	13/16, p=0.01	cDNA sequence BC049349
Olf146	4.81E-02	4.82	13/16, p=0.01	olfactory receptor 146
Gsbs	3.23E-02	4.02	12/13, p<0.05	G substrate
Ceacam2	3.79E-02	4.01	14/16, p=2.69E-03	carcinoembryonic antigen-related cell adhesion molecule 2
LOC100044500	5.24E-03	3.86	14/16, p=2.69E-03	similar to Dsg2 protein
Taf4b	3.10E-04	3.69	16 /16, p=6.33E-05	TAF4B RNA polymerase II, TATA box binding protein (TBP)-associated factor
Gsbs	2.17E-02	3.67	12/13, p<0.05	G substrate
Vnn3	4.82E-02	3.66	13 /16, p=0.01	vanin 3
Onecut2	6.70E-03	3.54	16 /16, p=6.33E-05	one cut domain, family member 2
Il5	6.79E-03	3.39	15/16, p=4.65E-04	interleukin 5
Nefn	2.71E-02	3.29	13 /16, p=0.01	neurofilament, medium polypeptide
Sncg	2.58E-02	3.14	13 /16, p=0.01	synuclein, gamma
Nefl	4.46E-02	3.08	12/13, p<0.05	neurofilament, light polypeptide
Ppp2r2c	4.64E-02	3.02	12/13, p<0.05	protein phosphatase 2 (formerly 2A), regulatory subunit B (PR 52), gamma isoform
H28	2.19E-02	2.97	13 /16, p=0.01	histocompatibility 28
Illdr2	2.03E-02	2.83	14/16, p=2.69E-03	immunoglobulin-like domain containing receptor 2
Lin28a	3.27E-02	2.8	12/13, p<0.05	lin-28 homolog A (C. elegans)
Rnf17	1.42E-02	2.71	16 /16, p=6.33E-05	ring finger protein 17
Synn	7.83E-03	2.65	12/13, p<0.05	synemin, intermediate filament protein
Igdcc3	3.11E-02	2.6	13 /16, p=0.01	immunoglobulin superfamily, DCC subclass, member 3
Shroom3	3.82E-02	2.47	13 /16, p=0.01	shroom family member 3
Ttl6	1.96E-02	2.47	14/16, p=2.69E-03	tubulin tyrosine ligase-like family, member 6
Trim6	4.25E-02	2.46	13 /16, p=0.01	tripartite motif-containing 6
Klk1b4	4.36E-02	2.42	11/16, p=0.13	kallikrein 1-related peptidase b4
Fabp7	2.44E-02	2.4	13 /16, p=0.01	fatty acid binding protein 7, brain
Cartpt	1.72E-02	2.39	12/13, p<0.05	CART prepropeptide
E330037M01Rik	2.25E-03	2.35	15/16, p=4.65E-04	RIKEN cDNA E330037M01 gene
Gm3560	8.29E-03	2.31	14/16, p=2.69E-03	predicted gene 3560
Onecut1	3.21E-02	2.31	13 /16, p=0.01	one cut domain, family member 1
Accn4	1.46E-02	2.29	14/16, p=2.69E-03	amiloride-sensitive cation channel 4, pituitary
Rbpjl	4.47E-02	2.27	<11 of 16, p>0.05	recombination signal binding protein for immunoglobulin kappa J region-like
E330037M01Rik	1.61E-02	2.22	13 /16, p=0.01	RIKEN cDNA E330037M01 gene
Onecut2	3.16E-02	2.16	12/13, p<0.05	one cut domain, family member 2
Slc38a9	2.97E-02	2.13	12/13, p<0.05	solute carrier family 38, member 9
Cxcl13	8.62E-03	2.12	13 /16, p=0.01	chemokine (C-X-C motif) ligand 13
Ntrk1	3.19E-02	2.12	12/13, p<0.05	neurotrophic tyrosine kinase, receptor, type 1
B130011D17Rik	4.18E-02	2.09	11/16, p=0.13	RIKEN cDNA B130011D17 gene
Gsg1l	3.76E-02	2.07	11/16, p=0.13	GSG1-like
Myh3	3.58E-02	2.07	11/16, p=0.13	myosin, heavy polypeptide 3, skeletal muscle, embryonic
Mreg	1.37E-02	2.04	13 /16, p=0.01	melanoregulin
Onecut2	4.19E-02	2.03	<11 of 16, p>0.05	one cut domain, family member 2
Fam190a	1.38E-02	2.01	13 /16, p=0.01	family with sequence similarity 190, member A

LNP, and MxP and at epithelial contact sites between the fusing prominences. However, expression was reduced in CLP(+) embryos (Figure 2). In addition to this observation, immunohistochemistry showed less *Wnt9b* in the epithelium of the facial prominences of CLP(+) embryos at a time when the facial prominences should fuse (Figure 3). As demonstrated in previous studies on *Wnt9b*-/- gene deletion generated mice, *Wnt9b* is essential for mesenchy-

mal cell proliferation of facial prominences through WNT/ β -catenin signaling.^[23] Decreased *Wnt9b* expression in CL/Fr mice likely leads to hypoplasia of the prominences and delayed contact and apoptosis at epithelial contact sites, failure of fusion, and CLP.

Wnt9b, however, is likely not the only gene affected in CL/Fr mice since CLP occurs in 35% of newborn CL/Fr mice, which is higher than the incidence seen in other "A"

Table 3

Genes exhibiting greatest decreased expression in the CLP(+) compared to CLP(-) samples (Note: splice variants included as separate entries).

Gene symbol	p-value	Fold change	Rigorous analysis	Gene name
Prl2c3	3.14E-02	-4.93	14/16, p=2.69E-03	prolactin family 2, subfamily c, member 3
Pde1a	2.06E-02	-3.85	14/16, p=2.69E-03	phosphodiesterase 1A, calmodulin-dependent
Calb2	1.37E-02	-3.64	13 /16, p=0.01	calbindin 2
Pde1a	1.89E-02	-3.50	13 /16, p=0.01	phosphodiesterase 1A, calmodulin-dependent
a	3.68E-02	-3.35	13 /16, p=0.01	nonagouti
Cpxm2	4.85E-02	-3.26	13 /16, p=0.01	carboxypeptidase X 2 (M14 family)
Calb2	1.20E-02	-3.21	13 /16, p=0.01	calbindin 2
Gdf10	2.70E-02	-3.19	13 /16, p=0.01	growth differentiation factor 10
Wnt9b	4.05E-03	-3.11	15/16, p=4.65E-04	wingless-type MMTV integration site 9B
Calb2	6.71E-03	-3.08	15/16, p=4.65E-04	calbindin 2
Zfp572	2.11E-02	-3.05	14/16, p=2.69E-03	zinc finger protein 572
Avpr1a	6.10E-03	-3.02	14/16, p=2.69E-03	arginine vasopressin receptor 1A
Orm3	4.62E-02	-2.99	12/16, p<0.05	orosomucoid 3
Penk	2.07E-02	-2.92	15/16, p=4.65E-04	preproenkephalin
Hey2	2.11E-02	-2.86	13 /16, p=0.01	hairy/enhancer-of-split related with YRPW motif 2
Otop3	1.87E-02	-2.81	12/16, p<0.05	otopettrin 3
Pde1a	4.04E-02	-2.78	13 /16, p=0.01	phosphodiesterase 1A, calmodulin-dependent
Hdgfl1	1.44E-02	-2.76	14/16, p=2.69E-03	hepatoma derived growth factor-like 1
Col6a1	3.10E-02	-2.71	12/16, p<0.05	collagen, type VI, alpha 1
Runx2	2.30E-02	-2.66	12/16, p<0.05	runt related transcription factor 2
Penk	2.74E-02	-2.65	14/16, p=2.69E-03	preproenkephalin
Thy1	2.90E-02	-2.64	13 /16, p=0.01	thymus cell antigen 1, theta
Pde1a	4.73E-02	-2.63	12/16, p<0.05	phosphodiesterase 1A, calmodulin-dependent
Shank1	4.68E-02	-2.57	12/16, p<0.05	SH3/ankyrin domain gene 1
Irak3	4.24E-02	-2.54	11/16, p=0.13	interleukin-1 receptor-associated kinase 3
Olfir68	4.12E-02	-2.51	13 /16, p=0.01	olfactory receptor 68
Krt5	2.26E-02	-2.41	13 /16, p=0.01	keratin 5
Olfir355	2.83E-02	-2.36	13 /16, p=0.01	olfactory receptor 355
Ccdc113	2.21E-02	-2.32	13 /16, p=0.01	coiled-coil domain containing 113
Thy1	3.18E-02	-2.31	11/16, p=0.13	thymus cell antigen 1, theta
Aqp1	3.71E-02	-2.27	12/16, p<0.05	aquaporin 1
Wnt7a	2.63E-02	-2.26	12/16, p<0.05	wingless-related MMTV integration site 7A
Slc9a4	4.83E-02	-2.23	11/16, p=0.13	solute carrier family 9 (sodium/hydrogen exchanger), member 4
Adcy2	3.77E-02	-2.22	12/16, p<0.05	adenylate cyclase 2
Rgs6	1.56E-02	-2.19	13 /16, p=0.01	regulator of G-protein signaling 6
Kera	7.78E-03	-2.14	15/16, p=4.65E-04	keratocan
Mr1	5.31E-03	-2.14	15/16, p=4.65E-04	major histocompatibility complex, class I-related
Sp5	4.84E-03	-2.13	12/16, p<0.05	trans-acting transcription factor 5
Apcdd1	7.13E-03	-2.12	14/16, p=2.69E-03	adenomatosis polyposis coli down-regulated 1
Osr2	1.87E-02	-2.08	13 /16, p=0.01	odd-skipped related 2 (Drosophila)
Lrrc17	2.83E-02	-2.05	11/16, p=0.13	leucine rich repeat containing 17
Pkp1	2.05E-02	-2.05	13 /16, p=0.01	plakophilin 1
Klf4	4.08E-02	-2.03	11/16, p=0.13	Kruppel-like factor 4 (gut)
C1qtnf7	9.12E-03	-2.02	13 /16, p=0.01	C1q and tumor necrosis factor related protein 7
Ccl21a	4.57E-02	-2.00	11/16, p=0.13	chemokine (C-C motif) ligand 21A
Kcnmb2	5.53E-03	-2.00	12/16, p<0.05	potassium large conductance calcium-activated channel, subfamily M, beta member 2

strain mice.^[26] This suggests that disruption of multiple genetic and environmental factors add to the increased penetrance of CLP seen in CL/Fr mice.^[27–30] Previous studies with *Pbx* mutants, *Wnt9b*^{-/-}, and mice with disrupted WNT signaling due to misexpressed genes such as sonic hedgehog (*Shh*), showed reduced *Trp63* expression in the facial prominence epithelium overlapping spatiotemporally with *Wnt9b*, *Wnt3*, and other *Wnt* genes.^[22,24] Previous work suggested possible control and activation of *Trp63* through canonical Wnts. From this, we hypothesized that decreased *Wnt9b* leads to reduced *Trp63* in CL/Fr mice. However, our microarray data supported by qRT-PCR results did not indicate significant perturbations of *Trp63* or *Wnt3* in CL/Fr mice (**Figure 1b**). This suggests that *Trp63* expression may be maintained in CL/Fr mice due to redundancy or compensation by other *Wnt* genes that are expressed within the facial prominences and that a dramatic decrease in expression of *Wnt* may be necessary for a reduction in *Trp63* expression.

Regarding genes in the *clf2* locus, we identified two candidate genes from the array, *Ube2q11* and *Adcy2*, that may be affected in this region. In previous studies, it was postulated that gene(s) in the *clf2* locus on chromosome 13, may contribute to CLP occurrence in “A” strain mice by interacting epistatically with *Wnt9b* and affecting the degree of methylation of the IAP transposon located 3’ of *Wnt9b*. Studies show that low methylation levels of the transposon is associated with CLP.^[9,10,16] Of the two genes detected in our microarray though, *Ube2q11* showed a greater statistical probability of being the gene affected in the *clf2* locus (**Table 3**). *Ube2q11* is in the ubiquitin-conjugating enzyme family, and is responsible for catalyzing covalent attachment of ubiquitin to the target proteins in the second step of the ubiquitination reaction. The key player in the canonical *Wnt* program is β -catenin, a cytoplasmic protein that is regulated a destruction complex that involves ubiquitination for targeted proteasomal degradation.^[31] The brain and face share a close morphogenetic relationship and both genes are widely expressed in the brain during development.^[32] Thus, *Ube2q11* and possibly *Adcy2* may be implicated indirectly in cleft development; however, no specific role in the epigenetic modification of IAP can be speculated based on our results and raw expression data from the array shows very low detection of transcripts. Thus, the identity of the direct mechanism by which *clf2* modifies CLP in CL/Fr, remains elusive.

Additional genes that may contribute to the complicated genetic pathways of CLP were analyzed based on the microarray data, and we identified over 100 genes that are highly misexpressed (>2-fold; p-value ≤ 0.05). Many lie outside of the prospective critical loci. These genes may

be involved in the CL/Fr mutation secondarily from pathways affected by the *clf1* or *clf2* mutations, may have independent roles in facial prominence morphogenesis, or be a product of feedback signaling resulting from abnormal molecular events occurring in cleft tissues. Evidence exists suggesting a number of these candidates direct morphogenetic processes such as cell proliferation, differentiation, and apoptosis. The runt-related transcription factor (*Runx2*) and odd-skipped related transcription factor (*Osr2*) are two other genes associated with CLP that were significantly altered in our microarray analysis. *Runx2* regulates the differentiation of mesenchymal stem cells into osteoblasts and bone formation.^[33] Most mice deficient in *Runx2* presented cleft palate.^[34] *Osr2* is involved in regulating palatal shelf elevation and functions as a downstream target of *Pax9* during palatogenesis.^[35,36] The down-regulation of *Runx2* (-2.66 fold; p<0.05) and *Osr2* (-2.08 fold; p<0.01) in CL/Fr tissues may indicate a secondary effect resulting in cleft palate. Further investigation is necessary to confirm the expression values of these genes and to identify their role in craniofacial morphogenesis.

We were not able to clearly identify genes from our microarray analysis that *Wnt9b* is known to regulate. *Wnt9b* regulates FGF signaling pathways in the ectoderm of the nasal prominence. Reduced levels of *Fgf8*, 10 and 17 along with reduced cell proliferation of facial mesenchyme in mice deficient of *Wnt9b* has been reported.^[23] Furthermore, proliferation of the palatal mesenchyme was reduced in the palatal shelves of CL/Fr mice.^[37,38] Our initial qRT-PCR studies on the most highly upregulated gene in the array, *Sst* (**Table 1**) showed a 1.72-fold up-regulation in CL/Fr tissues (**Figure 5**). *Sst* is a growth hormone-inhibiting hormone with many known functions, which include inhibiting cell proliferation and promoting apoptosis.^[39] Variable up-regulation of *Sst* in the facial prominences could lead to a decrease in growth hormone release, which may slow the growth of the MxPs and MNP and prevent fusion of the prominences in the transient nasal fin regions, leading to clefts in these individuals. Inhibition of cell proliferation by *Sst* is consistent with the effect seen in tissues with reduced FGF signaling as in *Wnt9b* knockout mice. It is possible that *Sst* may have even countered the effect of FGF signaling to inhibit cell proliferation in CLP(+) mice. However, further work will be required to understand this potential mechanism.

The Ca^{2+} -calmodulin stimulated phosphodiesterase 1A (*Pde1a*), previously shown to regulate β -catenin/Tcf signaling was another highly misexpressed gene; down-regulated 3.85 fold in the array (**Table 3**). Previous work demonstrated that inhibition of PDE1A in vascular smooth muscle cells inhibit β -catenin signaling through

up-regulation of protein phosphatase 2A (PP2A), an isoform of which (*Ppp2r2c*) was up-regulated 3.02-fold in the array.^[40] In addition to this, a gene encoding calcium-binding protein, calbindin-2 (*Calb2*), with roles in calcium homeostasis was also downregulated 3.64-fold in the array (Table 3). Thus, misregulation of these key players in the Pde1a/Pp2a/ β -catenin/Tcf signaling pathway may be contributing to the CLP defect. These genes and perhaps many of the other highly misregulated genes listed in Tables 2 and 3 may be targets of the Wnt/ β -catenin signaling or involved in unrelated pathways. This suggests that the etiology of CLP in CL/Fr is highly complex, and thus future studies should focus on elucidating the molecular mechanisms involved with these genes and the role they play in facial development.

Conclusion

The genetic mechanisms involved in the development of CLP are undoubtedly very complex. *Wnt9b* is shown here to be significantly downregulated in CL/Fr mice as seen in other “A” strain mice, emphasizing its important role in craniofacial morphogenesis. However, the hyperpenetration of CLP in CL/Fr mice compared to other “A” strain mice suggests that other factors such as the misexpression of many other key genes outside of the prospective critical loci, and perhaps environmental factors as well, may play important roles in the development of CLP in CL/Fr. Future studies should focus on validating the highly misexpressed genes in the microarray. Subsequently, studies should be aimed at determining whether these genes are downstream targets of *Wnt9b* signaling, and then if so, identifying the mechanisms by which abnormal signaling by these genes leads to CLP.

Acknowledgements

Dr. Y. Lan provided the *Wnt9b* probe for *in situ* analysis. This work was supported by grants R01 DK064752 (SL), HCF 2001265 (SL), HCF 60316 (KSKF).

References

1. Prevalence (number of cases) of cleft lip and palate. National Institute of Dental and Craniofacial Research <http://www.nidcr.nih.gov/> 2014 (accessed in Oct 25, 2016)
2. Parker SE, Mai CT, Canfield MA, Rickard R, Wang Y, Meyer R, Anderson P, Mason CA, Collins JS, Kirby RS, Correa A. Updated national birth prevalence estimates for selected birth defects in the United States. *Birth Defects Res (Part A)* 2010;88:1008–16.
3. Dixon MJ, Marazita ML, Beaty TH, Murray JC. Cleft lip and palate: synthesizing genetic and environmental influences. *Nat Rev Genet* 2011;12:167–78.
4. Kalter H. The history of the A family of inbred mice and the biology of its congenital malformations. *Teratology* 1979;20:213–32.
5. Juriloff DM. Mapping studies in animal models. In: Wyszynski DF, editor. *Cleft lip and palate. From origin to treatment*. New York: Oxford Press; 2002. pp. 265–82.
6. Kadowaki S, Sakamoto M, Kamiishi H, Tanimura T. Embryologic features of term fetuses and newborns in CL/Fr mice with special reference to cyanosis. *Cleft Palate Craniofac J* 1997;34:211–7.
7. Juriloff DM, Harris MJ, Mah DG. The *clf1* gene maps to a 2- to 3-cM region of distal mouse chromosome 11. *Mamm Genome* 1996;7:789.
8. Juriloff DM, Harris MJ, Brown CJ. Unraveling the complex genetics of cleft lip in the mouse model. *Mamm Genome* 2001;12:426–35.
9. Juriloff DM, Harris MJ, Dewell SL. A digenic cause of cleft lip in A-strain mice and definition of candidate genes for the two loci. *Birth Defects Res A Clin Mol Teratol* 2004;70:509–18.
10. Plamondon JA, Harris MJ, Mager DL, Gagnier L, Juriloff DM. The *clf2* gene has an epigenetic role in the multifactorial etiology of cleft lip and palate in the A/WySn mouse strain. *Birth Def Res A Clin Mol Teratol* 2011;91:716–27.
11. Carinci F, Pezzetti F, Scapoli L, Martinelli M, Avantaggiato A, Carinci P, Padula E, Baciliero U, Gombos F, Laino G, Rullo R, Cenzi R, Carls F, Tognon M. Recent developments in orofacial cleft genetics. *J Craniofac Surg* 2003;14:130–43.
12. Carinci F, Scapoli L, Palmieri A, Zollino I, Pezzetti F. Human genetic factors in nonsyndromic cleft lip and palate: an update. *Int J Pediatr Otorhinolaryngol* 2007;71:1509–19.
13. Fontoura C, Silva RM, Granjeiro JM, Letra A. Association of WNT9B gene polymorphisms with nonsyndromic cleft lip with or without cleft palate in a Brazilian nuclear families. *Cleft Palate Craniofac J* 2015;52:44–8.
14. He F, Chen Y. Wnt signaling in lip and palate development. *Front Oral Biol* 2012;16:81–90.
15. Juriloff DM, Harris MJ, McMahon AP, Carroll TJ, Lidral AC. *Wnt9b* is the mutated gene involved in multifactorial nonsyndromic cleft lip with or without cleft palate in A/WySn mice, as confirmed by a genetic complementation test. *Birth Defects Res A Clin Mol Teratol* 2006;76:574–9.
16. Juriloff DM, Harris MJ, Mager DL, Gagnier L. Epigenetic mechanism causes *Wnt9b* deficiency and nonsyndromic cleft lip and palate in the A/WySn mouse strain. *Birth Defects Res A Clin Mol Teratol* 2014;100:772–88.
17. Livak KJ, Schmittgen TD. Analysis of relative gene expression data using real-time quantitative PCR and the $2^{-(\Delta\Delta Ct)}$ method. *Methods* 2001;25:402–8.
18. Bustin SA, Benes V, Garson JA, Hellems J, Huggett J, Kubista M, Mueller R, Nolan T, Pfaffl MW, Shipley GL, Vandesompele J, Wittwer CT. The MIQE guidelines: minimum information for publication of quantitative real-time PCR experiments. *Clin Chem* 2009;55:611–22.
19. Lan Y, Ryan RC, Zhang Z, Bullard SA, Bush JO, Maltby KM, Lidral AC, Jiang R. Expression of *Wnt9b* and activation of canonical Wnt signaling during midfacial morphogenesis in mice. *Dev Dyn* 2006;235:1448–54.
20. Fogelgren B, Kuroyama MC, McBratney-Owen B, Spence AA, Melahn LE, Anawati MK, Cabatbat C, Alarcon VB, Marikawa Y, Lozanoff S. Misexpression of *Six2* is associated with heritable frontonasal dysplasia and renal hypoplasia in 3H1 Br mice. *Dev Dyn* 2008;237:1767–79.
21. Sokal RR, Rohlf FJ. *Biometry: the principles and practice of statistics in biological research*. New York (NY): WH Freeman; 1995.

22. Ferretti E, Li B, Zewdu R, Wells V, Hebert J, Karner C, Anderson M, Williams T, Dixon J, Dixon M, Depew M, Selleri L. A conserved Pbx-Wnt-p63-Irf6 regulatory module controls face morphogenesis by promoting epithelial apoptosis. *Dev Cell* 2011;21:627–41.
23. Jin Y-R, Han XH, Taketo MM, Yoon JK. Wnt9b-dependent FGF signaling is crucial for outgrowth of the nasal and maxillary processes during upper jaw and lip development. *Development* 2012;139:1821–30.
24. Kurosaka H, Iulianella A, Williams T, Trainor P. Disrupting hedgehog and WNT signaling interactions promotes cleft lip pathogenesis. *J Clin Invest* 2014;124:1660–71.
25. Diewert VM, Wang K-Y, Tait B. A new threshold model for cleft lip in mice. *Ann NY Acad Sci* 1993;678:341–3.
26. Young N, Wat S, Diewert VM, Browder LW, Hallgrímsson B. Comparative morphometrics of embryonic facial morphogenesis: Implications for cleft-lip etiology. *Anat Rec (Hoboken)* 2007;290:123–39.
27. Bronsky PT, Johnston MC, Sulik KK. Morphogenesis of hypoxia-induced cleft lip in CL/Fr mice. *J Craniofac Genet Dev Biol Suppl* 1986;2:113–28.
28. Martin DA, Nonaka K, Yanagita K, Nakata M. The effect of dam strain on the craniofacial morphogenesis of CL/Fr mouse fetuses. *J Craniofac Genet Dev Biol* 1995;15:117–24.
29. Nonaka K, Sasaki Y, Watanabe Y, Yanagita K, Nakata M. Effects of fetus weight, dam strain, dam weight, and litter size on the craniofacial morphogenesis of CL/Fr mouse fetuses affected with cleft lip and palate. *Cleft Palate Craniofac J* 1997;34:325–30.
30. Nonaka K, Sasaki Y, Martin DA, Nakata M. Effect of the dam strain on the spontaneous incidence of cleft lip and palate and intrauterine growth of CL/Fr mouse fetuses. *J Assist Reprod Genet* 1995;12:447–52.
31. Clevers H. Wnt/beta-catenin signaling in development and disease. *Cell* 2006;127:469–80.
32. Marcucio RS, Young NM, Hu D, Hallgrímsson B. Mechanisms that underlie co-variation of the brain and face. *Genesis* 2011;49:177–89.
33. Ducy P, Zhang R, Geoffroy V, Ridall AL, Karsenty G. *Osf2/Cbfa1*: a transcriptional activator of osteoblast differentiation. *Cell* 1997;89:747–54.
34. Aberg T, Cavender A, Gaikwad JS, Bronckers AL, Wang X, Waltimo-Siren J, Thesleff I, D'Souza RN. Phenotypic changes in dentition of *Runx2* homozygote-null mutant mice. *J Histochem Cytochem* 2004;52:131–9.
35. Lan Y, Ovitt CE, Cho ES, Maltby KM, Wang Q, Jiang R. *Odskipped related 2 (Osr2)* encodes a key intrinsic regulator of secondary palate growth and morphogenesis. *Development* 2004;131:3207–16.
36. Zhou J, Gao Y, Lan Y, Jia S, Jiang R. *Pax9* regulates a molecular network involving *Bmp4*, *Fgf10*, *Shh* signaling and the *Osr2* transcription factor to control palate morphogenesis. *Development* 2013;140:4709–18.
37. Sasaki Y, Tanaka S, Hamachi T, Taya Y. Deficient cell proliferation in palatal shelf mesenchyme of CL/Fr mouse embryos. *J Dent Res* 2004;83:797–801.
38. Sasaki Y, Taya Y, Saito K, Fujita K, Aoba T, Fujiwara T. Molecular contribution to cleft palate production in cleft lip mice. *Congenit Anom (Kyoto)* 2014;54:94–9.
39. Barnett P. Somatostatin and somatostatin receptor physiology. *Endocrine* 2003;20:255–64.
40. Jeon K-I, Jono H, Miller C, Cai Y, Lim S, Liu X, Gao P, Abe J-I, Li J-D, Yan C. *Ca2+*/calmodulin-stimulated PDE1 regulates the beta-catenin/TCF signaling through PP2A B56 gamma subunit in proliferating vascular smooth muscle cells. *FEBS J* 2010;227:5026–39.

Online available at:
www.anatomy.org.tr
 doi:10.2399/ana.16.033
 QR code:



deomed®

Correspondence to: Scott Lozanoff, PhD

Department of Anatomy, Biochemistry and Physiology, University of Hawaii John A. Burns School of Medicine, Honolulu, Hawaii, USA

Phone: +1 808 692 1442

e-mail: lozanoff@hawaii.edu

Conflict of interest statement: No conflicts declared.

This is an open access article distributed under the terms of the Creative Commons Attribution-NonCommercial-NoDerivs 3.0 Unported (CC BY-NC-ND3.0) Licence (<http://creativecommons.org/licenses/by-nc-nd/3.0/>) which permits unrestricted noncommercial use, distribution, and reproduction in any medium, provided the original work is properly cited. *Please cite this article as:* Takagi B, Hong T, Hynd TE, Fong KSK, Fogelgren B, Nonaka K, Lozanoff S. Reduction in *Wnt9b* and associated gene expression in the embryonic midface of CL/Fr mice with heritable cleft lip and palate. *Anatomy* 2016;10(3):182–192.

The relationship between the carotid canal and mandibular condyle: an anatomical study with application to surgical approaches to the skull base via the infratemporal fossa

Fernando Alonso¹, Shenell Bernard², Paul A. Irwin¹, R. Isaiah Tubbs¹, Joe Iwanaga¹, Marios Loukas², Rod J. Oskouian^{1,3}, R. Shane Tubbs¹

¹Seattle Science Foundation, Seattle, Washington, USA

²Faculty of Medicine, St. George's University, Grenada, West Indies

³Swedish Neuroscience Institute, Swedish Medical Center, Seattle, Washington, USA

Abstract

Objectives: To review the relationship of the internal carotid artery, and carotid canal to the mandibular condyle, specifically from an infratemporal fossa approach. Skull base procedures which involve the middle cranial fossa utilize an infratemporal fossa approach either as the primary or adjunct surgical approach often performed with access osteotomies. In these surgeries, injury to the internal carotid artery and carotid canal may occur leading to many vascular complications ranging from internal carotid artery transection and thrombosis to embolism of distal communicating segments. Hence, knowing the relationship of these important structures is of utmost importance for skull base surgeons. In addition, the necessity for this knowledge is critical for clinicians to be able to understand the mechanism by which medial displacement of the mandibular condyle may cause blunt internal carotid artery injury in the evaluation of trauma patients. Identification of these structures and understanding their relationship on imaging may be used in the decision process to perform angiography based imaging.

Methods: Twenty dry skulls were utilized for a total of forty sides and the distance between the proximal carotid canal and the medial aspect of the mandibular condyle was measured.

Results: The average distance between the mandibular condyle and the carotid canal on right and left sided specimens was 1.03 cm and 1.11 cm, respectively. The length ranged from 0.2 cm to 1.7 cm. No significant differences were found between right and left sides.

Conclusion: A clear understanding of the anatomical relationship between the carotid canal and the head of the mandible, an easily identifiable landmark, is important for clinicians and surgeons alike. A substantial distance variability was observed in the samples studied. The understanding of this relationship should help identify patients at risk for ICA injury during surgical approaches and in the trauma setting.

Keywords: anatomy; infratemporal fossa; neurosurgery; skull base; vascular injury

Anatomy 2016;10(3):193–199 ©2016 Turkish Society of Anatomy and Clinical Anatomy (TSACA)

Introduction

Vascular relationships are important in relation to the skull base (**Figure 1**). Infratemporal approaches are often challenging and made more hazardous by the disruption of anatomy due to tumor displacement and invasion. Approaches involving the infratemporal fossa (ITF) may cause injury to the internal carotid artery (ICA)

leading to the need for repair, ligation and/or sacrifice. Anatomical knowledge of this relationship is of utmost importance.^[1]

The ICA is one of the terminal branches of the common carotid artery, which frequently originates at the C3-C5 vertebrae where the common carotid artery bifurcates into the internal and external branches.^[2]

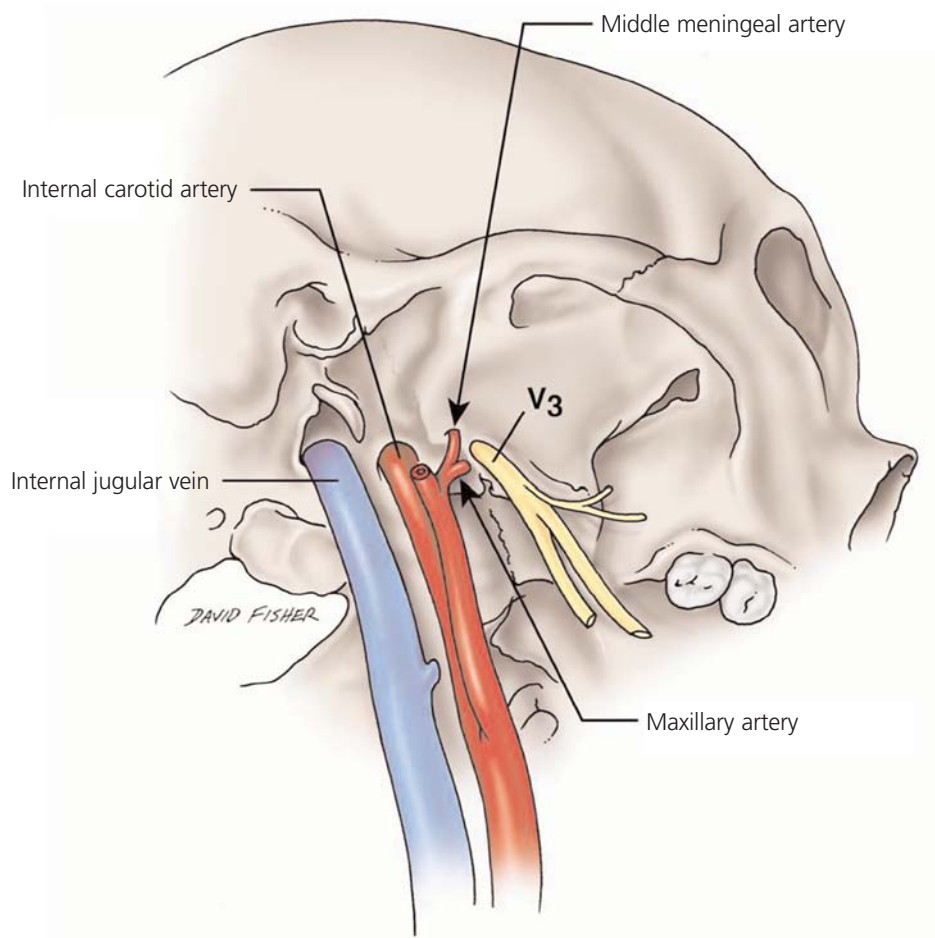


Figure 1. Schematic drawing of the vascular relationships at the skull base. Note the relationship between the medial edge of the mandibular fossa and the internal carotid artery as it enters the carotid canal. [Color figure can be viewed in the online issue, which is available at www.anatomy.org.tr]

Bouthillier et al.^[3] created a new classification system of the ICA using a numerical scale in the direction of blood flow, and described its segments according to a detailed understanding of the anatomical structures surrounding it and the compartments through which it travels. Commonly used today, it comprises seven segments: C1, cervical; C2, petrous; C3, lacerum; C4, cavernous; C5, clinoid; C6, ophthalmic; and C7, communicating.^[3]

The cervical segment of the ICA begins at the level of the common carotid artery bifurcation. This segment is found inside the carotid sheath with the internal jugular vein lateral to the artery, and the vagus nerve usually in a posterolateral course.^[1] Inside the carotid sheath, the ICA is surrounded by areolar tissue containing fat, a venous plexus, and postganglionic sympathetic nerves. Rostrally, as the ICA enters the carotid canal, the carotid sheath divides into two layers. The inner layer continues as the periosteum of the carotid canal, and the outer layer continues as the periosteum of the extracranial sur-

face (exocranium) of the skull base. The cervical segment of the ICA ends when it enters the carotid canal of the petrous bone anterior to the jugular foramen.^[3] The ICA does not branch prior to entering the carotid canal. The carotid canal, which encompasses the petrous ICA, terminates at the vertical line of the posterolateral margin of foramen lacerum.

As the carotid artery traverses the canal its direction is dependent upon the windings of its passage.^[4] The entrance of the carotid canal is bordered anterolaterally by a bony lamina that is part of the tympanic bone called the vaginal process.^[3] The periosteal lining of the carotid canal is densely adherent to a fibrocartilaginous ring at the entrance of the carotid canal.^[5] The opening of the carotid canal is most often oval.^[6] Its long axis shows a mediorostral to laterodorsal orientation with its largest diameter being 3–4.5 mm in newborns, 4–8 mm in two year olds, 6–7 mm in adolescents and adults on the right side and 6–8 mm on the left.^[6]

As the artery exits from the internal orifice of the canal and ascends into the cranium, it encounters the body of the sphenoid bone. It is reflected ventrally and inferiorly through the cavernous sinus. It then rotates dorsally, beneath the anterior clinoid process, projecting superiorly and posteriorly, giving rise to the clinoid, ophthalmic and ultimately the communicating branches.

The first portion of the carotid canal is directed superiorly and anteriorly; its angle to the Frankfurt horizontal plane was measured as 113–135° in newborns, 110–130° in 5-year olds, and 86–110° in adults.^[6] The length of the ascending portion of the canal was 3.5–4.5 mm in newborns, 5.7 mm in 1-year olds, 7.3 mm in 3-year-olds, 10 mm in 15-year olds and 6.5–13.5 mm in adults.^[6]

The aim of this study was to measure the distance between the medial edge of the mandibular condyle and the proximal carotid canal to review the relationship of the internal carotid artery, and carotid canal to the mandibular condyle, specifically from an ITF approach.

Materials and Methods

Twenty adult dry skulls were utilized for a total of forty sides and the distance between the proximal carotid canal at its lateral edge and the medial aspect of the mandibular condyle was measured (Figures 2 and 3). Specimens were derived from 12 males and 8 females. Measurements were made with microcalipers and were taken three times each and the average taken and recorded. Three of the authors (RIT, PAI, RST) made all the measurements. Photographs were taken of the specimens to document each skull's unique anatomy. Statistical analysis was performed using Statistica software (StatSoft, Inc., Gaithersburg, MD, USA). Statistical significance was set at $p < 0.05$.

Results

The average distance between the medial edge of the mandibular condyle and the lateral edge of the proximal carotid canal on right and left sided sides was 1.03 cm and 1.11 cm, respectively. The length ranged from 0.2 cm to 1.7 cm. No significant differences were found between right and left sides or sex. No specimen was found to have signs of temporomandibular joint disease or dislocation. None of the specimens were found to have damage or anomalies of the skull base near the regions studied.

Discussion

Anatomy of the infratemporal fossa

The ITF is defined as the area under the floor of the middle cranial fossa.^[7,8] It gives passage to several major cerebral vessels and cranial nerves.^[7] Knowledge of the surgical



Figure 2. The skull base and the relationship between the medial edge of the mandibular head and the beginning of the carotid canal. [Color figure can be viewed in the online issue, which is available at www.anatomy.org.tr]

anatomy of the ITF is important to safely expose pathology of the parapharyngeal space, the distal cervical ICA, the extracranial course of cranial nerves VII through XII, and the lateral cranial base. Although a variety of surgical approaches to this region have been developed, the surgical anatomy is complex and remains challenging, often made more difficult by tumors that encase or displace key anatomical structures, increasing the complexity of surgical approaches.^[7]

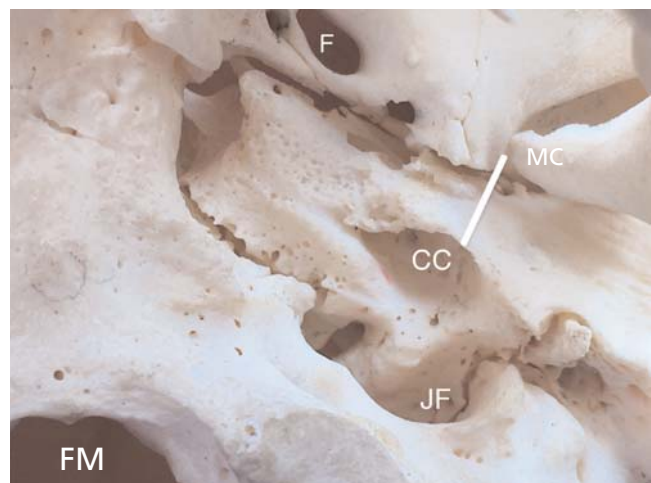


Figure 3. The skull base and the relationship between the medial edge of the mandibular condyle (MC), opening of the proximal carotid canal (CC), jugular foramen (JF), foramen ovale (F), and foramen magnum (FM). The distance between MC and CC is seen as the white line. [Color figure can be viewed in the online issue, which is available at www.anatomy.org.tr]

Bejjani et al.^[7] determined direct foraminal measurements of dried human skulls and noted the relationship of these foramina to each other and various landmarks. The anatomic relationships of muscles, nerves, arteries, and veins were carefully recorded, with special emphasis regarding the relationship of these structures to the styloid diaphragm.^[7]

The styloid diaphragm is a key element in understanding the surgical anatomy of the ITF. It is oriented inferiorly and anteriorly being attached to the exocranial surface of the base of the cranium along a line from the anterior border of the mastoid process, through the styloid and vaginal (tympanic bone) processes, ending at the anterior border of the carotid canal.

The styloid diaphragm divides the ITF into the prestyloid region and the retrostyloid region. The prestyloid region contains the parotid gland and associated structures, including the facial nerve and external carotid artery. The retrostyloid region contains major vascular structures (ICA, internal jugular vein) and the initial exocranial portion of the lower cranial nerves IX through XII.^[7]

If the mandible is laterally retracted and the medial pterygoid muscle is detached, the infratemporal space can be reached. In order to dislocate and mobilize the mandibular condyle, the attachment of the stylomandibular and sphenomandibular ligaments to the mandible are divided, dislocating the temporomandibular joint anteriorly. If more space is necessary, the condyle may be resected.^[2,5]

Using landmarks for the exocranial portion of the lower cranial nerves is useful in identifying them and avoiding injury during approaches to the high cervical ICA, the upper cervical spine, and the ITF.^[7] Its inferior boundary is the horizontal plane passing through the inferior border of the angle of the mandible and the roof, the infratemporal surface of the greater sphenoid wing and the exocranial surface of the petrotympanic region. The medial boundary is the lateral wall of the pharynx and the skin covering the parotid gland and the masseter.^[7,8]

Anteriorly, it is limited by the maxillary tuberosity, the pterygomandibular raphe, and the muscles attached to it. Posteriorly, it is limited by the cervical prevertebral fascia and the underlying muscles.^[8,9]

Identification of the ICA within the surgical field

A comprehensive knowledge of the anatomical relationship of the infrapetrous ICA and its adjacent structures is crucial (**Figure 4**).^[9] It is often difficult in cases of pathology to recognize these structures within a surgical field.^[10]

Tumors of the skull base with carotid artery involvement either require carotid ligation, subtotal resection or

have been deemed inoperable.^[11] Due to its course in the temporal bone, ICA can restrict surgical procedures for lesions extending to the middle skull base and ITF. Preservation of the ICA is demanded and techniques have been developed in order to assist the surgeon in its conservation.^[2,12-18]

The Matas test (percutaneous compression of the carotid artery) and its newer variations have assisted the surgeon in the evaluation of carotid artery sacrifice and the need for bypass. First described in 1911 by Rudolph Matas, if percutaneous compression of the carotid artery produced neurological signs then it was inferred that the patient would not tolerate complete surgical occlusion.^[19,20] However, the technical difficulty of producing a prolonged complete occlusion of the carotid artery by percutaneous compression is considerable and failure to produce neurologic signs by compression, could not guarantee that the patient would tolerate complete surgical occlusion. This test has greatly been modified by contemporary endovascular techniques to be safer and

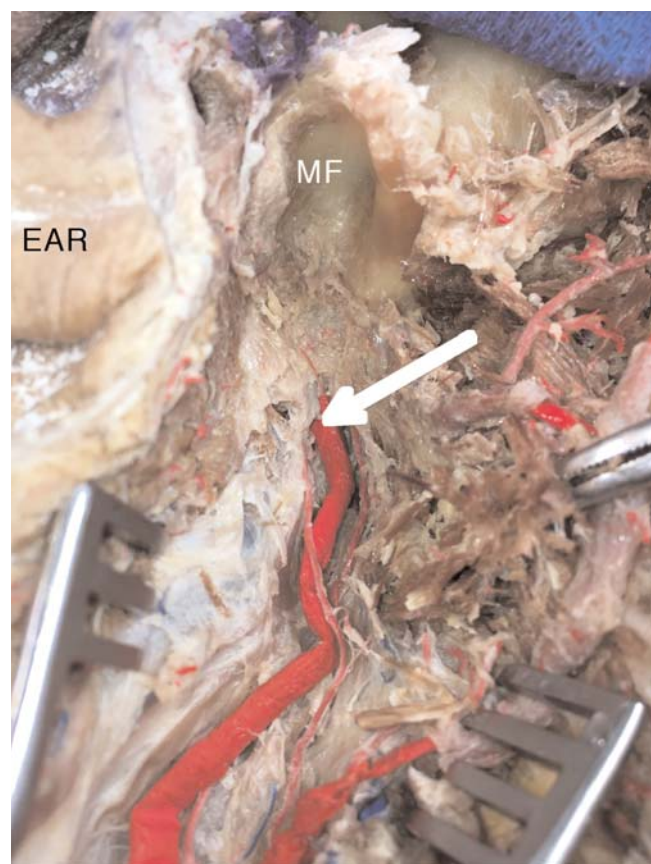


Figure 4. Cadaveric view of a trans-TMJ approach to the skull base. Note the intimate relationship between the medial edge of the mandibular fossa (MF) and the distal ICA at the skull base. [Color figure can be viewed in the online issue, which is available at www.anatomy.org.tr]

more reliable, being largely replaced by balloon test occlusion. ICA ligation can lead to complications due to inadequate circulation in the acute period with subsequent infarction. Ligation of the ICA carries a high risk in patients over 50 years and should not be undertaken unless as an emergency. Even in younger patients, careful preoperative study with bilateral carotid angiography is needed.^[19]

The absence of symptom development during a balloon test occlusion does not guarantee that a patient may become subsequently symptomatic after carotid artery sacrifice.^[21] Non-acute complications of carotid artery sacrifice include thrombosis and emboli of its distal branches. If the posterior communicating artery is large, this may rarely result in infarction of the posterior cerebral artery.^[19] However, performing a BTO can eliminate the need for a high flow radial artery or saphenous venous bypass and allow the clinician to perform a low flow STA-MCA bypass.^[22]

As an alternative to carotid artery ligation, Urken et al.^[11] proposed carotid artery bypass using autogenous saphenous vein graft with distal anastomosis to the infratemporal portion of the ICA. This procedure has been used for malignant skull base neoplasms removed en bloc with sacrifice of a portion of the ICA.^[11]

Sekhar demonstrated usage of a subtemporal-preauricular ITF approach to remove neoplasms involving the lateral and posterior cranial base. This approach has been found useful for the removal of neoplasms involving the clivus, sphenoidal area, petrous apex, orbit, cavernous sinus, middle fossa, infratemporal fossa and the retro- and parapharyngeal areas. However, complications may arise due to ICA thrombosis and middle cerebral artery injury.^[5]

In an attempt to prevent complications associated with ICA injury or ligation. Kawakami et al.^[12] proposed performing radical surgery of malignant tumor occupying the ITF with en bloc resections of the tumor. This was achieved with preservation of the ICA. A substantial operative space was secured during surgery after early identification and opening of the carotid canal. In opening the canal, the carotid triangle can be first identified then shaved and cut as far as the spine of the sphenoid, allowing visualization of the tumor and the ICA. This permits en-bloc resection of the tumor with preservation of the ICA.^[12]

With the advent and refinement of endovascular techniques, carotid sacrifice and subsequent bypass procedures may be avoided. Severe encasement of the ICA, a major factor in achieving gross total resection, may lead to arterial rupture. Stenting can be used to reinforce

the cervical and infratemporal portions of the ICA with good success.^[23]

The ITF approaches to the skull base were first introduced by Fisch for various lesions situated in the infralabyrinthine and apical compartments of the petrous pyramid and surrounding portions of the skull base. The aim of the type B and type C ITF approaches is to have control of the ICA.^[9,24] In ITF approaches type B and type C, the main landmarks used during manipulation of the ICA are the basal turn of the cochlea, Eustachian tube, foramen spinosum, mandibular nerve and anterior foramen lacerum.^[9,25]

Talebzadeh et al.^[26] measured a transverse distance average of 37.5 mm from the carotid artery to the zygomatic arch. This ranged from 29 mm to 48 mm. The most medial aspect of the temporomandibular joint is the most lateral aspect of the ITF. In a study performed by Aslan et al.^[9] to clarify the anatomic relationship between surgical landmarks in type b and type c ITF approach, the cochleariform process (CP) was used as their landmark for surgical orientation. The mean distance of the CP to the ICA genu was 9.2 ± 1.6 mm, while the mean distance from the cochlea to the ICA was 1.6 ± 0.9 mm.^[9] Mason utilized an endoscopic approach and CT imaging, to find a mean distance to the petrous ICA of 16.34 mm from the foramen rotundum, 4.88 mm from the ovale, and 5.11 mm from the spinosum in males. For females, the values were 16.4 mm from the rotundum and 4.36 mm each from the ovale and spinosum.^[14] Additionally, their study made observations as to the existence and locations of any dehiscence of the carotid canal. Carotid canal dehiscence localization is of extreme importance during surgery with a frequency of approximately 20%. The primary location of dehiscence was found to be the superior wall of the horizontal portion of the carotid canal. Dehiscence of the vertical portion is extremely rare.^[9] Lawton and Spetzler^[27] estimate the risk of ICA rupture by tumor infiltration to be approximately 18%, exceeding the risk of revascularization procedures.

In a study of 605 facial trauma patients with mandibular condyle fractures by Vranis, it was found that 5.5 percent of patients had concomitant ICA injury. Severe vascular injury, defined as a Biffel grade greater than one, was present in 6 percent of extracapsular mandibular condyle fractures.^[28] Injury to the ICA can occur by several mechanisms including medial dislocation of the condylar head with impingement of the carotid artery, medial dislocation of the inferior fragment of the condylar fracture, posterior translation of the ramus as it may compress the ICA against the verte-

bral transverse process and lateral displacement of the fracture if it allows the ramus of the mandible to migrate superiorly and medially.^[28] This emphasizes the need for the recognition of the proximity of the ICA to the mandibular condyle as it exceeds its surgical use and should be suspected in the evaluation of patients with facial trauma.

Our present study found the average lengths between the mandibular fossa and the carotid canal on right and left sided specimens were 1.03 cm and 1.11 cm, respectively. The length ranged from 0.2 cm to 1.7 cm. It is an important landmark as this area is simple to identify and often encountered during access osteotomies.^[1,29-31]

Conclusion

An anatomical understanding of the relationship of the carotid canal, which encases only a segment of the ICA, is of immense importance for the surgeon. Special care and a strong anatomical knowledge are needed to prevent complications such as ICA laceration, thrombosis and subsequent emboli. This is more critical when there is invasion or dehiscence of the ICA by tumor pathology. We describe the approximate distance between the most medial border of the mandibular fossa, an easily identifiable landmark during mandibulotomy or dislocation of the mandibular condyle, and the carotid canal. Preoperative identification through imaging is critical as our series revealed significant variation among skull samples.

References

- Sanna M, Shin SH, Piazza P, Pisanis E, Vitullo F, Di Lella F, Bacciu A. Infratemporal fossa approach type a with transcondylar-transtubercular extension for Fisch type C2 to C4 tympanojugular paragangliomas. *Head Neck* 2014;36:1581-8.
- Sekhar LN, Schramm VL Jr, Jones NF, Yonas H, Horton J, Latchaw RE, Curtin H. Operative exposure and management of the petrous and upper cervical internal carotid artery. *Neurosurgery* 1986;19:967-82.
- Bouthillier A, van Loveren HR, Keller JT. Segments of the internal carotid artery: a new classification. *Neurosurgery* 1996;38:425-33.
- Smith NR. Surgical anatomy of the arteries: with plates and illustrations. Baltimore (MD): J. N. Toy and W. R. Lucas; 1835. p. 61-2.
- Sekhar LN, Schramm VL, Jones NF. Subtemporal- preauricular infratemporal fossa approach to large lateral and posterior cranial base neoplasms. *J Neurosurg* 1987;67:488-99.
- Lang J. Skull base and related structures: atlas of clinical anatomy. 2nd ed. Stuttgart: Schattauer; 1996. p. 60-180.
- Bejjani GK, Sullivan B, Salas-Lopez E, Abello J, Wright DC, Jurjus A, Sekhar LN. Surgical anatomy of the infratemporal fossa: the styloid diaphragm revisited. *Neurosurgery* 1998;43:842-52; discussion 852-3.
- Fisch U, Mattox D. Microsurgery of the skull base. New York (NY): Thieme Medical Publishers; 1988. p. 286-301.
- Aslan A, Balyan FR, Taibah A, Sanna M. Anatomic relationships between surgical landmarks in type b and type c infratemporal fossa approaches. *Eur Arch Otorhinolaryngol* 1998;255:259-64.
- Guo YX, Sun ZP, Liu XJ, Bhandari K, Guo CB. Surgical safety distances in the infratemporal fossa: three-dimensional measurement study. *Int J Oral Maxillofac Surg* 2015;44:555-61.
- Urken ML, Biller HF, Haimov M. Infratemporal carotid artery bypass in resection of base of skull tumor. *Laryngoscope* 1985;95:1472-7.
- Kawakami K, Kawamoto K, Tsuji H. Opening of the carotid canal in the skull base surgery: drilling of the carotid canal triangle. *No Shinkei Geka* 1993;21:1013-9.
- Catalano PJ, Bederson J, Turk JB, Sen C, Biller HF. New approach for operative management of vascular lesions of the infratemporal internal carotid artery. *Am J Otol* 1994;15:495-501.
- Mason E, Gurrola J 2nd, Reyes C, Brown JJ, Figueroa R, Solares CA. Analysis of the petrous portion of the internal carotid artery: landmarks for an endoscopic endonasal approach. *Laryngoscope* 2014;124:1988-94.
- Sabit I, Schaefer SD, Couldwell WT. Modified infratemporal fossa approach via lateral transantral maxillotomy: a microsurgical model. *Surg Neurol* 2002;58:21-31.
- Leonetti JP, Bencotter BJ, Marzo SJ, Borrowdale RW, Pontikis GC. Preauricular infratemporal fossa approach for advanced malignant parotid tumors. *Laryngoscope* 2012;122:1949-53.
- Froelich SC, Abdel Aziz KM, Levine NB, Pensak ML, Theodosopoulos PV, Keller JT. Exposure of the distal cervical segment of the internal carotid artery using the trans-spinosum corridor: cadaveric study of surgical anatomy. *Neurosurgery* 2008;62:ONS354-61; discussion ONS361-2.
- Suhardja AS, Cusimano MD, Agur AM. Surgical exposure and resection of the vertical portion of the petrous internal carotid artery: anatomic study. *Neurosurgery* 2001;49:665-9; discussion 669-70.
- Voris HC. Complications of ligation of the internal carotid artery. *J Neurosurg* 1951;8:119-31.
- Wang H, Lanzino G, Kraus RR, Fraser KW. Provocative test occlusion or the matas test: who was rudolph matas? *J Neurosurg* 2003;98:926-8.
- Couldwell WT, Liu JK, Amini A, Kan P. Submandibular-infratemporal interpositional carotid artery bypass for cranial base tumors and giant aneurysms. *Neurosurgery* 2006;59:ONS353-9; discussion ONS359-60.
- Almefty K, Spetzler RF. Management of giant internal carotid artery aneurysms. *World Neurosurg* 2014;82:40-2.
- Sanna M, Piazza P, De Donato G, Menozzi R, Falcioni M. Combined endovascular-surgical management of the internal carotid artery in complex tympanojugular paragangliomas. *Skull Base* 2009;19:26-42.
- Fisch U, Pillsbury HC. Infratemporal fossa approach to lesions in the temporal bone and base of the skull. *Arch Otolaryngol* 1979;105:99-107.
- Liu J, Pinheiro-Neto CD, Fernandez-Miranda JC, Snyderman CH, Gardner PA, Hirsch BE, Wang E. Eustachian tube and internal carotid artery in skull base surgery: an anatomical study. *Laryngoscope* 2014;124:2655-64.

26. Talebzadeh N, Rosenstein TP, Pogrel MA. Anatomy of the structures medial to the temporomandibular joint. *Oral Surg Oral Med Oral Pathol Oral Radiol Endod* 1999;88:674–8.
27. Lawton MT, Spetzler RF. Internal carotid artery sacrifice for radical resection of skull base tumors. *Skull Base Surg* 1996;6:119–23.
28. Vranis NM, Munding GS, Bellamy JL, Schultz BD, Banda A, Yang R, Dorafshar AH, Christy MR, Rodriguez ED. Extracapsular mandibular condyle fractures are associated with severe blunt internal carotid artery injury: analysis of 605 patients. *Plast Reconstr Surg* 2015;136:811–21.
29. Maheshwari GU, Chauhan S, Kumar S, Krishnamoorthy S. Access osteotomy for infratemporal tumors: two case reports. *Ann Maxillofac Surg* 2012;2:77–81.
30. Ye ZX, Yang C, Chen MJ, Abdelrehem A. A novel approach to neoplasms medial to the condyle: a condylectomy with anterior displacement of the condyle. *Int J Oral Maxillofac Surg* 2016;45:427–32.
30. Vilela MD, Rostomily RC. Temporomandibular joint-preserving preauricular subtemporal-infratemporal fossa approach: surgical technique and clinical application. *Neurosurgery* 2004;55:143–53; discussion 153–4.

Online available at:
www.anatomy.org.tr
doi:10.2399/ana.16.035
QR code:



deomed®

Correspondence to: Joe Iwanaga, DDS, PhD
Seattle Science Foundation, 550 17th Ave, James Tower,
Suite 600, Seattle, WA, 98122, USA
Phone: +1 206 732 65 00, Fax: +1 206 732 65 99
e-mail: joei@seattlencefoundation.org

Conflict of interest statement: No conflicts declared.

This is an open access article distributed under the terms of the Creative Commons Attribution-NonCommercial-NoDerivs 3.0 Unported (CC BY-NC-ND3.0) Licence (<http://creativecommons.org/licenses/by-nc-nd/3.0/>) which permits unrestricted noncommercial use, distribution, and reproduction in any medium, provided the original work is properly cited. *Please cite this article as:* Alonso F, Bernard S, Irwin PA, Tubbs RI, Iwanaga J, Loukas M, Oskouian RJ, Tubbs RS. The relationship between the carotid canal and mandibular condyle: an anatomical study with application to surgical approaches to the skull base via the infratemporal fossa. *Anatomy* 2016;10(3):193–199.

Sex determination from the radiographic measurements of calcaneus*

Muhammet Bora Uzuner¹, Ferhat Geneci¹, Mert Ocak¹, Pınar Bayram², İbrahim Tanzer Sancak³, Anıl Dolgun⁴, Mustafa Fevzi Sargon¹

¹Department of Anatomy, School of Medicine, Hacettepe University, Ankara, Turkey

²Department of Histology, School of Medicine, Ankara University, Ankara, Turkey

³TOBB University of Economics and Technology Hospital, Department of Radiology, Ankara, Turkey

⁴Department of Biostatistics, School of Medicine, Hacettepe University, Ankara, Turkey

Abstract

Objectives: The main reason why the calcaneus is chosen for the sex determination is due to its solid structure and resistance to postmortem changes. The comparison of calcanei in radiographies ensures the determination of the sex of corpses whose sex is unknown. A number of skeletons that have been studied as part of the sex determination studies, as well as the variability extents of the male and female samples in the physical and forensic anthropologies which deal with the analysis of the past and present biodiversity, provide information for the observation of data like age, height and sex that are essential for identification.

Methods: In this study, we used the radiographies of patients in the Radiology Department of TOBB University of Economics and Technology Hospital. A total of 143 individuals (including 66 male and 77 female patients) whose calcanei were anatomically normal were involved in the study. The participating individuals were divided into three groups: Group 1 consisted of individuals born in and before 1970, Group 2 consisted of individuals born between 1971 and 1985, and Group 3 consisted of individuals born in and after 1986. Sex distribution was similar in each of the three age groups. Metric and non-metric methods were used in the process of identification held with the aim of sex distinction. Metric measurements were made for eight parameters of the calcaneus, e.g. maximum width, body width, maximum length, minimum length, height of the facies articularis cuboidea, tuber angle, front angle and the tuber plantar angle.

Results: The maximum, minimum and average values of the conducted measurements were obtained. In each of the age groups, differences were observed between the metric lengths of the female and male parameters. Groups 1 and 2 showed similarities in the angular (alpha, beta, sigma) lengths and Group 3 showed similar values in alpha and sigma angles. A statistically significant difference was observed in the beta angle of Group 3. When all of the measurements of the three groups were compared, the maximum height, the minimum height and alpha angle showed similarities, whereas in other parameters a statistically significant difference was observed.

Conclusion: This study reveals the importance of calcaneus in the sex determination and suggests that it can be used as an alternative method in the forensic anthropology and forensic sciences.

Keywords: anatomy; calcaneus; forensic anthropology; radiography; sex determination

Anatomy 2016;10(3):200–204 ©2016 Turkish Society of Anatomy and Clinical Anatomy (TSACA)

Introduction

While determining the basic data such as age, height and sex in physical and forensic anthropology, the differences in calcaneus in between males and females are important.^[1,2] In cases with the presence of the majority of skele-

ton's parts, one can say that the individual's sex will be correctly determined with 90% of accuracy.^[3]

Different parts of skeletons have been analysed in the studies of sex determination. Based on Washburn's studies of sex determination in different societies, the most successful results were achieved using the pelvis.^[4]

*This study has been presented as an oral presentation at the XVII National Anatomy Congress in Eskişehir, Turkey in 2016.

Meanwhile, according to Şahiner and Yalçın's reference to Scheuer, sex can be determined with 80% confidence using the cranium; with 90% confidence using the head and mandible, and with 80% confidence using the pelvis.^[5]

Sex determination can be made by the radiographic measurements of the calcaneus.^[6] This method ensures an alternative facility to possible problems arising from the post-mortem changes in the skeleton. The relevance of calcaneus in sex determination was asserted by a number of authors.^[6-9] The main reason why the calcaneus is chosen for the determination of sex is related to its solid structure and its resistance to post-mortem changes.^[6]

Materials and Methods

In this study, radiographs were obtained from the Department of Radiology of TOBB University of Economics and Technology Hospital. The calcanei of 66 male and 77 females (a total of 143 individuals), anatomically normal in every aspect, were used (Ethics committee approval numbered GO16 / 68 with meeting number 2016/08).

The radiographs were divided into three groups. Group 1 contained individuals born in and before 1970 (n=43), Group 2 consisted of patients born in between 1971-1985 (n=40), and Group 3 included patients born in 1986 and afterwards (n=60). Grouping was done because of the foot's anatomy and changes in bone development in different age groups. The bony mass reaches to its maximum density in the ages of 30-35. After this age interval, the bone turnover results in the loss of bone mass.^[10] Because of this, individuals younger than 30 were included in a separate group, Group 3. Group 1 included people older than 45 years old due to the possibility of osteoporosis after the age of 45.^[11] In the identification process used for the sex determination, metric and non-metric methods were used. In this study, the metric methods were chosen.

After determining the following eight parameters from the latero-lateral radiographies of calcaneus, we conducted the metric measurements with the eFlim program which is appropriate to the PACS system that is used in the TOBB University of Economics and Technology Hospital (Figure 1).

Maximum width (a-g): The distance in between the most posterior point of calcaneus and the highest point of the height of facies articularis cuboidea.

Body width (b-g): The distance in between the most posterior point of calcaneus and lowest point of the height of facies articularis cuboidea.

Maximum length (e-f): The distance in between the most superior and most inferior points of the calcaneus.

Minimum length (c-d): The distance in between the deepest points of the superior and inferior surfaces calcaneus.

The height of facies articularis cuboidea (a-b): The distance in between the highest and lowest points of facies articularis cuboidea.

Tuber angle (α): The angle in between the line drawn from uppermost point of facies articularis cuboidea to most anterior point of calcaneus' superior surface and the line drawn from the most anterior point of calcaneus' superior surface to the most posterior point of this surface (Figure 2).

Anterior angle (β): The angle in between the line drawn from the lowest point of facies articularis cuboidea to most posterior point of calcaneus's superior surface and the line drawn from the lowest point facies articularis cuboidea to most posterior point of the inferior surface of calcaneus (Figure 2).



Figure 1. Measurements for maximum width (a-g), body width (b-g), maximum length (e-f), minimum length (c-d), and height of facies articularis cuboidea (a-b).

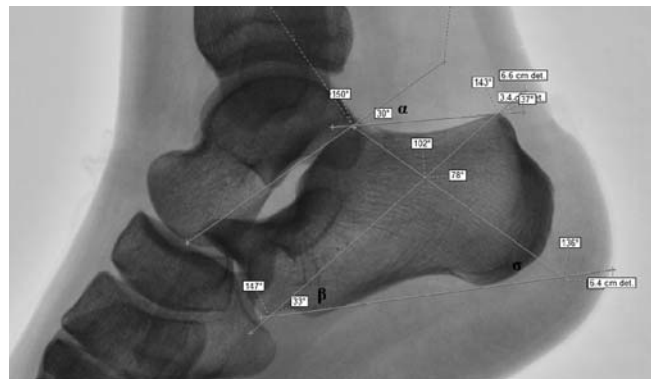


Figure 2. Tuber angle (α), anterior angle (β) and tuber plantare angle (Σ).

Tuber plantare angle (Σ): The angle in between the line drawn from the most posterior point of calcaneus to the line of most inferior point of calcaneus and the line drawn from the intersection of the previous parameters to most posterior point of superior surface of calcaneus (Figure 2).

Statistical analysis

Mean \pm standard deviation (SD) and median values were used to describe the quantitative variables. Also, frequency and percentages were given for the nominal data. Normality assumption was checked by Shapiro Wilk's test. Since data did not conform to normal distribution, non-parametric statistical tests were used. The distribution of qualitative variables among study groups was analyzed by chi-square test. Within each age group, Mann-Whitney U test was used to compare females and males in terms quantitative variables. Kruskal-Wallis test (with the Conover-Dunn multiple comparison technique) was used to compare quantitative variables among age groups. For all analyses, IBM SPSS Statistics for Windows (Version 21.0, Armonk, NY) was used and statistical significance was set at $p < 0.05$.

Results

Among males 24.2% of (16/66) were in Group 1, 30.3% (20/66) were in Group 2 and 45.5% (30/60) of were in Group 3. Among females, 35.1% of (27/77) were in the Group 1, 26% (20/77) were in Group 2, and 39% (30/77) of were in Group 3. The sexes in the age groups were observed to be similar ($p = 0.372$). Mean, standard deviation and median values for each parameter among age groups are shown in Table 1. In each of the age groups, the defining statistics of each sex were separately defined (Table 2). The statistically significant differ-

ence according to sex was observed in the parameters a-g, b-g, b-a, e-f, c-d for all parameters ($p < 0.001$). The difference between the age groups was determined in a-g ($p = 0.012$), b-g ($p = 0.014$), b-a ($p = 0.025$), tuber angle (α) ($p = 0.002$), and anterior angle (β) ($p = 0.036$) measurements.

In the first group, significant statistical difference was observed in all of the parameters ($p < 0.05$) except for the tuber angle (α) ($p = 0.17$), the anterior angle (β) ($p = 0.343$) and tuber plantare angle (Σ) ($p = 0.92$) (Table 2). In the second group, statistically significant difference was observed in all of the parameters ($p < 0.05$) except for the tuber plantare angle (α) ($p = 0.184$), the anterior angle (β) ($p = 0.673$) and tuber plantare angle (Σ) ($p = 0.585$) (Table 2). In the third group, statistically significant difference was observed in all of the parameters ($p < 0.05$) except for the tuber angle (α) ($p = 0.722$), and the tuber plantare angle (Σ) ($p = 0.051$) (Table 2).

Discussion

In females and males, Riepert et al.^[6] found the mean value of tuber angle 33.8° and 34.7° mean value of the anterior angle 40.1° and 41.2° and mean value of tuber plantare 73° and 72°, respectively. In our study, the mean value of tuber angle was 33.52° and 35.14°, mean value of anterior angle was 38.96° and 40.32° and mean value of tuber plantare was 46.03° and 46.59°, respectively. In the study of Riepert et al.,^[6] there was obviously a greater difference between males and females in the linear measurements than in angles. The authors found the male calcaneus significantly to be larger than the females. However, there was no difference in their proportions. In our study, the mean value of tuber plantare was found to be smaller than Riepert's research.^[6]

Table 1
Descriptive statistics of parameters among age groups [mean \pm SD (median)].

Variables	Group 1 (n=43)	Group 2 (n=40)	Group 3 (n=60)	p
Age	55.93 \pm 8.19 (54)	37.72 \pm 4.36 (38)	22.4 \pm 4.69 (22.5)	-
a-g	7.55 \pm 0.96 (7.7)	8.185 \pm 0.9 (8.1)*	8.012 \pm 0.97 (8.05)	0.012
b-g	6.93 \pm 0.87(7)	7.49 \pm 0.93 (7.6)*	7.29 \pm 0.91 (7.45)	0.014
b-a	2.3 \pm 0.35 (2.3)	2.49 \pm 0.33 (2.5)†	2.31 \pm 0.35 (2.3)	0.025
e-f	4.36 \pm 0.71 (4.5)	4.58 \pm 0.59 (4.65)	4.41 \pm 0.68 (4.5)	0.396
c-d	3.62 \pm 0.53(3.7)	3.75 \pm 0.48 (3.7)	3.77 \pm 0.60 (3.8)	0.463
Tuber angle (α)	32.81 \pm 5.39 (32)†	33.025 \pm 6.35 (33)†	36.13 \pm 5.42 (37)	0.002
Anterior angle (β)	41.09 \pm 5.39 (41)†	39.35 \pm 4.07 (39)	38.67 \pm 357 (39)	0.036
Tuber plantare angle (Σ)	46.86 \pm 3.52 (47)	45.65 \pm 3.75 (46.5)	46.3 \pm 2.77 (46)	0.339

*Significantly different from Group 3 ($p < 0.05$); †significantly different from the Group 1 ($p < 0.05$)

Table 2Descriptive statistics of parameters among gender and within each age group [mean \pm SD (median)].

Parameters	Groups	Males (n=16)	Females (n=27)	p
		Mean \pm SD (Median)	Mean \pm SD (Median)	
a-g	Group 1	8.25; 0.69 (8.3)	7.13; 0.84 (7.3)	<0.001
	Group 2	8.82; 0.57 (8.8)	7.55; 0.69 (7.65)	<0.001
	Group 3	8.52; 0.81 (8.7)	7.51; 0.83 (7.65)	<0.001
b-g	Group 1	7.6; 0.63 (7.5)	6.53; 0.75 (6.8)	<0.001
	Group 2	8.095; 0.65 (8)	6.88; 0.76 (6.95)	<0.001
	Group 3	7.75; 0.7 (7.75)	6.85; 0.87 (7)	<0.001
b-a	Group 1	2.49; 0.26 (2.45)	2.19; 0.34 (2.2)	0.004
	Group 2	2.67; 0.26 (2.65)	2.315; 0.28 (2.3)	<0.001
	Group 3	2.47; 0.3 (2.5)	2.15; 0.31 (2.15)	<0.001
e-f	Group 1	4.85; 0.48 (4.95)	4.062; 0.65 (4.1)	<0.001
	Group 2	4.985; 0.38 (4.9)	4.17; 0.46 (4.2)	<0.001
	Group 3	4.84; 0.52 (4.9)	3.98; 0.52 (4)	<0.001
c-d	Group 1	3.95; 0.41(4.1)	3.42; 0.50 (3.4)	0.001
	Group 2	3.97; 0.43 (4)	3.52; 0.40 (3.55)	0.001
	Group 3	4.01;0.51 (4)	3.52; 0.58 (3.45)	0.001
Tuber angle (α)	Group 1	33.93; 5.82(35.5)	32.14; 5.11 (31)	0.17
	Group 2	34.7; 7.18 (33.5)	31.35; 5.03 (32.5)	0.184
	Group 3	36.06; 6.07 (37)	36.2; 4.76 (36.5)	0.722
Anterior angle (β)	Group 1	42.56; 7.08 (42)	40.22; 3.99 (41)	0.343
	Group 2	39.05; 4.23 (38.5)	39.65; 3.97 (40)	0.673
	Group 3	39.96; 2.90 (39.5)	37.36; 3.74 (37)	0.003
Tuber plantare angle (Σ)	Group 1	3.56; 46.75 (46.5)	46.92; 3.55 (47)	0.92
	Group 2	45.8; 2.87 (47)	45.5; 4.53 (46)	0.585
	Group 3	47.03; 2.80 (47)	45.56; 2.56 (46)	0.051

In the comparison of the same parameters studied by Riepert et al.,^[6] Kim et al.,^[14] Zhang et al.,^[13] Introna et al.,^[9] Bidmos et al.^[8] and our study, morphometric measurements of the males were found to be higher than in females in all of the studies. However, in the study by Zhang et al.,^[13]

morphometric values were found to be smaller than our morphometric data both in males and females. This difference was thought to be related with genetical differences (Table 3).^[6,8,9,13,14] Studies found in the literature concluded that the measurements of males were found to be higher

Table 3

Morphometric data of the measurements of calcaneus.

	Method	Gender (n)	a-g	e-f	c-d	a-b
Present study	X-ray	Males (66)	8.55	4.9	3.9	2.53
		Females (77)	7.39	4.05	3.48	2.2
Riepert et al. ^[6]	X-ray	Males (436)	8.98	5.18	4.23	
		Females (364)	8.2	4.67	3.78	
Kim et al. ^[14]	Bones	Males (50)	8.05	4.91	3.95	2.72
		Females (54)	7.37	4.46	3.55	2.49
Zhang et al. ^[13]	X-ray	Males (148)	7.19		3.51	2.23
		Females (186)	6.52		3.12	1.96
Campobasso et al. ^[9]	Bones	Males (40)	7.91			2.45
		Females (40)	7.25			2.24
Bidmos et al. ^[12]	Bones	Males (58)	7.98	4.31		2.39
		Females (58)	7.36	4		2.09
Bidmos et al. ^[8]	Bones	Males (53)	8.47	4.77		2.29
		Females (60)	7.58	4.33		2.02

than the females (Table 3). The black community living in Europe had higher calcaneus measurement values than the ones living in Southern African society. Within the framework of this conclusion, according to Bidmos,^[15] sex and population cause to a difference in osteometric dimensions of calcaneus.

In the study of Bidmos and Dayal,^[16] the values of males' parameters were higher than the females'. The authors further maintained that the results gained by the osteometric methods provided an easy and fast way of determining sex.^[16] As already asserted in a number of studies. Kim et al.,^[14] also supported Bidmos and Dayal,^[16] claim that males possess higher measurement values as compared to females.^[14] On the other hand, while stating that it is difficult to statistically differentiate between white and black Americans by osteometric methods. Steele claimed that these methods could be used to determine sex in the community of Pueblo.^[17]

Conclusion

This research shows that the calcaneus plays an important role in the determination of sex. As it was observed that the measurements of length were an easy method for sex determination, the participants' angular measurements did not reveal any statistical differences. In conclusion, if supported by non-metric methods which are mostly used by the forensic anthropologists, radiographic analysis of the calcaneus can be used as an alternative method in the forensic anthropology and the forensic sciences.

References

1. Cox M, Mays S. Human osteology in archaeology and forensic science. London (UK): Greenwich Medical Media; 2000. p. 548.
2. France DL. Observational and metric analysis of sex in the skeleton. In: Reichs KJ, editor. Forensic osteology: advances in the identification of human remains. 2nd ed. Springfield (IL): Charles C. Thomas; 1998. p. 163–186.

Online available at:
www.anatomy.org.tr
doi:10.2399/ana.16.039
QR code:

deomed.



3. Zeyfeoglu Y, Hancı H. İnsanlarda kimlik tespiti. Sürekli Tıp Eğitimi Dergisi 2001;10:375–7.
4. Washburn SL. Sex differences in the pubic bone. Am J Phys Anthropol 1948;6:199–207.
5. Şahiner Y, Yalçın H. Erkek ve bayanlarda kafatası kemiğinden geometrik morfolometri metoduyla cinsiyet tayini ve ramus flexure. Atatürk Üniversitesi Veteriner Bilimleri Dergisi 2007;2:132–40.
6. Riepert T, Drechsler T, Schild H, Nafe B, Mattern R. Estimation of sex on the basis of radiographs of the calcaneus. Forensic Sci Int 1996;77:133–40.
7. Gualdi-Russo E. Sex determination from the talus and calcaneus measurements. Forensic Sci Int 2007;171:151–6.
8. Bidmos MA, Asala SA. Discriminant function sexing of the calcaneus of the South African whites. J Forensic Sci 2003;48:1213–8.
9. Introna F Jr, Di Vella G, Campobasso CP, Dragone M. Sex determination by discriminant analysis of calcanei measurements. J Forensic Sci 1997;42:725–8.
10. Demir A, Çivi S. Assessment of 10-year major osteoporotic and femur fracture risk of postmenopausal women using FRAX®. The Turkish Journal of Physical Medicine and Rehabilitation 2014;60:11–8.
11. Saka G, Ceylan A, Ertem M, Palancı Y, Toksöz P. Diyarbakır il merkezinde lise ve üzeri öğrenim görmüş 40 yaş üzeri kadınların menopoza dönemine ait bazı özellikleri ve kalsiyum kaynağı yiyecekleri tüketim sıklıkları. Dicle Tıp Dergisi 2005;32:77–83.
12. Bidmos MA, Asala SA. Sexual dimorphism of the calcaneus of South African blacks. J Forensic Sci 2004;49:446–50.
13. Zhang ZH, Chen XG, Li WK, Yang SQ, Deng ZH, Yu JQ, Yang ZG, Huang L. Sex determination by discriminant analysis of calcaneal measurements on the lateral digital radiography. Fa Yi Xue Za Zhi 2008;24:122–5.
14. Kim DI, Kim YS, Lee UY, Han SH. Sex determination from calcaneus in Korean using discriminant analysis. Forensic Sci Int 2013;228:177.e1–7.
15. Bidmos M. Adult stature reconstruction from the calcaneus of South Africans of European descent. J Clin Forensic Med 2006;13:247–52.
16. Bidmos MA, Dayal MR. Sex determination from the talus of South African whites by discriminant function analysis. Am J Forensic Med Pathol 2003;24:322–8.
17. Steele DG. The estimation of sex on the basis of the talus and calcaneus. Am J Phys Anthropol 1976;45:581–8.

Correspondence to: Muhammet Bora Uzuner, MD
Department of Anatomy, School of Medicine,
Hacettepe University, Ankara, Turkey
Phone: +90 312 305 21 07
e-mail: bora.uzuner@hacettepe.edu.tr

Conflict of interest statement: No conflicts declared.

This is an open access article distributed under the terms of the Creative Commons Attribution-NonCommercial-NoDerivs 3.0 Unported (CC BY-NC-ND3.0) Licence (<http://creativecommons.org/licenses/by-nc-nd/3.0/>) which permits unrestricted noncommercial use, distribution, and reproduction in any medium, provided the original work is properly cited. *Please cite this article as:* Uzuner MB, Geneci F, Ocak M, Bayram P, Sancak İT, Dolgun A, Sargon MF. Sex determination from the radiographic measurements of calcaneus. *Anatomy* 2016;10(3):200–204.

Orbital indices in a modern Sinhalese Sri Lankan population

Navneet Lal¹, Jon Cornwall^{1,2,3}, George J. Dias⁴

¹Department of Physiology, University of Otago, Dunedin, New Zealand

²Graduate School of Nursing, Midwifery and Health, Victoria University of Wellington, Wellington, New Zealand

³Institute for Health Sciences, Zurich University of Applied Science, Zurich, Switzerland

⁴Department of Anatomy, University of Otago, Dunedin, New Zealand

Abstract

Objectives: An understanding of orbital morphology is relevant to forensic identification, craniofacial surgery, and anthropological analysis. Orbital index (OI), the relationship between the height and width of the orbit, varies between different populations of humans. This study examines modern Sinhalese Sri Lankan skulls to determine normal values for OI and explore how OI may vary with laterality and sex.

Methods: Measurements of fifty modern Sinhalese Sri Lankan skulls (origin Central Province, Sri Lanka) of known sex (34 male and 16 female) were undertaken for orbital height and width (bilaterally) using a digital caliper. OI was calculated using a standard formula ($[\text{orbital breadth} / \text{orbital height}] \times 100$). Statistical tests analysing OI and size for both sex and laterality were performed using unpaired and paired 2-tailed t-tests ($p < 0.05$), respectively.

Results: Overall mean (\pm standard deviation) OI was 81.29 ± 6.14 , with significant differences found between males (79.29 ± 5.65) and females (84.39 ± 5.59) OI. Left OI was significantly greater than right in both males (80.74 ± 5.85 vs. 77.83 ± 5.11) and females (85.47 ± 5.70 vs. 83.31 ± 5.39), indicating OI asymmetry. Individual heights and breadths of the orbits were symmetrical in both males and females.

Conclusion: Findings indicate OI asymmetry (left larger than right OI) and sexual dimorphism in this population of modern Sinhalese Sri Lankan skulls. Male orbits were microseme (OI < 83) and female mesoseme (OI 83–89), an unexpected finding as Asian populations supposedly have megaseme (OI > 89) orbits, therefore challenging previous assumptions on ethnic OI norms.

Keywords: measurement; orbit; orbital index; Sinhalese Sri Lankan

Anatomy 2016;10(3):205–210 ©2016 Turkish Society of Anatomy and Clinical Anatomy (TSACA)

Introduction

The orbits are craniofacial structures situated on either side of the sagittal plane within the skull and encroach equally upon the cranial and facial regions. Each orbit is composed of several bones arranged to form quadrilateral pyramids with their bases facing anterolaterally and slightly downward, and their apices projecting posteromedially.^[1-3] The orbits contain and protect the eyes, extra-ocular muscles and several neurovascular structures, and also allow for the accurate positioning of the visual axis,^[1,4] which is essential for binocular vision. As landmark features of the skull, morphometric characterisation of the orbits is of value for anthropology,^[5] tracing population origins, gaining insight into craniofacial growth due to

racial and sexual differences,^[6] and quantifying intraspecific variations and forensic osteology.^[1,2,4,7] Moreover, comprehensive assessment and preoperative planning in areas of neurosurgery, craniofacial surgery, congenital disfigurement and trauma require specific morphometric data on orbit morphology for the safety and efficacy of clinical treatment.^[8-11]

While orbit morphology has not changed significantly over recent human history, advances in surgical practice means that we are now able to utilise more detailed and specific information for the treatment of patients.^[12] Thus, obtaining data elucidating intraspecific variation, such as left right symmetry (laterality), sex, and racial differences in the morphological parameters of the orbit

will allow an increased depth, breadth and specificity of knowledge on orbital morphology. One well utilized parameter of orbital morphology is the orbital index (OI) which is defined as a ratio between the orbital height to its width (multiplied by 100).^[13] The use of this parameter is favoured for several reasons: 1) the OI is standardized and can be measured in the living and deceased, 2) measurement is rapid and trivial, 3) OI allows for the numerical quantification of descriptive features, and 4) numerous authors have published OI data on several populations, such that the development of a race and sex specific database can possibly be considered. From previous data, three categories of OI have emerged.^[14-20] Megaseme describes an OI of ≥ 89 and is supposedly typically seen in Mongoloid races with the exception of Inuits, while mesoseme describes an OI between 89 to 83 and is typically seen in Caucasians.^[19,21] Microseme describes an OI of ≤ 83 and is typically seen in Africans.^[19,21]

The following study aims to describe normal values and variations of OI found within a contemporary population of Sinhalese Sri Lankans. The study examines and described the relationships between OI, orbital shape, laterality and sex within these skulls with a view to inform and expand current knowledge of OI and orbital morphology.

Materials and Methods

Fifty modern Sinhalese Sri Lankan skulls of known sex (34 male and 16 female, from Central Province, Sri Lanka) were measured for orbital height and width using digital calipers (Tresna 0-150 mm digital caliper with 0.03 mm accuracy; Thermo Fisher, Auckland, New Zealand) (**Figure 1**) by a single individual with ten years experience in anatomy teaching and research. Skulls with any evidence of trauma or other lesions (*e.g.* disease) that may affect measurements of the orbit were excluded from the study. Measurement methodology was determined by consensus within the research team in consultation with published methods in the field; the research team included a maxillofacial surgeon with a PhD in anatomy and twenty years research experience (author GD). OI was calculated using a standard formula - [orbital breadth / orbital height] \times 100. Measurements were recorded and analyses performed using Microsoft Excel (Microsoft Corp., Albuquerque, NM, USA). Statistical tests assessing OI and size for both sex and laterality were performed using paired and unpaired 2-tailed homoscedastic t-tests ($p < 0.05$), respectively. All experimental procedures were undertaken in accordance with the Declaration of Helsinki on medical ethics; experimental protocols met local institutional ethical guidelines as per similar research on human remains held by an academic institution.^[22,23]

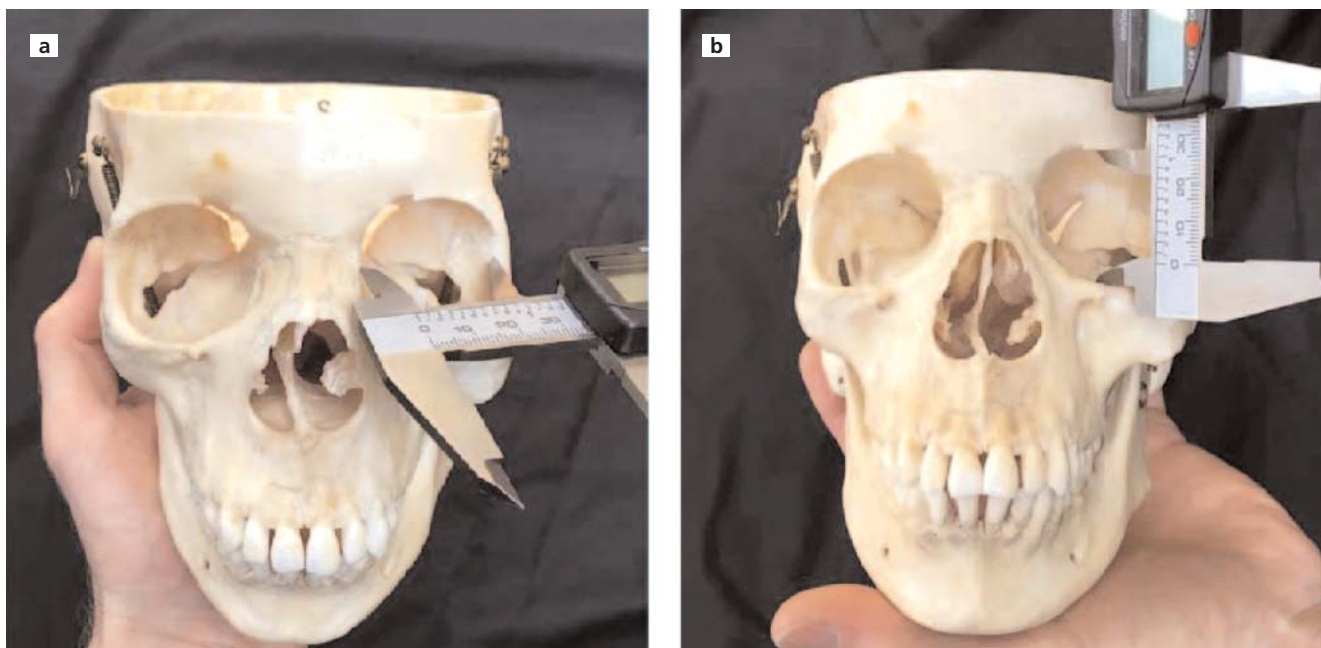


Figure 1. Demonstration of orbital measurements using a digital caliper. Measuring the width (**a**) and height (**b**) of the left orbit. [Color figure can be viewed in the online issue, which is available at www.anatomy.org.tr]

Results

Bilateral measurements from all 50 skulls were analysed. Overall mean (\pm standard deviation) OI for this population was 81.29 ± 6.02 , with mean male OI being significantly smaller than female OI (79.29 ± 5.48 vs. 84.39 ± 5.55 ; $p < 0.001$), respectively (**Table 1**). The left OI was significantly greater than right in both males (80.74 ± 5.85 vs. 77.83 ± 5.11 ; $p < 0.0001$) and females (85.47 ± 5.70 vs. 83.31 ± 5.39 ; $p = 0.032$), with significant differences also seen between males and females for both the left ($p = 0.0043$) and right ($p < 0.001$) sides, respectively, indicating OI asymmetry. The breadths of orbits were significantly different between males and females, with orbital breadth larger in males than in females for both left ($p < 0.001$) and right ($p < 0.001$) orbits (**Table 1**). The measurements for heights of orbits showed no significant difference for laterality or sex.

Discussion

In this population of contemporary Sinhalese Sri Lankan skulls, the mean OI was 81.29 ± 6.02 which places them in the microseme category. However, there were significant differences between males (79.29 ± 5.48) and females (84.39 ± 5.55) such that males were classified as microseme, while females as mesoseme. These differences appear to be the result of differences found in the breadths of the orbits, with male orbits being significantly wider than female orbits. Moreover, while individual orbital parameters such as height and breadth were symmetrical, orbital indices displayed left-right asymmetry. The left OI tended to be slightly smaller than the right OI in both males and females.

Orbital index

Previous studies describing OI in Asian populations found these populations typically characterized as megaseme (**Table 2**).^[24,25] However, our data shows that contemporary Sinhalese Sri Lankan males are microseme whilst females fit the mesoseme category. This is discrepant in two ways. First, microseme categorisation of our skulls

appears suggest that the orbits have a more rounded morphology than other Asian populations.^[1] When this is analyzed against other data from the Asian population, it appears that this discrepancy is evident with most of the data available on Egyptian^[2] and Indian subpopulations.^[12,14,15,18,19,21,26,27] Second, Asian populations seldom display OI sexual dimorphism (**Table 2**). However, this was clearly evident within the Sinhalese population, and may reflect the selection pressures placed on the sexes within the population at the time.

Orbital height and breadth

Orbital heights were consistent between males and females, and displayed left-right symmetry. The left (32.74 ± 1.96 mm vs. 32.65 ± 1.94 mm) and right (32.24 ± 2.19 mm vs. 32.35 ± 1.93 mm) orbital heights of both males and females respectively were within the range of with other neighbouring populations in India,^[12,14,15,18,19,21,26,27] but smaller than Egyptian,^[2] Korean,^[24] and most African populations (**Table 2**).^[9,13,17,28,29] Orbital breadth was larger in males (40.63 ± 1.92 mm, 41.47 ± 1.94 mm; left and right sides, respectively) than females (38.27 ± 2.1 mm, 38.91 ± 2.39 mm; left and right sides, respectively). These values were larger than those seen in Korean populations,^[24] smaller than Egyptian^[2] and most African populations, but within the range of most Indian populations (**Table 2**).^[12,14,15,18,19,21,26,27]

Laterality

Individually, the left and right orbital heights and breadths in males and females were not significantly different, suggesting left and right symmetry. However, when these parameters were used to derive OI, differences between the left and right sides in males and females became apparent. This indicates that individually, the differences found between the left and right side orbital height and width were not large enough to be detected by our statistical tests. Left-right asymmetry in orbital height or breadth was previously reported in Egyptian^[2] and Nigerian^[20] populations; morphological asymmetry is not unique to this

Table 1

Data and analyses of orbital size and indices of modern Sinhalese Sri Lankan skulls from Central Province.

	n	Left orbital height	Right orbital height	Left orbital breadth	Right orbital breadth	Left orbital index	Right orbital index
All	50	32.71 ± 1.94	32.28 ± 2.07	39.7 ± 2.29	40.46 ± 2.46	82.6 ± 6.2	79.98 ± 5.84
Males	34	32.74 ± 1.96	32.24 ± 2.19	$40.63 \pm 1.9^*$	$41.47 \pm 1.94^*$	$80.74 \pm 5.85^†$	$77.83 \pm 5.11^*$
Females	16	32.65 ± 1.94	32.35 ± 1.93	38.27 ± 2.1	38.91 ± 2.39	$85.47 \pm 5.7^†$	83.31 ± 5.39

* $p < 0.05$ females vs males (unpaired 2-tailed homoscedastic t-test); † $p < 0.05$ left vs right (paired 2-tailed homoscedastic t-test)

Table 2

Orbital indices data from this study and previously published work. Data from this study on the orbital indices of Sinhalese Sri Lankan skulls is presented for comparison with those from other ethnicities by sex and by classification.

Region	Population	Sex	Number	Orbital Index	Category	Author	Method, Source
Africa	Black Kenyan	Male	80	82.57	Microseme	Munguti et al. ^[30] 2013	Vernier caliper, dry skulls
		Female	70	83.48	Mesoseme		
		Mean		83.03	Mesoseme		
	Malawians	Male	70	94.35	Megaseme	Igbigbi and Ebite ^[13] 2010	Ruler, frontal X-ray
		Female	66	96.03	Megaseme		
		Mean		95.2	Megaseme		
	Nigerian	Male	78	89.59	Mesoseme	Orish and Ibeachu ^[20] 2016	Digital Vernier calipers, dry skulls
		Female	22	87.04	Mesoseme		
		Mean		88.32	Mesoseme		
	Nigerian	Male	Unknown	89.21	Megaseme	Ukoha et al. ^[28] 2011	Unknown
	Nigerian Binis	Male	63	78.21	Microseme	Anibor and Ighodae ^[17] 2013	Vernier caliper, frontal X-ray
		Female	37	75.82	Microseme		
Mean			77	Microseme			
Nigerian Urhobos	Male	236	78.15	Microseme	Ebeye and Otkipo ^[29] 2013	Not stated, living subjects	
	Female	152	78.57	Microseme			
	Mean		78.36	Microseme			
Asia	Egyptian	Male	30	82.27	Microseme	Fetouh and Mandour ^[2] 2014	Divider and ruler, dry skulls
		Female	22	83.5	Mesoseme		
		Mean		82.89	Microseme		
	Indian	Mean	68	80.07	Microseme	Kumar and Nagar ^[12] 2014	Vernier calipers, dry skulls
	Indian (North)	Mean	50	82.68	Microseme	Alam et al. ^[18] 2016	Vernier calipers, dry skulls
	Indian (North)	Male	60	81.15	Microseme	Maharana and Agarwal ^[19] 2015	Manual calipers, dry skulls
		Female	40	82.16	Microseme		
		Mean		81.66	Microseme		
	Indian (North)	Mean	30	81.65	Microseme	Kaur et al. ^[14] 2012	Vernier calipers, dry skulls
	Indian (Central)	Mean	64	81.88	Microseme	Gosavi et al. ^[15] 2014	Digital Vernier calipers, dry skulls
	Indian (South)	Male	105	84.62	Mesoseme	Mekala et al. ^[21] 2015	Manual calipers, dry skulls
		Female	95	85.46	Mesoseme		
		Mean		85.04	Mesoseme		
	Indian (South)	Mean	50	88.41	Mesoseme	Narasinga and Pramila ^[27] 2015	Vernier calipers, dry skulls
	Indian (South)	Male	130	81.13	Microseme	Patil et al. ^[26] 2014	Vernier calipers, dry skulls
		Female	70	81.32	Microseme		
		Mean		81.23	Microseme		
	Indonesian (Batak)	Unknown	11	99.26	Megaseme	Novita ^[25] 2006	Not stated, frontal X-ray
	Indonesian (Flores)	Unknown	10	106.63	Megaseme		
	Indonesian (Klaten)	Unknown	10	102.73	Megaseme		
	Korean	Male	41	100	Megaseme	Hwang and Baik ^[24] 1999	Vernier / Marshac calipers, dry skulls
		Female		98.55	Megaseme		
		Mean		99.28	Megaseme		
Sinhalese Sri Lankan	Male	34	79.29	Microseme	Current study	Digital Vernier calipers, dry skulls	
	Female	16	84.39	Mesoseme			
	Mean		81.29	Microseme			

Orbital indices (OI) are classified in the following manner: Microseme=OI<83; Mesoseme=OI 83–89; Megaseme=OI>89.

region and was identified in other morphological features such as the jugular foramen and the superior sagittal sinus.^[31] However, the majority of studies published on OI indicate left-right symmetry, though some of these observed differences were not statistically significant. Left-

right orbital index asymmetry is potentially a novel finding and may be a characteristic unique to our population of skulls. Previous OI studies seldom included left-right measurements and thereby data on laterality is lacking for many other populations where OI has been studied.

Sexual dimorphism

Sexual dimorphism was evident in the orbital breadth and OI, with male skulls exhibiting a larger breadth (40.63 ± 1.92 mm, 41.47 ± 1.94 mm; left and right sides, respectively) and smaller OI (79.29) than female skulls (38.27 ± 2.1 mm, 38.91 ± 2.39 mm; left and right breadths respectively; $OI = 84.39 \pm 5.55$). These data suggest that the females in our population of Sinhalese Sri Lankans had more rounded orbits than the males, whilst male orbits tended to be broader and more rectangular. In previous studies, OI sexual dimorphism was a feature most frequently seen in African^[9,13,17,20,24] and Egyptian^[2] populations, whereas sexual dimorphism in Indian and other Asian populations^[12,14,15,18,19,21,24-27] were not statistically significant. The existence and extent of OI sexual dimorphism might indicate a history of significant selection pressure that was specific to our population of Sinhalese Sri Lankans.

Comparison of methods between studies

The comparison of data generated in previous studies on OI is difficult due to the diverse nature of the methodologies employed by the various authors. Methods for the studies presented in **Table 2** vary between the use of calipers (digital or manual),^[12,21] measurement from X-ray,^[13,25] calculations from living individuals,^[29] transfer of measurements from a divider to a ruler,^[2] or methods not being clearly enough stated to allow reproduction of the study.^[28] Reliable measurements of orbital dimensions from an X-ray is particularly problematic given the potential for error in generating a measurement of an image (X-ray) that displays a two-dimension representation of a structure that has a three-dimensional morphology (height, width and depth). It is also not clear whether measurements from X-rays were normalized by calibration to account for any possible image distortion. Measurements from living individuals also create difficulty for investigators looking to reliably identify orbital margins and accurately determine maximum breadth and height in each case. In addition, some sample sizes in other studies are very small and may not be representative of the populations studied.^[25] Further, there are no consistently applied guidelines or criteria that studies follow which would allow confidence in the reliability of the measurement of the orbit and subsequent calculation of OI. Although the orbital measurements are recorded by taking the maximum orbital height and breadth, a standardized set of guidelines should be developed and utilized for this purpose to generate consistency of reporting and allow accurate comparison of future data. It is therefore suggested that any comparison between OI data in the presented studies (**Table 2**) be undertaken with caution given the variation in utilised methodologies.

Limitations

There is the potential for older, damaged, or well-handled skulls to be difficult to examine, especially if there is any damage around the orbital margins. None of the skulls used in this study had damage to the orbit that affected the measurement or recording. The sample size was small, in particular for the female skulls; despite this, the data do provide useful information from which to undertake a study with a larger sample size given the confirmation of variation in orbital morphology both between and within sexes. There was the potential for intra-observer variation of the recorded measurements; however, members of the research team oversaw practice of the technique to ensure consistency and repeatability, and the recorder was an anatomist who was experienced in such measurements (*e.g.* bony measurement using digital calipers), thereby minimising the potential for overt measurement errors.

Conclusion

Modern Sinhalese Sri Lankan male orbits can be classified as microseme ($OI < 83$) and female as mesoseme ($OI = 83-89$), which is an unusual finding given many Asian populations are said to have megaseme ($OI > 89$) orbits. This interesting finding thereby challenges previous suggestions regarding ethnic categorization and possible lack of ethnic variation for this morphological measure. Our findings identified the presence of left-right OI asymmetry (left larger than right OI) and sexual dimorphism in this population. This is a feature which has not been identified in neighbouring Indian populations and may be a characteristic unique to contemporary Sinhalese Sri Lankans.

References

1. Xing S, Gibbon V, Clarke R, Liu W. Geometric morphometric analyses of orbit shape in Asian, African, and European human populations. *Anthropological Science* 2013;121:1-11.
2. Fetouh FA, Mandour D. Morphometric analysis of the orbit in adult Egyptian skulls and its surgical relevance. *Eur J Anat* 2014;18:303-15.
3. Kumar SS, Gnanagurudasan E. Morphometry of bony orbit related to gender in dry adult skulls of South Indian population. *International Journal of Health Sciences and Research* 2015;5:207-14.
4. Pires LAS, Teixeira AR, Leite TFO, Babinski MA, Chagas CAA. Morphometric aspects of the foramen magnum and the orbit in Brazilian dry skulls. *International Journal of Medical Research and Health Sciences* 2016;5:34-42.
5. Oladipo GS, Olotu JE, Suleiman Y. Anthropometric studies of cephalic indices of the Ogonis in Nigeria. *Asian J Med Sci* 2009;1:15-17.
6. Evereklioglu C, Doganay S, Er H, Gunduz A, Tercan M, Balat A, Cumurcu T. Craniofacial anthropometry in a Turkish population. *Cleft Palate Craniofac J* 2002;39:208-18.

7. Giles E, Elliot O. Race identification from cranial measurements. *J Forensic Sci* 1962;7:147–57.
8. Lo LJ, Marsh JL, Kane AA, Vannier MW. Orbital dysmorphology in unilateral coronal synostosis. *Cleft Palate Craniofac J* 1996;33:190–7.
9. Munguti J, Mandela P, Butt F. Referencing orbital measures for surgical and cosmetic procedures. *Anatomy Journal of Africa* 2012;1:40–5.
10. Cheng AC, Lucas PW, Yuen HK, Lam DS, So KF. Surgical anatomy of the Chinese orbit. *Ophthal Plast Reconstr Surg* 2008;24:136–41.
11. Rehman KU, Shetty S, Williams R. An orbital depth guide for the repair of the orbital floor. *Br J Oral Maxillofac Surg* 2008;46:338.
12. Kumar A, Nagar M. Morphometry of the orbital region: “Beauty is bought by judgment of the eyes.” *International Journal of Anatomy and Research* 2014;2:566–70.
13. Igbigbi PS, Ebite LE. Orbital index of adult Malawians. *Anil Aggrawal's Internet Journal of Forensic Medicine and Toxicology* 2010;11:1.
14. Kaur J, Yadav S, Singh Z. Orbital dimensions - A direct measurement study using dry skulls. *Journal of Academia and Industrial Research* 2012;1:293–5.
15. Gosavi SN, Jadhav SD, Zambre BR. A study of orbital morphometry in Indian dry skulls. *Asian Journal of Biomedical and Pharmaceutical Sciences* 2014a;4:23–5.
16. Gosavi SN, Jadhav SD, Zambre BR. Orbital morphology with reference to bony landmarks. *Revista Argentina de Anatomia Clinica* 2014b;6:20–5.
17. Anibor E, Ihodae W. Orbital index of adult Binis in Edo State, Nigeria. *International Journal of Forensic Medical Investigation* 2015;2:17–9.
18. Alam MT, Rai R, Singh MK. Orbital dimensions and orbital index of adult human dry skulls: a direct measurement study. *International Journal of Science and Research* 2016;5:523–4.
19. Maharana SS, Agarwal RK. Variations in the dimensions of the orbit in the adult human skull (a dry bone study). *International Journal of Recent Biotechnology* 2015;3:20–2.
20. Orish CN, Ibeachu PC. Craniometric indices of Nigeria skulls. *International Journal of Anatomy and Applied Physiology* 2016;2:6–13.
21. Mekala D, Shubha R, Rohini Devi M. Orbital dimensions and orbital index: A measurement study on South Indian dry skulls. *International Journal of Anatomy and Research* 2015;3:1387–91.
22. Cornwall J, Stringer MD, Duxson M. The functional morphology of the thoracolumbar transversospinal muscles. *Spine (Phila Pa 1976)* 2011;36:E1053–61.
23. Cornwall J, Samarakoon L, Antony DJ, Dias GJ. Morphological and degenerative changes in a post-traumatic bifid mandibular condyle. *Anatomy* 2014;8:27–31.
24. Hwang K, Baik SH. Surgical anatomy of the orbit of Korean adults. *J Craniofac Surg* 1999;10:129–34.
25. Novita M. Facial, upper facial, and orbital index in Batak, Klaten, and Flores students of Jember University. *Dental Journal (Majalah Kedokteran Gigi)* 2006;39:116–9.
26. Patil GV, T Shishirkumar, D Apoorva, Sharif J, Sheshgiri C, Sushanth NK. Study of orbital index in human dry skulls of South Indian origin. *Int J Health Sci Res* 2014;4:125–8.
27. Narasinga RB, Pramila PM. A study of orbital index in dry skulls of North Coastal Andhra Pradesh. *International Journal of Basic Applied Medical Sciences* 2015;5:1–3.
28. Ukoha U, Egwu OA, Okafor IJ, Oguagu PC, Onwudingo O, Udemezie OO. Orbital dimensions of adult male Nigerians: a direct measurement study using dry skulls. *Int J Biol Med Res* 2011;2:688–90.
29. Ebeye OA, Otikpo O. Orbital index in Urhobos of Nigeria. *IOSR Journal of Dental and Medical Sciences* 2013;8:51–3.
30. Munguti J, Mandela P, Butt F. Sex differences in the cranial and orbital indices for a black Kenyan population. *International Journal of Medical Sciences* 2013;5:81–4.
31. Dias GJ, Perumal V, Smith C, Cornwall J. The relationship between jugular foramen asymmetry and superior sagittal sinus laterality. *Anthropological Science* 2014;122:115–20.

Online available at:
www.anatomy.org.tr
 doi:10.2399/ana.16.045
 QR code:

deomed®



Correspondence to: George Dias, PhD
 Department of Anatomy, University of Otago,
 PO Box 56, Dunedin, New Zealand
 Phone: +64 3 479 7092
 e-mail: george.dias@anatomy.otago.ac.nz

Conflict of interest statement: No conflicts declared.

This is an open access article distributed under the terms of the Creative Commons Attribution-NonCommercial-NoDerivs 3.0 Unported (CC BY-NC-ND3.0) Licence (<http://creativecommons.org/licenses/by-nc-nd/3.0/>) which permits unrestricted noncommercial use, distribution, and reproduction in any medium, provided the original work is properly cited. *Please cite this article as:* Lal N, Cornwall J, Dias GJ. Orbital indices in a modern Sinhalese Sri Lankan population. *Anatomy* 2016;10(3):205–210.

Macroscopic demonstration of the male urogenital system with evidence of a direct inguinal hernia utilizing room temperature plastination

Victor A. Ruthig^{1,2}, Steven Labrash², Scott Lozanoff², Monika A. Ward^{1,2}

¹*Institute for Biogenesis Research, John A. Burns School of Medicine, University of Hawai'i at Mānoa, Honolulu, HI, USA*

²*Department of Anatomy, Biochemistry and Physiology, John A. Burns School of Medicine, University of Hawai'i at Mānoa, Honolulu, HI, USA*

Abstract

The male urogenital system represents a morphologically complex region that arises from a common embryological origin. However, it is typically studied separately as the excretory system is dissected with the posterior wall of the abdomen while the reproductive features are exposed with the pelvis and perineum dissection. Additionally, the reproductive structures are typically dissected following pelvic and perineal hemisection obviating a comprehensive and holistic examination. Here, we performed a dissection of the complete male urogenital system utilizing a 70-year-old donor and room temperature silicon plastination. Identification of a direct inguinal hernia during the dissection facilitated a unique opportunity to incorporate a common abdominal wall defect into the plastination requiring a novel approach to retain patency of relevant structures. Results showed that the typical structures identified in medical gross anatomy were retained in addition to the hernia. Thus, the described approach and the resulting specimen provide valuable and versatile teaching tools for male urogenital anatomy.

Keywords: direct inguinal hernia; genital; male; reproductive; urogenital

Anatomy 2016;10(3):211–220 ©2016 Turkish Society of Anatomy and Clinical Anatomy (TSACA)

Introduction

In the adult male, the unity between the renal and genital systems and their supporting structures is somewhat subtle. However, the integration of these two systems is quite clear during the embryonic and fetal periods. There is a close developmental association between embryonic kidneys and primitive gonads. Both originate from the intermediate mesoderm in the pelvic region. However, after forming, the embryonic kidneys and testes migrate in opposite directions as their development continues.^[1,2] Between gestational week (gw), 6 and 9 the kidneys ascend into the abdominal cavity.^[1,3] By gw 6, in the male fetus, the primitive gonads are directed towards the testis fate by the Y chromosome, and specifically Y-encoded SRY.^[2,4] The testes descend abdominally between gw 8 to 12.^[2] Once the testes enter the inguinal canal around gw 24, they contribute to the formation of the canal as they migrate inferomedially to enter the scrotum by gw 35.^[5]

The common developmental origin of the kidneys and testes leads to common excretory sites for both systems while their divergent migration patterns result in long testicular vasculature extending from upper-mid abdomen to scrotum.^[1,2] In the adult male, the urethra is the common exit site for products of the kidneys and testes with their accessory glands. There is also a hormonal relationship between these two regions. From an endocrine perspective, the primary source of male testosterone are the Leydig cells of the testis.^[6] However, the adrenal glands that are positioned superior to the kidneys also serve as a source of androgens in the adult.^[7,8]

The common developmental origin of the testes and kidneys results in a persistent link in the adult. Because of this inherent association it seems logical to showcase these two systems in a single urogenital dissection. The involvement of the endocrine system and influence of migration on the vascular systems of these organs during develop-

ment also makes a clear case for maintaining pertinent vasculature with a urogenital dissection. However, general instructional dissection is usually performed regionally such that the kidneys and adrenal glands, and the pelvis and perineum are investigated separately.^[9] This type of division precludes observing the connectivity of structures in these two regions. For example, the typical procedure for viewing the erectile bodies of the penis is achieved through cross-sectional excision of the body.^[9] This approach obscures the longitudinal spatial relationships between the corpus spongiosum and the corpora cavernosa, particularly at the dorsal base of the glans. Likewise, the testes and accessory glands are often dissected as individual components so that the concept of their inherent connectedness is lost to the dissector and viewers.

The other common method for viewing the male genital system follows transverse sectioning at approximately L5 (lumbar vertebra 5) with subsequent hemisectioning of the pelvis. While a hemisection allows the observer an excellent *in situ* view of the main focal points of the male genitalia, the kidneys are often missing from this approach, as well as the vasculature of the testis. At the same time the inclusion of the bones and ligaments of the pelvis obscures spatial relationships between the bladder, prostate, urethra, erectile bodies, and muscles at the bulb and crura of the penis.

A dissection that retains the entire urogenital system and its associated vasculature as one entire unit would allow for a readily apparent comprehensive understanding of the interlinking between the renal and male reproductive systems along with the impact their embryological development has on the accompanying vasculature in the adult.

Here, our first goal was to perform a dissection that maintained connections between urogenital components so that critical spatial relationships between distant regions would be readily apparent. Our second goal was to eliminate non-urogenital structures to facilitate a 360-degree view of the entire system while avoiding organ transection in an effort to maintain normal morphology. Our third goal was to increase the instructional collection of anatomical plastinations for educational purposes among medical and allied medical students at our institution. During the dissection, a left direct inguinal hernia was discovered providing a unique opportunity to successfully preserve a hernia and its patency in the human male. To our knowledge, this study is the first description of plastination of a direct inguinal hernia except what seems to be an anecdotal observation of a hernia at a plastination demonstration.^[10,11] Thus, our fourth and final goal was to devise a method to preserve the direct hernia so that it could be demonstrated within the final plastinated specimen.

Materials and Methods

All procedures were performed in accordance with protocols approved by the biosafety committee at John A. Burns School of Medicine, University of Hawai'i at Mānoa. Human anatomical material was utilized following standard operating procedures.^[12]

Embalming

The body was washed thoroughly using antibacterial soap, with special care paid to the eyes, nose and mouth. The body was elevated above the table surface using body blocks at critical points (neck, shoulders, lumbar region and heels) to avoid constricting arteries in the back and buttocks. Anatomical embalming was a three-day process. Day 1: Embalming cannulas were placed in the carotid arteries directed superiorly into the head and inferiorly into the body. Injection was done at a moderate/high pressure and a slow flow rate (~6-8 oz. per min). The embalming solution consisted of: 1 L formaldehyde, 1 L of methanol, 2.5 L of isopropyl Alcohol, 0.5 L of glycerin and enough water to make 12 L of total embalming solution. There was no blood drainage during the embalming process. Once the head was perfused, cannulas were switched and the body injected with the remainder of the embalming solution. Day 2: 12 L of embalming solution was injected. Day 3: Another 12 L of embalming solution was injected. When the body was adequately perfused, the gluteal region was hypodermically injected to increase overall vascular pressure. The cadaver was placed into a heavy-duty body bag and stored.

Dissection

The dissection protocol was derived from several sources including: Clark's Anatomy and Physiology, Moore's Clinically Oriented Anatomy, Gilroy's Atlas of Anatomy, Tank's Dissector, and The Physiology of Reproduction.^[9,13-17]

Cutaneous tissue removal

Skin was removed from the abdominal, anterior and lateral pelvic, and thigh regions but the skin and fascia of the penis, scrotum and perineum were retained.

Excising the abdomen

An excision was made along the midline of the abdomen that ran from xiphoid process to pubic symphysis. The superior cut was extended laterally following the path of the costal margin. The inferior cut was extended laterally parallel but superior to the inguinal canal medially and superior to the inguinal ligament laterally.

Preparing the abdomen

Once the abdomen was opened, the alimentary canal and associated organs were removed from the abdominal cavity. The abdominal aorta and inferior vena cava were isolated. Both right and left kidney and adrenal glands were identified and the left and right renal arteries and veins were traced back to the abdominal aorta and inferior vena cava, respectively.

Kidneys and vessel release

The kidneys, renal vessels and ureters were manually released from the renal capsule and surrounding fascia while the adrenal attachment with the kidney was preserved. The right and left testicular veins were identified and retained at their origins. A pair of inferior incisions were performed along the internal and external iliac arteries and veins approximately 6 cm distal to their bifurcation at the common iliac artery and vein, respectively. Remaining vessels were removed.

Detachment of the rectum and anus

The legs were maximally abducted and a superficial incision was made that encircled the posterior scrotum. Externally the skin of the perineum was carefully reflected, up to the perimeter of the anus. Internally the connective tissue surrounding the anus and rectum was excised and both structures were removed from the perineum.

Degloving the penis

The skin around the root of the penis was reflected, except for skin of the scrotum. The penis was degloved by cutting the fascia (Buck's fascia) separating the skin from the erectile bodies; attachment to the scrotum was retained to facilitate removal of scrotal skin subsequently. Complete degloving was achieved by releasing the foreskin.

Removing the scrotum and freeing the testes

The skin of the scrotum was removed from the testes by excising the underlying dartos fascia. Care was taken to preserve the testes and spermatic cord structures including the pampiniform plexus, epididymides and ductus deferentes. Palpation was then used to locate the spermatic cord inside the inguinal canal. Palpation along the path of the spermatic cord was also used to bluntly check for the presence of any hernias. Once each testis was released, the spermatic cord was followed superiorly and loosened manually.

Removal of the urogenital system and vasculature from the body

The testes and spermatic cord were reflected superiorly into the abdominal cavity. Bone cutters were used to excise the left and right superior pubic and ischiopubic

rami. The entire urogenital system and vasculature were then removed from the abdominal and pelvic cavities.

Bone removal and perineal muscle dissection

The bulbospongiosus and ischiocavernosus muscles were separated from the isciopubic ramus as completely as possible, while simultaneously maintaining their connection to the bulb and crura of the penis respectively. The remaining portion of the deep transverse perineal muscle between the base of the penis and prostate was retained in an effort to protect the bulbo-urethral (Cowper's) glands and the intermediate part of (membranous) urethra within. The lateral puboprostatic ligament was identified and preserved. All excess tissue and muscle fragments were removed from the region so that relevant structures including the bulb and crura of the penis with bulbospongiosus, ischiocavernosus, deep transverse perineal, and external urethral sphincter muscles, prostate, urinary bladder, ureters, seminal vesicles and ductus deferentes were all clearly visible.

Dissection of the body of the penis

The remaining fascia was removed from the body of the penis. Care was taken to preserve the deep dorsal vessels of the penis. The fascia between the glans of the penis and corpora cavernosa was teased away facilitating separation of the corpora cavernosa from corpus spongiosum and glans.

Dissection of the body of the penis

Adipose and minor tissue remnants were removed from the surface of the bladder, seminal vesicles, and prostate. At the apex of the prostate, the deep transverse perineal muscle was delicately dissected revealing the bulbo-urethral glands and membranous urethra.

Inguinal hernia

During the dissection a direct inguinal hernia on the left side was discovered at the inferomedial margin of the medial inguinal fossa (Hesselbach's triangle). The protocol was modified slightly to preserve this pathology. The left spermatic cord and inguinal canal were preserved and remained attached to the lateral side of the herniated abdominal peritoneum. The medial side of the hernia was kept in contact with the left lateral portion of the bladder.

Plastination

Following dissection, the urogenital specimen was rinsed overnight in running tap water. A Foley catheter (18 Fr. 5cc) was introduced distally into spongy urethra. The specimen was placed in a chemically resistant bucket with a sealable lid (Gamma lids). Dehydration was performed in an explosion-proof freezer (-25°C, Lab-Line Frigid Cab)

in $\geq 97.5\%$ acetone bath. The percentage of acetone was checked weekly and adjusted to 97.5% after the 1st and the 2nd week and to 99.5% after the 3rd week. After greater than 99% of acetone was achieved, the specimen was considered dehydrated and transferred to room temperature. Degreasing occurred during submersion in acetone ($>99\%$ and fresh 100%, 4 weeks each) at room temperature. For impregnation, the specimen was removed from the acetone and submerged into a bath of PR10 silicone solution, NCS10 polymer/NCSVI cross-linker (Silicones, Inc.) diluted 100:8 in water, and placed in a medium sized vacuum chamber attached to an oil-free two-stage vacuum pump (Labport, KNF, Neuberger) at room temperature. Forced impregnation (2 cm Hg) was achieved after 48 hr.

Following impregnation, the specimen was removed from the vacuum chamber, placed on a wire rack, blotted with a paper towel, and allowed to drain for two days. The specimen was lightly coated with NCSIII (catalyst), wrapped in plastic foil and monitored daily. Curing was successfully achieved 30 days after impregnation.

Results

General appearance

The new dissection protocol and the established plastination process used at our institute (*see* Materials and Methods, and for more details) yielded a good quality specimen demonstrating the male urogenital system and associated vasculature (Figures 1 and 2).^[18] The plastination was

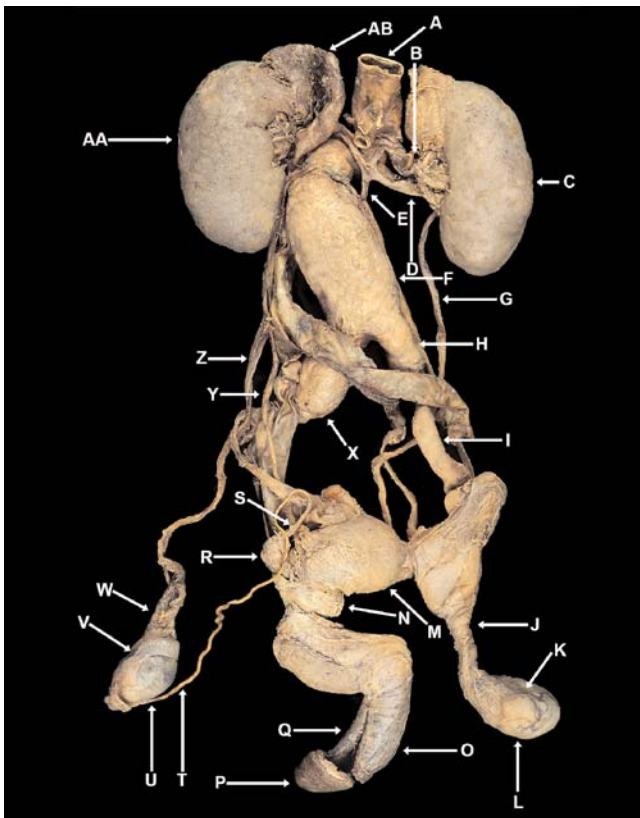


Figure 1. Anterior view of the urogenital system plastination. The structures shown represent a subset of structures required to be identified by medical students performing dissections in Gross Anatomy Laboratory listed in Table 1. A: abdominal aorta; B: left renal artery; C: left renal vein; E: left testicular vein; F: abdominal aorta aneurysm; G: left ureter; H: left common iliac artery; I: left external iliac artery; J: spermatic cord; K: anterior scrotal artery/vein; L: spermatic fascia/parietal layer tunica vaginalis; M: bladder; N: prostate; O: corpus cavernosum; P: glans penis; Q: corpus spongiosum and spongy urethra patent within; R: seminal vesicle; S: ampulla of ductus deferens; T: ductus deferens; U: testis/visceral layer tunica vaginalis/tunica albuginea; V: epididymis; W: pampiniform plexus; X: right common iliac artery aneurysm; Y: right ureter; Z: right testicular artery/vein; AA: right kidney; AB: right adrenal gland. [Color figure can be viewed in the online issue, which is available at www.anatomy.org.tr]

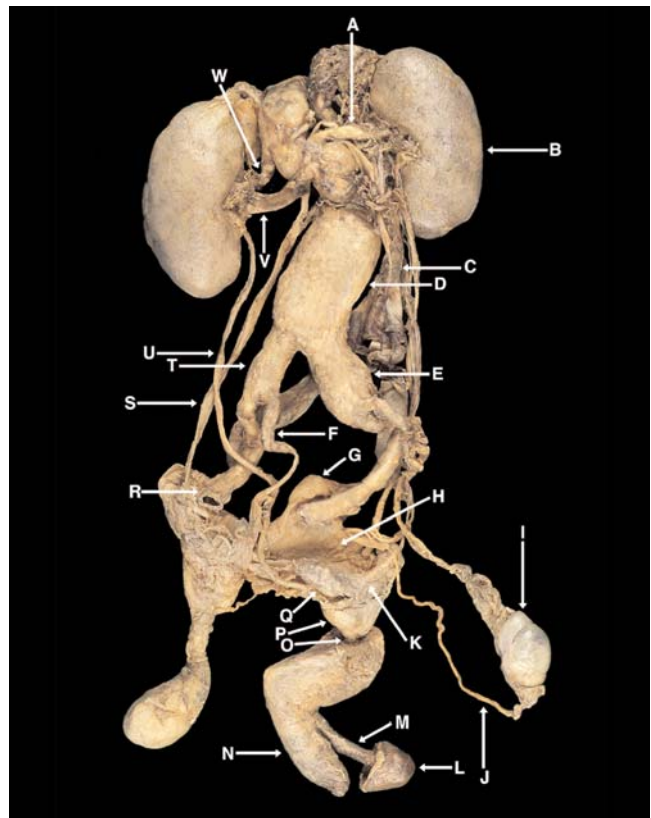


Figure 2. Posterior view of the urogenital system plastination. The structures shown represent a subset of structures required to be identified by medical students performing dissections in Gross Anatomy Laboratory listed in Table 1. A: right renal artery; B: right kidney; C: right renal vein; D: abdominal aorta aneurysm; E: right common iliac artery aneurysm; F: left internal iliac artery; G: median umbilical ligament of bladder; H: fundus of bladder; I: epididymis; J: ductus deferens; K: ejaculatory duct; L: glans penis; M: corpus spongiosum with spongy urethra patent within; N: corpus cavernosum; O: membranous urethra; P: prostate; Q: seminal vesicle; R: left external iliac artery; S: left testicular artery/vein; T: left common iliac artery; U: left ureter; V: left renal vein; W: left renal artery. [Color figure can be viewed in the online issue, which is available at www.anatomy.org.tr]

urable, and smaller vessels maintained their general shape (Figure 3, top and bottom right). The placement of a catheter in the urethra before plastination successfully kept the spongy urethra patent within the corpus spongiosum, which maintained shape (Figure 3, bottom left). The relationship of the erectile bodies and the muscles at their prox-

imal end was demonstrated while maintaining the overall structure of the penis (Figure 3, bottom left).

Male genital organs and glands

The vasculature of the testis at its superior pole retained shape. All three segments of the epididymis were clearly

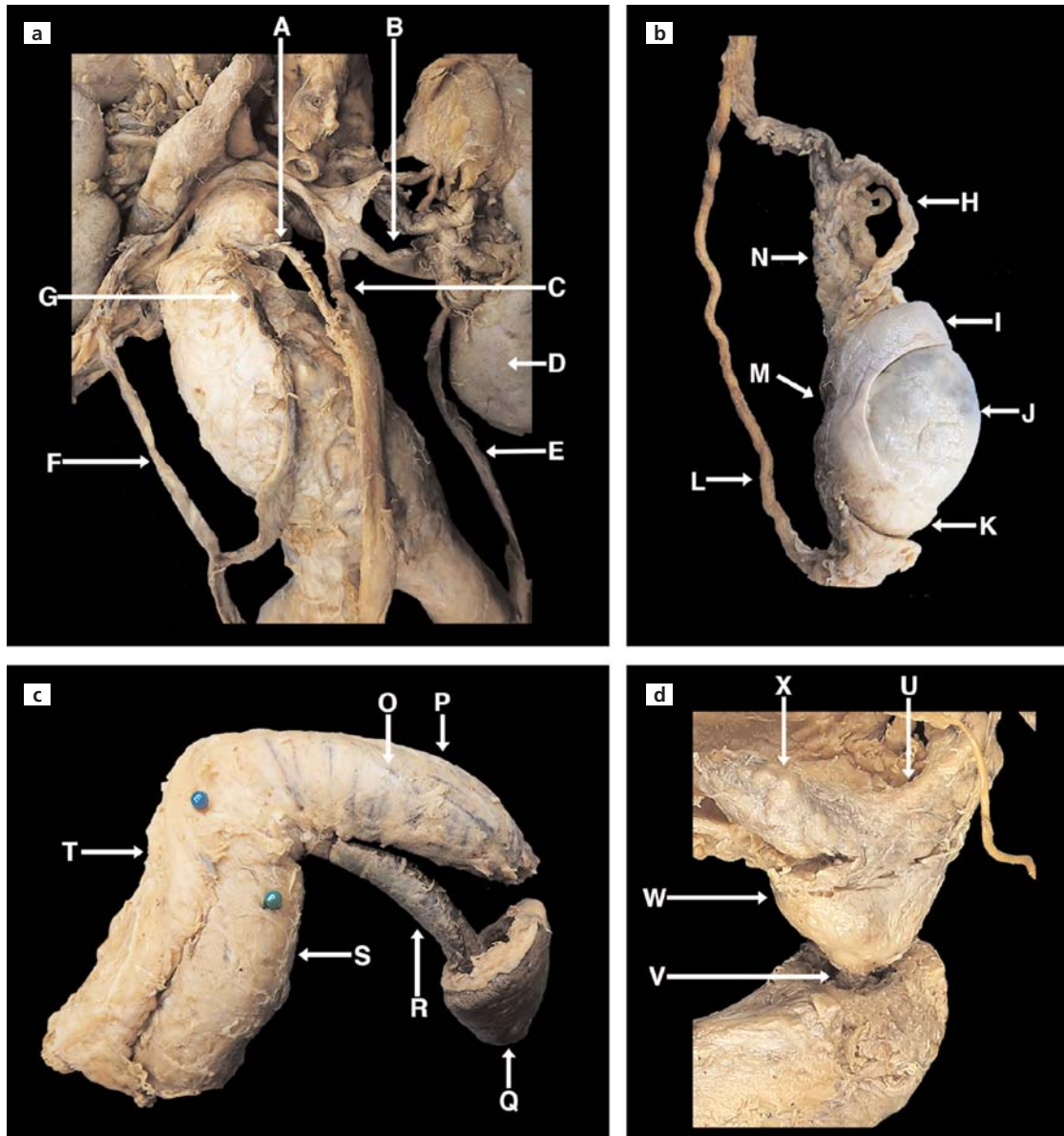


Figure 3. Higher magnification of selected structures. (a) The superior portions of testicular vasculature as they relate to renal structures. (b) A lateral view of the right testis showing the scrotal contents viewable when the spermatic fascia is removed. (c) The penis: the erectile muscles, erectile bodies and deep venous structures superficial to the corpora cavernosa. Specifically highlighting the association of the corpus spongiosum and the glans penis as the spongy urethra traverses the center of both structures. (d) Male reproductive glands and associated structures. A: left testicular artery; B: left renal vein; C: left testicular vein; D: left kidney; E: left ureter; F: right testicular vein; G: right testicular artery; H: testicular artery; I: caput epididymis; J: testis; K: caudate epididymis; L: ductus deferens; M: corpus epididymis; N: pampiniform plexus; O: deep dorsal vein of the penis; P: corpus cavernosum; Q: glans penis; R: corpus spongiosum; S: bulbospongiosus muscle (green pin head); T: ischiocavernosus muscle (blue pin head); U: right ejaculatory duct; V: membranous urethra; W: prostate; X: left seminal vesicle. [Color figure can be viewed in the online issue, which is available at www.anatomy.org.tr]

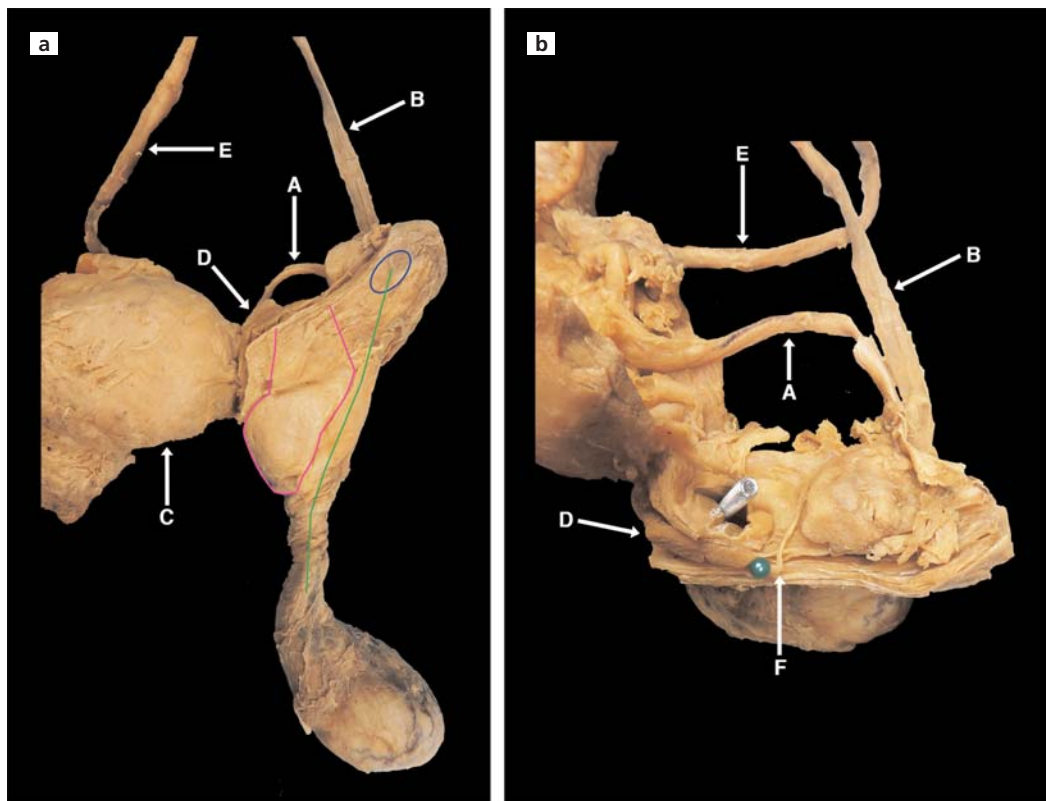


Figure 4. Demonstration of direct inguinal hernia and validity of the technique used to preserve pathology. (a) Left anterior view demonstrating path of abdominal peritoneum herniation (pink) in relation to spermatic cord (green) and deep inguinal ring (blue). (b) Left superior view demonstrating location of abdominal peritoneum herniation (needle) in relation to inferior epigastric artery and rectus abdominus muscle (green pin head). A: ductus deferens; B: testicular artery and vein; C: bladder; D: rectus abdominus muscle (green pin head); E: ureter; F: inferior epigastric artery. [Color figure can be viewed in the online issue, which is available at www.anatomy.org.tr]

visible as they follow the curvature of the posterior testis and direct sperm to the ductus deferens. The seminal vesicles and prostate along with the ejaculatory duct between them were maintained (Figure 3, top right). Most likely due to its small size and delicacy, the bulbo-urethral gland was inadvertently removed with the external urethral sphincter muscle during dissection to reveal the membranous urethra (Figure 3, bottom right).

Pathologies

The direct inguinal hernia remained patent after plastination (Figure 4). The abdominal peritoneum formed a thickened outer sheath and protruded laterally and inferiorly; however, it remained distinct from the inguinal canal and its contents (Figure 4, left). The herniated peritoneal pouch retained a position lateral to the urinary bladder and medial to the deep inguinal ring and protruded into the medial inguinal canal adjacent to the spermatic cord as the spermatic cord approached the superficial inguinal ring (Figure 4, left). The hernia also projected anteriorly

towards the anterior abdominal wall, but remained posterolateral to the rectus abdominus muscle (Figure 4, right). Thus, it protruded slightly medial to the medial inguinal fossa (Hesselbach's triangle). Distortion and closure of the hernia during plastination was prevented possibly due to the abnormal thickening of the peritoneum as well as the retention of its connections extraperitoneally (Figure 4, right). The retention of the spermatic fascia also preserved the anterior scrotal artery and vein (Figure 1).

After dissection it was obvious that a large abdominal tumor had caused extensive deformation of the abdominal aorta. The tumor and associated fibrous tissue covered the length of the abdominal aorta and common iliac arteries while further binding these vasculature structures to a fibrous mass that encased parts of the stomach, pancreas and large intestine. The same region also seemed to have suffered an abdominal aortic aneurysm (Figures 1 and 2). Despite these obstacles, the vasculature was maintained, though it appeared somewhat morphologically abnormal. The origins of the right and left testicular arteries and ter-

mination of the right and left testicular veins were intact and visible (Figure 3, top left).

Efficacy as a teaching tool

The plastination was assessed for instructional relevancy by determining the number of structures that could be identified compared to a standard list of structures required for observation by medical students during gross anatomy dissection of the abdomen and pelvis and perineum (Table 1). Typically, many prosections and plastinations are necessary to cover all of the structures on the list. However, over 50% of the structures on the list were identified on the single plastinated specimen generated in this study. Over one-third of the structures absent from

the specimen were either nerves that were not on the dissection or structures that would require transecting part of the dissection to be visible. The latter was specifically not performed to maintain the general morphology of the structures that were highlighted in the dissection.

Discussion

Here, we detailed an alternative way of dissecting the renal and male genital systems. Dissection was followed by a plastination method that can be used to preserve the specimen for years of instructional use. We produced a complete urogenital dissection that has been removed from the abdomen and pelvis in such a way that connections between components are readily apparent in a 360°

Table 1
Efficacy of specimen as teaching tool.

Male Urogenital Relevant Structures from MS1 Identify List*	
Structure Present (Figure #)	Structure Not Present
Adrenal gland (1)	Artery of the bulb (penis/vestibule)
Ampulla of ductus deferens (1)	Artery to ductus deferens
Bulbospongiosus m (3 bottom left)	Bulbo-urethral glands
Corpus cavernosum (3 bottom left)	Deep artery of the penis
Corpus spongiosum (3 bottom left)	Deep transverse perineal m
Deep dorsal vein of the penis (3 Bottom left)	Dorsal artery of the penis
Ductus deferens (1, 2, 3 top right, 4)	Dorsal nerve of penis/clitoris
Ejaculatory ducts (3 bottom right)	Ganglion of sympathetic trunk
Epididymis (1, 3 top right)	Internal pudendal artery
Fundus of bladder (2)	Internal urethral orifice [†]
Glans penis (1, 2, 3 bottom left)	Pelvic splanchnic nerves
Internal iliac artery (2)	Posterior scrotal/labial nerve
Ischiocavernosus m (3 bottom left)	Prostatic urethra [†]
Kidney (1, 2)	Prostatic duct [†]
Median umbilical ligament of bladder (2)	Prostatic plexus of veins
Membranous urethra (3 bottom right)	Prostatic capsule
Pampiniform plexus (1, 3 top right)	Prostatic utricle
Penis (3 bottom left)	Rete testis [†]
Prostate (1, 2, 3 bottom right)	Scrotum
Renal artery (1, 2)	Seminal colliculus
Renal vein (1, 2, 3 top left)	Seminiferous tubules [†]
Seminal vesicle (1, 2, 3 bottom right)	Sphincter urethrae [†]
Spermatic cord (1, 4 left)	Spongy urethra [†]
Testicular artery (1, 3 top, 4)	Trigone of bladder [†]
Testicular vein (1, 3 top, 4)	Tunica dartos
Testis (1, 3 top right)	Ureteric orifice [†]
Tunica albuginea (1)	Urethral artery
Tunica vaginalis (1)	
Ureter (1, 2, 3 top left, 4)	
Urinary bladder (1, 4 left)	
Total 30/57	Total 27/57
52.6%	47.4%

*Structures present on specimen were compared to the male urogenital relevant vocabulary list of structures typically required to be identified by medical students performing dissections in Gross Anatomy Laboratory. [†]Internal structure that requires transection of the prosection for viewing (in general transection was counter to the purpose of this dissection (see Results, Efficacy as a teaching tool).

view. This represents a valuable alternative to regional dissections, which treat the component parts as separate entities; or pelvic hemisection, which can at times omit components or mute their spatial relationships.

Thorough dissection of the erectile bodies after removal of the fascia encasing them (Buck's fascia) was a conscious dissection decision. This approach allowed for a much better understanding of the continuity between the corpus spongiosum and glans, while concurrently demonstrating the termination of the corpora cavernosa distally at the proximal end of the dorsal glans. These relationships cannot be studied when the penis is simply excised cross-sectionally midway along the body.

Tissue dehydration occurs as a result of the plastination process thus raising concerns regarding the retention of urethral morphology. Catheterization was performed in an attempt to overcome this problem. However, success was limited since the proximal portion could not be reached and the urethra lacked patency at its origin. Future efforts will utilize smaller tubing or perhaps something solid such as a rounded flexible plastic rod so that the entire length of the urethra can be catheterized with ease.

The demonstration of bladder morphology did not achieve expectations since the bladder became compacted unexpectedly during plastination. Despite this compaction, structures such as the fundus and median umbilical ligament of the bladder were visible. Future attempts may utilize packing or inflating the bladder, via a small incision, to maintain its shape.

Preservation of the testicular vasculature all the way to arterial origin at the abdominal aorta, and venous termination at either the inferior vena cava or the left renal vein was another significant component of the dissection. The decision to not transect the spermatic cord or its contents allowed similarities and differences between testicular vasculature to be observed. Specifically, the strong 90° angle of the left testicular vein at the left renal vein is anatomically divergent from the much more acute angle the right testicular vein forms with the inferior vena cava. This left-right disparity is linked to a higher prevalence of varicocele, a common male reproductive pathology affecting the pampiniform plexus, on the left side.^[19]

The fortuitous finding of a direct inguinal hernia necessitated divergence from our original dissection agenda. The presence of the direct inguinal hernia gave us an excellent opportunity to demonstrate a common male pathology from an anatomical viewpoint. When strategizing how best to preserve the pathology, the decision was made to forgo transection of the testis ipsilateral to the direct inguinal hernia. The intention was that by retaining the spermatic fascia and tissue around the inguinal canal,

the identifying features of the direct inguinal hernia would remain readily apparent after plastination.

About 75% of abdominal hernias in adults occur in the inguinal canal. A recent study found there were 770,000 cases in the United States during 2003, accounting for about 5% of Americans with a 9:1 male to female ratio.^[20-22] Examining for the presence of a hernia is typically performed as part of a routine physical for males and about 25% of American men are expected to have a medically recognizable inguinal hernia.^[23] Due to this prevalence, hernia repair has become the most common routine surgical procedure for general surgeons and is divided between two surgical treatments: mesh-free repair or tension-free mesh repair.^[20,24,25]

According to a recent randomized study of men who had asymptomatic or minimally symptomatic inguinal hernias 53% were indirect (i.e. entering the inguinal canal laterally via the spermatic cord and deep inguinal ring) and 41% were direct.^[26] Generally, indirect inguinal hernias are more prevalent in young men and boys while direct inguinal hernias are more prevalent in older men.^[27,28] Indirect inguinal hernia at a young age is most often due to persistent patency of the of processus vaginalis after development, while direct inguinal hernia in the elderly is thought to be linked to compromised integrity of the abdominal wall at the medial inguinal fossa (Hesselbach's triangle).^[27-31] Treatment of either kind of inguinal hernia is the same from a surgical perspective, but classification distinguishing between direct and indirect inguinal hernia, is still a dominant part of diagnosis.^[32] There is also a growing recommendation to not perform a preoperative diagnosis of direct versus indirect inguinal hernia, as the preoperative diagnosis often does not match the intraoperative findings.^[33,34]

The dissection and plastination technique described above allowed for observation of a clear and classic direct inguinal hernia in the context of surrounding structures and reproductive organs often affected by its presence. Although distinction between direct and indirect inguinal hernia may not be a critical part of preoperative diagnosis, intraoperative distinction is vital for treatment at the correct location. Further, there is still a great deal to be learned about inguinal hernias, especially in light of the continued discourse on proper treatment in regards to hernia recurrence and pain management of this common pathology.^[32,35] If we are afforded an opportunity to plastinate another hernia, it could be prudent to pack the hernia with material that can be removed after plastination to ensure patency of the specimen.

Originally one testis was to be transected from pole to pole after plastination to demonstrate the internal structures. The unexpected appearance of a direct inguinal her-

nia, which we opted to feature in our dissection, necessitated retaining the spermatic fascia and connective tissue of the spermatic cord of the ipsilateral testis. Barring the presence of another testis related pathology in future dissections, one testis will be kept intact while the other will be transected from pole to pole such that internal structures will be visible.

We have previously demonstrated the general effectiveness of plastinations as teaching tools.^[36] The specimen detailed in this manuscript represents a teaching tool with high impact in terms of medical education at our institution. This single specimen allows for viewing of the collection of anatomical structures, investigation of which would usually require two or more specimens. The specific vantage points that are offered by the specimen described here are rarely available to students, who instead work with specimens offering an obstructed view resulting from hemisectioning or visually lacking the relation between urogenital structures as occurs during regional dissection.

To summarize, the new dissection approach resulted in an excellent complete male urogenital dissection with vasculature along with an example of a common male pathology, the direct inguinal hernia. The final plastination enables a viewing perspective of the system from any orientation without obstruction while also enforcing the idea that it is a very connected system despite the spatial separation of its integral parts.

Acknowledgements

The authors thank Beth Lozanoff for assisting in the preparation of Figures 1, 2 and 4 (bottom right) and Michael Nicholas Hancock for assisting in the preparation of Figures 3 and 4 (top and bottom left). The authors are very grateful to Dr. Louis Moreau for expert clinical consultation. The authors wish to thank the altruistic individual who donated his body for the advancement of medical education and research through the Willed Body Program at the University of Hawai'i School of Medicine, Honolulu, HI. This study was funded with a grant from NIH; Grant number: HD072380.

References

- Larsen WJ, Sherman LS. Human embryology: development of the urogenital system. New York (NY): Elsevier Churchill Livingstone; 1993. p. 245.
- Sadler TW. Third to eighth weeks: the embryonic period; Urogenital system. In: Langman's medical embryology. 11th ed. Philadelphia (PA): Wolters Kluwer/Lippincott Williams and Wilkins; 2010. p. 77, 246–8, 260–1.
- du Bois AM. The embryonic kidney. In: Rouiller C, Muller AF, editors. The kidney: morphology, biochemistry, physiology. Vol. 1. New York (NY): Academic Press; 1969. p. 8–11, 48.
- Gubbay J, Collignon J, Koopman P, Capel B, Economou A, Münsterberg A, Vivian N, Goodfellow P, Lovell-Badge R. A gene mapping to the sex-determining region of the mouse Y chromosome is a member of a novel family of embryonically expressed genes. *Nature* 1990;346:245–50.
- Rotondi M, Valenzano F, Bilancioni E, Spano G, Rotondi M, Giorlandino C. Prenatal measurement of testicular diameter by ultrasonography: development of fetal male gender and evaluation of testicular descent. *Prenat Diagn* 2001;21:112–5.
- Chen H, Midzak A, Luo L-d, Zirkin BR. Aging and the decline of androgen production. In: Payne AH, Hardy MP, editors. The Leydig cell in health and disease. Totowa (NJ): Humana Press; 2007. p. 117–31.
- Sanford EJ, Paulson DF, Rohner TJ, Jr., Santen RJ, Bardin CW. The effects of castration on adrenal testosterone secretion in men with prostatic carcinoma. *J Urol* 1977;118:1019–21.
- Georgiadis EI, Matzoros C, Aliferis C, Batrinos M. Are adrenal and testicular androgen levels correlated? *Horm Metab Res* 1992;24:488–91.
- Tank PW. The abdomen; the pelvis and perineum. In: Grant's dissector. 15th ed. Philadelphia (PA): Lippincott Williams and Wilkins; 2013: 89–163.
- Walter T. Body Worlds: clinical detachment and anatomical awe. *Sociol Health Illn* 2004;26:464–88.
- von Hagens G, Tiedemann K, Kriz W. The current potential of plastination. *Anat Embryol (Berl)* 1987;175:411–21.
- Labrash S, Lozanoff S. Standards and guidelines for willed body donations at the John A. Burns School of Medicine, 2007. *Hawaii Med J* 2007;66:72,74–5.
- Clark RK. Your reproductive system; Your urinary system. In: Anatomy and physiology: understanding the human body. Sudbury (MA): Jones and Bartlett Publishers; 2005. p. 267–72, 371–88.
- Moore KL, Dalley AF, Agur AMR. Abdomen; pelvis and perineum. In: Clinically oriented anatomy. 6th ed. Philadelphia (PA): Wolters Kluwer/Lippincott Williams and Wilkins; 2010. p. 181–438.
- Schünke M, Schulte E, Schumacher U. Abdomen and pelvis. In: Gilroy AM, MacPherson BR, Ross LM, editors. Atlas of anatomy. 2nd ed. Stuttgart: Thieme; 2012. p. 124–48.
- Setchell BP, Maddocks S, Brooks DE. Anatomy, vasculature, innervation, and fluids of the male reproductive tract. In: Knobil E, Neill JD, Greenwald GS, Markert CL, Pfaff DW, editors. The physiology of reproduction. 2nd ed. Vol. 1. New York (NY): Raven Press; 1994. p. 1063–175.
- Benson GS. Male sexual function: erection, emission, and ejaculation. In: Knobil E, Neill JD, Greenwald GS, Markert CL, Pfaff DW, editors. The physiology of reproduction. 2nd ed. Vol. 1. New York (NY): Raven Press; 1994. p. 1489–506.
- Henry RW. Silicone plastination of Biological tissue: Room-temperature technique – North Carolina technique and products. *Journal of the International Society for Plastination* 2007;22:26–30.
- Saypol DC, Lipshultz LI, Howards SS. Varicocele. In: Lipshultz LI, Howards SS, editors. Infertility in the male. New York (NY): Churchill Livingstone; 1983. p. 299–313.
- Rutkow IM. Demographic and socioeconomic aspects of hernia repair in the United States in 2003. *Surg Clin North Am* 2003; 83:1045–51.
- Evers BM. Small Bowel. In: Sabiston DC, Townsend CM, editors. Sabiston textbook of surgery: the biological basis of modern surgical practice. 18th ed. Philadelphia (PA): Saunders/Elsevier; 2008. p. 873–916.

22. McIntosh A, Hutchinson A, Roberts A, Withers H. Evidence-based management of groin hernia in primary care - a systematic review. *Fam Pract* 2000;17:442-7.
23. Ruhl CE, Everhart JE. Risk factors for inguinal hernia among adults in the US population. *Am J Epidemiol* 2007;165:1154-61.
24. Conze J, Klinge U, Schumpelick V. Part XIII. Abdominal wall - hernias. In: Holzheimer RG, Mannick JA, editors. *Surgical treatment - Evidence-based and problem-oriented*. München: Zuckschwerdt Verlag; 2001. p. 611-8.
25. Holzheimer RG. Inguinal hernia: classification, diagnosis and treatment - classic, traumatic and Sportsman's hernia. *Eur J Med Res* 2005;10:121-34.
26. Fitzgibbons RJ Jr, Giobbie-Hurder A, Gibbs JO, Dunlop DD, Reda DJ, McCarthy M Jr, Neumayer LA, Barkun JS, Hoehn JL, Murphy JT, Sarosi GA Jr, Syme WC, Thompson JS, Wang J, Jonasson O. Watchful waiting vs repair of inguinal hernia in minimally symptomatic men: a randomized clinical trial. *JAMA* 2006;295:285-92.
27. Ein SH, Njere I, Ein A. Six thousand three hundred sixty-one pediatric inguinal hernias: a 35-year review. *J Pediatr Surg* 2006;41:980-6.
28. Nehme AE. Groin hernias in elderly patients. Management and prognosis. *Am J Surg* 1983;146:257-60.
29. van Wessem KJ, Simons MP, Plaisier PW, Lange JF. The etiology of indirect inguinal hernias: congenital and/or acquired? *Hernia* 2003;7:76-9.
30. Nano M. Technique for inguinal hernia repair in the elderly patient. *Am J Surg* 1983; 146:373-5.
31. Gianetta E, de Cian F, Cuneo S, Friedman D, Vitale B, Marinari G, Baschieri G, Camerini G. Hernia repair in elderly patients. *Br J Surg* 1997;84:983-5.
32. Jenkins JT, O'Dwyer PJ. Inguinal hernias. *BMJ* 2008;336:269-72.
33. Ralphs DN, Brain AJ, Grundy DJ, Hobsley M. How accurately can direct and indirect inguinal hernias be distinguished? *Br Med J* 1980;280:1039-40.
34. Sanjay P, Fulke JL, Shaikh IA, Woodward A. Anatomical differentiation of direct and indirect inguinal hernias: Is it worthwhile in the modern era? *Clin Anat* 2010;23:848-50.
35. Bay-Nielsen M, Nilsson E, Nordin P, Kehlet H. Chronic pain after open mesh and sutured repair of indirect inguinal hernia in young males. *Br J Surg* 2004;91:1372-6.
36. Tamura K, Stickley CD, Labrash SJ, Lozanoff S. Effectiveness of Plastinated anatomical specimens depicting common sports injuries to enhance musculoskeletal injury evaluation education. *Athletic Training Education Journal* 2014;9:174-81.

Online available at:
www.anatomy.org.tr
 doi:10.2399/ana.16.036
 QR code:



deomed®

Correspondence to: Victor A. Ruthig, MD

Institute for Biogenesis Research, John A. Burns School of Medicine,
 University of Hawai'i at Mānoa, Honolulu, HI, USA

Phone: +1 808-956-5556

e-mail: vruthig@hawaii.edu

Conflict of interest statement: No conflicts declared.

This is an open access article distributed under the terms of the Creative Commons Attribution-NonCommercial-NoDerivs 3.0 Unported (CC BY-NC-ND3.0) Licence (<http://creativecommons.org/licenses/by-nc-nd/3.0/>) which permits unrestricted noncommercial use, distribution, and reproduction in any medium, provided the original work is properly cited. *Please cite this article as:* Ruthig VA, Labrash S, Lozanoff S, Ward MA. Macroscopic demonstration of the male urogenital system with evidence of a direct inguinal hernia utilizing room temperature plastination. *Anatomy* 2016;10(3):211-220.

Bifid ribs: a comprehensive review

Andrea Andrea¹, Gabrielle Tardieu², Christian Fisahn^{1,3}, Joe Iwanaga¹,
Rod J. Oskouian^{1,3}, R. Shane Tubbs¹

¹Seattle Science Foundation, Seattle, Washington, USA

²Faculty of Medicine, St. George's University, Grenada, West Indies

³Swedish Neuroscience Institute, Swedish Medical Center, Seattle, Washington, USA

Abstract

Bifid or bifurcated ribs are a rare anatomical anomaly that accounts for approximately 28% of known rib abnormalities. Bifurcation always occurs at the sternal end of the rib and its two extremities are joined to a bifid costal cartilage. The presence of bifid rib is frequently accompanied by other anomalies, although this does not necessarily imply that it cannot occur as an isolated anomaly. The clinical significance of the latter has not been established. There have not been many studies done to investigate bifid rib closely aside from individual case reports, presumably due to the condition's extremely low incidence. However the detection of bifid ribs, though mostly incidental, has been proven advantageous for an early and well-rounded diagnosis. It has also revealed significant preventive benefits especially in the pediatric patient population. This review is written to provide a comprehensive summary of what is known about bifid ribs and incorporate substantial findings from clinical cases that have been reported in past literature.

Keywords: anatomy; bone; developmental; embryology; thorax; variation

Anatomy 2016;10(3):221–227 ©2016 Turkish Society of Anatomy and Clinical Anatomy (TSACA)

Introduction

Anatomical abnormalities of the ribs occur in an average 2% of the population.^[1,2] Bifid rib accounts for 28% of this percentage^[1] (**Figure 1**). When multiple bifurcations occur, they are mostly unilateral, although some bilateral cases have been reported.^[3] Bifurcation is most common at the third or fourth ribs, and occurs more on the right side than the left.^[3–5] Nearly all studies have reported a higher occurrence of bifid rib in males than females,^[4,5] except for one study that was published in 2015. Song et al.^[4] recognized two morphological patterns of bifid ribs: (1) Bifid rib has the appearance of a two-pronged fork with fissured, long and slender bifid space; and (2) bifid rib with a more rounded bifid space. These are coined fork and hole types, respectively.^[4] Song et al.^[4] also proposed the distinction between the developments of the two. The fork type is likely to have developed through the dividing of the rib in the anterior portion, while the hole type formed from the upper branch growing out of the lower branch of the bifurcation.^[4] The basis of the hypotheses was not elaborated upon.

The ribs are derived from the ventral extension of the sclerotomic mesenchyme that forms the vertebral arches.^[6] The entire extension of the thoracic region known as the 'primitive costal arch' undergoes chondrification followed by subsequent ossification and form the ribs.^[6] In a bifid rib, the distal parts of the osseous rib bifurcated at a 60° angle.^[6] Both the upper and lower divisions have their own costal cartilage.^[6] The costal cartilage again fuses to form the trunk that is connected to the sternum.^[6] Multiple cases reported in a study indicated that the upper intercostal space of the bifid rib was narrowed, while the lower intercostal space widened.^[4] It is presumed that the bifid intercostal space was filled with intercostal muscles.^[3,4] The distribution of nerves and blood vessels is relatively constant in all cases: Arterial and venous branches originate from the inner thoracic artery and vein ("upper costal branches") and ran towards the upper branch of the bifid ribs; while intercostal nerves ran along the lower margin of the lower branch instead of bifurcating, leaving the upper branch without an intercostal nerve.^[3,4,7]

Based on the aforementioned uniformity,^[4] put forward several hypotheses regarding the anatomical development of bifid ribs. The following lists the hypotheses along with the observation on which each one is grounded; (1) The upper branch is the abnormal portion of the bifurcation, judging from the fact that the distance from the lower branch is equal to the width of the lower intercostal space; (2) The lower division formed the original rib and the upper division grew out of the lower division, judging from the normal presence of intercostal muscles in the bifid intercostal space; (3) The intercostal muscle in the bifid space originated from muscles of the 3rd intercostal space and was separated from one another by the upper division of the bifurcation, judging from the fact that the artery supplying the bifid space branched from the upper (anterior) intercostal artery; (4) The intercostal nerve distribution, running along the lower margin of the lower division of the bifurcation but absent in the upper division, further strengthens the hypothesis that the lower branch did not grow out of the upper branch; and (5) The direction of growth of a bifid rib is dominantly lateral, rather than medial, judging from the fact that only the lateral portion of the upper division is present.

In 2006, Oostra and Maas^[8] also made a contribution in proposing the origins of bifid rib. They suggested that the anomaly had an early developmental origin, plausibly during the re-segmentation of the sclerotomes that leads to vertebral formation. Unlike other rib anomalies, bifid ribs do not generally co-occur with vertebral defects.^[1] Based on this fact, it is highly likely that the proposed defect in intersclerotomal fusion only concerned the laminar and costal sclerotome derivatives.^[8] In addition, Oostra and Maas^[8] noted a striking resemblance between the combination of anomalies in their case and a mice mutant known as the open brain (opb). The phenotypical features of this mutation include severe malformations of the vertebral column, mostly evident in the upper thoracic region.^[9] As expected, bifid rib is one of these malformations. The homozygously lethal mutation arose from a homozygous stop codon mutation in the Rab23 gene. This had led Oostra and Maas to ponder upon the possibility that a Rab23 mutation is somehow involved in the development of bifid ribs. This conception is indeed intriguing; however no known human developmental defect that is comparable to the opb mutant has been identified.

Chromosomal/Gene Studies

Scientists are divided in their opinion when it comes to the genetic nature of bifid ribs.^[7] Some argued for it



Figure 1. Isolated rib noting a bifid distal end. [Color figure can be viewed in the online issue, which is available at www.anatomy.org.tr]

being pathogenic^[10–12] while others gene-dependent.^[7,13,14] The recurring presence of bifid rib in genetic syndromes has led to the speculation that bifid rib is a gene-controlled pathological malformation.^[7] On the other hand, its extremely low incidence in the general population has suggested otherwise.^[7] The congeniality of bifid ribs is also clouded with uncertainty. It has not been determined whether the development of bifid ribs is pre- or post-natal.^[15]

In many occasions, a bifid rib is detected in the presence of genetic syndromes such as the nevoid basal cell carcinoma, otherwise known as Gorlin syndrome.^[7,13,16] Nevoid basal cell carcinoma syndrome (NBCCS) can be considered the most prominent genetic syndrome with which bifid ribs often co-occurs. The relationship between the rib anomaly and clinical diagnoses has yet to be determined.^[1] NBCCS is an autosomal-dominant disease with poor penetrance that is characterized by multiple basal cell carcinomas, jaw cysts, palmar/plantar pits, spinal/costal abnormalities, and primarily the calcification of the falx cerebri.^[16] In 1960, Gorlin and Goltz first pointed out the occurrence of bifid rib in conjunction with NBCCS and jaw cysts. While acknowledging the challenge in pinning the embryological origins of bifid rib, Gorlin and Goltz proposed the involvement of either a simple pleiotropic gene or multiple closely linked genes.^[11] Gorlin and Goltz^[11] also observed other symptoms that are potentially associated with the disease, such as skin lesions, while identifying the close relationship between the three. The interchangeable use of the designations NBCCS and the newly coined “Gorlin syndrome” has been common ever since.

Mutation in the *PTCH1* gene (the human homologue of the *Drosophila* segment polarity gene *patched*) is identified in 65–80% of individuals with NBCCS.^[16] Due to challenges presented by both the mutation screening itself and its interpretation, other methods such as radiological are commonly used in complementation.^[16] Radiological evaluation is especially valuable in the early diagnosis of NBCCS in the pediatric population before the development of the disease's more prominent clinical features (i.e. jaw cysts, basal cell carcinoma, falx cerebri calcification) develop in the teenage years/early twenties.^[16] While the occurrence of bifid rib is only present in 28% of NBCCS cases, its detection is rendered a crucial part of the syndrome's early diagnosis and can possibly reduce the severity of its long-term complications.^[17]

In 1963, Yunis and Gorlin^[18] took charge of the only published chromosomal study on bifid ribs in the context of NBCCS. They performed a karyotype analysis in family members of 2 unrelated individuals who are affected with Gorlin syndrome. Yunis and Gorlin detected an anomaly in chromosome number 1 in one of the affected individuals, in which an arm of one homologue was longer than the other homologue.^[18] The same anomaly was observed in another 4 (out of 11) members of this individual's family that were involved in the study, yet unaffected by the syndrome.^[18] No chromosome abnormality was observed in any member of the second family, affected or unaffected.^[18] In conclusion of their study, Yunis and Gorlin^[18] attributed the longer arm of the homologue to a partial trisomy with no harmful effect. They ruled the chromosome abnormality as irrelevant to Gorlin syndrome.^[18] While this result is not all too surprising, it is important to keep in mind that the study involved no more than two families. And as the case with all that may appear as trends on such a rare anomaly, careful considerations need to be taken prior to drawing any conclusion. Regardless, it will still be interesting to see the results of a chromosomal study directed more towards bifid rib itself rather than Gorlin syndrome—especially recalling the aforementioned fact that bifid rib is only observed in approximately 28% of reported cases on Gorlin syndrome.^[1]

In favor of the gene-dependent hypothesis, two studies that were done in 1995 reported a possible correlation between a couple mice genes, *Hoxc-9* and *Mrf4*, and the bifurcation at the distal parts of the ribs.^[13,14] The question on whether or not a comparable trend persists in humans has not been investigated. Also supporting this side of the argument, Edgar J. Martin noticed that

the incidence of bifid ribs is significantly higher among Samoans in contrast with other populations.^[15] In 1960, Martin conducted a research in an attempt to shed light on the matter. Samoans are categorized as the native inhabitants of Samoa, an isolated group of islands in the South Pacific.^[15] The population consists of a self-contained ethnic unit of Polynesian ethnicity, numbering about 115,000 around the time of study.^[15] From close examination of the subjects' chest radiography, Martin and his colleagues have found that up to 8.4% Samoan adults were affected by rib abnormalities, though a correlation with other disorder(s) was not identified.^[15,19] By the end of his study, the general factors that might be involved in the development of bifid ribs in general and its high incidence among Samoans remain elusive to Martin. Shifting focus away from the Samoans and back to the general population, Osawa et al.^[7] thought that it is highly unlikely for the anomaly to be gene-controlled. After all, it only affects barely 1% of most populations.^[7] Altogether, this argument seems to have the more acceptable stance that suits the minimal understanding on the nature of bifid ribs.

Symptoms, Complications and Case Studies

There have been a decent number of case reports written worldwide on the diagnoses of bifid ribs, whether as an isolated symptom or in association with other malformations. This section aims to explore and summarize such reports:

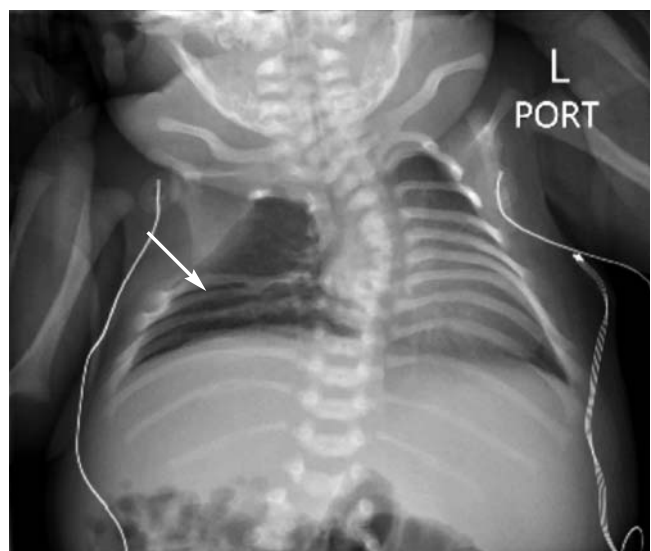


Figure 2. AP chest radiograph of an infant noted to have missing ribs and a bifurcated rib (arrow).

An emphasis will be laid on observations that were obtained from chest radiography (*i.e.* x-ray/roentgenogram) (Figures 2 and 3), mainly during routine check-ups and general physical evaluations. MRI and CT scan (Figure 4) are often utilized to follow up the initial detection of an anomaly.^[20] These supplementary methods have been proven helpful in pinpointing more specific symptoms.^[20-22]

While bifid rib is generally described as asymptomatic, a number of literatures have noted symptoms that were experienced by patients diagnosed with the condition: respiratory difficulty, neurological complaints, chest deformity, chest pain, dyspnea, and hemoptysis.^[6,23] The diagnosis of bifid rib is considered very challenging especially in children with multiple other anomalies, and is therefore often overlooked.^[1]

Radiographic examination of the ribs can yield noteworthy diagnostic clues that point to other diseases.^[20] The diseases that have been reported include, but are not limited to: congenital bone dysplasia, acquired metabolic diseases, iatrogenic conditions, neoplasms, vertebral segmentation, spondylocostal and spondylothoracic dysostosis, and thoracic outlet syndrome.^[1,20] Other studies have identified additional diseases/malformations that can be associated with bifid rib specifically: deficient lateral clavicle, mandibular hypoplasia, macrocephaly, mental retardation, chest wall tumor, and costal fracture.^[4,24] Unlike other rib anomalies, bifid rib usually occurs in the absence of vertebral defects.^[1]

Considering mesodermal origins of the ribs, it is sensible that costal abnormalities are often associated with defects in organs of mesodermal origin such as the heart and kidney.^[1] Cardiac, renal, and urogenital defects are among the most prevalent symptoms associated with rib abnormalities, whether as part of genetic syndromes or isolated congenital malformations.^[1,20] Yet, associated abnormalities in endo- and ectoderm derived structures is also existent. Martinez-Frias et al.^[25] suggested that such phenomenon arises from the disturbance of what was introduced as developmental field, a part of an embryo that coordinately produces identical reaction(s) to various dysmorphogenetic courses. They proposed that its disturbance leads to multiple anomalies that are mostly contiguous, but sometimes distantly located.^[25]

Several case reports featured the detection of bifid rib in deceased individuals. Most of these observations were made following a cadaveric dissection; yet in one particular case, multiple rib bifurcations were detected in a preserved anatomical specimen.^[8] Upon detecting bifid rib(s) during a cadaveric dissection, researchers often



Figure 3. AP chest radiograph of a child noting an incidental bifid rib (arrow).



Figure 4. 3D CT reconstruction of a patient with multiple spine anomalies and also found to have bifid ribs (arrows). [Color figure can be viewed in the online issue, which is available at www.anatomy.org.tr]

noted additional features that could point to NBCCS. However, this does not necessarily mean that the respective individuals were ever diagnosed with the syndrome while living.

Association with Gorlin Syndrome

In 2013, Stickley et al.^[17] discovered bifurcation of the right 4th rib in an 85-year-old female cadaver whose cause of death was identified as brain tumor. The costochondral joints were reportedly present on both superior and inferior portions of the bifid rib. No intercostal muscles or vessels were found within bifurcation. Rather, a single layer of fascia was present – superficial to the rib. A single vein was noted along the posterior inferior portion of the fascia. A narrowed intercostal space in the region of bifurcation was reported in comparison with the left, non-bifurcated ribs.

Song et al.^[4] report was based on the evaluation of three male cadavers (80, 59, and 50-years-old at death). A single bifurcation on the right 4th rib was detected in all three cases. No irregular observation was made regarding the vessel and nerve distribution in the bifid intercostal space(s) in all three cases. As discussed earlier, the bifid intercostal space was filled with intercostal muscles and supplied by the third anterior intercostal artery from the internal thoracic artery. The 4th intercostal nerve ran along the inferior margin of the bifid rib and innervated the intercostal muscles occupying the bifid space. However, in one case, a branch from the 3rd intercostal nerve supplied the bifid space in addition to the 4th intercostal nerve.

Osawa et al.^[7] reported two cases of bifid ribs in two adult Japanese male cadavers. The first case was involved a bifid right 3rd rib. The other revealed a rare case of bilateral bifid ribs of the right 3rd and left 4th ribs. There were no findings indicative of Gorlin syndrome.

Oostra and Maas^[8] reported on the skeleton of a newborn infant found to have bifurcation of the left 2nd to 5th ribs and the right 7th rib. Oostra and Maas considered the possibility of Gorlin syndrome for this case.^[8]

Association with Oral Anomalies and Occasional Skin Lesions

In 1964, Meerkoter and Sheer^[26] reported a case on a 19-year-old female Caucasian patient admitted to the Oral and Dental Hospital of the University of Witwatersrand in Johannesburg, South Africa. The patient initially came in to have her unerupted 3rd molars examined. Her physical evaluation noted the following additional obser-

vations: thoracic and lumbar skin lesions, and congenital cataracts. Her chest film revealed bifurcation on the left 3rd, 4th and 8th ribs, and the right 4th rib.

In 1951, Binkley and Johnson^[27] reported a case on a 30-year-old female Caucasian with multiple dental follicular cysts in both sides of the mandibles. According to the patient's account, the cysts were first detected when she was 16. The report also indicated the presence of innumerable hard papules at various parts of the body. Her chest roentgenogram revealed a bifid 6th rib.

In 1953, Gross^[28] reported a case on a 9-year-old boy with numerous papillary lesions in various areas of the body. The boy was diagnosed with epithelioma adenoides cysticum. Dental cysts were detected on the left side of mandible and maxilla. His chest roentgenogram revealed bifurcated left and right 6th ribs.

In 1960, Gorlin and Goltz^[11] reported a case on a 38-year-old female who ethnically identified as Jewish. She had multiple dentigerous cysts that were first identified when she was 7. Her chest x-ray revealed a bifid left 4th rib.

In 1960, Schamberg^[29] reported a case on an 18-year-old Caucasian with multiple maxillary and mandibular cysts, and multiple basal cell lesions on the skin. X-ray examination revealed bifid left and right 6th ribs.

Miscellaneous Extraordinary Cases

Bifid intrathoracic rib, also known as type II intrathoracic rib, involves bifurcation in the distal portion of the normal rib. This particular anomaly, accounting for 3 out of 41 intrathoracic rib cases, is characterized by an osseous prominence of a rib into the thoracic cavity.^[22] In 2006, Kamano et al.^[22] reported a case on bifid intrathoracic rib in a 21-year-old female. They proposed that the abnormality arose from the anterior-lateral portion of the depressed left 4th rib. Another case of bifid intrathoracic rib was reported by Bottosso and Ghaye in 2008.^[21] This time, the patient was a 79-year-old male who came in for a routine check-up. The abnormality was detected on the 6th rib. In both cases, the evaluation was done by chest radiography and CT scan.

Thoracic outlet syndrome (TOS) is a quite common abnormality with broad symptomology. It is characterized as the compression of subclavian vessels and brachial plexus in the cervicoaxillary region. In 2006, Cagli et al.^[30] reported a case on a 13-year-old girl with TOS that was caused by bifurcation of the first rib. Her chest film revealed bilateral cervical ribs that articulated with the first ribs, distally formed bifid ribs. She was successfully

treated by surgery, excising the variant rib to decompress neural elements.

In 1999, Guttentag and Salwen^[31] presented an unusual variant of bifid rib that involved a cartilaginous duplication of a rib segment that failed to ossify.

In 1926, Bloomberg^[32] reported a case on a 4-year-old with a striking outward appearance, referred to as the “pigeon breast” appearance. His general physical evaluation noted a firm, round prominence of the chest around the level of the 3rd rib on the right of the sternum. The lump was approximately two and a half inches in diameter. His chest roentgenogram revealed bifid right 3rd and 4th ribs. While traditionally the bulging of the chest wall had been solely associated with rickets, Bloomberg attributed this observation to the crowding by the extra costal branch from the bifurcation.

In contrast to the hard lump reported in Bloomberg’s cases, Batra and Lawner^[33] described a “palpable tenderness” during the physical evaluation of a 9-year-old Hispanic girl. She came to the outpatient clinic with complaints on pain in her right chest after a minor fall. Her chest radiography revealed a bifid right 5th rib. The relevance of the pain to the abnormality was not discussed further.

Conclusion

The detection of rib anomalies, while mostly incidental, plays a substantial role in tailoring an appropriate follow-up radiographic and laboratory evaluation. It has been established that the specific type of rib anomaly can help identify and define associated syndromes or malformations, which will in turn provide the patient with a complete and well-rounded diagnosis.^[1] Although bifid rib neither gives rise to severe clinical afflictions nor affects a great proportion of the population, its consideration especially in perspective of associated diseases has demonstrated preventative advantages. Early detection and therefore, prevention, is particularly vital in the pediatric patient population as it can possibly reduce the severity of long-term complications of an associated syndrome. The recommendation to further investigate other internal malformations following the detection of rib anomalies is therefore firmly corroborated.

References

1. Wattanasirichaigoon D, Prasad C, Schneider G, Evans JA, Korf BR. Rib defects in patterns of multiple malformations: a retrospective review and phenotypic analysis of 47 cases. *Am J Med Gen* 2003; 122A:63–9.
2. Silverman FN, Kuhn JP, editors. *Caffey’s pediatric x-ray diagnosis: an integrated/imaging approach*. 9th ed. St. Louis (MO): Mosby; 1993.
3. Rathinasabapathi MK, Perumallapalli HK. Bifid rib: a rare anomaly. *Medical Journal of Dr. D.Y. Patil University* 2015;8:670–1.
4. Song WC, Kim SH, Park DK, Koh KS. Bifid rib: anatomical considerations in three cases. *Yonsei Med J* 2009;50:300–3.
5. Etter LE. Osseous abnormalities in the thoracic cage seen in forty thousand consecutive chest photoroentgenograms. *Am J Roentgenol Radium Ther* 1944;51:359–63.
6. Patil VA, Lal V, Shaikh TP, Narayan P, Deolekar S. A rare case of bilateral bifid ribs: a case report. *International Journal of Research in Medical Sciences* 2014;2:1783–4.
7. Osawa T, Sasaki T, Matsumoto Y, Tsukamoto A, Onodera M, Nara E, Chen J-K, Fujimura A, Nozaka Y. Bifid ribs observed in the third and the fourth ribs. *Kaibogaku Zasshi* 1998;73:633–5.
8. Oostra RJ, Maas M. Bifid ribs and unusual vertebral anomalies diagnosed in an anatomical specimen. *Am J Med Genet A* 2006;140: 2135–8.
9. Spörle R, Schughart K. Paradox segmentation along inter- and intrasomatic borderlines is followed by dysmorphology of the axial skeleton in the open brain (opb) mouse mutant. *Dev Genet* 1998;22:359–73.
10. Schumacher R, Mai A, Gutjahr P. Association of rib anomalies and malignancy in childhood. *Eur J Pediatr* 1992;151:432–4.
11. Gorlin RJ, Goltz RW. Multiple nevoid basal-cell epithelioma, jaw cysts, and bifid rib: a syndrome. *N Engl J Med* 1960;262:908–12.
12. Koutnik AW, Kolodny SC, Hooker SP, Roche WC. Multiple nevoid basal cell epithelioma, cysts of the jaw, and bifid rib syndrome: report of a case. *J Oral Surg* 1975;33:686–9.
13. Suemori H, Takahashi N, Noguchi S. Hoxc-9 mutant mice show anterior transformation of the vertebrae and malformation of the sternum and ribs. *Mech Dev* 1995;51:265–73.
14. Zhang W, Behringer RR, Olsen EN. Inactivation of the myogenic bHLH gene MRF4 results in up-regulation of myogenin and rib anomalies. *Genes Dev* 1995;9:1388–99.
15. Martin EJ. Incidence of bifidity and related rib abnormalities in Samoans. *Am J Phys Anthropol* 1960;18:179–87.
16. Kimonis VE, Mehta SG, DiGiovanna JJ, Bale SJ, Pastakia B. Radiological features in 82 patients with nevoid basal cell carcinoma (NBCC or Gorlin) syndrome. *Genet Med* 2004;6:495–502.
17. Stickley CD, Tamura K, Labrash SJ, Lozanoff S. Bifurcation of the fourth rib as a possible indicator of Gorlin’s syndrome in an 85-year-old female cadaver. *International Journal of Anatomical Variations* 2013;6:86–9.
18. Yunis JJ, Gorlin RJ. Chromosomal study in patients with cysts of the jaw, multiple nevoid basal cell carcinomata and bifid rib syndrome. *Chromosoma* 1963;14:146–53.
19. Rist E, Gally L, Trocme C. L’ossification des cartilages costaux dans l’espèce humaine. *Presse Medicale* 1928;36:641–4.
20. Glass BJ, Norton KI, Mitre SA, Kang E. Pediatric ribs: a spectrum of abnormalities. *Radiographics* 2002;22:87–104.
21. Bottosso N, Ghaye B. Bifid intrathoracic rib. *JBR-BTR* 2008;91:86–7.
22. Kamano H, Ishihama T, Ishihama H, Kubota Y, Tanaka T, Satoh K. Bifid intrathoracic rib: a case report and classification of intrathoracic ribs. *Intern Med* 2006;45:627–30.
23. Kupeli E, Ulubay G. Bony bridge of a bifid rib. *Clev Clin J Med* 2010;77:232–3.

24. Scheepers S, Andronikou S. Beware the bifid rib. *South African Journal of Radiology* 2010;14:104.
25. Martinez-Frias ML, Frias JL, Opitz JM. Errors of morphogenesis and developmental field theory. *Am J Med Genet* 1998;76:291–6.
26. Meerkotter VA, Shear M. Multiple primordial cysts associated with bifid rib and ocular defects. *Oral Surg Oral Med Oral Pathol* 1964; 18:498–503.
27. Binkley GW, Johnson HH Jr. Epithelioma adenoids cysticum: basal cell nevi. agenesis of corpus callosum and dental cysts. *AMA Arch Derm Syphilol* 1951;63:73–84.
28. Gross PP. Epithelioma adenoides cysticum with follicular cysts of maxilla and mandible. *J Oral Surg (Chic)* 1953;11:160–5.
29. Schamberg IL. Basal cell nevi. *Arch Dermatol* 1960;81:269.
30. Cagli K, Ozcakar L, Beyazit M, Sirmali M. Thoracic outlet syndrome in an adolescent with bilateral bifid ribs. *Clin Anat* 2006;19: 558–60.
31. Guttentag AR, Salwen JK. Keep your eyes on the ribs: the spectrum of normal variants and diseases that involve the ribs. *Radiographics* 1999;19:1125–42.
32. Bloomberg MW. Bifurcate ribs - an unusual cause of deformity of the chest. *Can Med Assoc J* 1926;16:807–8.
33. Batra D, Lawner BJ. Bifid fifth rib in a 9-year-old girl with chest pain. *J Am Osteopath Assoc* 2006;106:359–60.

Online available at:
www.anatomy.org.tr
 doi:10.2399/ana.16.034
 QR code:



deomed®

Correspondence to: Joe Iwanaga, DDS, PhD
 Seattle Science Foundation, 550 17th Ave, James Tower,
 Suite 600, Seattle, WA, 98122, USA
 Phone: +1 20673265 00, Fax: +1 2067326599
 e-mail: joei@seattlencefoundation.org

Conflict of interest statement: No conflicts declared.

This is an open access article distributed under the terms of the Creative Commons Attribution-NonCommercial-NoDerivs 3.0 Unported (CC BY-NC-ND3.0) Licence (<http://creativecommons.org/licenses/by-nc-nd/3.0/>) which permits unrestricted noncommercial use, distribution, and reproduction in any medium, provided the original work is properly cited. *Please cite this article as:* Andrea A, Tardieu G, Fisahn C, Iwanaga J, Oskouian RJ, Tubbs RS. Bifid ribs: a comprehensive review. *Anatomy* 2016;10(3):221–227.

Mesenchymal stem cells in skin wound healing

Işıl Aydemir, Şamil Öztürk, Pınar Kılıçaslan Sönmez, Mehmet İbrahim Tuğlu

Department of Histology and Embryology, School of Medicine, Manisa Celal Bayar University, Manisa, Turkey

Abstract

The integrity of healthy skin plays a crucial role in maintaining physiological homeostasis of the human body. Chronic conditions such as diabetes mellitus or peripheral vascular diseases can lead to impaired wound healing. Skin wound healing purposes focusing on the main phases of wound healing, *i.e.*, inflammation, proliferation, epithelialization, angiogenesis, remodeling, and scarring. This is a complex process, which is dependent on many cell types and mediators interacting in a highly sophisticated temporal sequence. Although some interactions during the healing process are crucial, redundancy is high and other cells or mediators can adopt functions or signaling without major complications. Mesenchymal stem cells have an alternative role due to special properties such as the capacity for self-renewal and multi-lineage differentiation, immunomodulatory effect, alleviation of inflammatory response, induction of angiogenesis, regulation of extracellular matrix remodeling, excellent migration and secretion of growth factors and cytokines in wound healing. We summarized current research on the mechanisms of mesenchymal stem cells with their isolation, specific markers, differentiation capacity, and the functional activities to evaluate wound healing application.

Keywords: mesenchymal stem cell; skin; wound healing

Anatomy 2016;10(3):228–234 ©2016 Turkish Society of Anatomy and Clinical Anatomy (TSACA)

Introduction

The skin has a crucial role in protecting the body against external factors, such as mechanical strokes and infections. During the maintenance of the body homeostasis, integrity of skin is provided *via* fluid balance, flexibility, thermal regulation and keratinocytes exhibiting high mitotic activity. The keratinocytes in the basal layer of the skin generate the other epidermal layers and allow tissue renewal. They could fail to provide tissue regeneration in some chronic cases, especially diabetic wounds, peripheral vascular diseases and burn injuries.^[1]

Wound healing is a complex process that depends on the presence of various types of cells, growth factors, cytokines and elements of the extracellular matrix. In condition of wound healing, alternative therapies are attempted such as mesenchymal stem cells because of the loss of skin tissue. For this purpose, stem cells have a potential use in wound healing treatments. Many growth factors such as epidermal growth factor (EGF), fibroblast growth factor (FGF), platelet-derived growth factor (PDGF), transforming growth factor (TGF), and vascular endothelial growth factor (VEGF) are also important

for stem cell behavior in skin wound. The role of stem cells with biological activity of growth factors regulate skin environment during pathological conditions of skin. Therefore, knowledge concerning the mechanisms of wound healing is extremely essential from clinical point of view.^[2]

Studies in recent years have reported various stem cells for chronic wound healing, *e.g.* skin-derived precursor cells (SKPs), epidermal stem cell (EpSCs), amnion-derived mesenchymal stem cells (AMSCs), synovium mesenchymal stem cells (SMSCs), bone marrow-derived stem cells (BMSCs) and adipose-derived stem cells (ASCs). These are effective in cell proliferation, promoting angiogenesis, granulation and immunomodulation. However, the researchers in agreement on the use of the MSCs due to their advantages.^[3–9]

Mesenchymal stem cells (MSCs) have been a subject of an increased interest due to their ability to give rise to most of the tissues and their role in wound healing in organs has been extensively studied. Advances in the mechanism of these cells in promoting wound healing, including alleviation of inflammatory response, induc-

tion of angiogenesis, and promotion of migration of mesenchymal stem cells to the site of tissue injury show their potential use as tissue regenerative cells and tools for gene delivery.^[10]

In the current review, we aimed to summarize the characteristic properties of MSCs and their potential use in skin wound healing clinically. Thereby, as an alternative therapy using MSCs is exhibited with advantages in the dermatology area.

Mesenchymal Stem Cells

The potential of alternative methods to increase migration of MSCs into wound areas has also been demonstrated. Taking advantage of the association between MSCs with M2 macrophages and microRNA, methods to enhance the immunomodulatory capacity of MSCs have been successful. New measures to enhance angiogenic capabilities have also exhibited effectiveness, often demonstrated by increased levels of proangiogenic vascular endothelial growth factor. Also, hypoxia has been shown to have strong wound-healing potential in terms of increasing MSC efficacy.^[11] There are many sources for MSCs such as bone marrow and adipose tissue. BMSCs and ASCs can be obtained practically with surgical operation. Derivation of MSCs from the source necessitate different culture substance such as the use of higher (>10%) concentrations of horse and bovine serum and addition of various hormonal supplements and extracellular matrix (ECM) proteins such as collagen and

fibronectin. Their morphological shape is similar to fibroblasts *in vitro* during confluent stage (**Figure 1**). MSCs represent an extremely rare cell type within the bone marrow, comprising 0.01% to 0.001% of all mononuclear cells, compared to 1% for the hematopoietic stem cell (HSC). This rarity has made the identification of the MSCs niche within the bone marrow difficult, although surface marker expression analysis suggests a perivascular location. MSCs define pluripotent cells including stromal stem cells, multipotent stromal cells, mesenchymal stromal cells, and multipotent adult progenitor cells (MAPC).^[10-12]

Murine multipotent bone marrow MSCs were originally identified by Friedenstein on the basis of their adherence to tissue culture plastic *in vitro*, their ability to form colony-forming unit-fibroblasts (CFU-F) *in vivo*, and their potential for differentiation into adipocytic, osteocytic, chondrocytic, and muscular lineages. They were also shown to be able to differentiate following implantations *in vivo*. Depletion of hematopoietic cell contaminants by elimination of non-adherent cells or by surface marker-based negative selection is also routinely used to separate MSCs from HSCs. They show spindle, star-shaped, and large flattened cell morphology with surface markers indicative of self-renewal and multipotency. The identification of subpopulations of MSCs with varying degrees of commitment to one or more stromal cell types by specific antibodies is common during culture expansion *in vitro*.^[13-15]

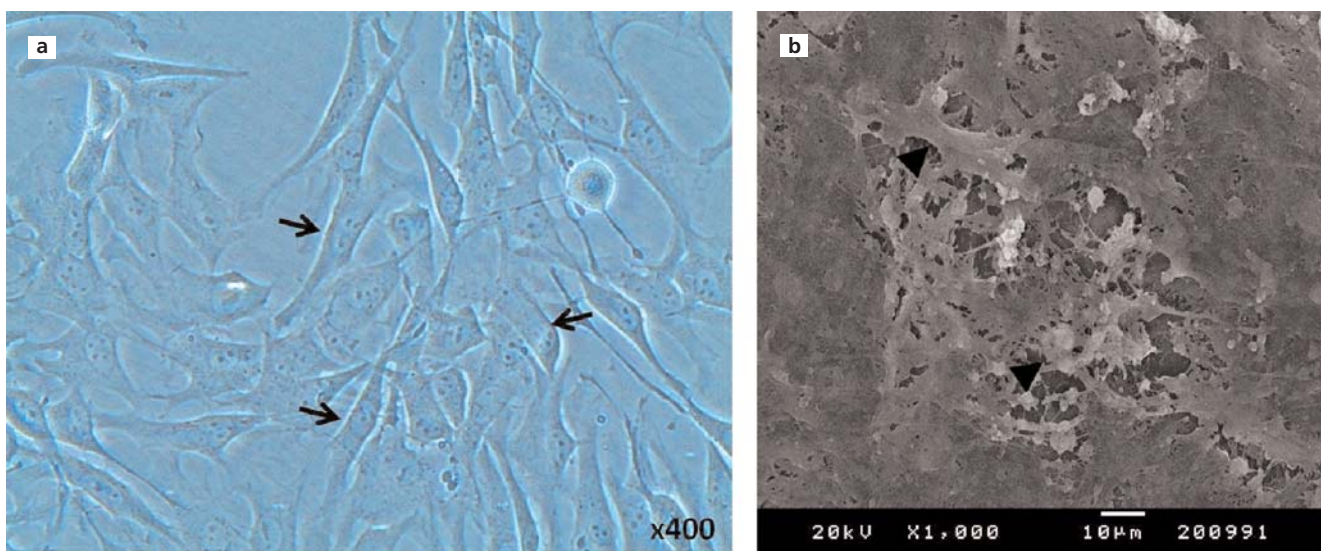


Figure 1. Inverted (a) and scanning electron microscope (b) images of MSCs *in vitro* culture conditions. MSCs were in shape of fibroblast-like on culture flask (a) and titanium disk (b). Arrows and arrow heads: MSCs. Magnification $\times 400$ in a and Scale bar $10\ \mu\text{m}$ in b. [Color figure can be viewed in the online issue, which is available at www.anatomy.org.tr]

MSCs share the expression of a number of key genes with embryonic stem cells (ESCs), namely, the transcription factors OCT-4 and SOX-2, which are involved in the maintenance of pluripotency. Additionally, MSCs are positive for the ESCs surface marker SSEA-4.^[16,17]

Human and murine MSCs are typically negative for hematopoietic markers CD34 and CD45, although freshly isolated MSCs often contain subpopulations of cells that express a low level of these markers (**Figure 2a**). Human MSCs typically are positive for surface markers CD44 (H cell adhesion molecule, HCAM), CD73 (5'-nucleotidase), CD90 (Thy-1 surface antigen), CD105 (endoglin), CD106 (vascular cell adhesion molecule-1, VCAM-1) and STRO-1 (**Figure 2b**).^[18,19] Murine MSCs share this expression pattern, with the exception of STRO-1, but express the stem cell antigen-1 (Sca-1).^[20] New surface markers with high differential expression on MSCs compared to other bone marrow cells have been recently proposed, including low-affinity nerve growth factor receptor (LNGFR/CD271) and integrin alpha-1 (CD49a), both of which have been used to purify a relatively homogeneous population of multipotent cells from bone marrow.^[21]

Differentiation of MSCs into lineage specific cells is controlled by external factors in the environment, including cell-cell and cell-ECM adhesion and cytokine, chemokine, and growth factor availability. A number of genes expressed upon differentiation of MSCs into mature cells of mesenchymal bone marrow lineages such as adipocyte, osteocyte and chondrocyte have been well characterized. The transcription factors RUNX-2 and OSTERIX control the differentiation of osteoblasts and

the formation of bone.^[22,23] Differentiation of MSCs into adipocytes is highly dependent on the peroxisome proliferator-activated receptor gamma (PPAR γ) proteins, as well as the C/CAAT enhancer binding proteins.^[24,25] A number of soluble mediators display powerful effects on MSCs proliferation and differentiation. Bone morphogenic proteins (BMP), which are members of the TGF- β family, stimulate the differentiation of MSCs into osteocytes, chondrocytes, and adipocytes. Selection of a particular lineage is dependent on the receptor engaged, with BMP receptor-IA and -IB inducing adipocyte or osteoblast differentiation, respectively. Additionally, BMP when coupled with Wnt inhibit the proliferation of undifferentiated MSCs. In contrast, transforming growth factor (TGF)- β 1 stimulates the proliferation of MSCs, while suppressing differentiation. TGF- β activates inhibitory Smads which suppress BMP signaling, providing a molecular basis for the antagonistic effects of different TGF- β family members. The Wnt family of proteins influence MSC phenotype through both canonical and non-canonical signaling pathways, but their effect seems concentration dependent. Canonical Wnt3a increases proliferation of MSC, while non-canonical Wnt5a suppresses proliferation, although high levels of canonical Wnt may also have an inhibitory effect. The cytokines interleukin (IL)-1 and tumor necrosis factor (TNF)- α provide another example of antagonistic control over MSC phenotype, as these molecules suppress adipogenesis and enhance osteogenesis through PPAR γ inhibition.^[26] Platelet-derived growth factor (PDGF) mediates the differentiation of MSC into pericytes by activating through the receptors PDGFR- α ,

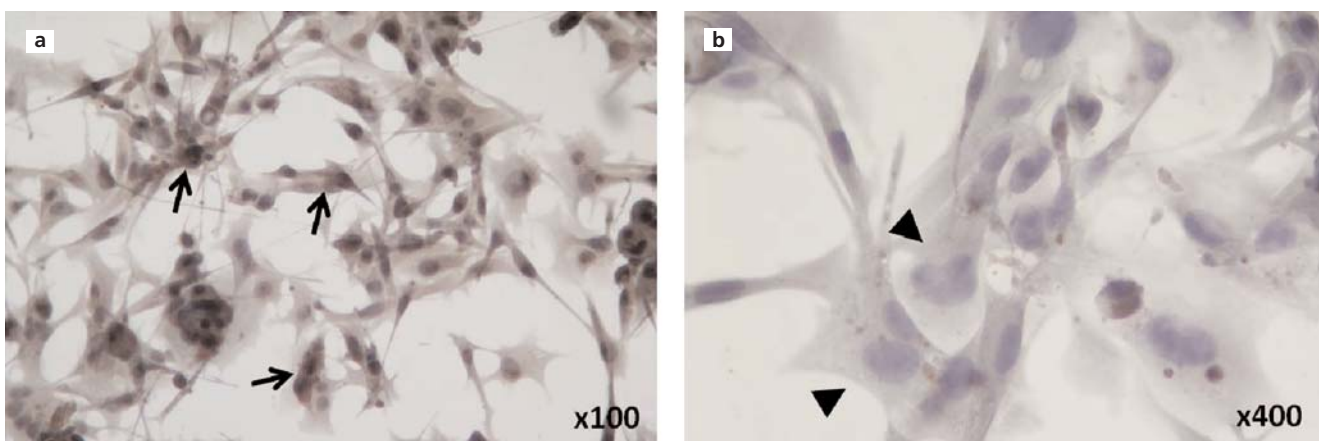


Figure 2. Immunohistochemistry staining of Stro-1 and CD45 in MSCs. MSCs were immunopositivity with Stro-1 (**a**), whereas CD45 staining was negative (**b**). **Arrows:** immunopositive cells, **arrows heads:** immunonegative cells. Magnification $\times 100$ in **a** and $\times 400$ in **b**. [Color figure can be viewed in the online issue, which is available at www.anatomy.org.tr]

ROCK, and the polymerization of α -SMA whereas PDGFR- β signaling inhibits ROCK and promotes α -SMA depolymerization.^[27,28] Characterization, isolation and facilities of MSCs have been defined well, so utilization of MSCs are still attempted.

Wound Healing and MSCs

The complex process of wound healing occurs in overlapping phases, including inflammation, proliferation, angiogenesis, epidermal restoration, and wound contraction and remodeling. As pro-inflammatory reactions play indispensable roles in initiating wound repair, sustained and prolonged inflammation exhibit detrimental effects on skin wound closure. Regeneration processes in wound healing are normally mediated through complex interactions among the extracellular matrix, cells and paracrine factors. Failed or disorganized healing processes caused by one or several impaired mechanisms would lead to difficulty in wound healing in many diseases.^[29]

A number of the therapies developed for chronic wounds, including negative pressure therapy, hyperbaric oxygen therapy, antimicrobial therapy, bioengineered skin equivalents, maggot debridement therapy, growth factors, have limited success. The cell transplantation incorporated in the matrix material or implanted in the wound bed has gained recent interest. The stem and progenitor cells originally thought to replace organ-specific cells have recently been discovered to also deploy their potential for wound healing through chemotaxis of host cells and as a source for cell signaling molecules.^[1,30]

In non-healing wounds, MSCs based therapies have the potential to activate a series of coordinated cellular processes, including angiogenesis, inflammation, cell migration, proliferation and epidermal terminal differentiation. As pro-inflammatory reactions play indispensable roles in initiating wound repair, sustained and prolonged inflammation exhibit detrimental effects on skin wound closure. Regeneration processes in wound healing are normally mediated through complex interactions among extracellular matrix, cells and paracrine factors. Failed or disorganized healing processes caused by one or several impaired mechanisms would lead to difficult-to-heal wounds in many diseases. The beneficial effects of MSC in promoting wound repair have been widely supported by numerous studies.^[31,32]

Prior studies have shown that MSCs can alter the cytokine secretion profile of a variety of immune cells towards anti-inflammatory behaviors. This feature of MSCs likely plays important functions in promoting wound repair beyond the inflammatory phase, and is

particularly useful for inflammation-associated disorders such as infection, diabetes and critical limb ischemia.^[33] Cells can contribute to tissue regeneration by effective and prolonged cytokine secretion at the wound site, immunomodulative properties, and cellular recruitments. Adipose-derived stromal cells (ASCs) have been described since 2002, are easily harvested by a subcutaneous biopsy, have high mesenchymal stem cell density per gram of adipose tissue, and possess differentiation, immunomodulative, and angiogenic properties similar to those of BMSCs. The ability of implanted ASCs to differentiate into endothelial cells was described, as was their capacity to release large amounts of proangiogenic growth factors (particularly SDF-1 α and VEGF).^[34]

Thus, the methods that potentially augment the immunomodulatory functions of MSCs may provide clinical benefits when treating chronic wounds in conjunction with MSCs. In clinical therapies to treat hard-to-heal and chronic lesions, MSCs present a promising opportunity, and fundamental understandings of MSC actions in wound healing are crucial for clinical success. Normal wound healing requires coordinated and dynamic tissue remodeling process, including coagulation and hemostasis, cell migration and proliferation, inflammation, angiogenesis, and extra cellular matrix remodeling. Failed or disrupted healing stages are often seen in chronic wounds due to a variety of underlying disorders, such as diabetes, vascular abnormalities or burns. Previous studies have reported that progenitor cells, particularly MSCs, could improve cutaneous repair, and MSCs could utilize multiple mechanisms to promote wound healing.^[35]

MSCs provide many key growth factors to induce cell migration and proliferation. Particularly, pro-angiogenic factors secreted by MSCs can stimulate the survival, proliferation and branching of vascular cells *in vitro* and *in vivo*. MSC-induced neovascularization through VEGF and bFGF could be a crucial step in directing efficient supplies of the cells required for the effective healing processes. MSCs can also maintain an optimal context for tissue remodeling by dynamically modulating the immune environment. Stem cells have been used successfully to treat both chronic and acute wounds by accelerating wound healing, enhancing re-epithelialization, promoting angiogenesis, exhibiting plasticity, and releasing paracrine signaling molecules. These cells can be delivered to the wounds either directly (*e.g.*, through spraying, injecting, or systemic administration) or *via* skin scaffolds. For example, successful delivery of autologous MSCs using a fibrin spray system directly to acute and chronic wounds in mice and humans has been reported.^[36,37]

MSCs were also shown to increase vascular density in the wounds along with the rate of re-epithelialization. The effect of activin signaling on the homing of stem cells to skin wound has been reported. It was also found that JNK and ERK signaling pathways were involved in activin signaling and eventually the homing of stem cells. The role of stem cells in wound healing has been shown to be performed through several pathways, such as JNK and ERK59, and with the involvement of different factors and mediators, such as KGF-1 and PDGF-BB.^[38]

The properties of the extracellular matrix (ECM) and its contribution to wound-healing changes throughout the lifespan. Younger skin can mount a robust response by producing ECM that can adapt to the mechanical demands of an injury, whereas older skin shows considerable atrophy and a prolonged and blunted healing response with heightened inflammation and differences in signal transduction that results in decrease in ECM production. The healing in older animals also involves a protective and non-inflammatory response characterized by reduced matrix molecule production and reduced scarring. The study about an *in vitro* model of aged rat skin suggests that age-associated disadvantages in healing may arise from overexpression of MMPs, particularly MMP2, consistent with findings that protease expression and activity are increased in older human adults. Age-related changes in hormonal status affect repair. MMPs, particularly MMP2, are elevated principally in older postmenopausal females, and estrogen replacement therapy can stimulate the migration and proliferation of keratinocytes and elaboration of matrix.^[39,40]

The important cell types in this process include platelets which recruit inflammatory cells and form a provisional matrix, and macrophages which include several phenotypes and regulate the cytokine environment in the wound influencing proliferative responses and wound closure. Matrix metalloproteinases (MMPs) are active throughout wound healing, aiding in phagocytosis, angiogenesis, cell migration during epidermal restoration, and tissue remodeling.^[39]

In chronic wounds, resident cells proliferate less and show morphology similar to that seen in senescent cells. Fibroblasts from chronic VLU, particularly ulcers of long duration, show poorer responses to platelet-derived growth factor (PDGF), alterations in transforming growth factor beta (TGF- β) and TGF- β type II receptor expression, and abnormal phosphorylation of key signal transduction proteins. Decreased receptor expression in cells in these wounds is similar to that in cells exposed to low oxygen tension, suggesting chronic wounds are hypoxic.^[41]

There are some FDA-approved cellular treatment products for wound healing. One of them is Gintuit, a product based on an allogeneic cultured keratinocytes and fibroblasts in bovine collagen. It is an allogeneic cellularized scaffold product indicated for topical (non-submerged) application to a surgically created vascular wound bed in the treatment of mucogingival conditions in adults. The active ingredients of GINTUIT are the allogeneic keratinocytes, allogeneic dermal fibroblasts, and bovine Type I collagen. *In vitro* studies have shown that GINTUIT secretes human growth factors and cytokines, and contains extracellular matrix proteins. The efficacy analysis of GINTUIT was based on two six-month, prospective, randomized, within-subject controlled (matched for teeth and gingival condition), treatment comparison clinical trials. Another FDA-approved cellular treatment product is Apligraf. It is a living cell-based product for chronic venous leg ulcers and diabetic foot ulcers. Apligraf is supplied as a living, bi-layered skin substitute. The lower dermal layer combines bovine type 1 collagen and human fibroblasts (dermal cells), which produce additional matrix proteins. The upper epidermal layer is formed by promoting human keratinocytes (epidermal cells) first to multiply and then to differentiate to replicate the architecture of the human epidermis. Unlike human skin, Apligraf does not contain melanocytes, Langerhans' cells, macrophages, and lymphocytes, or other structures such as blood vessels, hair follicles or sweat glands.^[42]

Indeed, the topical application of growth factors in an attempt to heal human chronic wounds has been reported with mixed reviews, highlighting the complexities of the chronic wound pathology. The drug Regranex, a recombinant human platelet-derived growth factor-BB (rhPDGF-BB), is currently the only growth factor with U.S. Food and Drug Administration (FDA) approval for treatment of DFUs, as it has been shown to improve healing in DFUs in randomized clinical trials.^[43]

Stem cells have proven to be a useful tool in cell-based therapies for a wide collection of diseases. For ASCs, the development of detailed and differentiation protocols for various cell types, optimization of *in vivo* delivery methods, and mitigation of immune response in allogeneic transplantations are some of the challenges that need to be overcome. Many of these challenges have been considered and investigated of late, but additional work is necessary in order to bridge the gap between findings in basic science and the clinical treatment of diseases with stem cell-based regenerative medicine.^[44]

Conclusion

In view of these studies, MSCs offer the potential to be used in wound healing. Despite the fact that resources of MSCs are very different, BMSCs and ASCs can be isolated easily from the adults; embryonic sources are proved troublesome in terms of ethics. In addition to their abilities of self-renewal and proliferation, MSCs can promote the cells *in vivo* for migration, angiogenesis, immunomodulation, so these facilities enhance their reliability and allow for their clinical use in dermatology.

References

- Sorg H, Tilkorn DJ, Hager S, Hauser J, Mirastschijski U. Skin wound healing: an update on the current knowledge and concepts. *Eur Surg Res* 2016;58:81–94.
- Pikuća M, Langa P, Kosikowska P, Trzonkowski P. Stem cells and growth factors in wound healing. *Postepy Hig Med Dosw* 2015; 69:874–85.
- Tuca AC, Ertl J, Hingerl K, Pichlsberger M, Fuchs J, Wurzer P, Pfeiffer D, Bubalo V, Parvizi D, Kamolz LP, Lang I. Comparison of Matrigel and atriderm as a carrier for human amnion-derived mesenchymal stem cells in wound healing. *Placenta* 2016;48:99–103.
- Motegi SI, Ishikawa O. Mesenchymal stem cells: the roles and functions in cutaneous wound healing and tumor growth. *J Dermatol Sci Epub* 2016 DOI 10.1016/j.jdermsci.2016.11.005.
- Yao Z, Li H, He W, Yang S, Zhang X, Zhan R, Xu R, Tan J, Zhou J, Wu J, Luo G. P311 accelerates skin wound reepithelialization by promoting epidermal stem cell migration through Rho A and Rac1 activation. *Stem Cells Dev Epub* 2016 Dec 8.
- Tao SC, Guo SC, Li M, Ke QF, Guo YP, Zhang CQ. Chitosan wound dressings incorporating exosomes derived from microrna-126-overexpressing synovium mesenchymal stem cells provide sustained release of exosomes and heal full-thickness skin defects in a diabetic rat model. *Stem Cells Transl Med Epub* 2016 DOI 10.5966/sectm.2016-0275
- Surrao DC, Boon K, Borys B, Sinha S, Kumar R, Biernaskie J, Kallos MS. Large-scale expansion of human skin-derived precursor cells (hSKPs) in stirred suspension bioreactors. *Biotechnol Bioeng* 2016;113:2725–38.
- Shi R, Jin Y, Cao C, Han S, Shao X, Meng L, Cheng J, Zhang M, Zheng J, Xu J, Li M. Localization of human adipose-derived stem cells and their effect in repair of diabetic foot ulcers in rats. *Stem Cell Res Ther* 2016;7:155.
- Rajabian MH, Ghorabi GH, Geramizadeh B, Sameni S, Ayatollahi M. Evaluation of bone marrow derived mesenchymal stem cells for full-thickness wound healing in comparison to tissue engineered chitosan scaffold in rabbit. *Tissue Cell* 2016 Epub DOI 10.1016/j.tice.2016.11.002.
- Prockop DJ. Repair of tissues by adult stem/progenitor cells (MSCs): controversies, myths, and changing paradigms. *Mol Ther* 2009;17:939–46.
- Lee DE, Ayoub N, Agrawal DK. Mesenchymal stem cells and cutaneous wound healing: novel methods to increase cell delivery and therapeutic efficacy. *Stem Cell Res Ther* 2016;7:37.
- Li H, Ghazanfari R, Zacharaki D, Lim HC, Scheduling S. Isolation and characterization of primary bone marrow mesenchymal stromal cells. *Ann N Y Acad Sci* 2016;1370:109–18.
- Owen M, Friedenstein AJ. Stromal stem cells: marrow-derived osteogenic precursors. *Ciba Found Symp* 1988;136:42–60.
- Cakiroglu F, Osbahr JW, Kramer J, Rohwedel J. Differences of cell surface marker expression between bone marrow- and kidney-derived murine mesenchymal stromal cells and fibroblasts. *Cell Mol Biol (Noisy-le-grand)* 2016;62:11–7.
- Battula VL, Tremel S, Bareiss PM, Gieseke F, Roelofs H, de Zwart P, Müller I, Schewe B, Skutella T, Fibbe WE, Kanz L, Bühring HJ. Isolation of functionally distinct mesenchymal stem cell subsets using antibodies against CD56, CD271, and mesenchymal stem cell antigen-1. *Haematologica* 2009;94:173–84.
- Matic I, Antunovic M, Brkic S, Josipovic P, Mihalic KC, Karlak I, Ivkovic A, Marijanovic I. Expression of OCT-4 and SOX-2 in Bone marrow-derived human mesenchymal stem cells during osteogenic differentiation. *Open Access Maced J Med Sci* 2016;4:9–16.
- Kfoury Y, Scadden DT. Mesenchymal cell contributions to the stem cell niche. *Cell Stem Cell* 2015;16:239–53.
- Maleki M, Ghanbarvand F, Reza Behvarz M, Ejtemaei M, Ghadirkhomi E. Comparison of mesenchymal stem cell markers in multiple human adult stem cells. *Int J Stem Cells* 2014;7:118–26.
- Mohammadi Z, Afshari JT, Keramati MR, Alamdari DH, Ganjibakhsh M, Zarmehri AM, Jangjoo A, Sadeghian MH, Ameri MA, Moinzadeh L. Differentiation of adipocytes and osteocytes from human adipose and placental mesenchymal stem cells. *Iran J Basic Med Sci* 2015;18:259–66.
- Baustian C, Hanley S, Ceredig R. Isolation, selection and culture methods to enhance clonogenicity of mouse bone marrow derived mesenchymal stromal cell precursors. *Stem Cell Res Ther* 2015;6: 151.
- Walmsley GG, Atashroo DA, Maan ZN, Hu MS, Zielins ER, Tsai JM, Duscher D, Paik K, Tevlin R, Marecic O, Wan DC, Gurtner GC, Longaker MT. High-throughput screening of surface marker expression on undifferentiated and differentiated human adipose-derived stromal cells. *Tissue Eng Part A* 2015;21:2281–91.
- Liu Y, Strecker S, Wang L, Kronenberg MS, Wang W, Rowe DW, Maye P. Osterix-cre labeled progenitor cells contribute to the formation and maintenance of the bone marrow stroma. *PLoS One* 2013; 8:e71318.
- Lin SS, Ueng SW, Niu CC, Yuan LJ, Yang CY, Chen WJ, Lee MS, Chen JK. Effects of hyperbaric oxygen on the osteogenic differentiation of mesenchymal stem cells. *BMC Musculoskelet Disord* 2014; 15:56.
- Zhang LY, Xue HG, Chen JY, Chai W, Ni M. Genistein induces adipogenic differentiation in human bone marrow mesenchymal stem cells and suppresses their osteogenic potential by upregulating PPAR α . *Exp Ther Med* 2016;11:1853–8.
- Menicainin D, Bartold PM, Zannettino AC, Gronthos S. Genomic profiling of mesenchymal stem cells. *Stem Cell Rev* 2009;5:36–50.
- Xu J, Li Z, Hou Y, Fang W. Potential mechanisms underlying the Runx2 induced osteogenesis of bone marrow mesenchymal stem cells. *Am J Transl Res* 2015;7:2527–35.
- Amos PJ, Mulvey CL, Seaman SA, Walpole J, Degen KE, Shang H, Katz AJ, Peirce SM. Hypoxic culture and in vivo inflammatory environments affect the assumption of pericyte characteristics by human adipose and bone marrow progenitor cells. *Am J Physiol Cell Physiol* 2011;301:C1378–88.
- Ling L, Nurcombe V, Cool SM. Wnt signaling controls the fate of mesenchymal stem cells. *Gene* 2009;433:1–7.
- Portou MJ, Baker D, Abraham D, Tsui J. The innate immune system, toll-like receptors and dermal wound healing: a review. *Vascul Pharmacol* 2015;71:31–6.

30. Frykberg RG, Banks J. Challenges in the treatment of chronic wounds. *Adv Wound Care (New Rochelle)* 2015;4:560–82.
31. Hocking AM. Mesenchymal stem cell therapy for cutaneous wounds. *Adv Wound Care (New Rochelle)* 2012;1:166–71.
32. Li M, Xu J, Shi T, Yu H, Bi J, Chen G. Epigallocatechin-3-gallate augments therapeutic effects of mesenchymal stem cells in skin wound healing. *Clin Exp Pharmacol Physiol* 2016;43:1115–24.
33. Tamama K, Kerpedjieva SS. Acceleration of wound healing by multiple growth factors and cytokines secreted from multipotential stromal cells/mesenchymal stem cells. *Adv Wound Care (New Rochelle)* 2012;1:177–82.
34. Lafosse A, Dufey C, Beauloye C, Horman S, Dufrene D. Impact of hyperglycemia and low oxygen tension on adipose-derived stem cells compared with dermal fibroblasts and keratinocytes: importance for wound healing in type 2 diabetes. *PLoS One* 2016;11:e0168058.
35. Maxson S, Lopez EA, Yoo D, Miagkova AD, LeRoux MA. Concise review: role of mesenchymal stem cells in wound repair. *Stem Cells Transl Med* 2012;1:142–9.
36. Ojeh N, Pastar I, Tomic-Canic M, Stojadinovic O. Stem cells in skin regeneration, wound healing, and their clinical applications. *Int J Mol Sci* 2015;16:25476–501.
37. Tao H, Han Z, Han ZC, Li Z. Proangiogenic features of mesenchymal stem cells and their therapeutic applications. *Stem Cells Int* 2016;2016:1314709.
38. Ghieh F, Jurjus R, Ibrahim A, Geagea AG, Daouk H, Baba BE, Chams S, Matar M, Zein W, Jurjus A. The use of stem cells in burn wound healing: a review. *Biomed Res Int* 2015;2015:684084.
39. Midwood KS, Williams LV, Schwarzbauer JE. Tissue repair and the dynamics of the extracellular matrix. *Int J Biochem Cell Biol* 2004;36:1031–7.
40. Ballas CB, Davidson JM. Delayed wound healing in aged rats is associated with increased collagen gel remodeling and contraction by skin fibroblasts, not with differences in apoptotic or myofibroblast cell populations. Wound repair and regeneration: official publication of the Wound Healing Society [and] the European Tissue Repair Society. 2001;9:223–37.
41. Kim BC, Kim HT, Park SH, et al. Fibroblasts from chronic wounds show altered TGF-beta-signaling and decreased TGF-beta Type II receptor expression. *J Cell Physiol* 2003;195:331–6.
42. Zaulyanov L, Kirsner RS. A review of a bi-layered living cell treatment (Apligraf®) in the treatment of venous leg ulcers and diabetic foot ulcers. *Clin Interv Aging* 2007;2:93–8.
43. Agren MS, Steenfors HH, Dabelsteen S, et al. Proliferation and mitogenic response to PDGF-BB of fibroblasts isolated from chronic venous leg ulcers is ulcer-age dependent. *J Invest Dermatol* 1999;112:463–9.
44. Wankhade UD, Shen M, Kolhe R, Fulzele S. Advances in adipose-derived stem cells isolation, characterization, and application in regenerative tissue engineering. *Stem Cells Int* 2016;2016:3206807.

Online available at:
www.anatomy.org.tr
 doi:10.2399/ana.16.043
 QR code:



deomed®

Correspondence to: Mehmet Ibrahim Tuğlu, MD
 Department of Histology and Embryology, School of Medicine,
 Manisa Celal Bayar University, Manisa, Turkey
 Phone: +90 236 233 07 18, Fax: +90 236 233 14 66
 e-mail: mituglu@yahoo.com

Conflict of interest statement: No conflicts declared.

This is an open access article distributed under the terms of the Creative Commons Attribution-NonCommercial-NoDerivs 3.0 Unported (CC BY-NC-ND3.0) Licence (<http://creativecommons.org/licenses/by-nc-nd/3.0/>) which permits unrestricted noncommercial use, distribution, and reproduction in any medium, provided the original work is properly cited. *Please cite this article as:* Aydemir I, Öztürk Ş, Kılıçaslan Sönmez P, Tuğlu Mİ. Mesenchymal stem cells in skin wound healing. *Anatomy* 2016;10(3):228–234.

Absence of the celiac trunk in a rectal cancer patient: case report

Deniz Tihan^{1,2}, Serdar Babacan², Tuncer Ergin³, Uygur Teomete⁴, Özgür Dandin⁵, İlker Kafa²

¹Department of General Surgery, Şevket Yılmaz Training and Research Hospital, Bursa, Turkey

²Department of Anatomy, School of Medicine, Uludağ University, Bursa, Turkey

³Department of Radiology, Gülhane Military Medical Academy, School of Medicine, Ankara, Turkey

⁴Department of Radiology, Miller School of Medicine, University of Miami, Miami, Florida, USA

⁵Department of General Surgery, Bursa Military Hospital, Bursa, Turkey

Abstract

Trifurcation of the celiac trunk (CT) was first described by Haller in 1756 and named as '*Tripus Halleri*'. It is found as a normal anatomical feature in 85% of the human population in CT images, and variations are observed for the remaining 15%. The rarest CT variation is the absence of CT which is found in 0.4% of the population. Although agenesis of CT is often asymptomatic, this variation should be considered while planning surgical interventions in the abdomen. Hereby, we report a case of the absence of the CT together with independent origin of the left gastric, splenic and common hepatic arteries from the ventral wall of the abdominal aorta.

Keywords: celiac artery; celiac trunk; variation

Anatomy 2016;10(3):235–238 ©2016 Turkish Society of Anatomy and Clinical Anatomy (TSACA)

Introduction

The celiac trunk (CT; celiac artery) the first visceral branch that originates from the abdominal aorta (AA), is a wide and short artery arising just below the aortic hiatus at the level of T12–L1.^[1] Its average length is 1–3 cm and average diameter 5–8 mm.^[2–5]

Trifurcation of the CT was first described by Haller in 1756 and named '*Tripus Halleri*'. Since then it is considered as a normal anatomical form.^[1,3,6] According to Haller, the CT has three branches: common hepatic artery (CHA) which supplies the liver, left gastric artery (LGA) which supplies the stomach, and the splenic artery (SA) which usually arises as tributary elsewhere in this trunk supplying the spleen. The other divisions of CT rarely occur in the human.^[1,3–5]

Variations of the arteries of the CT and their relationship to surrounding structures are of particular importance from a surgical perspective.^[3] Currently, frequent use of diagnostic and interventional radiologic modalities allows clinicians to diagnose such vascular

variations easily.^[7,8] In this case report, we present a rare variation of the CT incidentally diagnosed in a rectal cancer patient.

Case Report

A forty-seven-year-old female patient was admitted to Şevket Yılmaz Training and Research Hospital, Bursa, Turkey with a minimal acute rectal bleeding. She had no significant medical history but non-insulin-dependent diabetes mellitus and 30.8 kg/m² body mass index. Physical examination revealed minimally haematochezia and a markedly elevated CEA level (162.7 ng/mL) was found on blood tests. Colonoscopy was performed and an ulcerated mass was detected at the proximal part of the rectum. The patient underwent biopsy and colorectal adenocarcinoma was diagnosis with histopathological examination. Computed axial tomography scanning was performed to investigate metastasis, and the absence of the CT was found incidentally: the left gastric, splenic and common hepatic arteries were found to arise independently from the anterior wall of the AA (**Figure 1**).

The patient underwent an anterior resection with complete total mesorectal excision. During the exploration, no visceral ischemia was observed due to anomalous pattern of the CT, thus no intervention was performed to the vascular anomaly. The patient was discharged from the hospital on the fourth postoperative day after the anterior resection. After that, she had chemotherapy treatment and no medical or surgical problem due to operation or CT abnormality occurred during her follow-up period. Written informed consent was obtained from the patient for this case report.

Discussion

During embryological development, right and left dorsal aortas spread out into the segments of embryo by giving dorsal, lateral end ventral branches around the fourth week of development. Each segmental artery of the dor-

sal intersegmental arteries of the body wall, lateral splanchnic arteries of the mesonephric ridge and ventral splanchnic arteries of the digestive tube become permanent after forming a single aorta by the fusion of the two dorsal aortas under the fourth thoracal vertebra. Although many of the ventral splanchnic arteries evanesce, three roots (CT, SMA, IMA) in the mesenterium become permanent.^[9,10]

Anatomical variations of the CT and its branching pattern are frequently detected during cadaveric dissections and diagnostic radiological imaging.^[11] Although these variations are usually asymptomatic, they may become important in patients undergoing diagnostic angiography for gastrointestinal bleeding or prior to an operative procedure. They should be considered while planning surgery on the abdominal part of the oesophagus, stomach, duodenum, liver, pancreas, gallbladder and

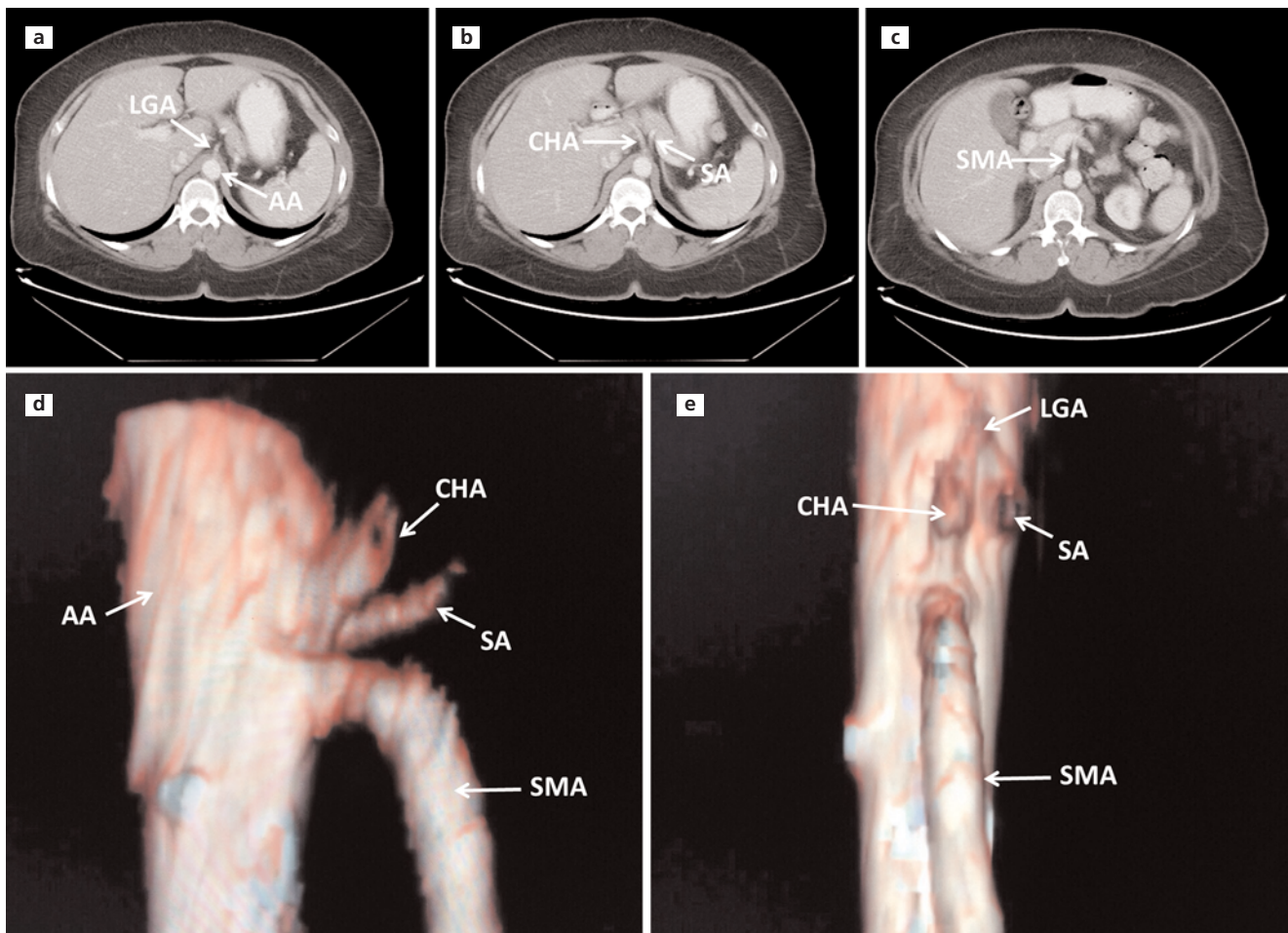


Figure 1. Radiological image of absence of the CT. (a–c) Computed axial tomography images; (d, e) 3D reconstruction of computed axial tomographic angiography. AA: abdominal aorta; CHA: common hepatic artery; LGA: left gastric artery; SA: splenic artery; SMA: superior mesenteric artery. [Color figure can be viewed in the online issue, which is available at www.anatomy.org.tr]

spleen.^[11] Furthermore, with the advance of interventional techniques for hepatic tumors and the increasing frequency of endovascular procedures and advanced hepatopancreatobiliary surgical procedures such as liver transplantation from the living donors accurate depiction of the CT and its branches has become more important.^[5,7,8,11,12]

The anatomical variations of CT have been studied in detailed and classified into six types for the first time in 1928 by Adachi.^[13] However, not all variations of CT branching have been described in Adachi's classification. Studies have shown that the CT can divide into from two to five or even six different branches in very rare cases; furthermore, all three components branch from the AA independently, so the trunk itself may be absent, described as 'agenesis of celiac trunk'.^[3,14,15]

The anatomical variations of CT are due to developmental changes in the ventral splanchnic arteries.^[15] Anatomical variations of the CT, superior mesenteric artery (SMA), and inferior mesenteric artery (IMA) have a considerable input in the diversity of the abdominal arterial supply and several branching patterns at this level have been described; yet, the most important one is the congenital absence of the CT, where the LGA, SA, and CHA arise directly from the AA.^[12]

In 1935, Morita^[16] described the first classification system that included an absent CT as a morphological type and the variational pattern of the arteries. He suggested five types with 15 subtypes. According to this classification, the present anomalous case belongs to Type 5 (*Typus primitivus*), a result of the absence or disappearance of the longitudinal anastomotic channels during the embryonic period, and the four ventral splanchnic arteries grew independently.^[17]

In the article by Zagyapan et al.,^[15] digital subtraction angiography data were collected from 152 consecutive donor patients who underwent orthotopic liver transplantation; there was no absence of the CT amongst these cases.

Vanieratos et al.^[11] examined 77 adult human cadavers. The absence of the CT was detected in two of the 77 cases (2.6%). Ugurel et al.^[18] reported that the CT was absent in one in 100 cases (1%). Prakash et al.^[11] found anatomical variations of the CT in seven of 50 cadavers. The CT was absent in 2.4% of the cases.

In a case report and literature review published by Matusz et al.,^[17] the absence of the CT was reported as varying from 0% to 1.96% in cadaveric dissections, from 0% to 1.11% in surgical findings and from 0.1% to 1% in radiodiagnostic analyses.

Panagouli et al.^[19] searched four databases and collected 36 studies with a total number of 12,196 cases – the largest series in the literature – in 2013. They reported the classical trifurcation in the 89.42% (n=10,906) of the cases and bifurcation of the CT in 7.4% of the pooled samples (n=903). The authors concluded that the rarest variation was the absence of CT with an incidence of 0.38% (n=46).

Babu and Khrab^[20] reported a new classification of the CT including most of the variations reported by authors until that time. They compiled the variations of CT under 16 types. 1. Type I: normal trifurcation; 2. Type IIa: hepatosplenic trunk; 3. Type IIb: hepatogastric trunk; 4. Type IIc: gastrosplenic trunk; 5. Type III: no coeliac trunk; 6. Type IVa: coeliacomesenteric trunk; 7. Type IVb: hepatomesenteric trunk; 8. Type IVc: gastro mesenteric trunk; 9. Type IVd: splenomesenteric trunk; 10. Type IVe: hepatosplenomesenteric trunk; 11. Type IVf: gastrosplenomesenteric trunk; 12. Type V: coeliacolic trunk; 14. Type IVa: coeliophrenic trunk (CT+ CIPA - common inferior phrenic artery); 14. Type IVb: coeliophrenic trunk (CT+ RIPA - right inferior phrenic artery); 15. Type IVc: coeliophrenic trunk (CT+ LIPA - left inferior phrenic artery); 16. Type IVd: coeliophrenic trunk (CT+ RIPA + LIPA). Amongst these variations, the case reported in this study was classified under Type III (Figure 2).

The absence of the CT is mostly asymptomatic. The variations, particularly the absence of CT, have no negative effect for the blood supply of the visceral organs. As a matter of fact, independent CHA, LGA and SA may even prevent a large visceral ischemia which may occur in the situation of a massive thromboembolism of the CT.

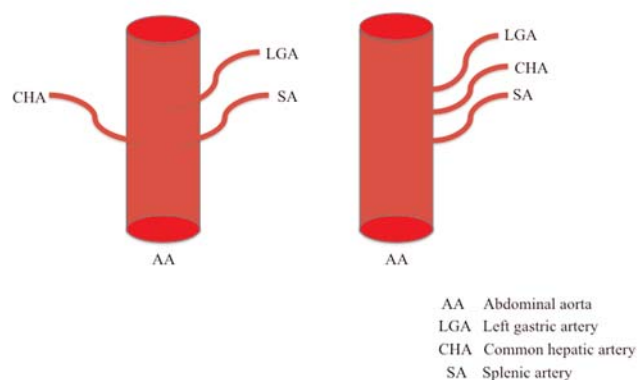


Figure 2. Schematic illustration of the absence of the CT, Type III as described by Babu and Khrab.^[20] AA: abdominal aorta; CHA: common hepatic artery; LGA: left gastric artery; SA: splenic artery. [Color figure can be viewed in the online issue, which is available at www.anatomy.org.tr]

The variations in the originating of the CHA, SA and LGA from the AA should be considered by surgeons and interventional radiologists. They should be kept in mind while planning of intraabdominal and/or retroperitoneal surgical operations.

References

- Venieratos D, Panagouli E, Lolis E, Tsaraklis A, Skandalakis P. A morphometric study of the celiac trunk and review of the literature. *Clin Anat* 2013;26:741–50.
- Malnar D, Klasan GS, Miletic D, Bajek S, Vranic TS, Arbanas J, Bobinac D, Coklo M. Properties of the celiac trunk – anatomical study. *Coll Antropol* 2010;3:917–21.
- Nayak SR, Prabhu LV, Krishnamurthy A, Kumar CG, Ramanathan LA, Acharya A, Sinha AP. Additional branches of celiac trunk and its clinical significance. *Rom J Morphol Embryol* 2008;49:247–9.
- Songür A, Toktaş M, Alkoç O, Acar T, Uzun I, Baş O, Özen OA. Abdominal aorta and its branches: morphometry – variations in autopsy cases. *Eur J Gen Med* 2010;7:321–5.
- Göktay AY, Seçil M, Dicle O. Çölyak trunkus ve hepatic arterlerin normal dallanma varyasyonları: anjiografik bulgular. *Tanışal ve Girişimsel Radyoloji* 2001;7:226–31.
- Yılmaz MT, Tezer M, Cicekbasi AE, Aydın A.D, Salbacak A. A case report of coeliacomesenteric trunk. *Biomedical Research* 2013;24:150–2.
- Özbülül NI. CT angiography of the celiac trunk: anatomy, variants and pathologic findings. *Diagn Interv Radiol* 2011;17:150–7.
- Gorantia VR, Nayak BS, Potu BK. Variations of the celiac trunk and its branches associated with the shift of vascular hilum (porta hepatis) of the liver. *Bratisl Lek Listy* 2012;113:120–2.
- Yalçın B, Kocabıyık N, Yazar F, Ozan H, Özdoğmuş Ö. Variations of the celiac trunk. *Gülhane Tıp Dergisi* 2004;46:163–5.
- Sağiroğlu O, Karakaş S, Ögetürk M, Çetin A, Esen G. Truncus coeliacus ve dalları. *Turgut Özal Tıp Merkezi Dergisi* 1997;4:350–9.
- Prakash, Rajini T, Mokhasi V, Geethanjali BS, Sivacharan PV, Shashirekha M. Coeliac trunk and its branches: anatomical variations and clinical implications. *Singapore Med J* 2012;53:329–31.
- Yi SQ, Terayama H, Naito M, Hirai S, Alimujang S, Yi N, Tanaka S, Itoh M. Absence of the celiac trunk: case report and review of the literature. *Clin Anat* 2008;21:283–6.
- Adachi B. Das arterien system der Japaner. Vol 2. Kyoto: der Kaiserlich Japanischen Universitaet; 1928. p. 18.
- Gielecki J, Zurada A, Sonpal N, Jablonska B. The clinical relevance of coeliac trunk variations. *Folia Morphol (Warsz)* 2005;64:123–9.
- Zagyapan R, Kürkcüoğlu A, Bayraktar A, Pelin C, Aytekin C. Anatomic variations of the celiac trunk and hepatic arterial system with digital subtraction angiography. *Turk J Gastroenterol* 2014;25:104–9.
- Morita M. Reports and conception of three anomalous cases on the area of the coeliac and the superior mesenteric arteries. *Igaku Kenkyu (Acta Med)* 1935;9:159–72.
- Matusz P, Miclaus GD, Ples H, Tubbs RS, Loukas M. Absence of the celiac trunk: case report using MDCT angiography. *Surg Radiol Anat* 2012;34:959–63.
- Uğurel MS, Battal B, Bozlar U, Nural MS, Tasar M, Ors F, Sağlam M, Karademir I. Anatomical variations of hepatic arterial system, celiac trunk and renal arteries: an analysis with multidetector CT angiography. *Br J Radiol* 2010;83:661–7.
- Panagouli E, Venieratos D, Lolis E, Skandalakis P. Variations in the anatomy of the celiac trunk: a systematic review and clinical implications. *Ann Anat* 2013;195:501–11.
- Babu D, Khrab P. Coeliac trunk variations: review with proposed new classification. *International Journal of Anatomy and Research* 2013;1:165–70.

Online available at:
www.anatomy.org.tr
doi:10.2399/ana.16.038
QR code:



deomed®

Correspondence to: Serdar Babacan, MD
Department of Anatomy, School of Medicine,
Uludağ University, Bursa, Turkey
Phone: +90 545 226 46 47
e-mail: sbabacan@uludag.edu.tr

Conflict of interest statement: No conflicts declared.

This is an open access article distributed under the terms of the Creative Commons Attribution-NonCommercial-NoDerivs 3.0 Unported (CC BY-NC-ND3.0) Licence (<http://creativecommons.org/licenses/by-nc-nd/3.0/>) which permits unrestricted noncommercial use, distribution, and reproduction in any medium, provided the original work is properly cited. *Please cite this article as:* Tihan D, Babacan S, Ergin T, Teomete U, Dandin Ö, Kafa İ. Absence of the celiac trunk in a rectal cancer patient: case report. *Anatomy* 2016;10(3):235–238.

Bilateral double parotid ducts: a case report*

Hülya Üçerler, Z. Aslı Aktan İkiz, Fatme Soylu, Narmin Farajiband, Mustafa Deniz Yörük, Pınar Çağmır

Department of Anatomy, School of Medicine, Ege University, Izmir, Turkey

Abstract

The parotid duct is formed by the confluence of two ducts in the gland which ascend and descend at right angle to the main duct. While crossing the masseter muscle, it can receive the accessory parotid duct. Although the anatomical course of this duct is well known, the reports on its normal anatomical variations and morphometry are very few. During routine dissection in the Department of Anatomy of Ege University School of Medicine, double parotid ducts were observed bilaterally in a 72-year-old male cadaver. These were traced carefully and neighboring anatomic structures were demonstrated. The two ducts on both sides merged with each other to form the main parotid duct that had a straight course running horizontally towards the anterior border of the masseter muscle. The length of the main parotid duct was 20.02 mm on the right side and 16 mm on the left side. The distance between tragus and the union point of the double ducts was 52 mm on the right side and 58.72 mm on the left side. Detailed morphometry and location of the double parotid ducts are useful for diagnostic and therapeutic luminal procedures.

Keywords: double parotid duct; parotid duct; parotid gland; sialography; Stensen's duct

Anatomy 2016;10(3):239–241 ©2016 Turkish Society of Anatomy and Clinical Anatomy (TSACA)

Introduction

The parotid gland is the largest salivary gland in the human projecting forwards on the surface of masseter muscle. In 20% of cases, the accessory parotid gland lies between the zygomatic arch above and the parotid duct below. Small ducts from the accessory gland drain into the parotid duct.^[1-3]

The parotid duct, also known as the Stensen's duct after the Danish neuroanatomist Neils Stensen, begins with the confluence of two main tributaries within the anterior part of the gland. It appears at the anterior border of the upper part of the parotid gland and passes across the masseter. The parotid duct turns medially to reach the oral cavity at the anterior border of the muscle. A single duct usually drains the parotid gland.^[1,4-6] This duct is formed by the confluence of the two ducts in the gland which ascend and descend at a right angle to the main duct.^[4] It can receive the accessory parotid duct while crossing the masseter.^[1] The lumen of the parotid duct is about 3 to 4 mm in diameter and its length is about 5 cm.^[1,3,4]

Although the anatomical course of this duct is well known, the reports on its normal anatomical variants and morphometry are very few.^[7] Understanding the variations of the parotid duct is important for the assessment of new diagnostic and therapeutic techniques.^[7] Besides, the proper knowledge of the normal topographic anatomy and variations of the parotid duct provides easy understanding of the analysis of radiographic images and computerized tomographic scans used in sialography.^[3] The aim of current study was to report a rare anomaly of the parotid duct because of its clinical importance for both diagnostic and therapeutic procedures.

Case Report

During routine dissection in the Department of Anatomy, Ege University School of Medicine, bilateral double parotid ducts were observed in a formalin-fixed 72-year-old male cadaver. The cadaver had no trace of scars, adhesions or signs of trauma or operation. All measurements were taken using a stainless steel caliper with an accuracy of 0.02 mm. The dissection was approved by the Ethics Committee of Ege University, School of Medicine and the

*This study has been presented as a poster at the XXIV International Symposium on Morphological Sciences (ISMS) in Istanbul, Turkey in 2015.

study conforms to the provisions of the Helsinki Declaration of 1964 and all subsequent revisions. Parotid ducts on both sides were traced carefully and neighboring anatomical structures were demonstrated. The two ducts on both sides merged with each other and formed the main parotid duct. The duct then had a straight course and ran horizontally towards the anterior border of the masseter (Figures 1 and 2). Diameters were measured from the anterior border of the masseter muscle on both sides (Tables 1 and 2).

Discussion

There are few studies on the surface anatomy of the parotid duct based on cadaver dissections and analyzing sialograms.^[5] The duplication of the parotid duct as a previously unreported anomaly was observed in the dissection laboratory of Ege University School of Medicine by Aktan et al. (2001).^[4] This was a unilateral anomaly, on the right side. The fusion of the upper and lower ducts was outside the gland 4.8 cm beyond their emergence from it. They pierced the buccinator as a single duct. The distance from the union point to the buccinator muscle was 0.7 cm.

Stringer et al.^[5] scanned fifty healthy adults using ultrasound to redefine the surface anatomy of the parotid duct. The duct was on the middle half line between the

Table 1

Double parotid duct measurements on the right and left sides.

	Upper duct Right (mm)	Lower duct Right (mm)	Upper duct Left (mm)	Lower duct Left (mm)
Length	12.14	20.82	10	27.3
Diameter	5.52	5.6	5.98	5.34
Distance between tragus and emergence point	46.2	36.9	47.98	36.8
Distance between zygomatic arch and duct	21.94	27.2	22.74	29.3

Table 2

Measurements of the main parotid duct after fusion of the two ducts on the right and left sides.

	Right (mm)	Left (mm)
Distance between lower border of tragus and center of philtrum	134.5	129.34
Distance between lower border of tragus and labial commissure	96.74	98.64
Length (union point-buccinator piercing)	20.02	16
Distance between lower border of tragus and union point of double ducts	52	58.72

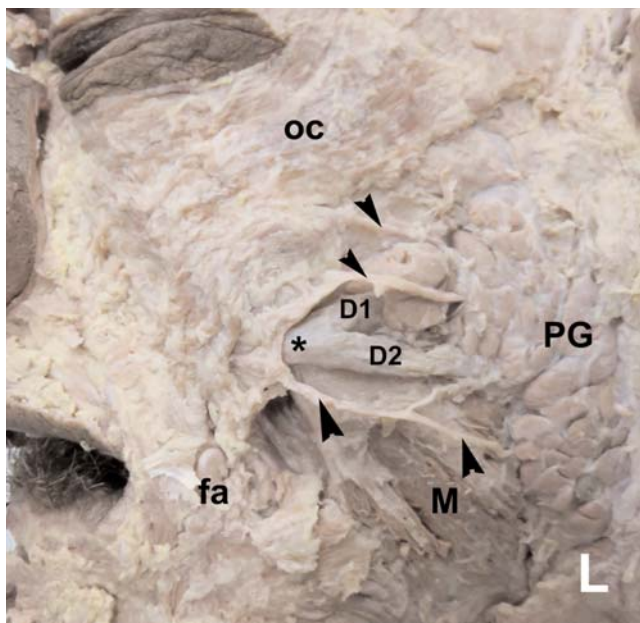


Figure 1. Double parotid ducts (left side). D1: upper parotid duct; D2: lower parotid duct; fa: facial artery; M: masseter muscle; oc: orbicularis oculi muscle; PG: parotid gland, *main parotid duct, arrowheads: facial nerve. [Color figure can be viewed in the online issue, which is available at www.anatomy.org.tr]

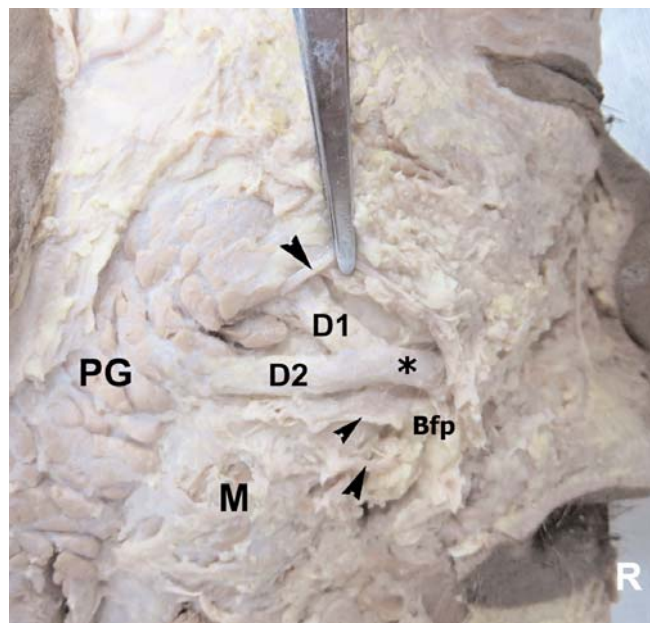


Figure 2. Double parotid ducts (right side). Bfp: buccal fat pad; D1: upper parotid duct; D2: lower parotid duct; M: masseter muscle; PG: parotid gland; *main parotid duct; arrowheads: facial nerve. [Color figure can be viewed in the online issue, which is available at www.anatomy.org.tr]

lower border of the tragus and the cheilion in more than 90% of the individuals. The lower duct was in this region in our cadaver also; the upper duct was not crossing, but over this line. Fernandes et al.^[3] also reported this rare variation of the parotid duct during a dissection on the right side in a 46-year-old male cadaver. The lengths of the superior and inferior ducts were 26.49 mm and 37.25 mm, respectively.

The presence of double parotid ducts can be explained on the basis of development of the parotid gland. The parotid gland arises from the epithelial lining the primitive oral epithelium as an elongated furrow, spreading back towards the ear. It can be recognized in human embryos about 8 mm long, at the sixth week of gestational age. It runs between the mandibular and maxillary prominences, and then converts into a tube and loses its connection with the epithelium of the mouth except its ventral end. It grows dorsally and invaginates into the adjacent mesenchyme in the cheek region. The tube persists as the parotid duct and its blinded end sprouts to several epithelial branches that proliferate to form secretory portion (acini) of the gland at the tenth week of gestational week.^[1,4,8] In cases with double parotid ducts, the epithelial sprout was bifurcated and each branch invaginated into the adjacent mesenchyme separately. These branches made two variant ducts.^[8] Astik and Dave^[2] reported double parotid ducts bilaterally in a 50-year-old male cadaver in 2011 during routine dissection. They reported that the cell-matrix interactions and growth factors had importance on morphogenesis and cyto-differentiation of the parotid gland and development of this variation.

The knowledge of the actual dimensions of the excretory ducts is important in duct endoscopy and lithotripsy.

This variation also has clinical importance for parotid gland surgery and facial cosmetic surgeries.^[2] In CT sialography and CT fistulography, double parotid ducts may be confused with congenital fistula from accessory parotid gland. Additionally, the duct may be severed by a facial laceration and is at risk of iatrogenic injury during facial surgery and injection of botulinum toxin into masseter muscle, because of its superficial location.^[5] To keep in mind the double parotid duct variation will reduce iatrogenic injury risks and improve diagnosis of parotid duct injury.

References

1. Standring S (editor). Gray's anatomy: the anatomical basis of clinical practice. 29th ed. Edinburgh (Scotland): Elsevier Churchill Livingstone; 2005. p. 515–7.
2. Astik RB, Dave UH. Embryological basis of bilateral double parotid ducts: a rare anatomical variation. *International Journal of Anatomical Variations* 2011;4:141–3.
3. Fernandes ACS, Lima RG, Rossi MA, Aguiar MC. Parotid gland with double duct: an anatomic variation description. *Int J Morphol* 2009;27:129–32.
4. Aktan ZA, Bilge O, Pinar YA, İkiz AO. Duplication of the parotid duct: a previously unreported anomaly. *Surg Radiol Anat* 2001;23:353–4.
5. Stringer MD, Mirjalili SA, Meredith SJ, Muirhead JC. Redefining the surface anatomy of the parotid duct: an in vivo ultrasound study. *Plast Reconstr Surg* 2012;130:1032–7.
6. Perrini P, Lanzino G, Parenti GF. Niels Stensen (1638–1686): scientist, neuroanatomist, and saint. *Neurosurgery* 2010;67:3–9.
7. Horsburgh A, Massoud TF. The salivary ducts of Wharton and Stenson: analysis of normal variant sialographic morphometry and a historical review. *Ann Anat* 2013;195:238–42.
8. Hassanzadeh Taheri MM, Afshar M, Zardast M. Unilateral duplication of the parotid duct, its embryological basis and clinical significance: a rare cadaveric case report. *Anat Sci Int* 2015;90:197–200.

Online available at:
www.anatomy.org.tr
doi:10.2399/ana.16.042
QR code:



deomed®

Correspondence to: Hülya Üçerler, MD
Department of Anatomy, Ege University, School of Medicine,
Bornova, Izmir, Turkey
Phone: +90 232 3903993
e-mail: hulyaucerler@gmail.com, hulya.ucerler@ege.edu.tr

Conflict of interest statement: No conflicts declared.

This is an open access article distributed under the terms of the Creative Commons Attribution-NonCommercial-NoDerivs 3.0 Unported (CC BY-NC-ND3.0) Licence (<http://creativecommons.org/licenses/by-nc-nd/3.0/>) which permits unrestricted noncommercial use, distribution, and reproduction in any medium, provided the original work is properly cited. *Please cite this article as:* Üçerler, H, Aktan İkiz, ZA, Soyly F, Farajiband N, Yörük MD, Çağmın P. Bilateral double parotid ducts: a case report. *Anatomy* 2016;10(3):239–241.

Partial corpus callosum agenesis and colpocephaly: a case report*

Ayşegül Güngör Aydın¹, Esat Adıgüzel², Aylin Aksoy³, Kemalettin Acar⁴

¹Department of Neuroscience, Graduate School of Health Sciences, Pamukkale University Denizli, Turkey

²Department of Anatomy, School of Medicine, Pamukkale University, Denizli, Turkey

³Department of Pathology, Council of Forensic Medicine, Antalya, Turkey

⁴Department of Forensic Medicine, School of Medicine, Pamukkale University, Denizli, Turkey

Abstract

Callosal abnormalities are mostly described as central nervous system malformations and can be symptomatic or asymptomatic. Herein, we report an autopsy case of a 50-year-old Syrian immigrant male with poor academic performance, presented with partial agenesis of the corpus callosum and colpocephaly. He was evidently asymptomatic until death. The cause of death was determined to be hypothermia. Autopsy revealed a corpus callosum of 3 cm only in the anterior part. Posterior part of the corpus callosum, anterior, posterior and hippocampal commissures were absent. On coronal sections, inferior horn of the lateral ventricle was dilated. Histopathological examination showed petechial microhemorrhagic areas and congestion in the brain. This case report was presented to demonstrate a good example of corpus callosum agenesis in asymptomatic individuals except for poor academic performance. Furthermore, this is the first corpus callosum agenesis in medical literature encountered during medicolegal autopsy in an adult case.

Keywords: autopsy; corpus callosum agenesis; malformation; poor academic performance; postmortem

Anatomy 2016;10(3):242–245 ©2016 Turkish Society of Anatomy and Clinical Anatomy (TSACA)

Introduction

Corpus callosum (CC) is a flat bundle of axonal fibers that connects the two cerebral hemispheres and forms the roof of the lateral ventricles. It is a major midline structure and comprises of approximately 200 million axons.^[1] Corpus callosum which is completely formed by 18–20th weeks of gestation is one of the latest maturing structures of the brain, and growth is not fully complete until the third decade of life. The formation of sulcus medianus telencephali medii (SMTM), a median groove in the dorsal lamina reuniens, and massa commissuralis, a large cell mass inside the SMTM formation, seem to be critical steps in the development of the corpus callosum.^[2,3] Being exposed to infection, chemical agents and hypoxia during/before or shortly after formation of these structures may likely result in complete or partial agene-

sis of corpus callosum, respectively. Thus, the portion of corpus callosum present in individuals with callosal abnormalities might be taken as an indication of the time of the insult.^[3]

Callosal abnormalities are mostly described as central nervous system (CNS) malformations and can be symptomatic or asymptomatic. The overall incidence of CNS malformations is about 1 in 100 births.^[4] The prevalence of corpus callosum agenesis in the general population is approximately 7 per 1000, but 3 per 100 in the developmentally delayed population. Because callosal agenesis is often asymptomatic, the actual prevalence of corpus callosum agenesis is not clear.^[5,6]

Most cases of abnormal CC were associated with other CNS structural abnormalities like cortical dysplasia,

This work has been presented at the XIV Turkish Neuroscience Congress, May 26–29, 2016, Ankara, Turkey.

dilatation of the occipital horns of the lateral ventricles (colpocephaly), and white matter fibers that developmentally curl back and fail to bridge the two hemispheres (Probst bundles). In addition to these structural anomalies, corpus callosum agenesis is commonly accompanied by other neurodevelopmental abnormalities such as reduced extracallosal white matter volume, abnormalities of the cerebral ventricles, hippocampal commissure, anterior commissure, cerebellar vermis, cerebellar hemispheres and brainstem.^[7,8]

We presented here a case of a man with corpus callosum agenesis who was evidently asymptomatic until death. This case was encountered during routine medicolegal autopsy. He was a Syrian immigrant, there was no information for his medical history. Our limited knowledge about the case was that he had poor academic performance and he was known as gullible, but was able to continue his daily life. This case report was presented to demonstrate a good example of corpus callosum agenesis in asymptomatic individuals except poor academic performance. We discuss the postmortem findings in the light of current knowledge of functional outcomes in individuals with corpus callosum agenesis.

Case Report

The case was a 50-year-old Syrian immigrant male whose medical history was unknown. His body was found in his room by his brother. A medicolegal autopsy was performed according to routine protocols. He was 75 cm in

weight and 165 cm in height, and his appearance was consistent with his stated age. The autopsy revealed no signs related to violent or traumatic cause of death. The postmortem interval was estimated as twelve hours. Brain and brainstem were removed by using standard autopsy techniques and weighed as 1465 g. There were no unusual findings at the skull base. The cerebral hemispheres were symmetrical. The dura and leptomeninges were unremarkable. The morphological examination of brain showed mild congestion and venous distension. The surface of the occipital lobes was collapsed because of colpocephaly. The circle of Willis was usual. The olfactory bulbs and tracts were normal. The brainstem was separated from the cerebral hemispheres by a section at the level of the midbrain. The cerebral hemispheres were bisected along the mid-sagittal plane. The corpus callosum was inspected and photographed at the interhemispheric aspect. The corpus callosum of 3 cm was present only in the anterior part. Posterior part of the corpus callosum, anterior, posterior and hippocampal commissures were absent (**Figure 1**). Two cerebral hemispheres were adherent in the lower part of the medial surface of the frontal lobe. There was no cingulate gyrus, and gyri of temporal lobe run vertically to diencephalon in the medial surface. There were no interhemispheric cysts or tumors. Serial sectioning was performed in the coronal plane at 2 cm interval from the frontal to the occipital poles. Each slice was photographed separately for further evaluation. On coronal sections, inferior horn of the lateral ventricle was

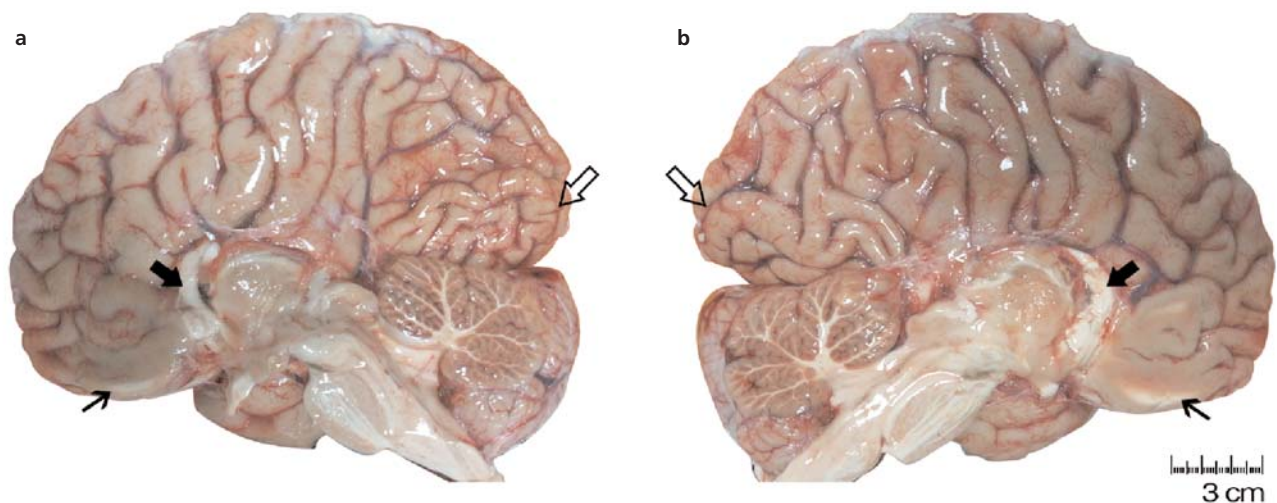


Figure 1. Mid-sagittal aspect of cerebral hemispheres of the case with partial agenesis of corpus callosum. Right cerebral hemisphere (a), left cerebral hemisphere (b). The corpus callosum of 3 cm was present in the anterior part (thick arrows). Posterior part of corpus callosum, anterior, posterior and hippocampal commissures were absent. Two cerebral hemispheres were adherent in the lower part of the medial surface of the frontal lobe (thin arrows). The surface of occipital lobes were collapsed because of colpocephaly (open arrows). [Color figure can be viewed in the online issue, which is available at www.anatomy.org.tr]

dilated and colpocephaly was determined (Figure 2). Left pole of temporal lobe had small cortical lytic-necrotic areas and was disrupted during the dissection. Occipital lobe was thinner than the other lobes. Cerebellum was sectioned along the sagittal plane. The cerebellar folia and dentate nuclei were unremarkable. The aqueduct and the fourth ventricle were of normal configuration, and the spinal cord was normal. Results of routine postmortem toxicological analysis were unremarkable. This case report complies with the current laws of the country (Turkey) in which the study was performed.

Histopathological examination

Routine medicolegal histopathologic examination showed petechial microhemorrhagic areas and congestion in the brain and cerebellum, autolytic changes and areas of focal fat necrosis and fresh microhemorrhage in parenchyma and peripheral adipose tissue of pancreas, autolytic changes in superficial epithelium, mild moderate chronic gastritis, multifocal fresh microhemorrhagic areas, swelling of epithelial cells and vacuolization in focal areas, extremely dilatation and severe congestion in submucosal vessels in the stomach. Considering the findings at autopsy and histopathologic examination, the cause of death was determined to be hypothermia.

Discussion

This is a case study of a 50-year-old man who died due to hypothermia and presented with partial agenesis of the corpus callosum and colpocephaly. Regarding information given by his relative, he could continue his daily life but he had poor academic performance. He immigrated from Syria and was living in poor conditions and poverty recently.

Most of the prevalence studies about corpus callosum agenesis were performed using neuroimaging techniques such as ultrasound and magnetic resonance imaging (MRI), especially during the prenatal and postnatal periods.^[9,10]

Recent neonatal and prenatal imaging studies suggest that corpus callosum agenesis occurs in at least 1:4,000 live births,^[11] and other imaging studies demonstrated that 3–5% of the individuals assessed for neurodevelopmental disorders have corpus callosum agenesis.^[12]

In a prevalence study by Kidron et al.^[13] determined four distinct callosal defect groups which are complete (absence of all components), partial (presence of a short remnant), hypoplastic (thinning of the all parts of the corpus callosum), and mixed defects (partial corpus callosum agenesis with thinning of the residual part of the corpus callosum). However, regardless of CC morphology,



Figure 2. Coronal section through occipital lobe showing disproportionate enlargement of the occipital horn of the lateral ventricle (colpocephaly) (black arrows indicate the cut edge of occipital horn of the lateral ventricle). [Color figure can be viewed in the online issue, which is available at www.anatomy.org.tr]

Brescian et al.^[7] classified agenesis of CC in two groups according to the presence of Probst bundles. In Type 1, primary agenesis of CC, Probst bundles are present and along with the enlargement of the occipital horns of the lateral ventricles (colpocephaly). Conversely, in Type 2, Probst bundles and commissural axons are absent.^[7] Some researchers also classified agenesis of corpus callosum with the presence of other cerebral or systemic abnormalities. In this classification, “isolated type” is without any other abnormalities, while “complex type” is concomitant with cerebral or extracerebral abnormalities such as holoprosencephaly, cyst formation, metabolic diseases.^[14,15]

Taking into consideration the mentioned classifications, this case is a partial agenesis according to Kidron classification, and presence of colpocephaly is appropriate with Type 1 of Brescian classification, but without MRI it was not possible to evaluate Probst bundles.^[7,13] Lastly, it may be considered as complex type of corpus callosum agenesis, due to accompanying poor academic performance. Comparing this case with the classification studies based on the fetal period may be controversial, because this is an adult case.

It is reported that the majority of cases with isolated agenesis of the corpus callosum show no symptoms. A systematic review of the literature recently suggested that about 65% of cases with complete agenesis of the corpus callosum had normal intelligence and neurodevelopment at postnatal period.^[14] Cases with corpus callosum agenesis may accompany other anomalies without showing any symptoms; therefore, it should be considered that these anomalies may not only be related to corpus callosum agenesis.

Our case report had several limitations. First of all, because it was a medicolegal autopsy case, we had limited time to perform detailed postmortem anatomical dissection, we could not keep the whole brain tissue. Furthermore, we did not have enough information about the medical history of the case; also, we could not confirm the information received from the relatives. On the other hand, we could take postmortem standard histopathological and toxicological examination reports.

Conclusion

This is the first corpus callosum agenesis in medical literature encountered during medicolegal autopsy in an adult. The authors emphasize that the clinical anatomy and forensic medicine cooperation may contribute significantly to medical literature. In conclusion, this case underlines the need for increased awareness of corpus callosum agenesis from the point of clinical findings. Also, corpus callosum agenesis should be considered in individuals with poor academic performance. Neuroimaging techniques can be useful to identify the causes of poor academic performance.

Acknowledgments

The authors thank to Gökçen Köşeler for helping the preparation of the figures.

References

1. Aboitiz F, Montiel J. One hundred million years of interhemispheric communication: the history of the corpus callosum. *Braz J Med Biol Res* 2003;36:409–20.
2. Ramaekers G. Embryology and anatomy of the corpus callosum. In: Ramaekers G, Njikiktjien C, editor. *Pediatric behavioural neurology: the child's corpus callosum*. Vol 3. Amsterdam: Suyi Publications; 1991. p. 24–39.
3. Barkovich AJ, Norman D. Anomalies of the corpus callosum: Correlation with further anomalies of the brain. *AJR Am J Roentgenol* 1988;151:171–9.
4. Gianluigi P, McGahan JP, Nyberg DA. Cerebral malformations. In: Nyberg DA, McGahan JP, Pretorius DH, Pulu G, editors. *Diagnostic imaging of fetal anomalies*. Philadelphia (PA): Lippincott Williams and Wilkins; 2002. p. 221–91.
5. Derbali F, Ben FF, Rezgui A, Karmani M, Hajji R, Ben AO, Mzabi A, Laouani C. The corpus callosum agenesis: a case report. *American Journal of Medical Case Reports* 2015;3:27–29.
6. Jeret JS, Serur D, Wisniewski K, Fisch C. Frequency of agenesis of the corpus callosum in the developmentally disabled population as determined by computerized tomography. *Pediatr Neurosci* 1985; 12:101–3.
7. Brescian NE, Curiel RE, Gass CS. Case study: a patient with agenesis of the corpus callosum with minimal associated neuropsychological impairment. *Neurocase* 2013;20:606–14.
8. Hetts SW, Sherr S, Chao S, Gobuty S, Barkovich AJ. Anomalies of the corpus callosum: An MR analysis of the phenotypic spectrum of associated malformations. *AJR Am J Roentgenol* 2006;187:1343–8.
9. Contro E, Nanni M, Bellussi F, Salsi G, Grisolia G, Sanz-Cortès M, Righini A, Rizzo N, Pulu G, Ghi T. The hippocampal commissure: a new finding at prenatal 3D ultrasound in fetuses with isolated complete agenesis of the corpus callosum. *Prenat Diagn* 2015;35:919–22.
10. Tang PH, Bartha AL, Norton ME, Barkovich AJ, Sherr EH, Glenn OA. Agenesis of the corpus callosum: an MR imaging analysis of associated abnormalities in the fetus. *AJNR Am J Neuroradiol* 2009; 30:257–63.
11. Glass H, Shaw GM, Ma C, Sherr EH. Agenesis of the corpus callosum in California 1983–2003: a population-based study. *Am J Med Genet A* 2008;146A:2495–500.
12. Bodensteiner J, Schaefer GB, Breeding L, Cowan L. Hypoplasia of the corpus callosum: a study of 445 consecutive MRI scans. *J Child Neurol* 1994;9:47–9.
13. Kidron D, Shapira D, Ben SL, Malinger G, Lev D, Cioca A, Sharony R, Lerman ST. Agenesis of the corpus callosum. An autopsy study in fetuses. *Virchows Arch* 2016;468:219–30.
14. Santo S, D'Antonio F, Homfray T, Rich P, Pulu G, Bhide A, Thilaganathan B, Papageorghiou AT. Counseling in fetal medicine: agenesis of the corpus callosum. *Ultrasound Obstet Gynecol* 2012; 40:513–21.
15. Guillermo Davila-Gutierrez. Agenesis and dysgenesis of the corpus callosum. *Semin Pediatr Neurol* 2002;9:292–301.

Online available at:
www.anatomy.org.tr
doi:10.2399/ana.16.044
QR code:



deomed®

Correspondence to: Esat Adıgüzel, MD
Department of Anatomy, School of Medicine,
Pamukkale University, Denizli, Turkey
Phone: +90 542 711 80 31
e-mail: adiguzel@pau.edu.tr

Conflict of interest statement: No conflicts declared.

This is an open access article distributed under the terms of the Creative Commons Attribution-NonCommercial-NoDerivs 3.0 Unported (CC BY-NC-ND3.0) Licence (<http://creativecommons.org/licenses/by-nc-nd/3.0/>) which permits unrestricted noncommercial use, distribution, and reproduction in any medium, provided the original work is properly cited. *Please cite this article as:* Güngör Aydın A, Adıgüzel E, Aksoy A, Acar K. Partial corpus callosum agenesis and colpocephaly: a case report. *Anatomy* 2016;10(3):242–245.

Correction: (P-135) Double enamel pearl whit buds: a case report

Özkan G¹, Akkoç RF¹, Demirdaş K², Artaş G³, Ögetürk M¹

¹Department of Anatomy, Faculty of Medicine, Frat University, Elazığ, Turkey

²Dental Clinic, 1st Harput Street, Yalı Apt 4, Elazığ, Turkey

³Department of Medical Pathology, Faculty of Medicine, Frat University, Elazığ, Turkey

Author names for abstract of poster presentation published in Volume 10, Supplement 2, September 2016, page 178 – P-135 “Double enamel pearl whit buds: a case report” is erroneously published as: Özkan G¹, Akkoç RF¹, Demirdaş K², Ögetürk M¹. Corrected version is as follows: Özkan G¹, Akkoç RF¹, Demirdaş K², Artaş G³, Ögetürk M¹.

Anatomy 2016;10(3):246 ©2016 Turkish Society of Anatomy and Clinical Anatomy (TSACA)

Author Index to Volume 10, 2016

(The bold typed references are the ones in which the person is the first author.)

A		F	
Abbas OL	94	Farajiband N	239
Abbasoğlu Y	99	Farrell SF	153
Abegaz BA	148	Fazlıoğulları Z	16
Abo El-Khair DM	114	Fisahn C	221
Acar K	242	Fogelgren B	182
Adalı F	99	Fong KSK	182
Adıgüzel E	242		
Akinjisola AA	8	G	
Akkin SM	iii, 75, 158	Gbadamosi IT	105, 170
Aksoy A	242	Geneci F	200
Aktan İkiz ZA	239	Gülçebi İdrizoğlu M	50
Alonso F	193	Güngör Aydın A	242
Andrea A	143, 221	Gürses İA	177
Arayombo BE	21		
Arogundade TT	170	H	
Aseta FB	87	Hassan A	159
Ayan DM	94	Hızay A	30
Aydemir I	228	Hong T	182
		Horata E	99
		Hynd TE	182
B			
Babacan S	235	I-İ	
Barco Ríos J	156	Irwin PA	193
Barut Ç	46, 134	Ivashchuk G	143
Barut Ç		Iwanaga J	193, 221
Baykan R	94	İkidag MA	75
Bayram P	200		
Beker Acay M	99	K	
Bernard S	193	Kaçar D	46, 134
		Kafa İ	235
C-Ç		Karabulut AK	16
Carcak N	50	Keskin H	99
Cornwall J	138, 205	Keş H	99
Cüce MA	75	Khan S	153
Çağımni P	239	Kılıçaslan Sönmez P	228
		Komolafe AO	8, 21
D		Korkmaz E	177
Dada-Habeeb SO	170	Kürkçüoğlu A	40, 94
Dandin Ö	235		
Demir N	30	L	
Demirel BM	30	Labrash S	211
Demirkan E	94	Lal N	205
Dias GJ	205	Lambe E	105, 170
Dilli A	40	Loukas M	143, 193
Dolgun A	200	Lozanoff S	182, 211
Duque Parra JE	156	Macar O	99
		Malek AK	87
E		Mwachaka PM	87
Ebeye OA	1		
Eboh DE	1	N	
El-Habeby MM	114	Natsis K	71
El-Kholy WB	114	Nonaka K	182
El-Safti FEA	114		
El-Sherif NM	114	O-Ö	
Ergin T	235	Obasi KK	105, 170
Essa TM	159	Ocak M	200

Odula PO	87	Süzen B	30
Ogunlade O	21	Şengül G	iii, 85
Ogunlade O	8	Şimşek M	94
Oğuz N	30		
Olajide OJ	170	T	
Olayode AA	8, 21	Takagi B	182
Omotoso GO	170	Tanrıöver G	30
Onyia NS	1	Tardieu G	221
Oskouian RJ	143, 193, 221	Teomete U	235
Owolabi AR	21	Tihan D	235
Oyewopo AO	105	Tor O	99
Öktem H	40	Tubbs RI	193
Özkan Ö	94	Tubbs RS	143, 193, 221
Özkılıç Ş	75	Tuğlu Mİ	228
Özkubat I	94	Turamanlar O	99
Özsoy U	30		
Öztürk A	177	U-Ü	
Öztürk Ş	228	Uysal E	75
		Uysal İİ	16
P		Uzuner MB	200
Pelin C	40	Üçerler, H	239
Puelles L	60	Ünver Doğan N	16
R		W	
Robinson B	138	Ward MA	211
Romero Reverón R	157	Woldeyes DH	148
Ruthig VA	211		
		Y	
S-Ş		Yaşargil DCH	78
Saka OS	8, 21	Yaşargil MG	78
Saker E	143	Yazıcı C	40
Sancak İT	200	Yıldırım FB	30
Sargon MF	200	Yılmaz Onat F	50
Sarıkcıoğlu L	30	Yörük MD	239
Sevinç Ö	134		
Sika-Paotonu D	138	Z	
Soylu F	239	Ziylan T	16
Soysal H	40		

Acknowledgment

www.anatomy.org.tr

Anatomy 2016;10:248, © 2016 TSACA

Acknowledgment of Reviewers for Volume 10, 2016

The Editorial Staff of Anatomy expresses their appreciation to the following reviewers who have evaluated the manuscripts for Volume 10, 2016.

Esat Adıgüzel	Ali Fırat Esmer	Levent Sarıkçıoğlu
Dilek Akakın	Yakup Gümüşalan	Süleyman Ümit Şehirli
Gökhan Akkoyunlu	İlker Mustafa Kafa	Gülgün Şengül
Nihal Apaydın	Lütfiye Kanıt	Mehmet İbrahim Tuğlu
Ebru Ballı	Piraye Kervancıoğlu	Emel Ulupınar
Çağatay Barut	Zeliha Kurtoğlu	Altuğ Yavaşoğlu
Ayhan Cömert	Davut Özbağ	Özlem Yılmaz
Yusuf Özgür Çakmak	Mustafa Fevzi Sargon	N. Dilara Zeybek

Table of Contents

Volume 10 / Issue 3 / December 2016

(Continued from back cover)

Teaching Anatomy

- Macroscopic demonstration of the male urogenital system with evidence of a direct inguinal hernia utilizing room temperature plastination** 211
Victor A. Ruthig, Steven Labrash, Scott Lozanoff, Monika A. Ward

Reviews

- Bifid ribs: a comprehensive review** 221
Andrea Andrea, Gabrielle Tardieu, Christian Fisahn, Joe Iwanaga, Rod J. Oskouian, R. Shane Tubbs
- Mesenchymal stem cells in skin wound healing** 228
Işıl Aydemir, Şamil Öztürk, Pınar Kılıçaslan Sönmez, Mehmet İbrahim Tuğlu

Case Reports

- Absence of the celiac trunk in a rectal cancer patient: case report** 235
Deniz Tihan, Serdar Babacan, Tuncer Ergin, Uygur Teomete, Özgür Dandin, İlker Kafa
- Bilateral double parotid ducts: a case report** 239
Hülya Üçerler, Z. Aslı Aktan İkiz, Fatme Soylu, Narmin Farajiband, Mustafa Deniz Yörük, Pınar Çağırın
- Partial corpus callosum agenesis and colpocephaly: a case report** 242
Ayşegül Güngör Aydın, Esat Adıgüzel, Aylin Aksoy, Kemalettin Acar

Erratum

- Correction: (P-135) Double enamel pearl whit buds: a case report** 246
Özkan G, Akkoç RF, Demirdaş K, Artaş G, Ögetürk M

Index

- Author Index to Volume 10, 2016** 247

Acknowledgment

- Acknowledgment of Reviewers for Volume 10, 2016** 248

On the Front Cover:

Schematic drawing of the vascular relationships at the skull base. Note the relationship between the medial edge of the mandibular fossa and the internal carotid artery as it enters the carotid canal. From Alonso F, Bernard S, Irwin PA, Tubbs RI, Iwanaga J, Loukas M, Oskouian RJ, Tubbs RS. The relationship between the carotid canal and mandibular condyle: an anatomical study with application to surgical approaches to the skull base via the infratemporal fossa. *Anatomy* 2016;10(3):193–199.

Colored images of the published articles can be found in the online version of the journal which is available at www.anatomy.org.tr

Table of Contents

Volume 10 / Issue 3 / December 2016

Original Articles

- Ultrastructure of the placenta in gestational diabetes mellitus** **159**
Abdelghany Hassan, Tarek M. Essa
- Moringa protects against nicotine-induced morphological and oxidative damage in the frontal cortex of Wistar rats** **170**
Ismail Temitayo Gbadamosi, Gabriel Olaiya Omotoso, Olayemi Joseph Olajide, Shakirat Opeyemi Dada-Habeeb, Tolulope Timothy Arogundade, Ezra Lambe, Kosisochukwu Kingsley Obasi
- Reporting detailed information and acknowledging donor-cadavers: good practice recommendation for anatomists** **177**
İlke Ali Gürses, Esranur Korkmaz, Adnan Öztürk
- Reduction in *Wnt9b* and associated gene expression in the embryonic midface of *CL/Fr* mice with heritable cleft lip and palate** **182**
Brennan Takagi, Trudy Hong, Thomas E. Hynd, Keith S. K. Fong, Ben Fogelgren, Kazuaki Nonaka, Scott Lozanoff
- The relationship between the carotid canal and mandibular condyle: an anatomical study with application to surgical approaches to the skull base via the infratemporal fossa** **193**
Fernando Alonso, Shenell Bernard, Paul A. Irwin, R. Isaiah Tubbs, Joe Iwanaga, Marios Loukas, Rod J. Oskouian, R. Shane Tubbs
- Sex determination from the radiographic measurements of calcaneus** **200**
Muhammet Bora Uzuner, Ferhat Geneci, Mert Ocak, Pınar Bayram, İbrahim Tanzer Sancak, Anıl Dolgun, Mustafa Fevzi Sargon
- Orbital indices in a modern Sinhalese Sri Lankan population** **205**
Navneet Lal, Jon Cornwall, George J. Dias

(Contents continued on inside back cover)